HYBRID MACHINE MODELLING AND CONTROL

by

Lale Canan Tokuz

This thesis is submitted in partial fulfilment of the requirements
for the degree of Doctor of Philosophy of the
Council for National Academic Awards.

Mechanisms and Machines Group
Liverpool Polytechnic
February 1992

CONTENTS

ACKNOWLEDGEMENTS

I would like to thank my academic supervisor, Prof. J. Rees Jones for his interest, guidance and encouragement during the course of the work. He gave me understanding of programmable systems and hybrid machines. Without his help and suggestions this work would not have been possible.

I would wish to thank Dr. G. T. Rooney, my second supervisor for his suggestions for the theoretical and the experimental work.

I would like to acknowledge the interest and support of Unilever Research Ltd. and Molins Advanced Technology Group which acted as collaborating establishments for the work.

My thanks are due to Mr Steve Caulder who has prepared the electronic circuits for the experimental work and generously helped on computer control issues.

I would like to express my thanks to Dr. M. J. Gilmartin, the director of research, and present and past members of the Mechanisms and Machines Group of the Liverpool Polytechnic who have indirectly helped in the completion of this work. In particular, Dr. K. J. Stamp who has been very supportive and helpful throughout the work.

Thanks are given to all technicians in the Department of Mechanical Engineering, also to the staff of the Mechanical Engineering Workshop.

I would also like to express my thanks to Dr. Sedat Baysec who advised me to work with Prof. J. Rees Jones and join the Mechanisms and Machines Group of the Liverpool Polytechnic.

Finally, I would wish to thank my mother and father and my sister, Gonca who have given continuous encouragement and support throughout the work.

Lale Canan Tokuz

HYBRID MACHINE MODELLING AND CONTROL

by

Lale Canan Tokuz

ABSTRACT

Non-uniform motion in machines can be conceived in terms of linkage mechanisms or cams which transform the notionally uniform motion of a motor. Alternatively the non-uniform motion can be generated directly by a servo-motor under computer control. The advantage of linkage mechanisms and cams is that they are capable of higher speeds. They usually admit the means of introduction of dynamic balancing without extra parts and a high degree of energy conservation exists within the arrangement in motion. The advantage of servo-motors is that it is easier to re-program their motion to provide the versatility required of many manufacturing processes.

To generate non-uniform mechanism motion, two alternative techniques are envisaged in the work presented.

(i) where a servo-motor drives a linkage to produce an output. The motion transformation is determined with the geometry of the linkage. The mechanism acts as a non-uniform inertia buffer between the output and the motor.

(ii) where a constant speed motor acts in combination with a servo-motor and a differential mechanism to produce the output motion of a linkage.

Machines of these two kinds combine both linkage and a programmable driver. The first configuration is referred to a *programmable machine*, the second one is referred to as a *hybrid machine*. The focus of interest here is on the hybrid machine. One anticipated benefit, the second would have over the first, is that the size of the servo-motor power requirement should come down.

In order to explore the idea an experimental rig involving a slider-crank mechanism is designed and built. Initially a computer model is developed for this so-called hybrid machine. The motion is implemented on an experimental rig using a sampled data control system. The torque and power relations for the system are considered. The power flow in the rig is analysed and compared with the computer model. The merits of the hybrid machine are then compared with the programmable machine. The hybrid machine is further represented with bond graphs. Lastly, the observations on the present work are presented as a guide for the development and use of hybrid machines.

INTRODUCTION

Non-Uniform Mechanism Motion

There are currently two alternative transmission systems for generating non-uniform motion: *conventional mechanisms* and *programmable servo-drives*.

i) *Conventional Mechanisms*

The driving power in conventional machines is usually obtained from one single constant speed motor. Power is transmitted to the drive shaft through a series of belts, gears and chains to obtain uniform motion while cams and linkages are used for non-uniform motion transformations to meet the peculiar needs of the process at one or several outputs. Over the years, designers of production machinery have answered needs of the market by using these components.

In the design of such transmission systems, the assumption made is that the size and shape of the products to be handled by a particular machine are known for its lifetime. Once installed, the motion profile cannot be easily changed. Only cam phase adjustments and minor changes of link lengths could be possible. Although they can be designed to satisfy high-speed mass production, such arrangements are generally considered to be inflexible when required to meet frequent changes in either manufacturing processes or products, particularly when short change-over time is the paramount requirement. Complex mechanistic solutions that may provide this versatility sometimes become expensive or are difficult to design.

However, these traditional linkage/flywheel systems present highly efficient regenerative capacity. Well-designed systems are capable of higher speeds with adequate dynamic balancing. Well-known applications are found in power presses or internal combustion engines, for example. Here the flywheel acts as an inertia buffer between load and the power source. When the press makes a stroke, work is done on the material between the tools. The energy is given out by the flywheel and it is restored from the source of power. The schematic

representation of conventional mechanical transmission can be seen in Figure I.1.(a).

ii) ***Programmable Servo-Drives***

Programmable transmission systems are accepted as the basis of a new generation of production machines which offer short change-over times, operational reliability and flexibility, design simplicity. The machine can handle different products without changing any parts in the machine with significant shopfloor flexibility. Many application examples are found in most types of packaging machine to more traditional machines, grinding etc. Figure I.1.(b) represents a programmable transmission schematically.

In programmable transmission systems, a module consists of three basic elements: *the motor*, *the drive* and *the control system*.

The motor, the main element, is an electrical device that generates the non-uniform motion. It takes advantage of the developments in digital technology in power devices and in new magnetic materials. Stepper motors, dc brush motors or brushless servo-motors constitute the broad type that are suitable for many applications. Each type of motor has benefits and drawbacks in terms of its suitability for a particular application.

Stepper motors have simplicity in construction with low cost. No feedback components are needed. These motors have three main types as permanent magnet, variable reluctance and hybrid steppers. They are simple to drive and control in an open-loop configuration. However, loss of accuracy may happen as a result of operating open-loop. They can cause excessive heating and they are noisy at high speeds. *DC brush motors* have benefits of smoothness for the whole speed range. A wide variety of configurations is available for different applications, ie: low inertia, moving coil, ironless rotor etc. The closed-loop control eliminates the risk of positional errors. The addition of feedback components does increase the cost. Several drawbacks of these motors are related to their commutator and brushes that are subject to wear and require maintanence. These also prevent the motor being used in hazardous environments or in a vacuum. Undoubtedly *brushless motors* combine best performance features of stepper and DC brush motors. They can produce high peak torques and operate at very high speeds. The only drawback results from their cost and complexity, and need for additional feedback components.

The second basic element, *the drive* is what makes the difference between a conventional system and a programmable system. It is an electronic power amplifier which delivers the power to operate the motor in response to control signals. In general, the drive will be specifically designed to operate with a particular type of motor. A stepper drive can not be

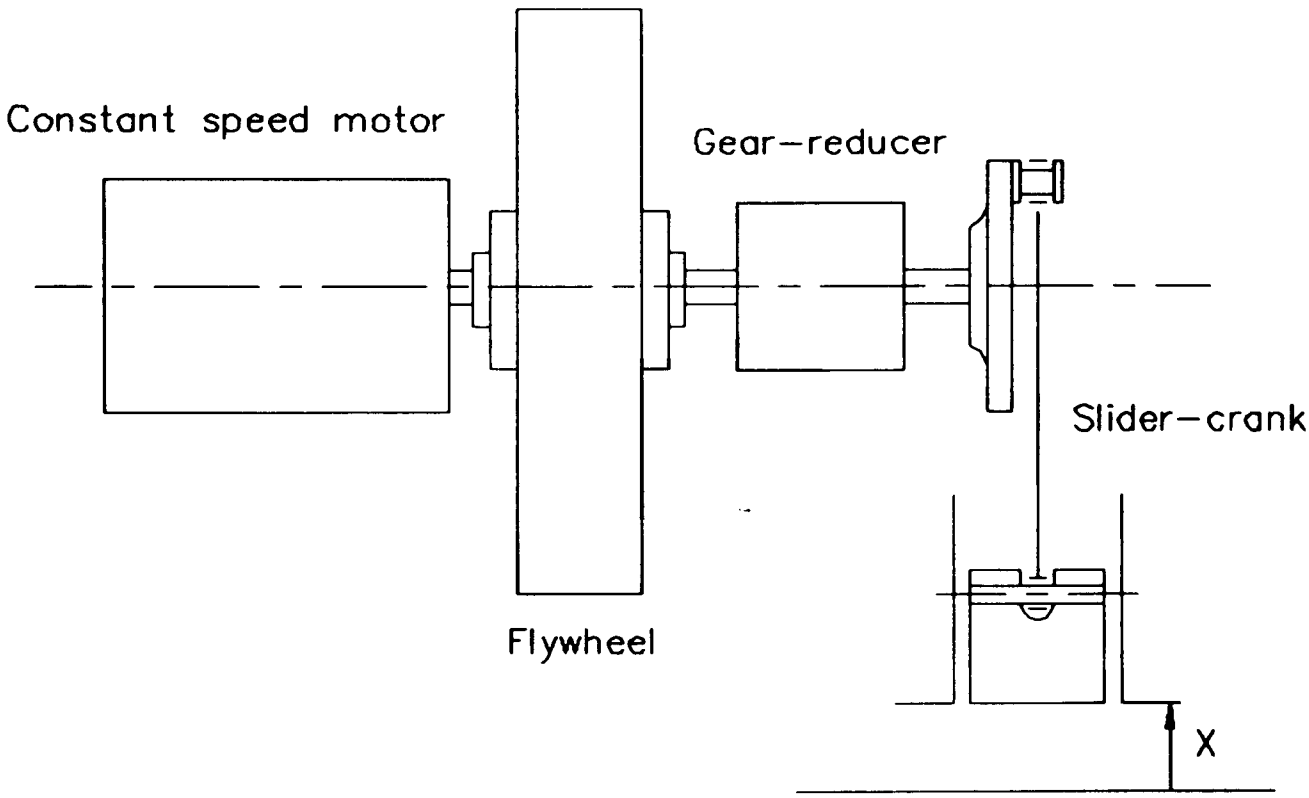

Figure 1.1. Conventional Mechanical and Programmable Transmission.

used to operate a DC brush motor, for example.

The *control system* determines the actual task performed by the motor such as controlling variables like position, speed, torque. They refer to position, velocity or torque control systems in which the angular position of the motor shaft is required to be controlled with addition of a shaft encoder, or the motor velocity is required to follow a given velocity profile as motor/tachometer combination or in the case of motor torque control with torque sensors respectively. These control systems all have a common purpose to ensure that command signals are obeyed immediately and exactly. The control function required can be distributed between a host controller, such as a desk-top computer. One controller can operate in conjunction with several drives and motors in a multi-axis system. So together with three basic elements, the non-uniform motion can be generated at the motor shaft output at the end.

However, for all of very basic rotary motions even this drive concept needs a transforming mechanism, such as a leadscrew or a rack and pinion, or a coupler and slider to complement the motion generation or to reach a required working point. The speed of operation of these programmable drives is limited by their dynamic bandwidth and torque capacity particularly when the mass of parts is added to a rotor. Complex non-uniform motion with high harmonic content will test performance limits. In direct generation of alternating type non-uniform motions these motors have to provide the required current to produce accelerating and decelerating torques. By constrast this involves an energy interchange between the mechanical and electrical components that may not be allowed for and prove very inefficient.

iii) ***Hybrid Machines***

A configuration which combines the above two types of non-uniform motion generation, conventional and programmable, presents new alternatives referred here as *hybrid machines* [1.1]. The prospect is one balancing the advantage and disadvantage of each transmission system and offer a better transmission configuration maximizing benefits of both.

The study and application of hybrid machines for non-uniform motion had not been previously explored and a suitable configuration was not clear. Here one possibility was thought to involve a *differential mechanism*. Inputs from a uniform motion constant speed motor and a programmable motion servo-motor would, therefore, be summed in a differential gear-unit to produce the non-uniform motion at the output of a linkage.

The differential is a commonly used transmission mechanism for addition and subtraction purposes. By using a differential device it may be possible to make the motion programmable

and regenerative. Thus there will be a regenerative prime mover where energy is stored in kinetic form and available when required.

Figure I.2 shows a schematic representation of a hybrid machine in the herein configuration. The expected benefits of this hybrid arrangement would be a reduced size of the servo-motor power requirements, more efficient use of energy, reduced change-over time with the programmed motions and potentially higher speeds with programmable features.

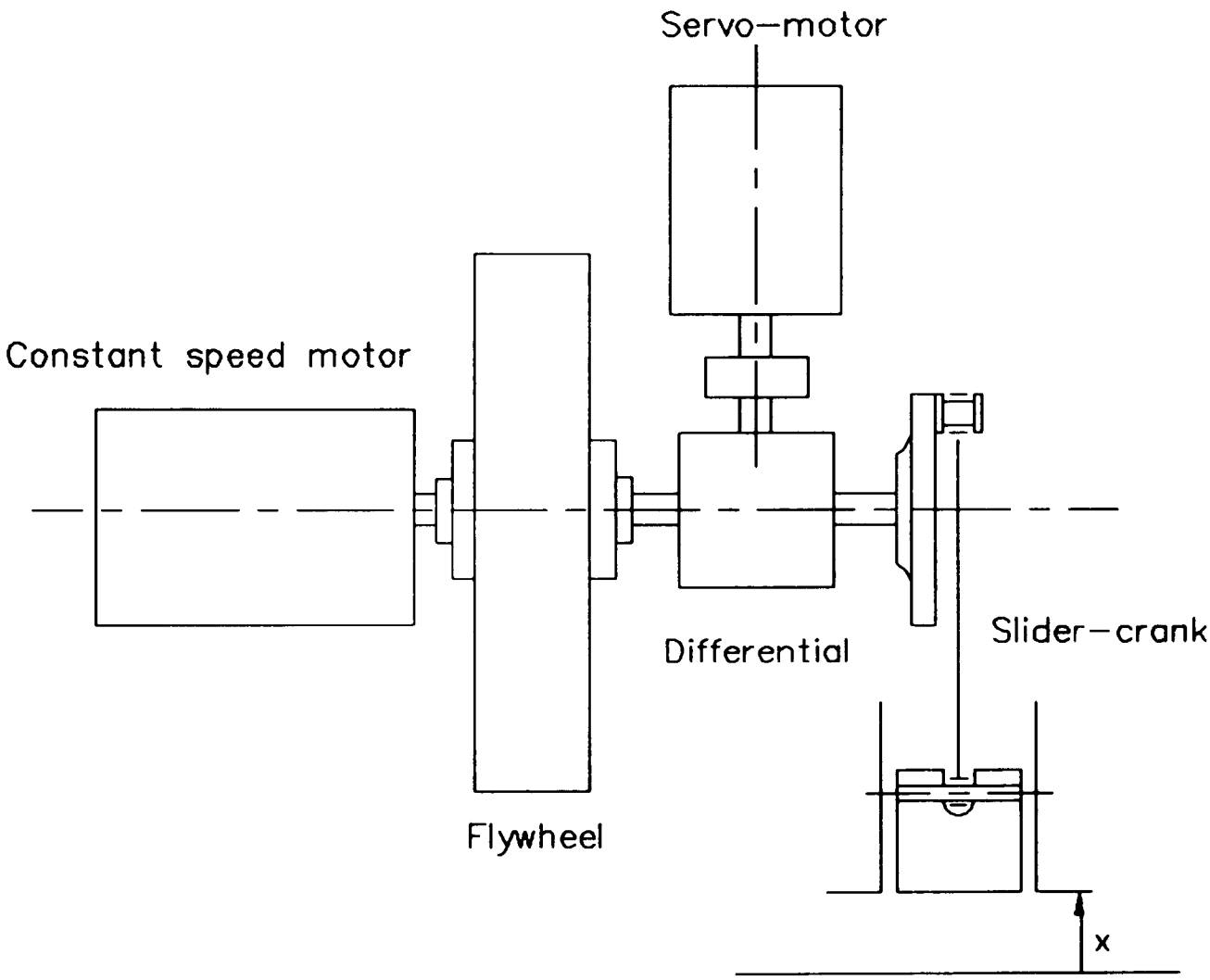

Figure I.2. Hybrid Machines.

From the above introduction, a summarizing table of advantages and disadvantages are given for the alternative transmission systems and also the expected benefits for the hybrid machines. This is shown in Table I.1.

Mainly the objective here is to study hybrid machines by modelling and experiment and subsequently deduce their important performance characteristics in terms of input torques and power rating for drive optimization. Conclusions will be presented in a form suitable as a design guide for hybrid machines through the study of two available transmission systems.

NON–UNIFORM MECHANISM MOTION

	Advantages	Disadvantages
CONVENTIONAL TRANSMISSION	regenerative (flywheels)	difficult machine layout
	low power requirements	low versatility
		long change–over time
PROGRAMMABLE TRANSMISSION	programmable	heavy current requirements
	simpler machine layout	inefficient use of energy
	short change–over time	higher power requirements
HYBRID MACHINES	regenerative	
	programmable	
	short change–over time	
	reduced servo–motor size	

Table 1.1. Non-Uniform Mechanism Motion.

Two degrees of freedom mechanisms

Linkage mechanisms with two or more degrees of freedom are known as *adjustable mechanisms.* In them discrete or continuous adjustability of the mechanism during operation can be possible. The requirement may be changes of a coupler curve or mechanism stroke adjustment, for example.

Here two degrees of freedom mechanisms can be considered in two groups: *linkages and cams* and *differential mechanisms.*

i) Linkages and Cams

In a single degree of freedom application, the position of an output member is directly dependent upon the dimensions of the links and the position of the input member. For example, four bar linkages can be used as function generators, such that the output moves as some function of the input as:

$$\theta = f(\phi)$$

or a slider-crank mechanism provides a linear reciprocating output as a function of input crank angle like;

$$x = f(\theta)$$

When the motion is implemented using cams, uniform motion of an input member is converted into a non-uniform motion of the output member. The output motion may be either shaft rotation, slider translation or follower motions created by direct contact between the input cam shape and the follower. The cam rotates at a constant angular velocity and the follower moves up and down. The motion of the follower depends on the cam profile. During the upward motion the cam drives the follower. In the return motion the follower is driven by the action of springs unless it a closed track cam or conjugate cam pair. It gives a relation between the crank rotation and the follower displacement as:

$$z = f(\theta)$$

However, if the requirement is that of obtaining output related to more than one input, then two degrees of freedom have to be provided by the mechanism. The seven bar linkage, the three slider linkage and three dimensional cams can be given as examples. In a two degree of freedom mechanism, two separate inputs control a single output. With two inputs available,

the arrangement provides an enlarged versatility but mechanical complication.

One of the simplest two degrees of freedom applications can be seen in *the seven bar linkage*, which is in Figure I.3.(a). The linkage is capable of generating

$$\theta_3 = f(\theta_1, \theta_2)$$

where θ_3 is the displacement of the output link and θ_1, θ_2 are the displacements of the two input links.

The second example is the *three slider linkage*. The relation between inputs and the output is given as;

$$x_3 = f(x_1, x_2)$$

where x_3 is the slider output and x_1, x_2 are the displacements of the two input sliders. A three slider linkage can be seen in Figure I.3.(b).

In *three dimensional cams*, the motion of the follower depends not only upon the rotation of the cam but it is also dependent on the axial motion of the cam. They are capable of generating functions of two independent variables. But they are difficult to manufacture and are quite expensive. A three dimensional cam is given in Figure I.3.(c). The output motion can be written with a mathematical relation as:

$$z = f(x, \theta)$$

where z is the output, x is the axial motion of the cam and θ is the angular displacement of the cam.

ii) Differential Mechanisms

Differential mechanisms are used to sum up two different motions, where the output is linearly dependent on two inputs. This fact is the characteristic of the differential in which gives the ability to act as a two degree of freedom mechanism. There are many different types of differentials available according to the function required at the output. We may include *linkage*, *screw*, *bevel* and *spur gear differentials*, for example.

When the differential mechanism is used for simple adding purposes, both inputs and output are linear. This device is known as a ***linear differential.***

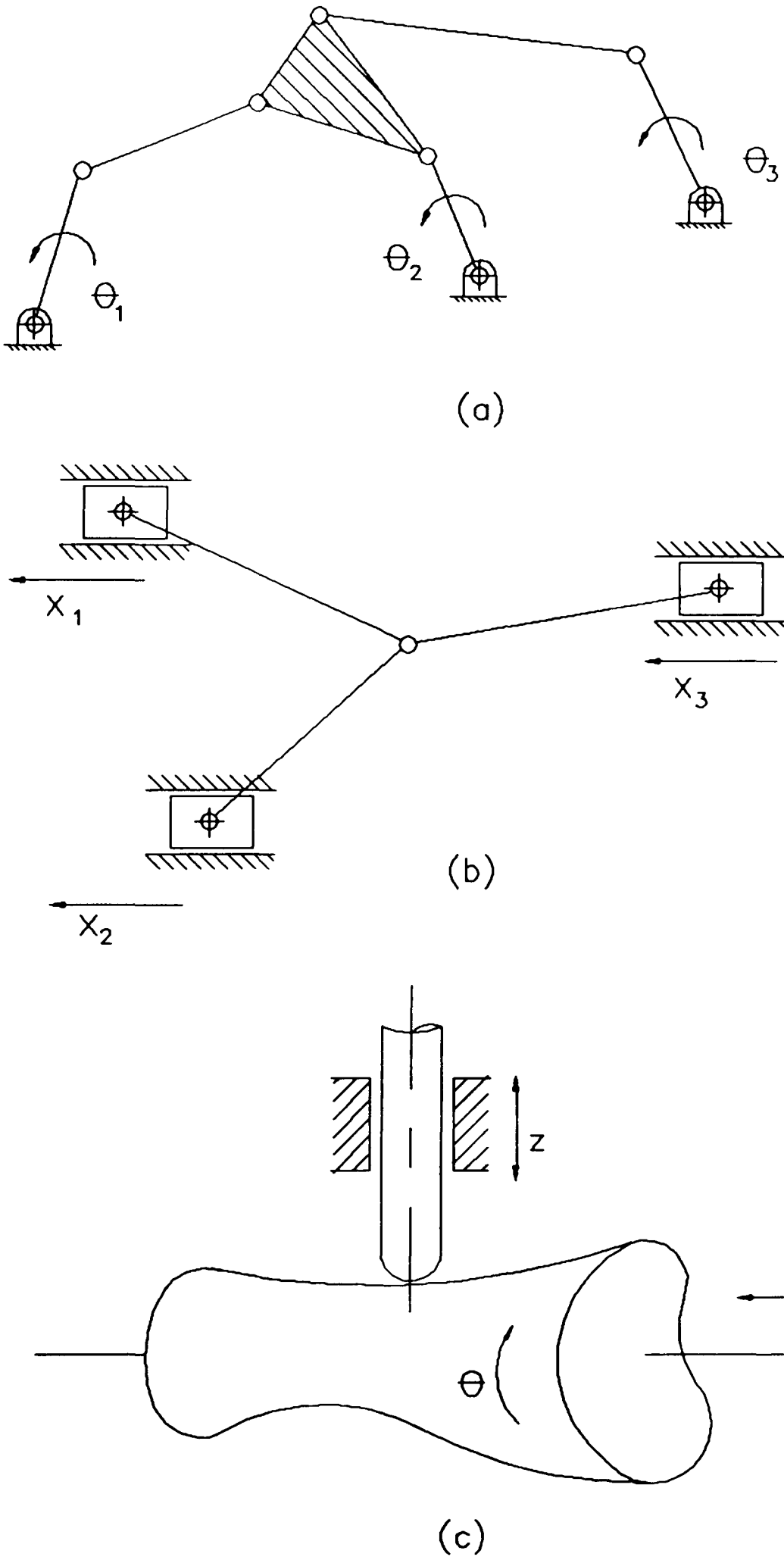

Figure I.3. Two degree of freedom mechanisms.

It is shown in Figure I.4.(a). Here the motion of bar 4, x_4 is expressed as:

$$x_4 = f(x_2, x_3)$$

where x_2 and x_3 are the linear inputs from bars 2 and 3. The mechanism can also be used for subtraction by adding negative portions to the scales.

When the inputs are rotary and the requirement is to have a linear output, this is achieved with a *screw differential* [1.2]. A sketch of a screw differential is shown in Figure I.4.(b). The pointer is constrained to move only axially with the screw without any rotation. The inputs are fed to gears 2 and 3, and the addition is represented on a linear scale by pointer 4. The output of the pointer x_4 is written as:

$$x_4 = f(\theta_2, \theta_3)$$

where θ_2 and θ_3 are the angular displacements from the gears.

When it is required to add rotations rather than linear quantities *a bevel gear* or *a spur gear differential* is applied. Gear differentials are compact and have unlimited angular displacement capacity and they are the most commonly used mechanisms for addition and subtraction purposes. An example epicyclic unit holds kinematic relations between its members as:

$$\dot{\theta}_3 = f(\dot{\theta}_1, \dot{\theta}_2)$$

where $\dot{\theta}_3$ is the velocity of the output shaft, $\dot{\theta}_1$ and $\dot{\theta}_2$ are the velocities of the two inputs. This unit is represented schematically in Figure I.4.(c) as epicyclic of basic ratio ρ with rotating casing.

Thesis Structure:

Chapter 1 begins with a description of the experimental set-up for a hybrid arrangement and its components. The elements used in system control and measurement are explained. The torque and power measurement are studied.

Chapter 2 contains motion design considerations for different reciprocating motions of fixed stroke. Polynomial laws are applied to define the slider motions. Their derivation is examined in detail. Three characteristically different slider motions are chosen and presented for implementations on the hybrid arrangement.

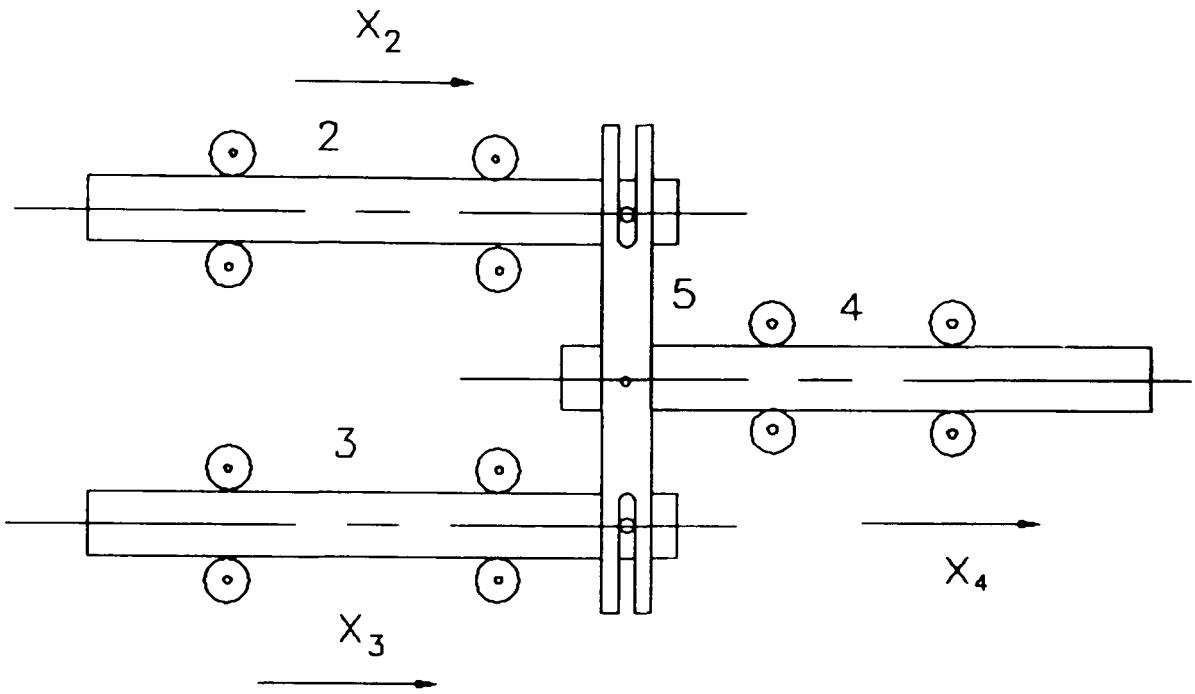

(a)

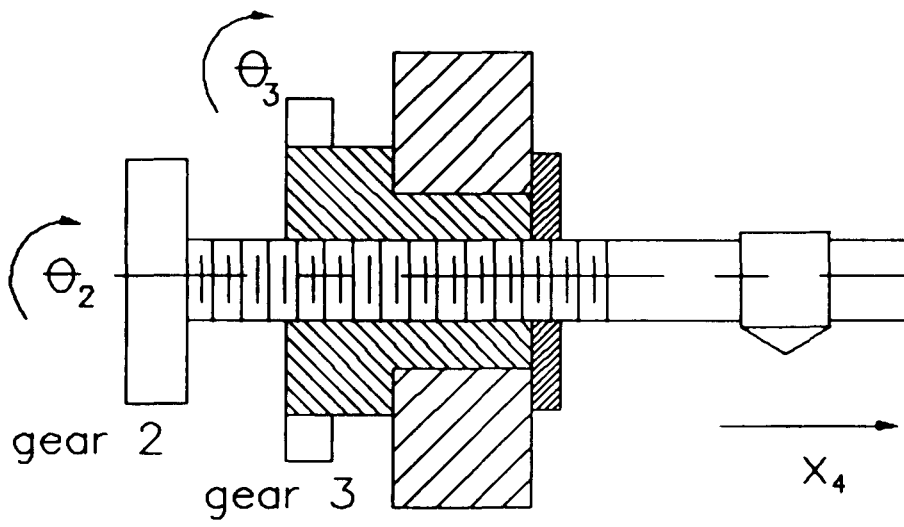

(b)

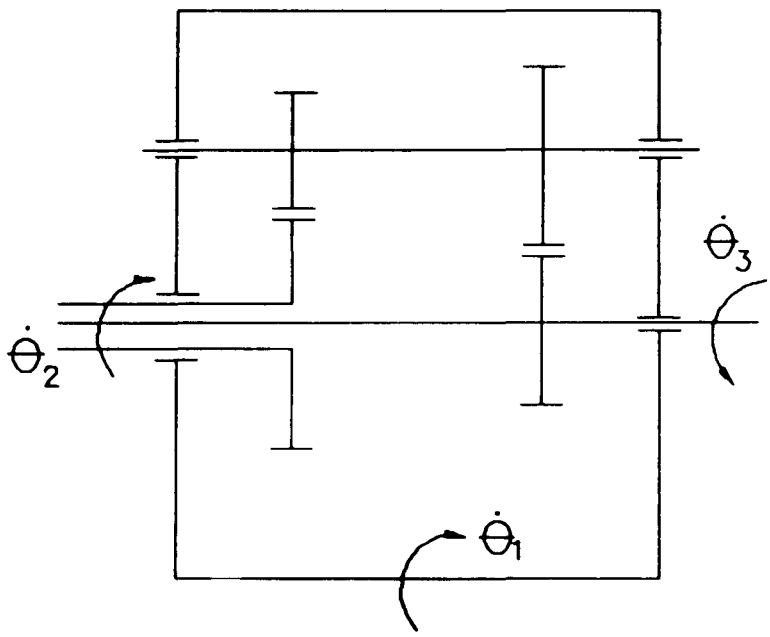

(c)

Figure I.4. Differential Mechanisms.

In chapter 3, kinematic and dynamic analysis for a slider-crank mechanism are studied. Inverse kinematic issues are included for the non-uniformly rotating crank. The differential equations of motion are derived using Lagrange's equations. The driving torques required are found for three different prescribed motions by using the equation of motion. The output crank motion is then separated into its components for the constant speed motor and the servo-motor input.

Chapter 4 contains a generalized approach to mathematical modelling of systems. It formulates a mathematical model of the hybrid arrangement using Lagrange's equations. With the model, the analysis of the real system response is carried out for test input signals and the designed motions.

Computer control issues are discussed in chapter 5. This chapter presents the controller hardware requirement to implement the required functional tasks. Also, the control hardware arrangement is described and the obtained system responses are presented. Later command motion tuning is introduced to the system.

These four chapters establish the mathematical and the experimental framework on which subsequent chapters are related for the torque and power calculations. So chapter 6 combines them and presents calculations for torque distribution and power flow in the hybrid arrangement. A modified experimental set-up is also described for torque and angular velocity measurement in this chapter.

Chapter 7 is devoted to the comparisons of theoretical and experimental results. A discussion on the system responses and modulated slider outputs are then followed with the results for theoretical and experimental torque distribution and power flow. The comparison of the programmable drive without differential and the hybrid arrangement is also included in this chapter with further comments for future use. Regenerative programmable systems are considered.

In chapter 8, fundamentals of bond graphs are included as an alternative way of interpreting the power flow in the system. The method of bond graph assembly is covered. To achieve bond graph modelling simplifying assumptions are made in the system equations. The hybrid arrangement is then represented by bond graphs to clarify the interactions among its components.

Finally the observations on the work achieved and recommendations for further work are presented in chapter 9.

CHAPTER 1
THE HYBRID ARRANGEMENT

1.1. Introduction

An arrangement that combines the two types of non-uniform motion generation is presented in this chapter. The main idea is to utilize the advantages and disadvantages of each alternative to offer a new alternative referred as a *hybrid machine* [1.1]. In this arrangement, the fundamental non-uniform motion requirement is derived from a linkage mechanism and the second input, which is programmable, is used to provide the modulation of that fundamental motion.

The experimental arrangement, based on a slider-crank mechanism, is built using suitable available motors, sensors and standard commercially available transmission elements. With this arrangement arbitrary reciprocating motions, with various characteristics but a fixed length of stroke, are to be achieved.

1.2. The General Description of The Experimental Arrangement

The arrangement, shown schematically in Figure 1.1 consists of

- dc servo-motor and servo-amplifier
- dc constant speed motor
- differential epicyclic gear-unit
- slider-crank mechanism

In the arrangement, the dc constant speed motor acts with a servo-motor and a differential gear-unit to produce an output that is connected directly to the crank of the mechanism. This arrangement is capable of operating alternatively from the constant speed input or the servo-driven input or a combination of each. General and top view of this arrangement are given in appendix 1 Figure A.1.1.

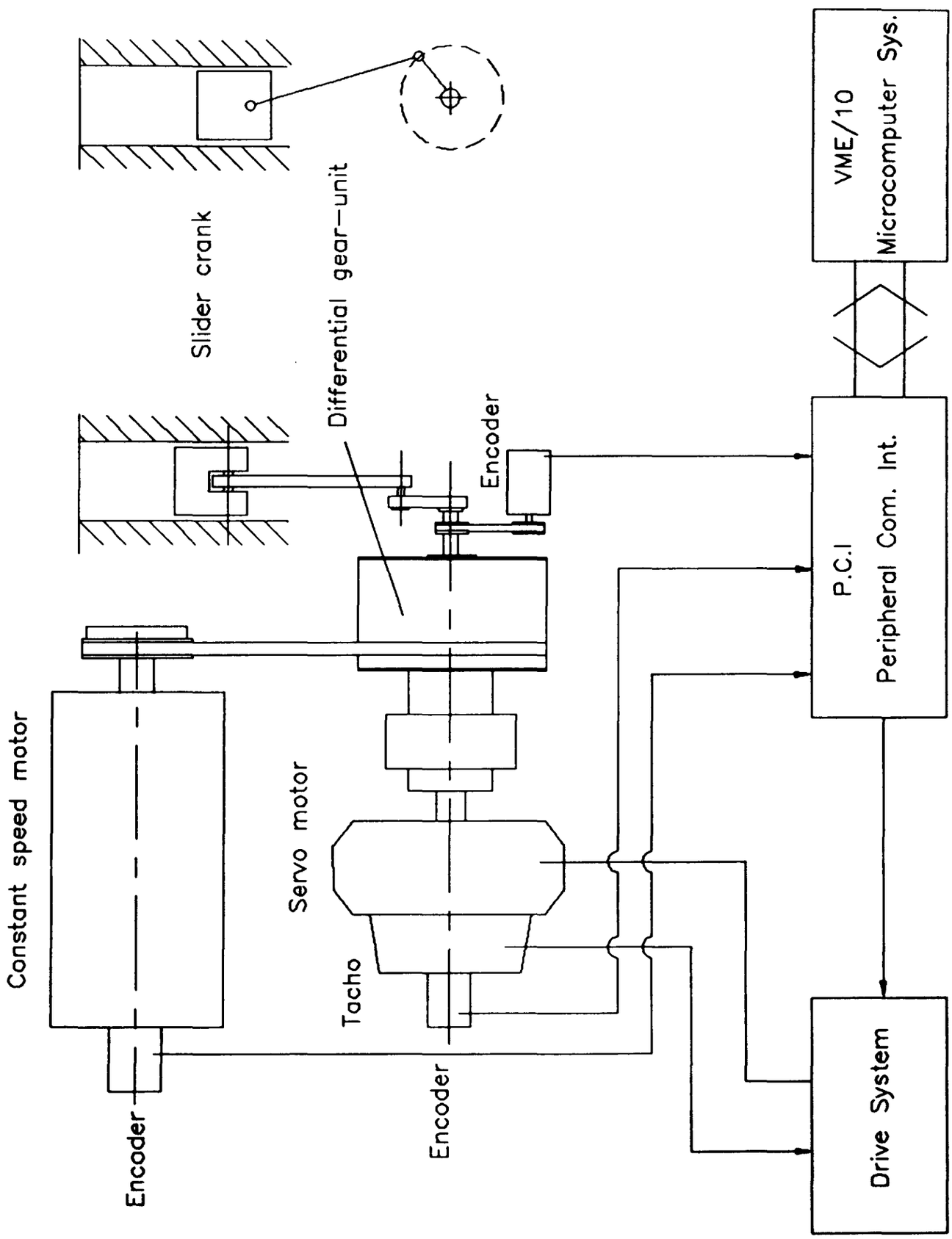

Figure 1.1. The Hybrid Arrangement.

1.2.1. The Drive Motors

The disc armature, printed circuit type dc servo-motor provides the programmable input. The essential element of this motor is its unique disc-shape armature with printed commutator bars in what is sometimes described as a *pancake* configuration, i.e., a large diameter and a narrow width.

Printed circuit motors have developed in response to the need for low inertia, high acceleration drives for actuators and servo applications. However, they possess some drawbacks because of their unique armature design. Since the current flow in a disc armature is radial, the windings are arranged across a rather large radius. This radius factor contributes to the relatively high moment of inertia of the armature. The thin printed circuit armature also has a brittle construction which can be considered a basic limiting factor in its applications.

The dc servo-motor used has a rated output power of 1 kW. Its rated torque in continuous operation is 3.2 N.m and its rated speed is limited at 3000 rpm. This motor is supplied with an integral tacho-generator. The dc servo-motor is driven by an amplifier which is controlled by a microcomputer.

The uniform motion input is generated by a dc shunt motor. The motor armature and the line of drive parts form the principal flywheel effect. The term 'shunt' is derived from the connection of the field and armature in parallel across the power supply. The shunt motor provides good speed regulation and it is generally used as a relatively constant speed motor. This motor has an output power of 0.75 kW and its maximum speed is 1500 rpm.

1.2.2. The Differential Gear-Unit

The differential used is an epicyclic gear-unit with multiple planet assemblies having their gears and shafts integral. It is comprised of three principal elements as follows:

— the casing (annulus) which carries the planets
— the central shaft
— the torque arm sleeve.

The kinematic relationship between the angular speeds of these three elements is given by the formula.

$$\dot{\theta}_3 = \rho\dot{\theta}_2 + (1-\rho)\dot{\theta}_1 \qquad (1.1)$$

where

$\dot{\theta}_1$ — angular speed of the casing (the constant speed motor)

$\dot{\theta}_2$ — angular speed of the torque arm sleeve (the servo-motor)

$\dot{\theta}_3$ — angular speed of the central shaft (the crankshaft)

ρ — gear ratio relating $\dot{\theta}_2$ to $\dot{\theta}_3$, when $\dot{\theta}_1$=0.

The gear ratio can be expressed in explicit form as:

$$\rho = \frac{\text{product of number of teeth in driving gears}}{\text{product of number of teeth in driven gears}} = \frac{Ab}{aB}$$

where A and B are the number of teeth in sun gears and a and b are the number of teeth in planet gears.

From Figure 1.1, we can see that the annulus of the differential gear-unit is driven by belts (Vee belts) and the servo-motor is coupled to the other input of the gear-unit with the reaction plate and a flexible coupling.

The differential gear-unit used is given with its dimensions and specifications in appendix 1 Figure A.1.3.(a). The accessories on the torque arm sleeve also shown in Figure A.1.3.(b) with a detailed drawing.

1.2.3. The Design of Slider-Crank Mechanism

The slider crank mechanism is used for the implementation of translating reciprocating motion in the present study. The design parameters of this mechanism are chosen to match with the drive capacity of available motors.

The slider-crank mechanism is shown in an assembly drawing in appendix 1 Figure A.1.4. In the assembly of the mechanism, the connecting rod and the crank are connected with a threaded bearing pin with sliding fit and fixed with a nut at the end. Needle bearings are used at the ends of the connecting rod with the outer race of the each needle bearing press fitted. The slider slides on a slideway plate which is screwed down to the base, which in turn is clamped on to a heavy tool bed. Rollers are fixed on the slideway plate to provide a sliding path to ensure reciprocating motion. The crankshaft, which connects the crank and the differential gear-unit, is also keyed to the crank and the differential gear-unit. The crankshaft is supported by means of two pillow blocks.

The sectional view of the slider-crank mechanism is given in Figure A.1.5.

1.3. System Control and Measurement

The control system is built around the memory mapped Input/Output (I/O) channel on a VME/10, 68010 microprocessor development system.

Several sensors are incorporated in the control system. There is a tachogenerator to sense the velocity and an incremental encoder to provide information about the shaft position. Wherever mechanical rotary motion has to be monitored, the encoder provides a necessary interface between the motor or the mechanism and the control unit. It transforms rotary movement into the electrical signals that are then conditioned; ie. the counters and microprocessors can easily count and synchronize the pulses.

To perform a closed-loop control action for the servo-system, a shaft encoder is connected via a flexible coupling directly to the servo-motor armature. The actual output is measured, fed back and compared to the desired input. Any difference between the two is the deviation from the desired input. This is amplified and used to correct the error.

In order to take additional measurements from the experimental arrangement shown in Figure 1.1, two incremental encoders are used, one fixed to the constant speed motor and other one fixed to the crankshaft. For this arrangement, it is also necessary to coordinate the command motion of the servo-motor to that of the constant speed motor irrespective of the operation of speed. In order to drive the servo-motor as a slave to the constant-speed motor, an encoder is indirectly connected to the annulus of the epicyclic unit. Thus pulses from the constant speed motor are taken to update the position command to direct the servo-motor.

The encoder on the crankshaft is only used for open-loop measurement for the system output. It is driven by means of a timing belt. This encoder is also used to enable the correlation between the crank position and the slider displacement. In order to allocate a certain position, like zero position of the crank which corresponds to zero slider displacement, a reference pulse from this encoder has been used to start the main control cycle.

The displacement of the slider is measured by means of a linear potentiometer which is fixed on the slider block. A voltage supply is connected to this potentiometer, the output is then fed to Analog-to-Digital Converter's (ADC) through the designed controller boards. The linear displacement of the slider is obtained in terms of ADC counts as experimental data reading.

The above control requirements for the servo-system and for the coordination of both motors are implemented by using a control hardware arrangement developed by ' Mechanisms and

Machines Group', Liverpool Polytechnic. The control hardware arrangement will be discussed in Chapter 5 in detail.

1.4. Torque and Power Measurement

In the second part of the study, the system torque and power outputs are measured. To achieve this, the *hybrid arrangement* is modified.

An inductive torque transducer is mounted between the differential gear-unit and the crank shaft by means of two flexible couplings. The torque transducer used incorporates a pulse pick-up transducer in its body. Thus to measure the angular velocity, signals coming from the pick-up are converted into a dc-voltage output with a frequency-to-voltage converter. Later the angular velocities are obtained by using pulse counting also. So with this set-up, the power flow and output is directly found by measuring torques and angular velocities. These measurements are presented in Chapter 6.

1.5. Conclusion

The *hybrid arrangement* and its components have been described in this chapter. A slider-crank is chosen for an example mechanism. The reason for this configuration is simply because of its suitability in many machine tool applications considerably in the stamping machines.

The technical requirements for the servo-system, the motion coordination and the means to achieve other measurements are discussed. According to the level of importance, as a first step, a closed-loop position control is achieved and the coordination of the constant speed motor and the servo-motor is performed. Output measurements are then taken from the crankshaft with corresponding slider displacements.

After completing the experiments and measurements for the first part, a modified experimental set-up is prepared with the inclusion of a torque transducer. The generated output torques and angular velocities are measured. The power flow from separate inputs of the system is then found.

Particularly starting from this chapter, the studies are carried on the hybrid arrangement. It is hoped that the results obtained would be able to reveal many unknown aspects of these types of machines and encourage their successful applications in the future.

CHAPTER 2
MOTION DESIGN

2.1. Introduction

The importance of motion design, implementation and control has become significant in recent years. This is the result of use of computers and microprocessors in the advancement of design and control techniques. Motion design especially has got the leading priority for the applications in high-speed production machinery.

Basically the developments have focused on the industrial processes that require intermittent or non-uniform motion. These motions could generally be implemented using linkage mechanisms and cams. Now the generation of non-uniform motion in machines using servo-motors is increasing more than ever. The servo-motors can perform a variety of motions by modulating the speed of a drive motor to produce a required characteristics for the output motion.

Motion design is a means of evaluation and adaptation of motion before its implementation into a system. The motions required may concern the position of a point, plane or body positions. This gives the description of motions with mathematical functions. We may, for example, wish to include harmonic laws, standard cam motion laws and polynomials etc. as suitable mathematical forms. This results in a need for a stronger mathematical basis on which to begin the design process.

In this chapter, motion design is studied in the context of a hybrid machine implementation. Characteristically different reciprocating motions are defined to match given boundary conditions using polynomial laws.

2.2. Motion Design

In motion design, the motion of a mechanical system is specified by the position expressed as

a function of time or is coordinated with the position of other moving elements. As a common practical way to conceive the required motion, the motion cycle is divided into a number of discrete segments. Position, velocity, acceleration and even jerk or higher derivatives are set as boundary conditions for the segments of motion. In addition, sometimes *via* or *intermediate points* are also included to control the dynamic properties of the motion between boundary conditions. Each segment is basically defined by its own law. A variety of mathematical functions are then used to describe the motion.

Mathematical forms of motion laws generally fit into two groups: *harmonic* and *polynomial laws*. The widest use of these laws is generally found in the field of cams. The experience of other studies [2.1], [2.2], [2.3] and [2.4] reveals that polynomial laws can be considered as a means of satisfying boundary conditions for the function and its derivatives and also for the computational simplicity. Polynomials are used throughout in the present study.

2.2.1. Polynomial Laws

The general form of the polynomial motion is given by:

$$x(t) = \sum_{i=0}^{n} c_i t^i \tag{2.1}$$

where x(t) is the desired output motion, c_i are the polynomial coefficients defining the law and n is the degree of the polynomial. The general derivative of a polynomial can be described as:

$$\frac{d^j}{dt^j} x(t) = \sum_{i=j}^{n} \frac{i!}{(i-j)!} c_i t^{i-j} \tag{2.2}$$

where j is the order of derivative.

The number of terms in the polynomial equation is dependent on the number of boundary conditions. In this work, the degree of polynomial law defining the motion law is made equal to the number of constraints used to define the motion minus one. The abbreivations x, $\dot{x}$, $\ddot{x}$ are used for the slider displacement, velocity and acceleration in the coming parts.

2.2.2. Solution of Polynomial Coefficients

The coefficients of a polynomial equation are determined by the formulation of matrices which include the imposed boundary conditions, given time intervals and the unknown coefficients. The equation for the nth order polynomial in terms of the independent variable time is written as:

$$x(t) = c_0 + c_1 t + c_2 t^2 + c_3 t^3 + \ldots\ldots\ldots + c_n t^n \tag{2.3}$$

Differentiation of this yields the following velocity equation,

$$\dot{x}(t) = c_1 + 2c_2 t + 3c_3 t^2 + \ldots\ldots\ldots + n\, c_n\, t^{n-1} \tag{2.4}$$

Similarly, the differentiation of velocity equation gives the acceleration:

$$\ddot{x}(t) = 2c_2 + 6c_3 t + \ldots\ldots\ldots\ldots + n\,(n-1)\, c_n\, t^{n-2} \tag{2.5}$$

When multi-segmented polynomials are implemented, the interval between two successive design points is considered as an individual segment. The continuity between these segments up to the second derivative is generally required for dynamic smoothness. The polynomials are solved for each successive segment. Final conditions of one segment give the initial conditions of the next one.

A division of a motion cycle into segments is shown in Figure 2.1. The suffix i and f represents the starting and end points of each segment respectively.

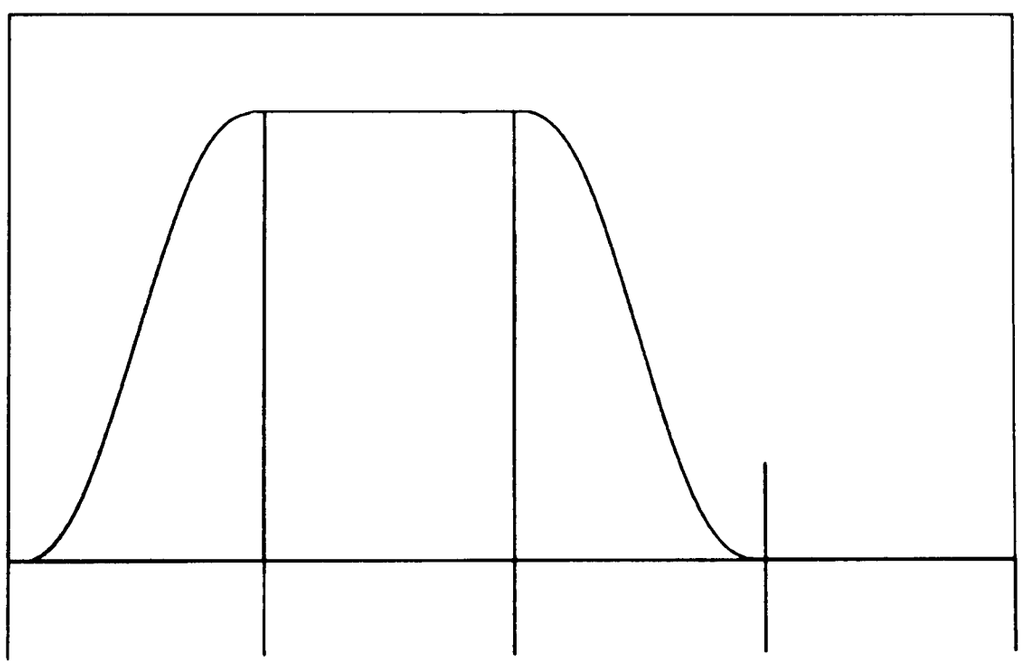

segment1	segment2	segment3	segment4	segment5
x_{1i} , x_{1f}	$x_{2i}=x_{1f}$, x_{2f}	$x_{3i}=x_{2f}$, x_{3f}	$x_{4i}=x_{3f}$, x_{4f}	$x_{5i}=x_{4f}$, x_{5f}
$\dot{x}_{1i}$, $\dot{x}_{1f}$	$\dot{x}_{2i}=\dot{x}_{1f}$, $\dot{x}_{2f}$	$\dot{x}_{3i}=\dot{x}_{2f}$, $\dot{x}_{3f}$	$\dot{x}_{4i}=\dot{x}_{3f}$, $\dot{x}_{4f}$	$\dot{x}_{5i}=\dot{x}_{4f}$, $\dot{x}_{5f}$
$\ddot{x}_{1i}$, $\ddot{x}_{1f}$	$\ddot{x}_{2i}=\ddot{x}_{1f}$, $\ddot{x}_{2f}$	$\ddot{x}_{3i}=\ddot{x}_{2f}$, $\ddot{x}_{3f}$	$\ddot{x}_{4i}=\ddot{x}_{3f}$, $\ddot{x}_{4f}$	$\ddot{x}_{5i}=\ddot{x}_{4f}$, $\ddot{x}_{5f}$

Figure 2.1. Division of a motion into segments.

In the studied motion examples, the specification of displacement, velocity and acceleration at each end of a single segment results in six boundary conditions. It thus requires the evaluation of six constant coefficients of a polynomial, the lowest order of which is of the form;

$$x(t)=c_0+ c_1t + c_2t^2 + c_3t^3 + c_4t^4 + c_5t^5 \tag{2.6}$$

$$\dot{x}(t)=c_1 + 2c_2t + 3c_3t^2 + 4c_4t^3 + 5c_5t^4 \tag{2.7}$$

$$\ddot{x}(t)=2c_2+ 6c_3t + 12c_4t^2 + 20c_5t^3 \tag{2.8}$$

The above equations from (2.6) to (2.8) can be assembled into a matrix form which involves the given boundary conditions separately. In a common representation, the unknown coefficients are c_i and the given input values x_i, $\dot{x}_i$, $\ddot{x}_i$ are the set of imposed boundary conditions at the corresponding time values of t_i. Each one of x_i, $\dot{x}_i$ to $\ddot{x}_i$ represent a simple condition for the required displacement, velocity and acceleration. Six boundary conditions yield a system of equations that can be assembled in 6x6 matrix form of equation (2.9) between any known time instants, like t_1 and t_2.

$$\begin{bmatrix} x_1 \\ \dot{x}_1 \\ \ddot{x}_1 \\ x_2 \\ \dot{x}_2 \\ \ddot{x}_2 \end{bmatrix} = \begin{bmatrix} 1 & t_1 & t_1^2 & t_1^3 & t_1^4 & t_1^5 \\ 0 & 1 & 2t_1 & 3t_1^2 & 4t_1^3 & 5t_1^4 \\ 0 & 0 & 2 & 6t_1 & 12t_1^2 & 20t_1^3 \\ 1 & t_2 & t_2^2 & t_2^3 & t_2^4 & t_2^5 \\ 0 & 1 & 2t_2 & 3t_2^2 & 4t_2^3 & 5t_2^4 \\ 0 & 0 & 2 & 6t_2 & 12t_2^2 & 20t_2^3 \end{bmatrix} \begin{bmatrix} c_0 \\ c_1 \\ c_2 \\ c_3 \\ c_4 \\ c_5 \end{bmatrix}$$

$$X \qquad\qquad A \qquad\qquad C \tag{2.9}$$

This can be written concisely in matrix form as:

$$\underline{X} = A\ \underline{C} \tag{2.10}$$

where A is the matrix containing the time instants, X is the vector containing the imposed boundary conditions and C is the vector including the unknown polynomial coefficients. The multiplication of this equation by the inverse of A gives the unknown coefficients C or

$$\underline{C} = A^{-1}\ \underline{X} \tag{2.11}$$

For a simplified motion and initial condition specification for zero time, the number of

coefficient is halfed as the others disappear on differentiation. If x_1, $\dot{x}_1$, $\ddot{x}_1$ and x_2, $\dot{x}_2$, $\ddot{x}_2$ are set as initial and final conditions for each segment, its matrix form is found as:

$$\begin{bmatrix} x_1 \\ \dot{x}_1 \\ \ddot{x}_1 \\ x_2 \\ \dot{x}_2 \\ \ddot{x}_2 \end{bmatrix} = \begin{bmatrix} 1 & 1 & 0 & 0 & 0 & 0 \\ 0 & 1 & 0 & 0 & 0 & 0 \\ 0 & 0 & 2 & 0 & 0 & 0 \\ 1 & t & t^2 & t^3 & t^4 & t^5 \\ 0 & 1 & 2t & 3t^2 & 4t^3 & 5t^4 \\ 0 & 0 & 2 & 6t & 12t^2 & 20t^3 \end{bmatrix} \begin{bmatrix} c_0 \\ c_1 \\ c_2 \\ c_3 \\ c_4 \\ c_5 \end{bmatrix} \tag{2.12}$$

Here, time instants appear as t instead of Δt. The inversion of the above C matrix gives the coefficients as:

$$c_0 = x_1$$

$$c_1 = \dot{x}_1$$

$$c_2 = \frac{\ddot{x}_1}{2}$$

$$c_3 = \frac{[20\ (x_2-x_1)-(12\dot{x}_1+8\dot{x}_2)t+(\ddot{x}_2-3\ddot{x}_1)t^2]}{2t^3}$$

$$c_4 = \frac{[30\ (x_1-x_2)+(16\dot{x}_1+14\dot{x}_2)t+(3\ddot{x}_1-2\ddot{x}_2)t^2]}{2t^4}$$

$$c_5 = \frac{[12\ (x_2-x_1)-6(\dot{x}_1+\dot{x}_2)t+(\ddot{x}_2-\ddot{x}_1)t^2]}{2t^5} \tag{2.13}$$

2.3. The Example Motions

This section considers three motions having different characteristics. These motions are specifically chosen to evaluate the applicability of the hybrid arrangement. They are given in the order of Rise-Return (R-R), Rise-Dwell-Return (R-D-R) and Rise-Return-Dwell (R-R-D) which involve a different number of segments for each one.

In order to carry all calculations on the segmented polynomial laws, a motion generation program which was in pascal was prepared.

In this program, the definition of motion starts with the specification of overall motion parameters such as maximum stroke, duration of motion for ech segment, control cycle time and the number of segments in the motion. After specifying these, the segment constraints or boundary conditions at various points are required one by one. Each one of the coefficients given in the equation (2.13) are then evaluated. They are substituted into each segment law to obtain the motion.

In each run of the program, the boundary conditions can be edited to alter the profile in each segment. What is required is to solve polynomials for each segment to get a smooth transition from one segment to the next. The observation during different motion trials is that, any small change in displacement condition results in large alterations in velocity and acceleration. So the velocity and acceleration have to be changed manually. This may provide difficulty in the optimum selection of the boundary conditions for the required motion.

2.3.1. Rise-Return Motion (R-R)

In this motion, the imposed boundary conditions include the displacement, velocity and acceleration resulting in the setting of six constraints for each segment.

Figure 2.2 shows the design motion of a slider in a slider-crank mechanism as a full line. This is to result from modulation of the crank speed. The dotted line represents the slider motion for a constant speed driven crank. The boundary conditions for this motion are given in for each segment separately in Table 2.1.

The example motion is divided into 4 segments. The stroke, already defined by the mechanism geometry, is equal to 0.12 m. The constant speed motor is considered to be running at 1500 rpm, at its rated maximum speed. After introducing the belt reduction and differential gear-unit, the crank finally rotates around 200 rpm.

In the first segment, the motion starts with zero displacement and velocity but with assigned slider acceleration. The slider motion is given a quick rise in the forward stroke. During the return stroke, the slider reaches a specific velocity at the end of the second segment. The third segment is required to have a constant velocity for about 50 ms. The mechanism then returns to its original position at the end of the fourth segment. The entire motion is desired to be continuous up to acceleration throughout the cycle. Compared with the constant speed driven slider output from Figure 2.2, here continuous modulations are required to provide quicker forward and slower return stroke. The motion cycle is desired to be completed in 300 ms.

Figure 2.3 shows the designed slider displacement, velocity and acceleration curves.

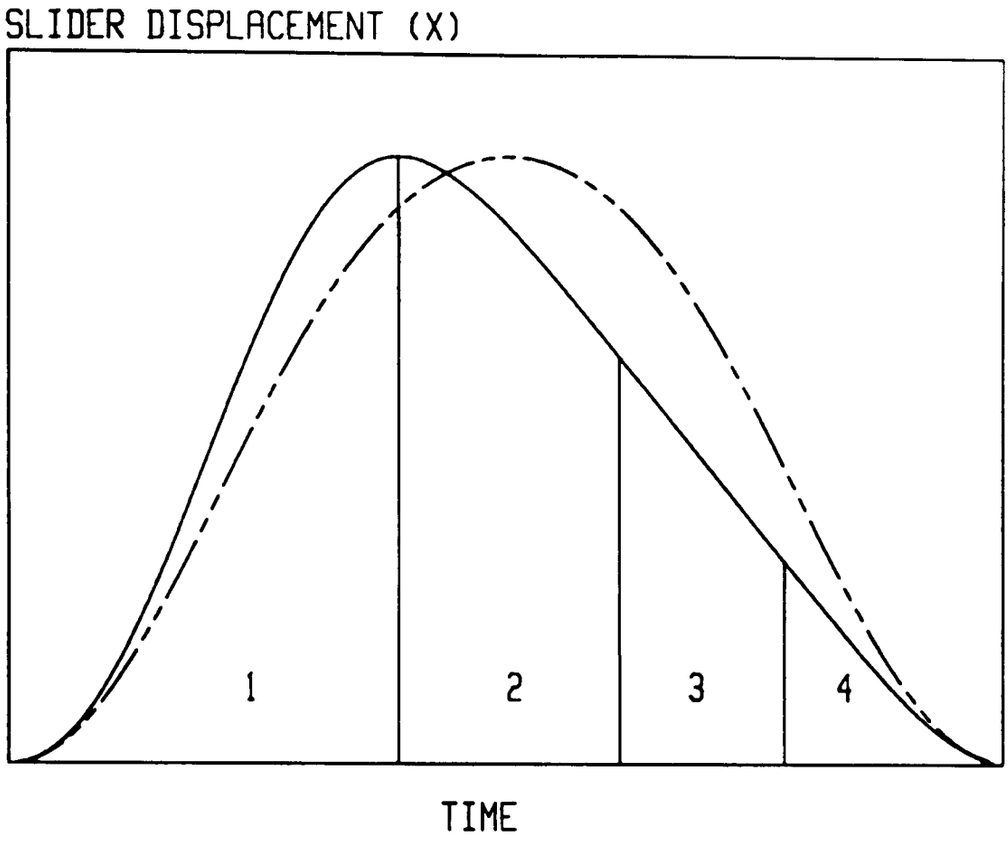

Figure 2.2. Modulated slider motion (R-R).

Table 2.1. Boundary Conditions for R-R Motion		
Time	Boundary Condition	
t_0	x_0, $\dot{x}_0$, $\ddot{x}_0$	x_0= 0.00 m $\dot{x}_0$= 0.00 m/s $\ddot{x}_0$= 34.20 m/s.s
t_1	x_1, $\dot{x}_1$, $\ddot{x}_1$	x_1= 0.12 m $\dot{x}_1$= 0.00 m/s $\ddot{x}_1$= -35.00 m/s.s
t_2	x_2, $\dot{x}_2$, $\ddot{x}_2$	x_2= 0.08 m $\dot{x}_2$= -0.80 m/s $\ddot{x}_2$= 0.00 m/s.s
t_3	x_3, $\dot{x}_3$, $\ddot{x}_3$	x_3= 0.040 m $\dot{x}_3$= -0.80 m/s $\ddot{x}_3$= 0.00 m/s.s
t_4	x_4, $\dot{x}_4$, $\ddot{x}_4$	x_4= 0.00 m $\dot{x}_4$= 0.00 m/s $\ddot{x}_4$= 34.20 m/s.s

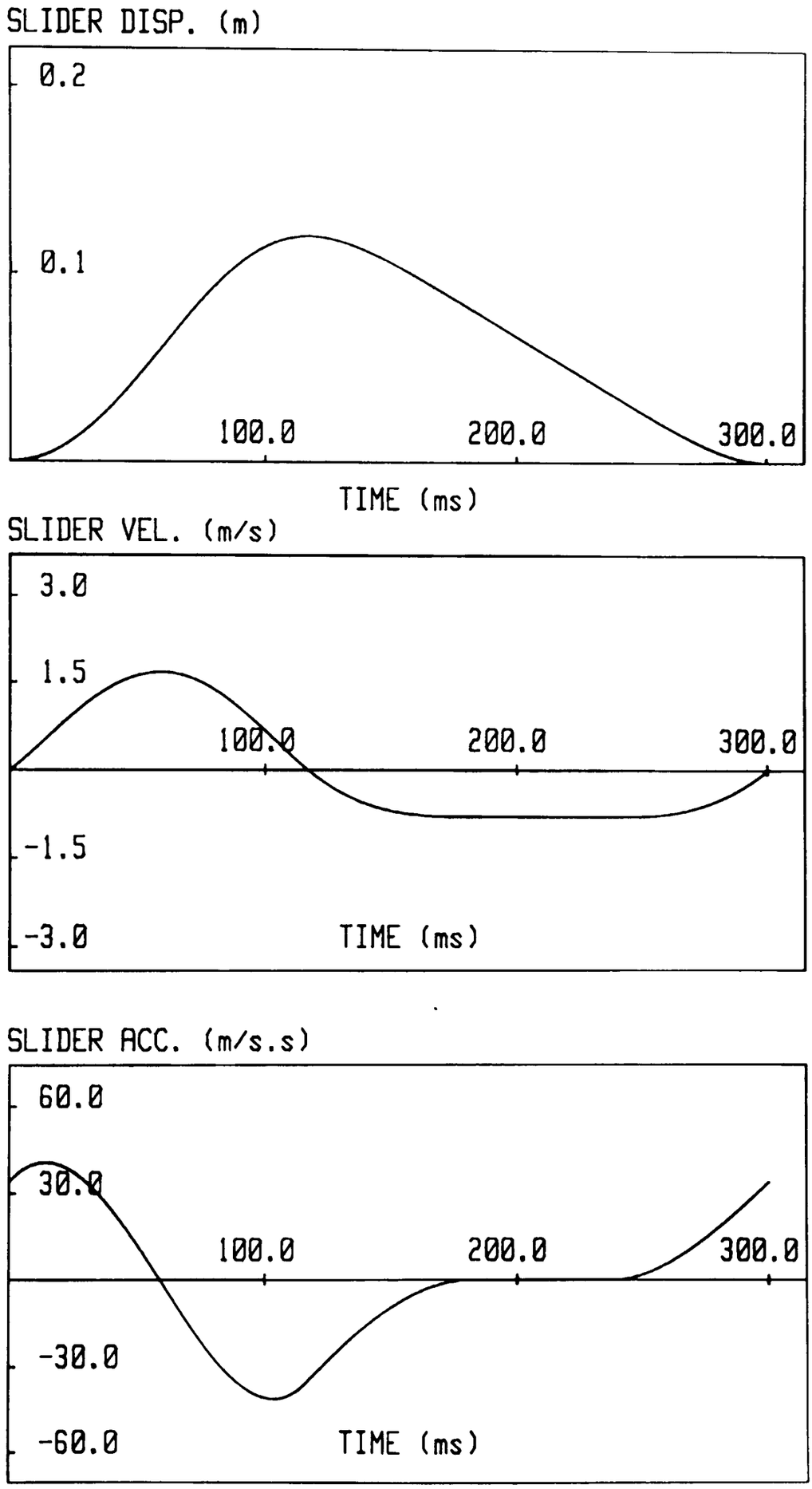

Figure 2.3. The Designed Slider Motion (R-R).

In order to get the above final form of the curves in this example, the velocity and acceleration are changed manually with guesses. Quite a wide range of curves were observed. At the end, one has been chosen. These motion points for the slider displacement, velocity and acceleration are then stored for further use in the necessary inverse solution of the displacement equations for modulated crank input.

One potential application of this type of continuous motion modulation is considered in a machine for cutting variable lengths of material, for example, paper, foil. This application demands an output which is continuously rotating but with cyclically fluctuating velocity. If desired, the flexibility for the cutting action to suit different cut lengths of material can simply be achieved.

2.3.2. Rise-Dwell-Return Motion (R-D-R)

A three segment, R-D-R motion has been considered. The motion is characterized by six constraints for each segments and 5th degree polynomials are used.

The modulated slider motion can be seen in Figure 2.4 as a full line with the constant speed driven slider motion as a dotted line. The assigned displacements, velocities and accelerations for boundary conditions are displayed in Table 2.2.

The constant speed motor rotates at 750 rpm for this motion. As a result of belt reduction g, which is 1/1.875, and the differential gear-unit reduction, $(1-\rho)$, which is equal to 0.260, the crank rotates about 100 rpm.

In the first segment, the boundary conditions are set to zero except for the assigned slider acceleration. This acceleration is made to be equal 100 rpm rotating crank driven slider for the same motion starting conditions with the constant speed motor driven crank. The motion starts with a quick forward stroke to reach its top dead centre. In the second segment, a 50-ms dwell is introduced to meet zero velocity and acceleration for this part of the motion. So the crank is due to stop at top dead centre as a result of imposed boundary conditions. The motion cycle is then completed with a faster return in the third segment and the slider finally returns to its starting point. The motion cycle lasts for 600 ms. The time for the rise and return periods is 275 ms that is an equal rise and return periods.

The designed slider displacement, velocity and acceleration curves are given in Figure 2.5. These slider curves are arrived at after many manual trials, with different guesses at each time.

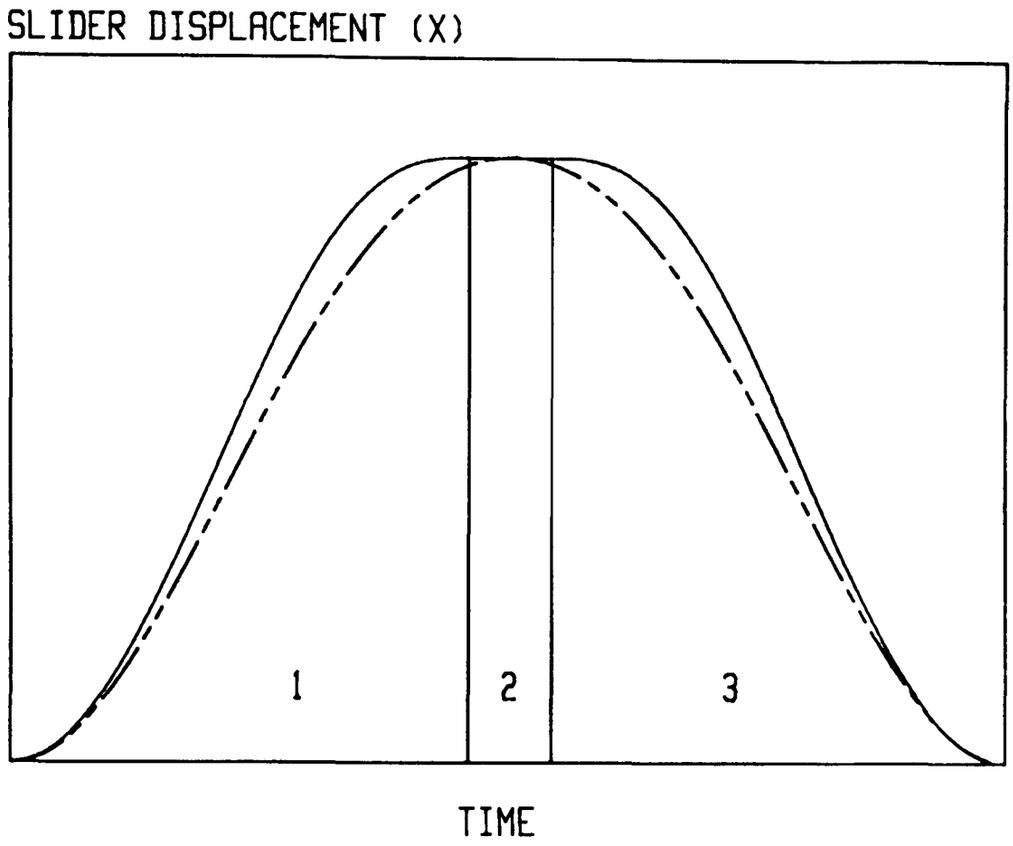

Figure 2.4. Modulated slider motion (R-D-R).

Table 2.2. Boundary Conditions for R-D-R Motion		
Time	Boundary Condition	
t_0	x_0, $\dot{x}_0$, $\ddot{x}_0$	x_0= 0.00 m $\dot{x}_0$= 0.00 m/s $\ddot{x}_0$= 8.56 m/s.s
t_1	x_1, $\dot{x}_1$, $\ddot{x}_1$	x_1= 0.12 m $\dot{x}_1$= 0.00 m/s $\ddot{x}_1$= 0.00 m/s.s
t_2	x_2, $\dot{x}_2$, $\ddot{x}_2$	x_2= 0.12 m $\dot{x}_2$= 0.00 m/s $\ddot{x}_2$= 0.00 m/s.s
t_3	x_3, $\dot{x}_3$, $\ddot{x}_3$	x_3= 0.00 m $\dot{x}_3$= 0.00 m/s $\ddot{x}_3$= 8.56 m/s.s

Basically, for this motion, what is actually required from the servo-motor is something more than just small modulations. In this application, both motors run at different speeds but the crank rotates with resultant zero angular velocity through the action of the differential gear-unit. With the servo-motor used, this raised a question about the capacity of the motor to

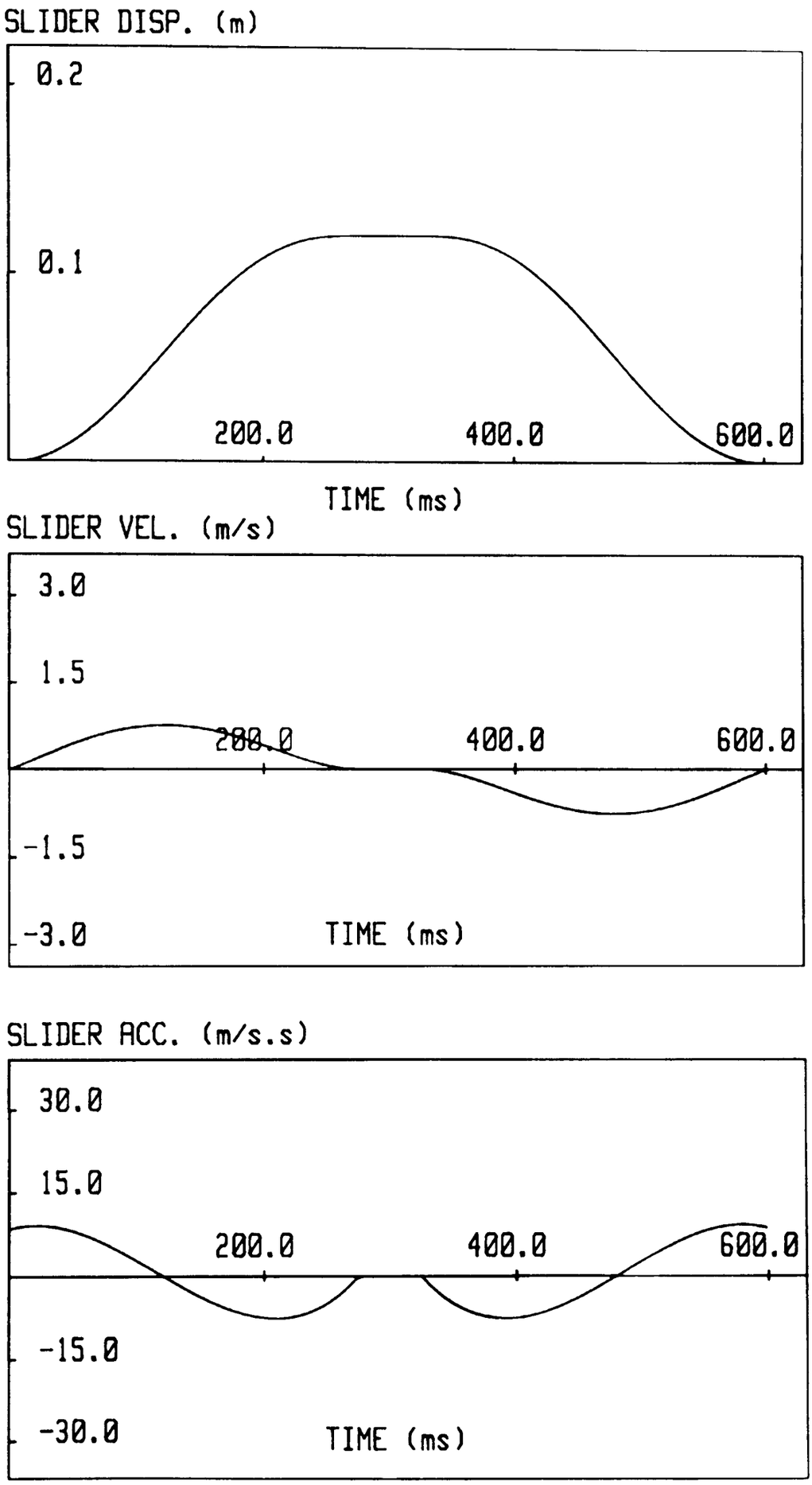

Figure 2.5. The Designed Slider Motion (R-D-R).

achive step change associated with the required accelerations just preceding and following a dwell. Even though an attempt has been made to match the motor and load inertia, to optimize performance with a speed of 1500 rpm the constant speed motor, the acceleration torque requirements of the servo-motor were too high. The dwell implementation was not possible. However, when the speed is reduced to its half, the benefits of motor and load matching are realized. That is why, the dc constant speed motor is operated at 750 rpm.

The potential application of this motion is considered for soap bar embossing. The operation requires near dwell conditions at the compression end of the stroke. This motion could describe an appropriate example by using a slider-crank configuration. Another potential application of dwell motion can be considered in assembly lines where the coordination of one machine element is essential with the other machine element. Sometimes this requires the motion to be designed to perform longer dwells within the cycle. After accepting the potential use of hybrid arrangements, it is up to the designer to deal with different motion characteristics whether they include a dwell or not.

2.3.3. Rise-Return-Dwell Motion (R-R-D)

Figure 2.6 and Table 2.3 show the slider motion and boundary conditions for the motion herein referred to as R-R-D.

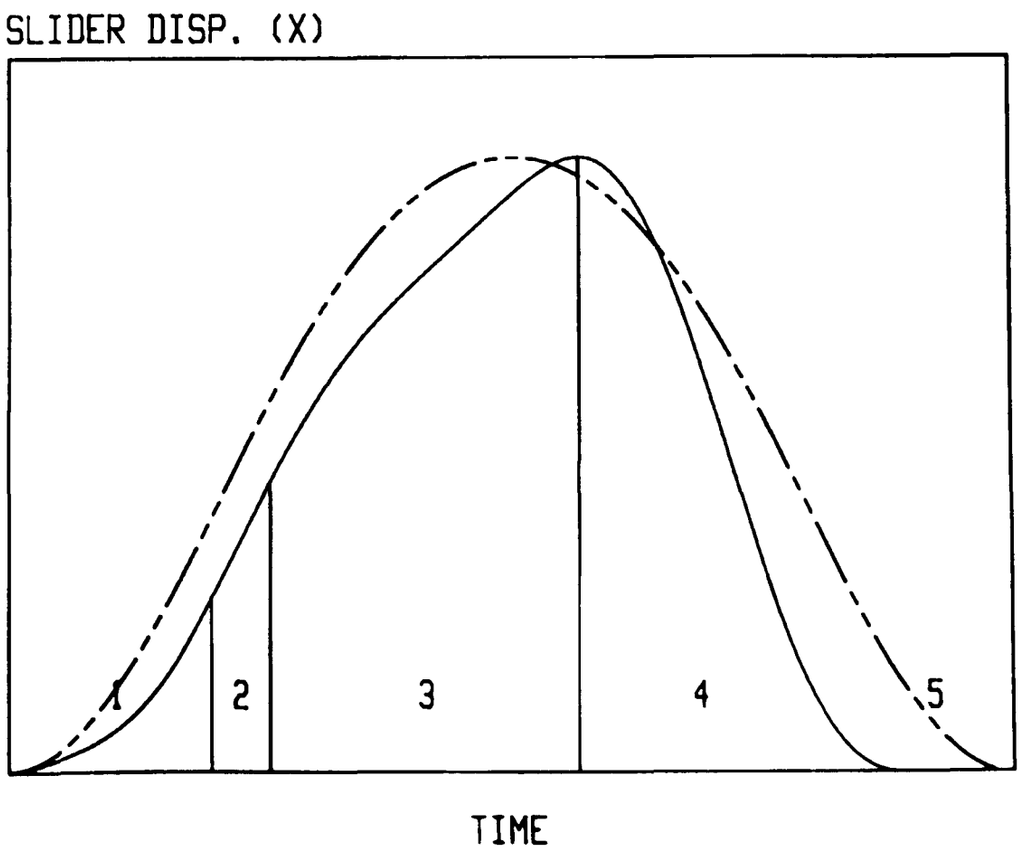

Figure 2.6. Modulated slider motion (R-R-D).

Table 2.3. Boundary Conditions for R-R-D Motion		
Time	Boundary Condition	
t_0	x_0, $\dot{x}_0$, $\ddot{x}_0$	x_0= 0.00 m $\dot{x}_0$= 0.00 m/s $\ddot{x}_0$= 8.56 m/s.s
t_1	x_1, $\dot{x}_1$, $\ddot{x}_1$	x_1= 0.034 m $\dot{x}_1$=0.64 m/s $\ddot{x}_1$=0.00 m/s.s
t_2	x_2, $\dot{x}_2$, $\ddot{x}_2$	x_2= 0.047 m $\dot{x}_2$= 0.64 m/s $\ddot{x}_2$= 0.00 m/s.s
t_3	x_3, $\dot{x}_3$, $\ddot{x}_3$	x_3= 0.12 m $\dot{x}_3$= 0.00 m/s $\ddot{x}_3$= -14.0 m/s.s
t_4	x_4, $\dot{x}_4$, $\ddot{x}_4$	x_4= 0.00 m $\dot{x}_4$= 0.00 m/s $\ddot{x}_4$= 0.00 m/s.s
t_5	x_5, $\dot{x}_5$, $\ddot{x}_5$	x_5= 0.00 m $\dot{x}_5$= 0.00 m/s $\ddot{x}_5$= 0.00 m/s.s

In that figure, the full line represents the designed slider motion and dotted line indicates the slider output for a constant speed driven crank. The cycle of motion is divided into five segments. All operating conditions for this dwell application are the same as the previous motion, i.e. the crankshaft rotates at 100 rpm.

In the first segment the motion begins from steady conditions of zero position, zero velocity and a finite acceleration. At the end of this segment the position and velocity reach particular values while the acceleration becomes zero. The second segment has a constant velocity which would enable the control of a impact velocity as the slider arrives at the object to be pushed. This continues for about 20 ms. The pusher reaches its top dead centre at the end of third segment. The return stroke is then completed with matching zero velocity and acceleration requirements in the forth segment. The fifth and final segment is a dwell for 60 ms and the overall motion cycle is performed in 600 ms.

The same motion generation program has again been used to find coefficients for this five segmented motion. Before the decision is made, the software has been run many times with different velocity and acceleration constraints. The final slider displacement, velocity and acceleration curves are given in Figure 2.7.

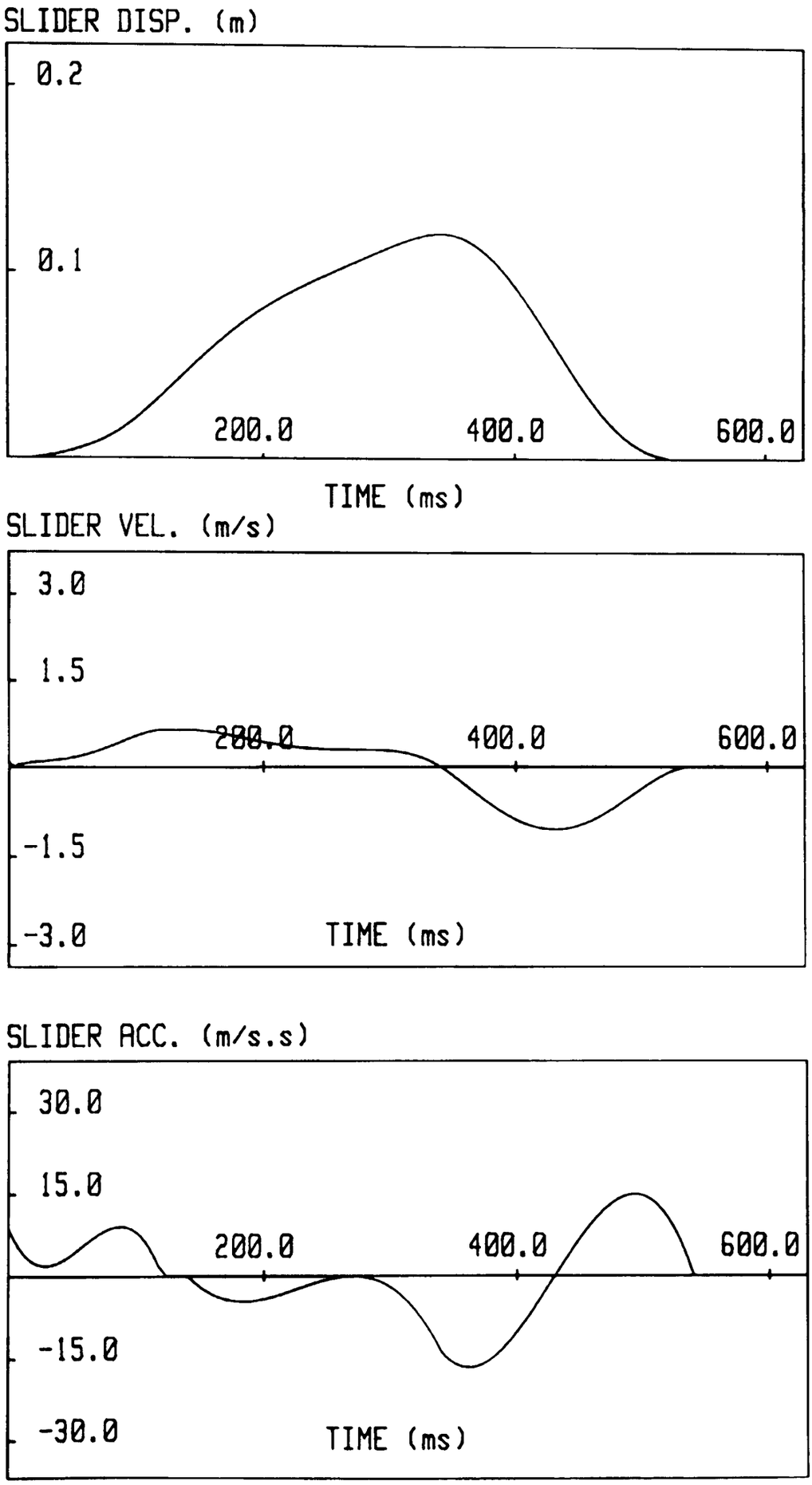

Figure 2.7. The Designed Slider Motion (R-R-D).

2.4. Conclusion

This chapter has presented a study on motion design for the hybrid arrangement. The motion design has been considered with polynomial laws and their solution method. A simple motion generation program was prepared to satisfy our specific requirements for the use of 5th degree polynomials. While designing the slider motions, some potential applications were focused on for the hybrid machines such as a high-speed programmable press and a high performance cut-to-length machine system requiring different modulations.

However, further work can be carried on the study of motion design for the application of different motion laws other than polynomials, making comparisons of the advantages that they might offer. For instance, in spite of many advantages, polynomials can show a peculiar behaviour, described as *meandering* between motion end points.

CHAPTER 3
KINEMATIC AND DYNAMIC ISSUES

3.1. Introduction

Linkage mechanisms are used to control position and in some cases velocity and acceleration of system components as a function of the given input. The higher derivatives of their motion are prescribed by defining the relation between the position and time, or relative position of some of their bodies. The design and understanding of linkage mechanisms is conveniently divided into two levels of analysis, namely *kinematic and dynamic.*

The kinematic analysis of a mechanism is the study of the geometry of its motion quite apart from the forces. It is concerned with the interrelation of displacement, velocity, acceleration and time. Knowing the physical relation between any two kinematic quantities and time is adequate to obtain a complete kinematic understanding of motion. To achieve this, the position, velocity and acceleration of members of a mechanism are typically determined by using linear algebraic equations specially derived for the mechanism of interest.

By contrast *the dynamic analysis* involves determination of the time history of position, velocity and acceleration of the system resulting from the action of external and internal forces. The equations of dynamics are differential or differential-algebraic equations. Lagrange's equations are commonly used as a basis for formulation.

In this chapter, initially, kinematic analysis is carried out for a slider-crank mechanism. This mechanism consists of a crank, a connecting rod and a slider moving inside linear roller bearings on a slideway in the set-up. Particular problems are seen in solving kinematic relationships when the motion of the slider is defined first. This issue is referred to here as the *inverse kinematic* problem. It is studied for a sliding output driven by a non-uniformly rotating crank of the hybrid arrangement. The equation of motion for a slider-crank is derived. The driving torques required to impose the three designed motions are calculated by using the equations of motion and the inverse crank motion points. The crank motion is then

separated into its components which are the inputs from the constant speed motor and the servo-motor.

3.2. Kinematic Analysis of a Slider-Crank Mechanism

Figure 3.1.(a) shows a sketch of a slider-crank mechanism in which link 1 is the frame, link 2 is the crank, link 3 is the connecting rod and link 4 is the slider. The crank angle, θ is defined as a function of time to control the position of the slider relative to the ground.

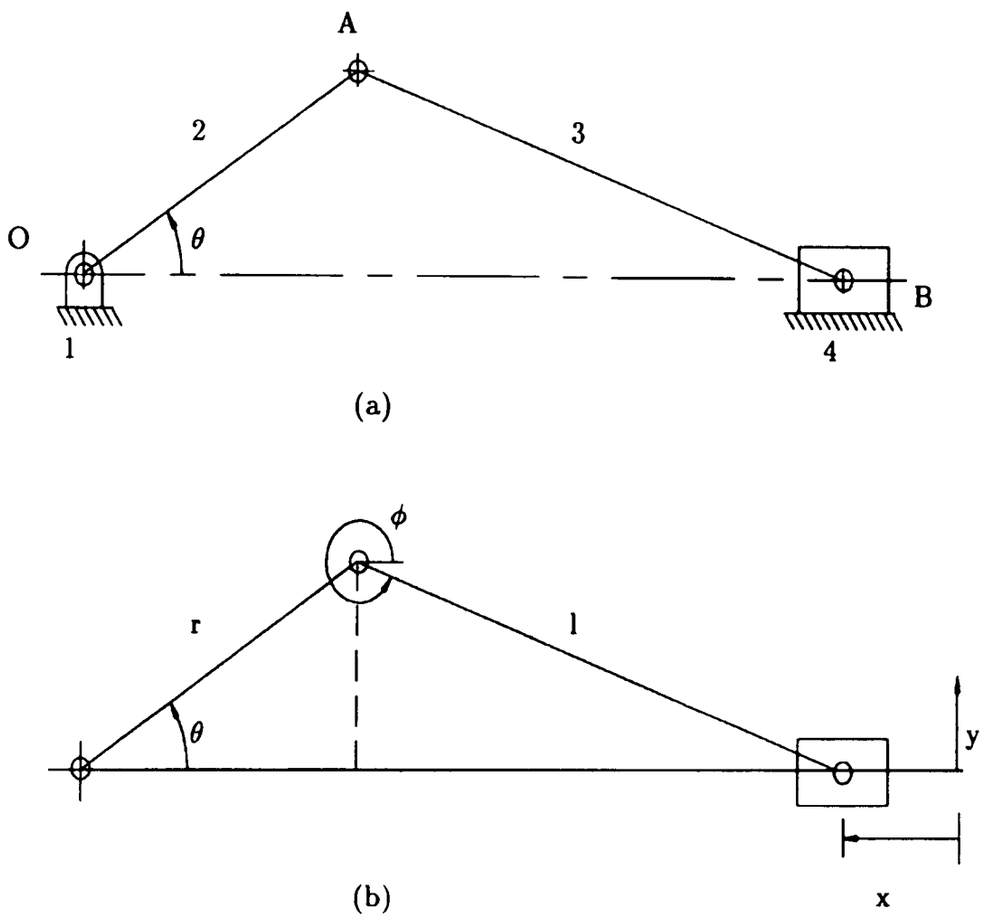

Figure 3.1. Slider-Crank Mechanism.

The constraint equations for the slider displacement, x and the slider offset, y are written in terms of the crank angle, θ and the coupler link angle, ϕ by using Figure 3.1.(b).

$$x = r + l - (r\cos\theta + l\cos\phi) \tag{3.1}$$

$$y = r\sin\theta + l\sin\phi \tag{3.2}$$

where r is the crank radius and l is the connecting rod length.

The basic approach is to write equations that represent the displacement of the driven part as

a function of varying angle of rotation of the driving part like in equation (3.1). The first and second time derivatives of equation (3.1) gives directly the velocity and acceleration equations for the slider respectively as:

$$\dot{x} = r\dot{\theta}\sin\theta + l\dot{\phi}\sin\phi \tag{3.3}$$

$$\ddot{x} = r(\ddot{\theta}\sin\theta + \dot{\theta}^2\cos\theta) + l(\ddot{\phi}\sin\phi + \dot{\phi}^2\cos\phi) \tag{3.4}$$

When the mechanism is taken as an in-line slider-crank, the offset for y is zero in Figure 3.1. So by equating y to zero in equation (3.2), a relationship between the crank angle, θ and the coupler link angle, ϕ is obtained.

3.2.1. Inverse Kinematics

When the constraints are set for the slider output or when the motion of slider is specially modified for a purpose, an inverse solution is required for the crank motion. This is the form of analysis where the known output motion characteristics can be used to determine input displacement, velocity and acceleration of the system from the kinematic equations.

In the present study, the inverse solutions are essentially required for the input crank displacement θ, the angular velocity $\dot{\theta}$, and the angular acceleration $\ddot{\theta}$. This is achieved by taking the squares of equations (3.1) and (3.2) first and summing them together, eliminating ϕ from the equations. The crank displacement is found as the following.

$$\cos\theta = \frac{l^2\text{-}r^2\text{-}(x\text{-}r\text{-}l)^2}{2r(x\text{-}r\text{-}l)} \tag{3.5}$$

where includes all known parameters for the mechanism.

To find the crank velocity and acceleration, the analytical solution is carried out by taking derivatives of equation (3.5). However, it is seen that singularity conditions present difficulty at limit positions of the mechanism, those corresponding to zero values of the crank angle. The inverse solution cannot be held properly. For this reason equation (3.3) and time derivatives of equation (3.2) are considered together, they are written in the following matrix form.

$$\begin{bmatrix} \dot{x} \\ \dot{y} \end{bmatrix} = \begin{bmatrix} r\sin\theta & l\sin\theta \\ r\cos\phi & l\cos\phi \end{bmatrix} \begin{bmatrix} \dot{\theta} \\ \dot{\phi} \end{bmatrix} \tag{3.6}$$

or rearranging above representation then,

$$\begin{bmatrix} \dot{\theta} \\ \dot{\phi} \end{bmatrix} = \begin{bmatrix} r\sin\theta & l\sin\theta \\ r\cos\phi & l\cos\phi \end{bmatrix}^{-1} \begin{bmatrix} \dot{x} \\ \dot{y} \end{bmatrix} \tag{3.7}$$

W A B

In closed form;

$$\underline{W} = A^{-1}\,\underline{B} \tag{3.8}$$

where W is the angular velocity vector, A is the coefficient matrix and B is the linear velocity vector. The solution lies in the inverse of the A matrix and is given as:

$$\dot{\theta} = \frac{\dot{x}}{r(\sin\theta - \cos\theta\tan\phi)} \tag{3.9}$$

$$\dot{\phi} = \frac{-\cos\theta\dot{x}}{[l\cos\phi(\sin\theta - \cos\theta\tan\phi)]} \tag{3.10}$$

where the values of $\dot{x}$ are available from the motion generation program which was used in the motion design, chapter 2, and $\dot{y}$ is zero.

In order to start the inverse solution program, the initial angular velocity of the crank is given as a finite value. This is to overcome numerical problems with the zero initial value of the denominator. The above approach gives the answer for the crank velocities. However, when the crank accelerations are required it still suffers from the singularity. Here the numerical differentiation has been applied for the crank accelerations.

Generally speaking obtaining a reasonable estimate of the derivative of a function at a given point is numerically a much more difficult problem than that of estimating its integral. There is a tendency to inaccuracy in the process of numerical differentiation of a function. In principle, we know that more accurate approximation of the acceleration function can be obtained by taking successively smaller values of time intervals Δt. The usual assumption is that the smaller the value of Δt the more accurate the approximation to the function. On the contrary, when Δt gets smaller some difficulties could arise. The approximation can be unreliable because of the rounding errors that occur during the evaluation. During the application of the numerical differentiation for the crank accelerations, these issues are always kept in mind.

Initially the crank motion points are found for the R-R motion. They are given in Figure 3.2 where they show the displacement, velocity and acceleration. These points are required to perform the characteristic slider motion shown in chapter 2, Figure 2.3. The motion cycle is completed in 300 ms. Δ t, the time interval used for the numerical differentiation is 1.66666 ms.

The solution points of the crank motion for the R-D-R and R-R-D motions are shown in Figure 3.3 and Figure 3.4.

Figure 3.3 and Figure 3.4 are the results of the inverse solutions applied to the R-D-R and R-R-D motions related to the slider outputs shown in chapter 2, Figure 2.5 and Figure 2.7. These motions are performed in 600 ms, used Δ t for the approximation of the acceleration function is 3.33333 ms.

When the numerical differentiation algorithm is performed, difference formulas, such as forward, backward, central and five point differences, are used to approximate the required derivative of the function. These difference formulas are included in a procedure in the program. When required, different difference formula can be called in each run of the program. The final step is up to the user to decide which method approximates the crank acceleration with better accuracy.

3.3. Dynamic Analysis of a Slider-Crank Mechanism

Lagrange's method of formulation is a common approach for finding the equations of motion for all dynamic systems. The method leads to the system equations of motion by using expressions for the system-energy function and its partial and time derivatives with respect to the defined coordinates.

3.3.1. Generalized Coordinates

For a system with n degrees of freedom, a set of n independent coordinates is required to specify the configuration of the system. These coordinates are designated by

$$q_1, q_2, q_3, \ldots\ldots\ldots, q_n$$

called *generalized coordinates*. A given coordinate q_i may be either a distance or an angle. The simultaneous positions of all points in the system can be determined by means of a set of generalized coordinates.

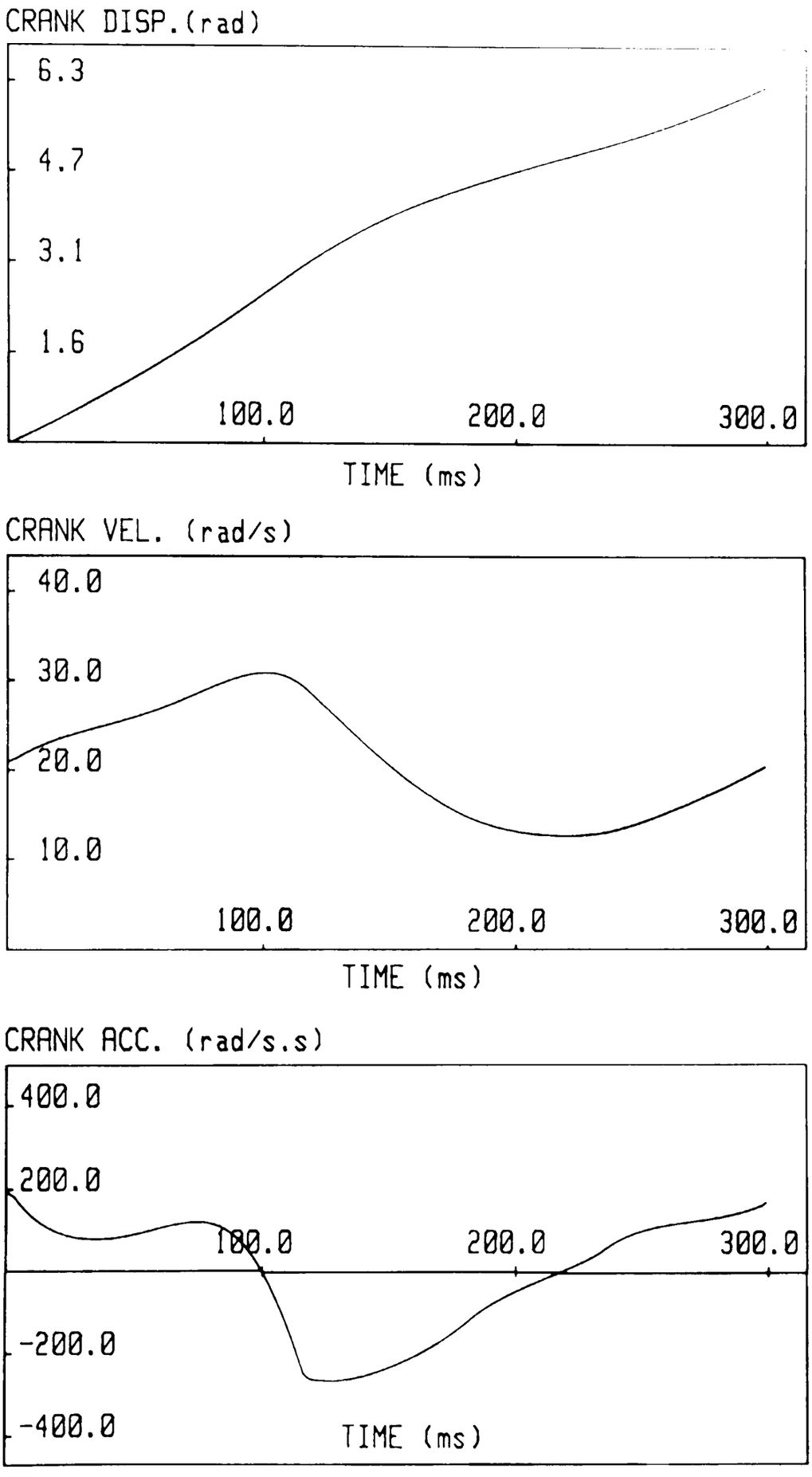

Figure 3.2. The inverse crank points for the R-R motion.

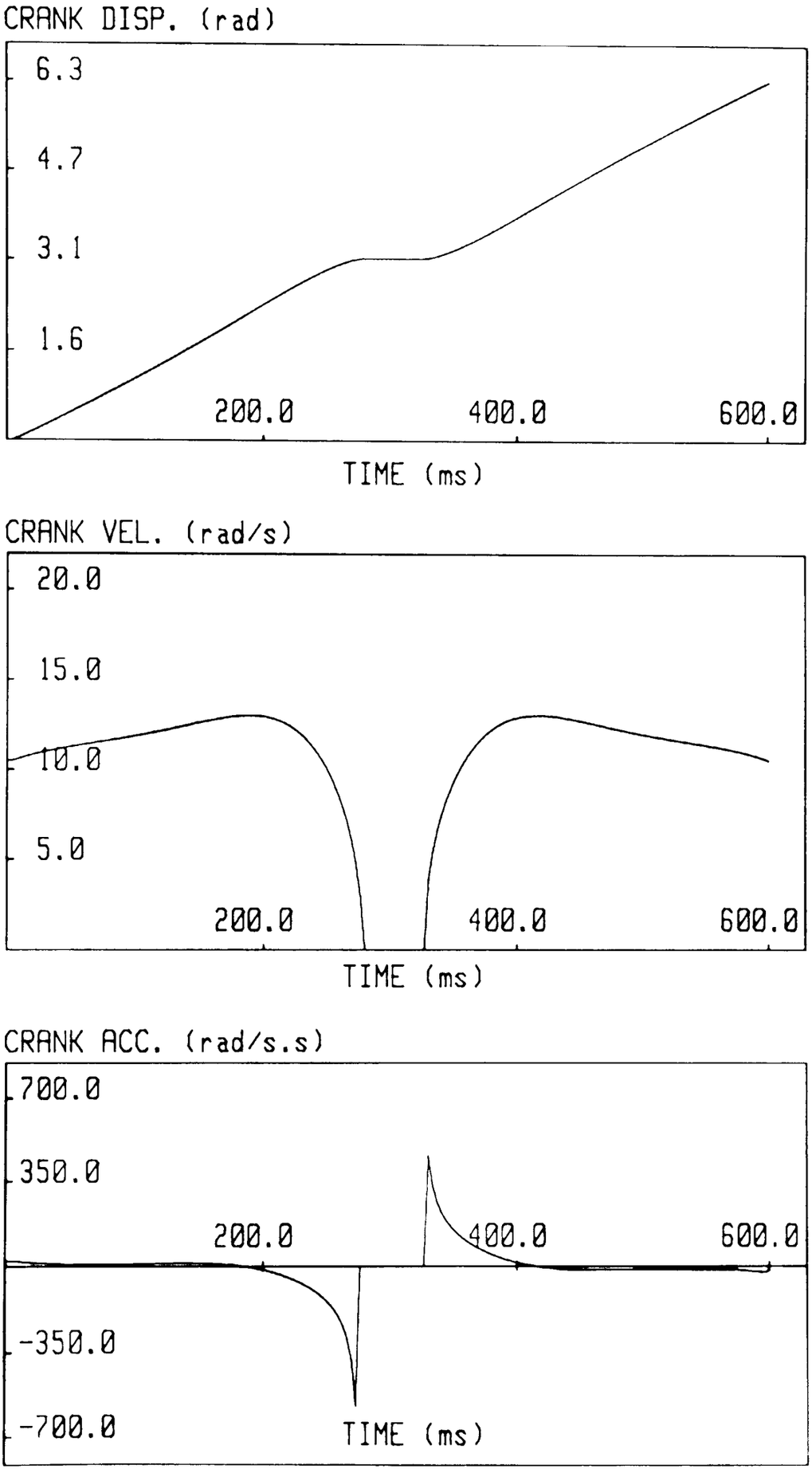

Figure 3.3. The inverse crank points for the R-D-R motion.

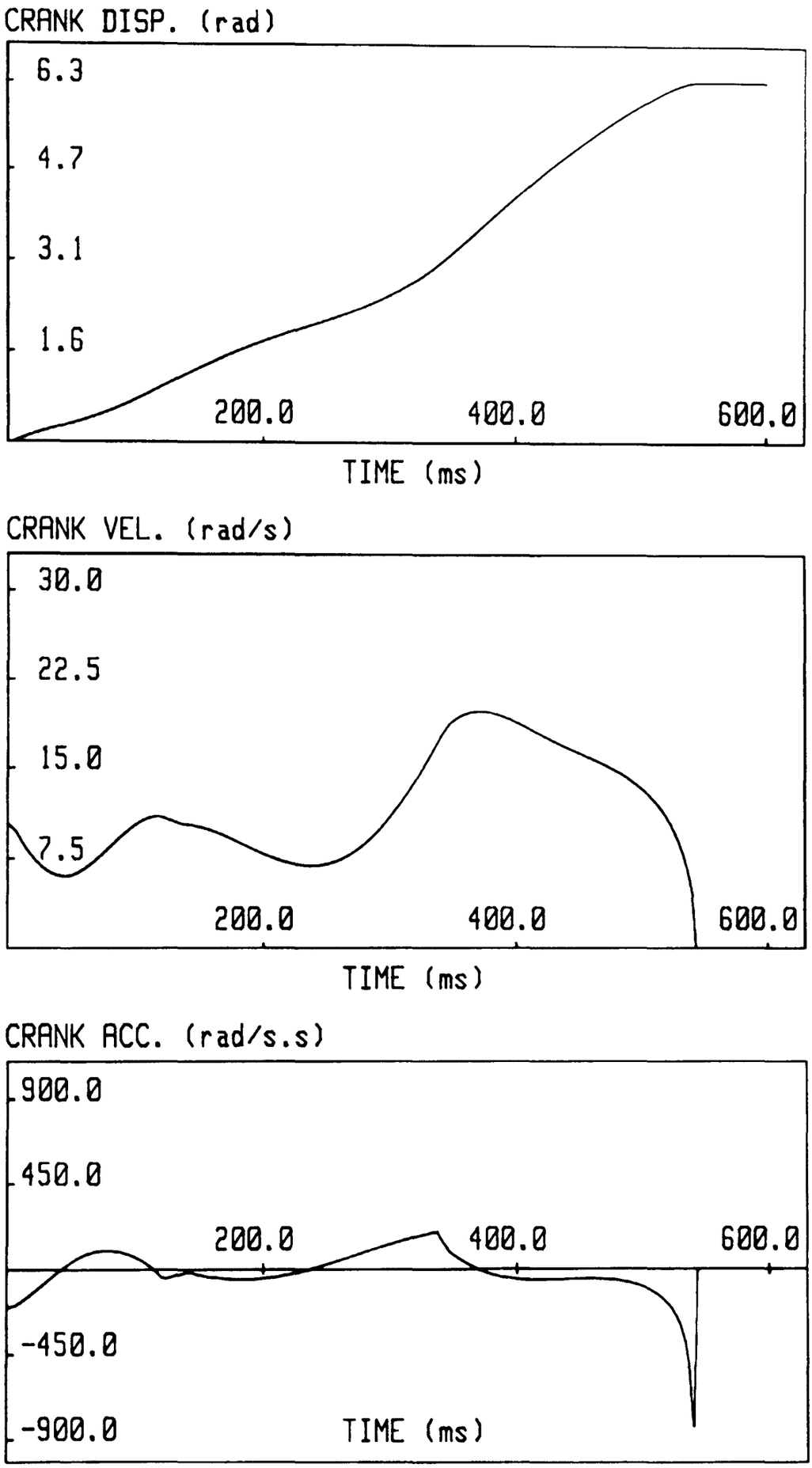

Figure 3.4. The inverse crank points for the R-R-D motion.

A system can also be shown with the *equations of constraints*. If the system is expressed with m coordinates and n degrees of freedom, (m>n) there must be m-n independent constraints to describe the system dynamics, i.e. x_1, x_2, x_3,..,x_m. Introducing any set of coordinates changes the solution methods of the equations of motion, but the dynamics of the system remains the same [3.4].

In the present study, Lagrange's equations of motion for generalized coordinates is applied throughout.

3.3.2. Lagrange's Equations

The differential equations of motion of the system are derived by using Lagrange's equations in the usual form:

$$\frac{d}{dt}\left(\frac{\partial L}{\partial \dot{q}_i}\right) - \frac{\partial L}{\partial q_i} = Q_i \qquad \text{for } i=1,2,\ldots,n \tag{3.11}$$

where L is the Lagrangian, q_i is the ith generalized coordinate, Q_i is the ith generalized force or torque depending upon q_i whether it represents a distance or an angle.

The Lagrangian of the system is defined as;

$$L = T - V$$

where T and V represent the kinetic and potential energy of the system, respectively. The kinetic energy is dependent on the generalized velocities. The potential energy depends explicitly only on the current position, it is independent of the generalized velocities.

Lagrange's equations here yield n equations for the n generalized coordinates. These equations describe the system dynamics depending upon the choice of the generalized coordinate. The choice of the generalized coordinates is free, but care is always taken that they give complete description of the motion of the system.

In addition to the above, there is another issue which classifies systems as *holonomic* and *nonholonomic* for a system of interest. In a system, if the number of generalized coordinates matches the number of degrees of freedom, it describes an *holonomic* system. However, if the number of generalized coordinates exceeds the number of degrees of freedom, it gives a *nonholonomic* system. These systems are generally much more difficult to work with than holonomic ones. For a nonholonomic system, Lagrange's equation of motion must be modified by describing a set of *constrained generalized coordinates* [3.4], [3.5].

3.3.3. Inverse Dynamics for Slider-Crank

The example that follows illustrates the use of Lagrange's equations to obtain the differential equation of motion for a slider-crank mechanism. The equation of motion is used to determine the driving torques that are required to achieve the programmable slider action with non-uniformly driven crank.

For a slider-crank, the number of generalized coordinates matches the number of degrees of freedom for a slider-crank. They describe an *holonomic* system and Lagrange's equations fully define the motion of the system.

The slider-crank model used is shown in Figure 3.5, where
r, l, r_1, l_1 — are the crank radius, the connecting rod length, the mass centres of the crank and the connecting rod,
m_2, m_3, m_4 — are the masses of the crank, the connecting rod and the slider,
J_2, J_3 — are the moment of inertias of the crank with the crankshaft and the connecting rod respectively.

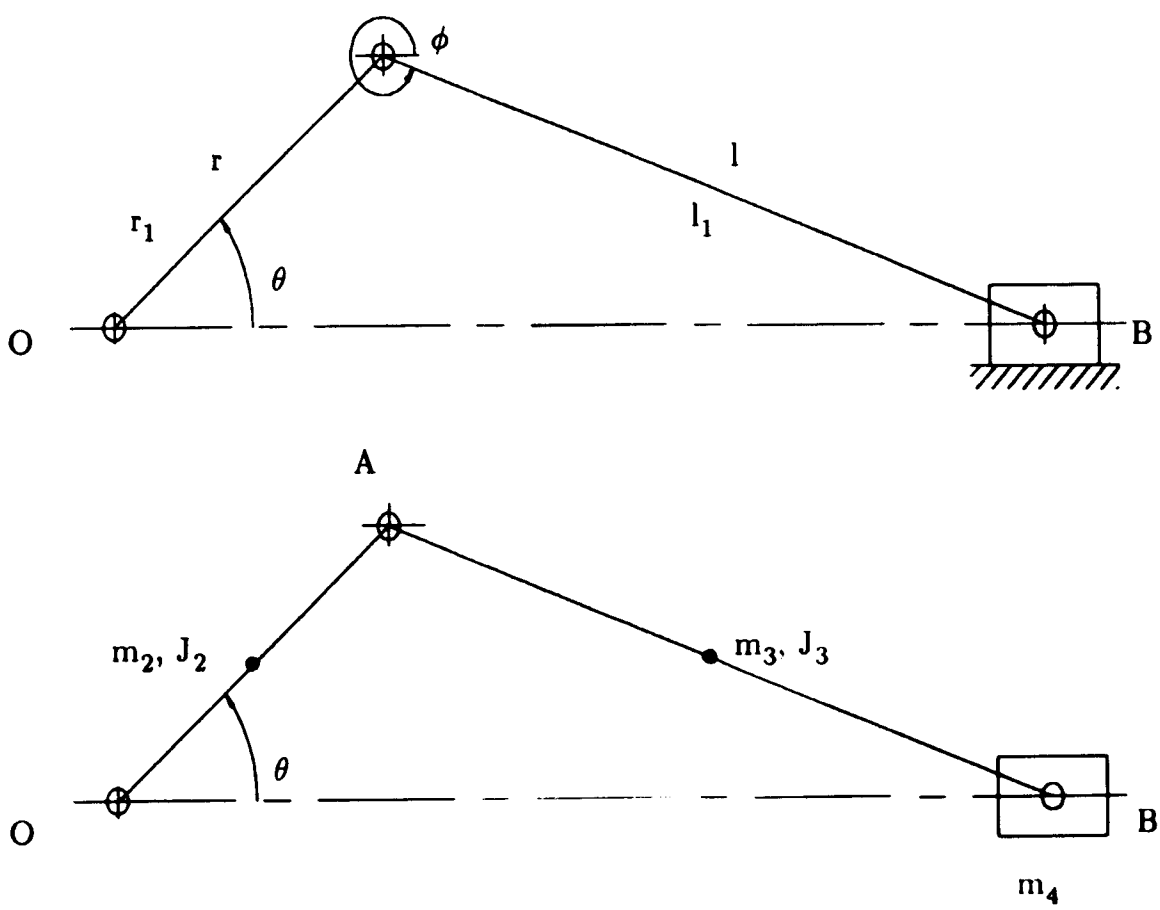

Figure 3.5. A Slider-Crank Model.

The slider-crank mechanism has a single degree of freedom resulting in one generalized coordinate as:

$$q_1 = \theta \tag{3.12}$$

The evaluation of Lagrange's equations for this mechanism is straight forward. The individual energy terms are given in appendix 2. The derivation results in a second order nonlinear differential equation in θ, with assigned masses and inertias. Its simplified form is given as the following.

$$\Big\{(J_2+m_2r_1^2)+(J_3+m_3l_1^2)[r^2\cos^2\theta/l^2-(y-r\sin\theta)^2]+(m_3+m_4)r^2\sin^2\theta+2(m_3l_1+m_4)[r^2\sin\theta\cos\theta$$

$$(y-r\sin\theta)/(l^2-(y-r\sin\theta)^2)^{1/2}]+[m_4r^2\cos^2\theta(y-r\sin\theta)^2/(l^2-(y-r\sin\theta)^2)]\Big\}\ddot{\theta}+\Big\{-(J_3+m_3l_1^2+$$

$$m_4(y-r\sin\theta)^2)\,[r^2\sin\theta\cos\theta/\,(l^2-(y-r\sin\theta)^2)]+(J_3+m_3l_1^2+\,m_4(l^2-(y-r\sin\theta)^2))\,[r^3\cos^3\theta$$

$$(y-r\sin\theta)/(l^2-(y-r\sin\theta)^2)^2]+(m_3+m_4)\,r^2\sin\theta\,\cos\theta+(m_3\,l_1/l+m_4)\,[r^2\cos^2\theta(y-\sin\theta)/(l^2-$$

$$(y-r\sin\theta)^2)^{1/2}]-(m_3l_1/l+m_4)\,[r^2\sin^2\theta(y-r\sin\theta)/(l^2-(y-r\sin\theta)^2\,)^{1/2}]+(\,m_3l_1/l+\,m_4)$$

$$[r^3\sin\theta\cos^2\theta/(l^2-(y-r\sin\theta)^2)^{1/2}]+(m_3l_1/l+m_4)[r^3\sin\theta\cos^2\theta(y-r\sin\theta)^2/(l^2-(y-r\sin\theta)^2)^{3/2}]+$$

$$m_4\,[r^3\cos^3\theta(y-r\sin\theta)^3/(l^2-(y-r\sin\theta)^2)^2]\Big\}\,\dot{\theta}^2=T \tag{3.13}$$

The numerical values for the link lenghts, centre of masses and the moment of inertias used in the evaluation of Lagrange's equations are;

$r = 0.06$ m	$r_1 = 0.02$ m
$l = 0.20$ m	$l_1 = 0.10$ m
$m_2 = 0.31697$ kg	$m_3 = 0.33606$ kg
$m_4 = 1.24123$ kg	
$J_2 = 0.00507$ kg.m.m	$J_3 = 0.00169$ kg.m.m

To calculate the required torques the equation of motion in equation (3.13) is included in a procedure. After finding the crank motion points for each example, to follow the prescribed motions, the required torques are calculated automatically afterwards by using available θ, $\dot{\theta}$ and $\ddot{\theta}$. Thus the driving torques are found for the R-R, R-D-R and R-R-D motions respectively. They are plotted as torque-angular displacement (T-θ) and torque-angular velocity (T-$\dot{\theta}$).

Figure 3.6 shows the torques required on the crank for the R-R motion. Correspondingly, Figure 3.7 and Figure 3.8 represent torques required for the R-D-R and R-R-D motions.

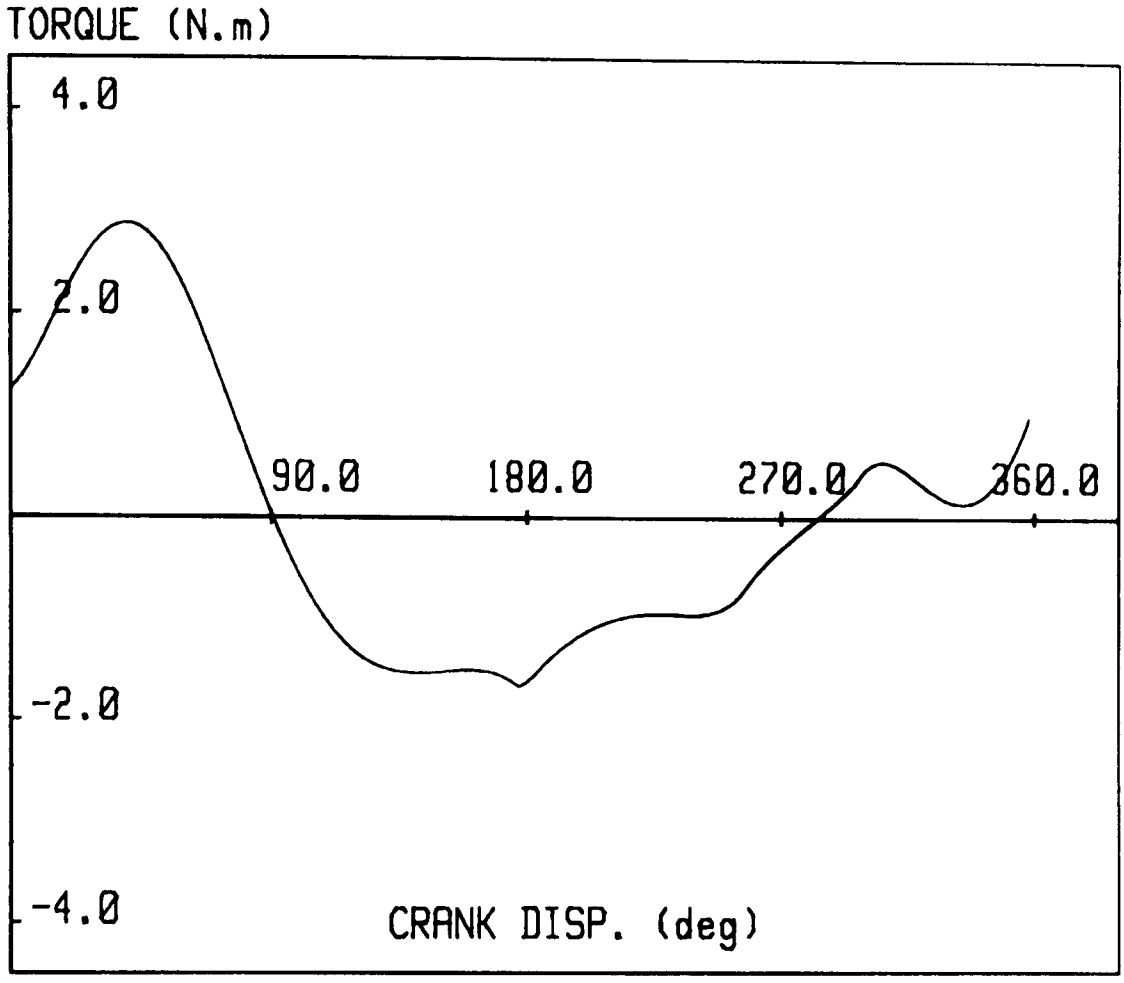

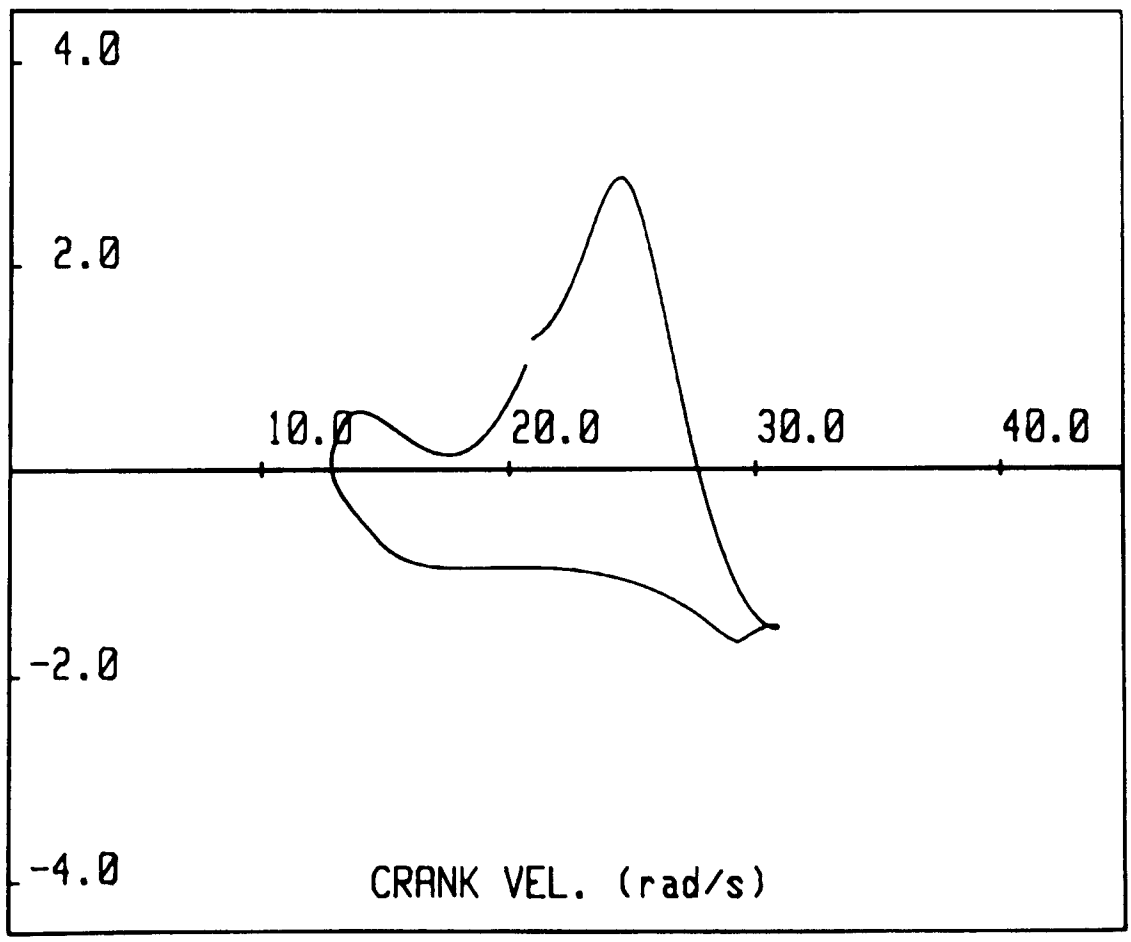

Figure 3.6. Torque-Disp. and Torque-Vel. Diagram for the R-R motion.

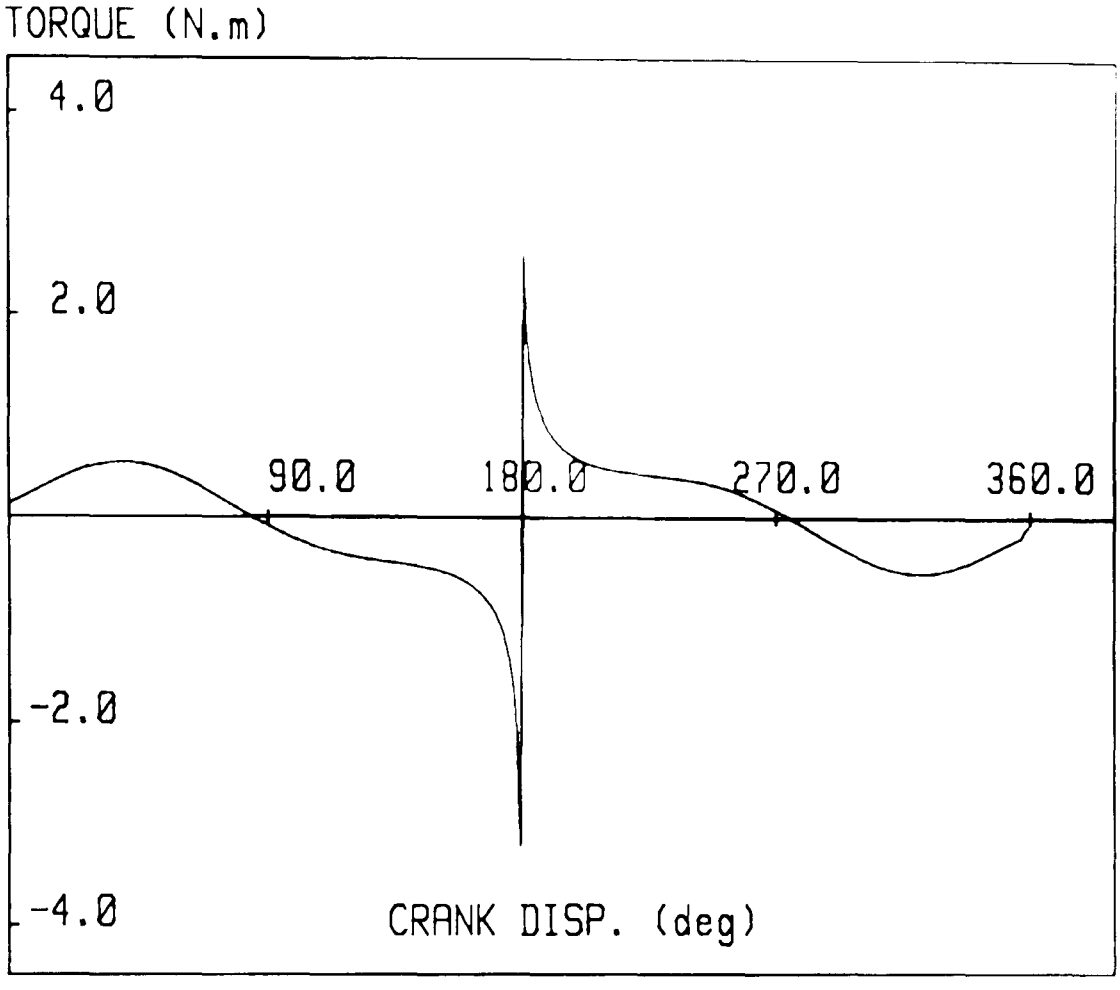

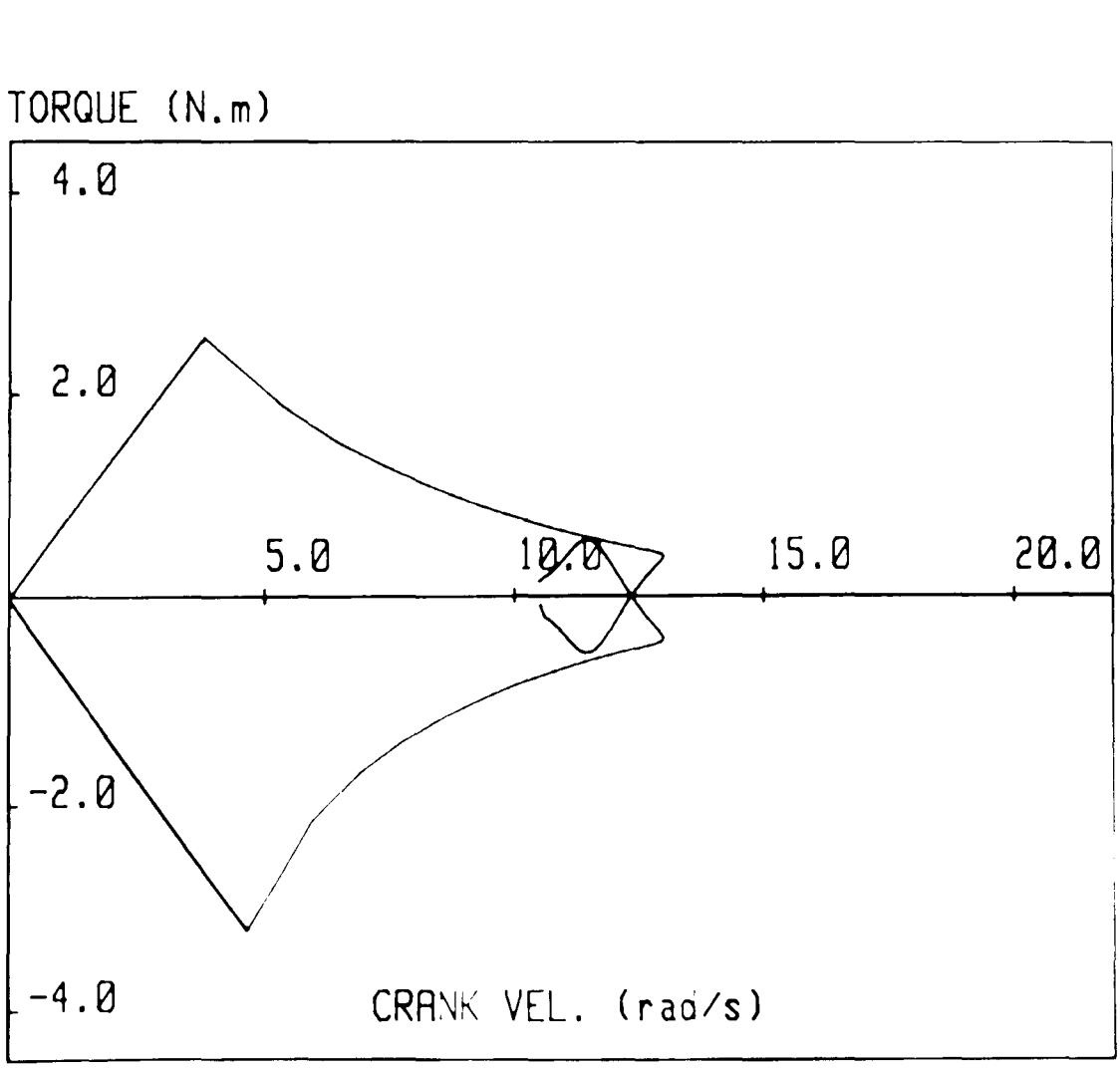

Figure 3.7. Torque-Disp. and Torque Vel. Diagram for the R-D-R motion.

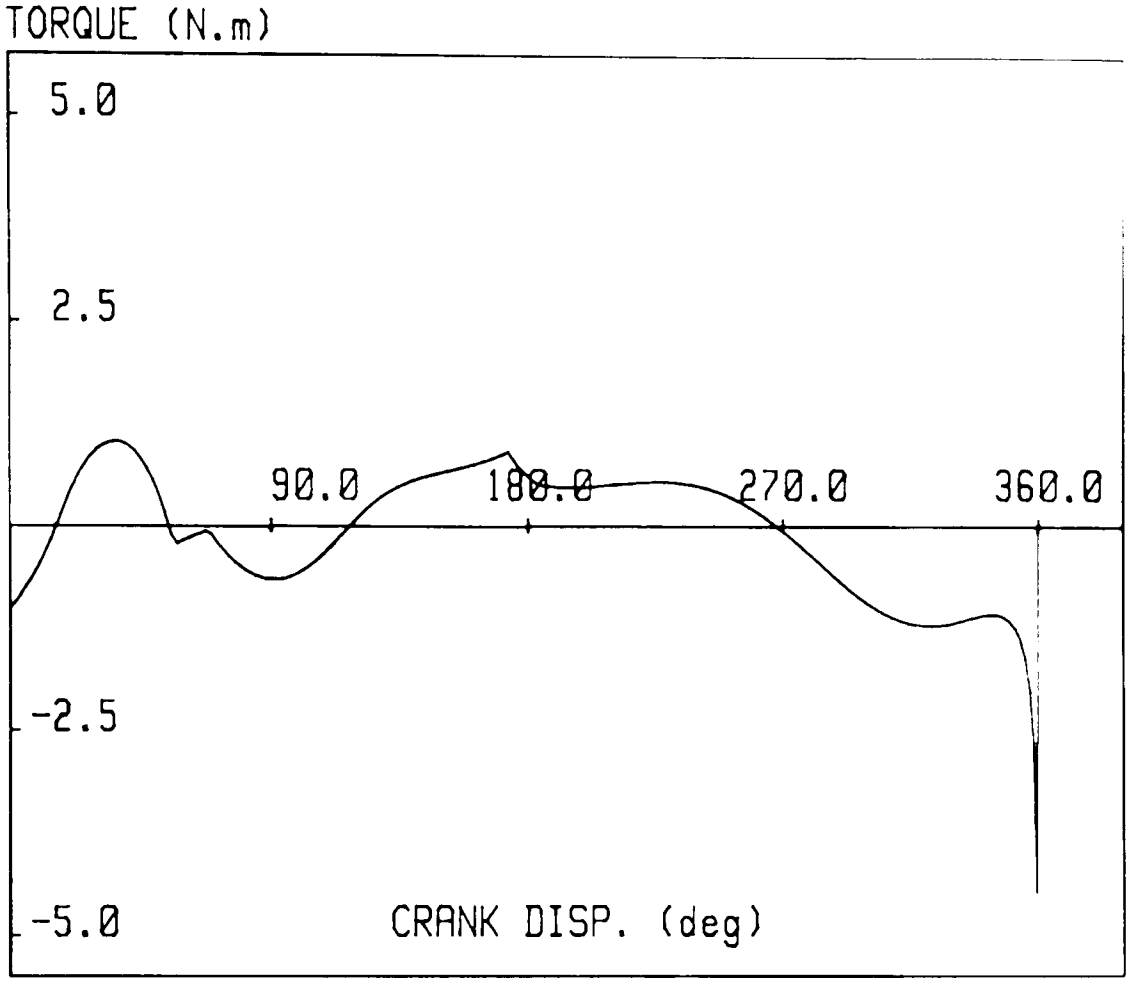

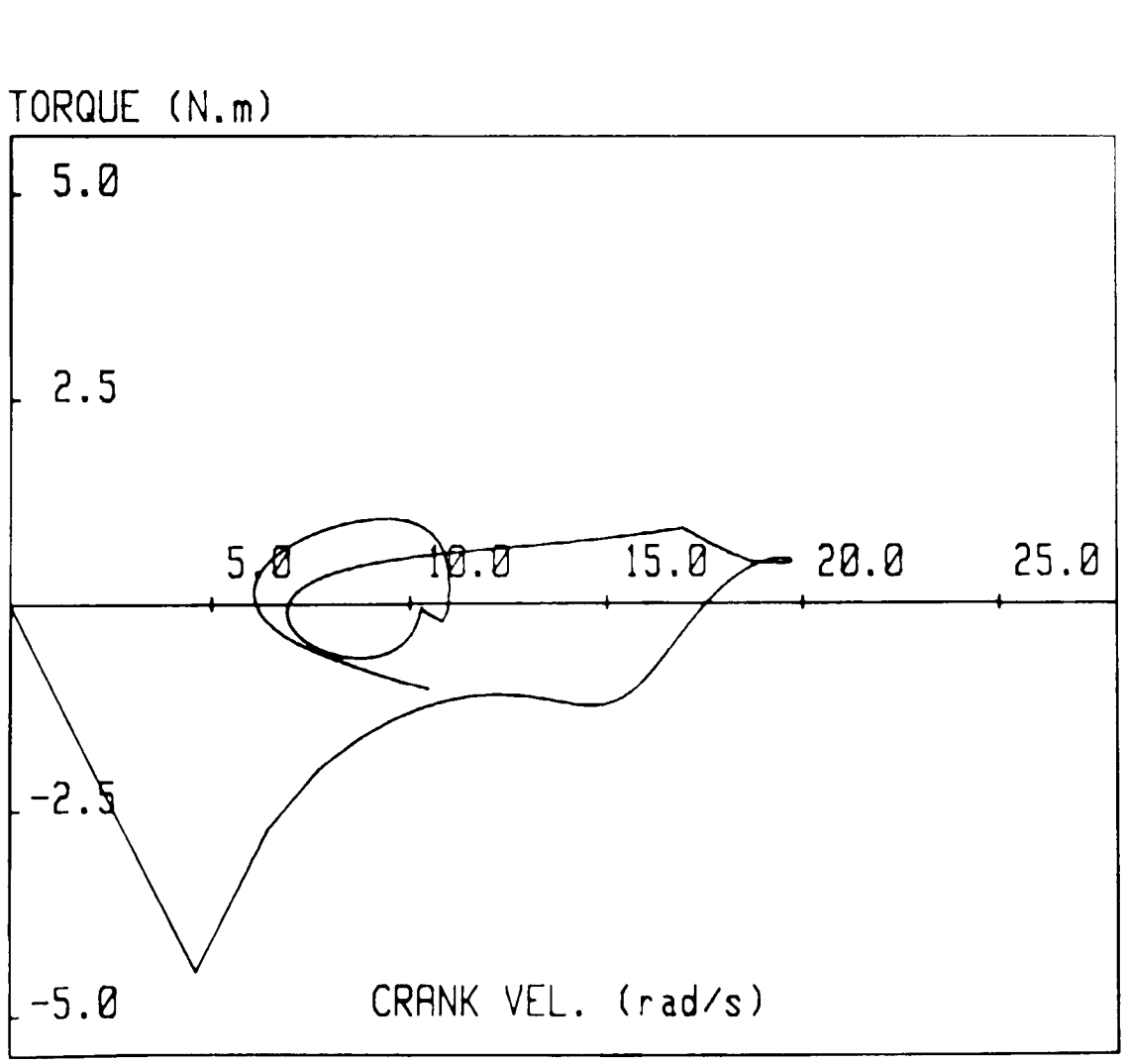

Figure 3.8. Torque-Disp. and Torque-Vel. Diagram for the R-R-D motion.

3.4. Determination of Separate Crank Inputs for the Hybrid Arrangement

After finding the crank motions from the inverse solutions, the contributions required from the separate inputs of the system are calculated, that is the uniform and the programmable motion input respectively.

What is found from the inverse solution is the output taken from the differential gear-unit. This output is a linear combination of the two inputs and is dependent on the internal gear ratio ρ. So knowing the constant speed motor input and using the kinematic relationship between two input displacements and velocities, the required servo-motor modulations are easily calculated.

Figure 3.9 shows the separate crank inputs required to perform for the R-R motion. The full line indicates the total crank motion. The constant speed motor input is represented as two dotted line curve and the programmable servo input is represented as one dotted line necessary compensated for the gear reduction of the differential gear-unit.

Similarly the following figure, Figure 3.10 gives the crank inputs for the implementation of the R-D-R motion, requiring a dwell at the end of the forward stroke.

The last figure, Figure 3.11 represents the crank inputs for the application of the R-R-D motion when achieving dwell at the end of the return stroke.

These solution curves are essential in the study whether it is carried out theoretical or experimental. The separate input curves from Figure 3.9 to Figure 3.11 are later referred as motion command points for the constant speed motor and the servo-motor when the theoretical and experimental system responses are calculated.

During the progress of this work, these crank solution points are obtained from the output of the gear reduction unit. They have been used as the main servo-motor command points in the positional control loop. θ-constant speed motor and θ-servo motor are indicated by θ_1 and θ_2 to attain θ-total at the crankshaft as θ_3. To find the actual command points for the servo-motor, θ_2 is multiplied by $1/\rho$.

3.5. Conclusion

The kinematic analysis, inverse kinematic issues and the dynamic analysis were considered for a slider-crank mechanism in this chapter. Numerical problems with inverse kinematics were solved by using different solution techniques.

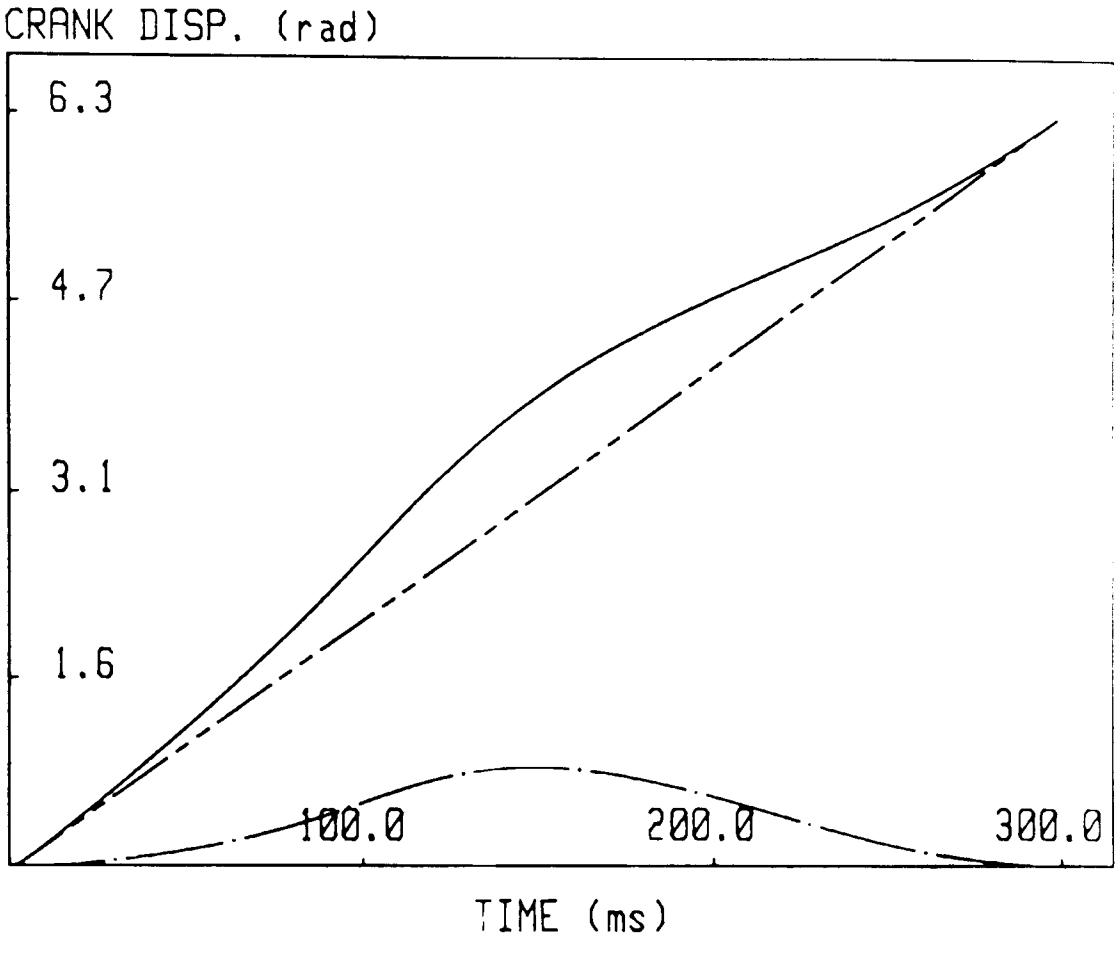

Figure 3.9. Separate crank inputs for the R-R motion.

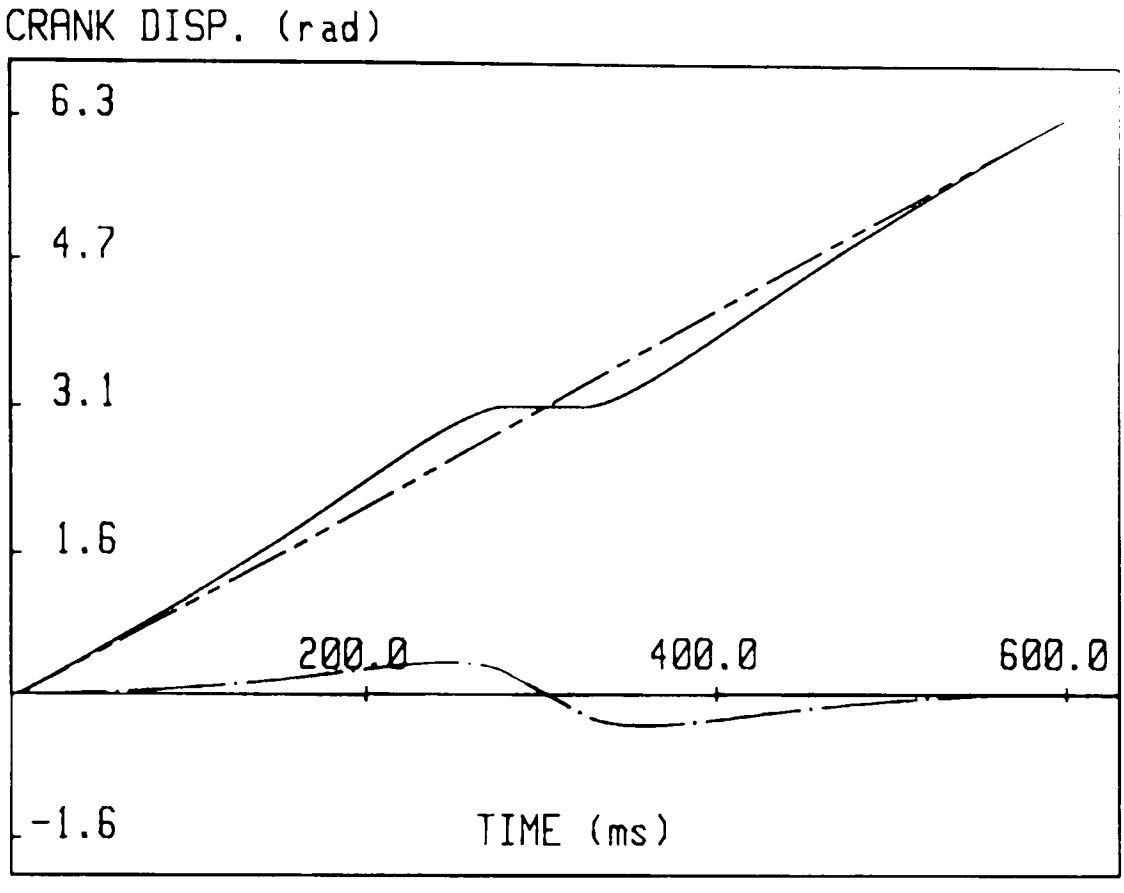

Figure 3.10. Separate crank inputs for the R-D-R motion.

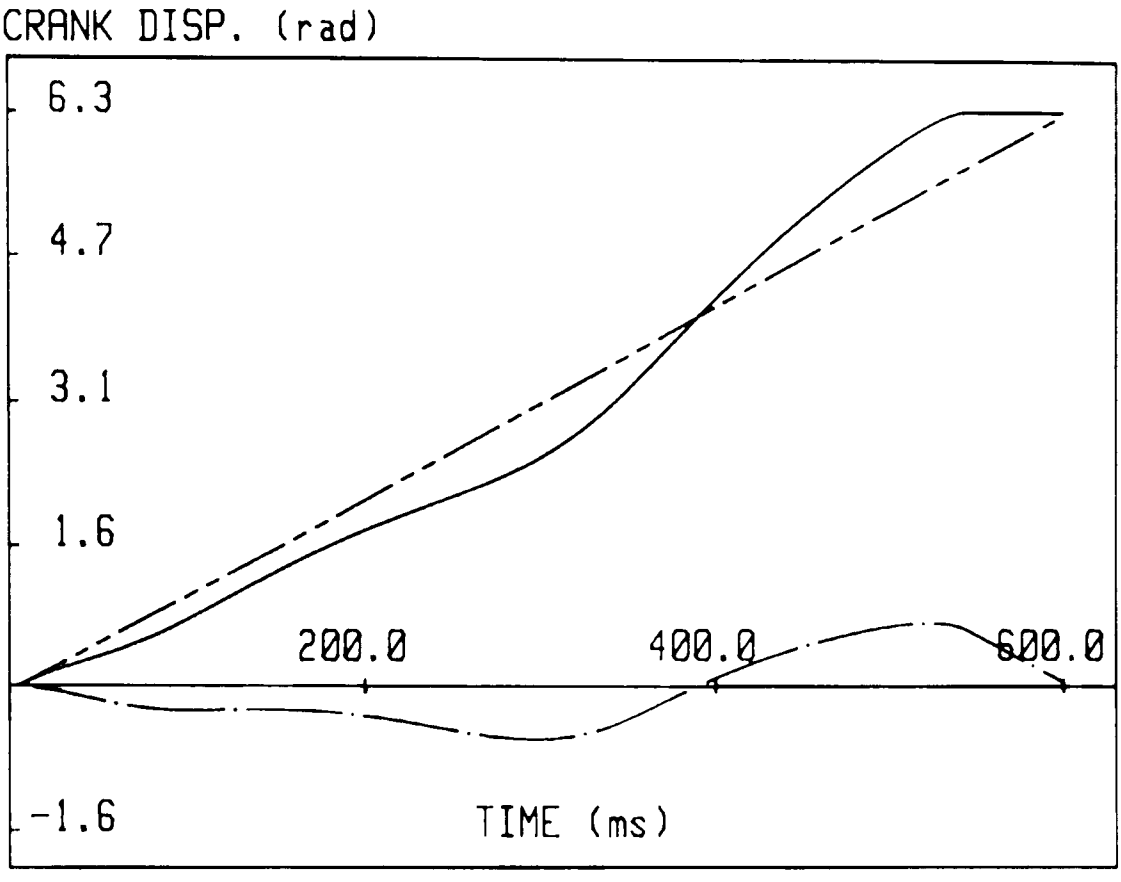

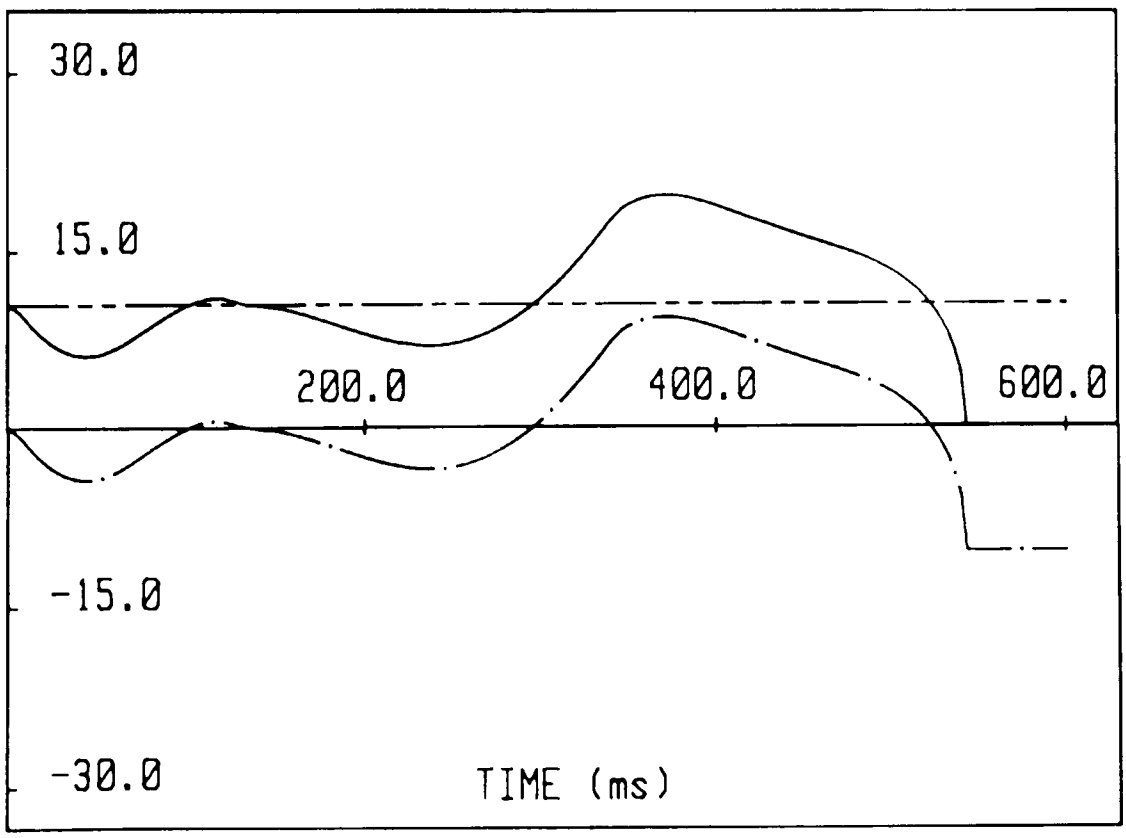

Total crank output ————————

Constant speed motor input — — — —

Servo motor input ——·——

Figure 3.11. Separate crank inputs for the R-R-D motion.

Lagrange's method of formulation was discussed and the equation of motion of a slider-crank was derived. The driving torques that were needed by the mechanism for the appraisal of the three prescribed motions were found.

Finally the crank inputs were separated into components as the constant speed motor input and the programmable servo-motor input. They were used for the further digital control study and during the calculation of the theoretical responses from the computer model in later chapters.

It was seen from the crank motions that, it was possible to introduce characteristically different motions. Once the solution was found for one example, the others were followed using the same procedure, just using available solution programs. The outputs certainly provided a superficial idea of a non-uniform motion requirement according to the motion chosen. Then it was possible to say something about the function of the servo-motor to achieve the designed motions.

CHAPTER 4
MATHEMATICAL MODELLING OF THE HYBRID ARRANGEMENT

4.1. Introduction

In this chapter, a mathematical model is presented to provide an adequate insight into the operation of the hybrid arrangement. Initially the differential equations of motion are derived by using *Lagrange's equations*. Once these equations are obtained, they are then solved to observe the dynamic behaviour of the system in terms of the response to either standard input signals, finite impulse function or square waveform or in terms of some kind of continually varying input for the required modulations. Example system responses from the derived mathematical model are presented.

4.2. Modelling of A System

Modelling is a common approach in problem solving. In order to understand and describe large-scale, interactive and complex systems of interest, the basic approach is to construct their models. Models can be applied in different ways, with the use of models, for example, we can

— describe the operation of a system as a functional dependance between interacting input and output variables,
— obtain the dynamic behaviour of a system,
— optimize an objective function of the system, by finding values for the important system variables,
— compare various alternative systems to determine the best.

Basically we may possibly start analysing a system using its mathematical representation, building its mathematical model, finding a solution method for the developed model and solving the model equations for a system of interest.

4.2.1. Mathematical Model

The relationships between the system variables can be modelled by using some mathematical structures like simple algebraic equations, differential equations or even systems of differential equations. This set of equations interpret the necessary fundamental relations and gives us a mathematical model to represent the dynamics of the system.

Mathematical models can be developed in different ways. Either they are purely theoretically based on the physical relationships, or purely on experiments on the existing system, or by a combination of both ways [4.2].

The development of a mathematical model requires many simplifying assumptions. In general, it is preferable to start from a simplified model making various assumptions and judiciously ignoring some properties of the system that may be present. If the effects of these ignored properties on the response are small, good matching will be obtained between the model and the experimental results. If not, it become necessary to selectively involve properties of the system where the importance of model-accuracy is a priority. Generally a compromise between limits of accuracy and complexity of the model is settled on at the end of the analysis.

4.2.2. Classification of Models

Models can be classified into several categories depending upon the kind of approximations made, the system equations derived and the properties of the system response obtained. When examined in detail, the models can be classified into two groups as *distributed parameter* and *lumped parameter* models. In a distributed parameter model, the dynamic behaviour of the system is described by partial differential equations. In a lumped parameter model ordinary linear or nonlinear differential equations are used for the same purpose.

Models can be considered as *stochastic* or *deterministic*. In a stochastic model, the relations between variables are given in terms of statistical values, whereas in a deterministic model, the probability is not concerned. Deterministic models include two classifications as *parametric* and *nonparametric* ones. Algebraic equations, differential equations and systems of differential equations are included in the examples of parametric models, whereas in a nonparametric model, the response is obtained directly from the experimental analysis. Theoretical model building gives a parametric model.

The classification of models can be further extended as *static* and *dynamic models*, *linear* and *nonlinear models* and *constant parameter* and *time-varying parameter models* etc. This

concept can be found in [4.2], [4,4] in detail.

4.2.3. Development of a Mathematical Model

A systematic procedure to develop a mathematical model for systems can be given in the following order.

- define the system, its components and parameters, dimensions and coordinates
- formulate the mathematical model, list the necessary assumptions
- write the differential equations describing the model
- solve the equations for the output variables
- examine the solution
- reanalyse and decide the real model.

This procedure is applied step by step in the following section.

4.3. The Derivation of Equations of Motion

The hybrid arrangement, with all of its components and the characteristics of the drives (motors), is considered in the model study presented. The energies of the system are expressed in terms of the generalized coordinates and Lagrange's equations are used to obtain the equations of motion directly.

Lagrange's equations for the generalized coordinates are included in chapter 3. They will not be discussed again here.

4.3.1. The Differential Equations of Motion for Hybrid Arrangement

Figure 4.1 shows the hybrid slider crank arrangement with its components and their assigned notations as it has been used throughout. By examining this figure, suitable set of coordinates to represent the configuration of the system are selected, such as one generalized coordinate associating with each degree of freedom.

The system has two degrees of freedom determined by inputs from a dc constant speed motor and a dc servo-motor. The generalized coordinates are the angular displacement of the respective motor armatures as:

$$q_1=\theta_1 \qquad q_2=\theta_2 \tag{4.1}$$

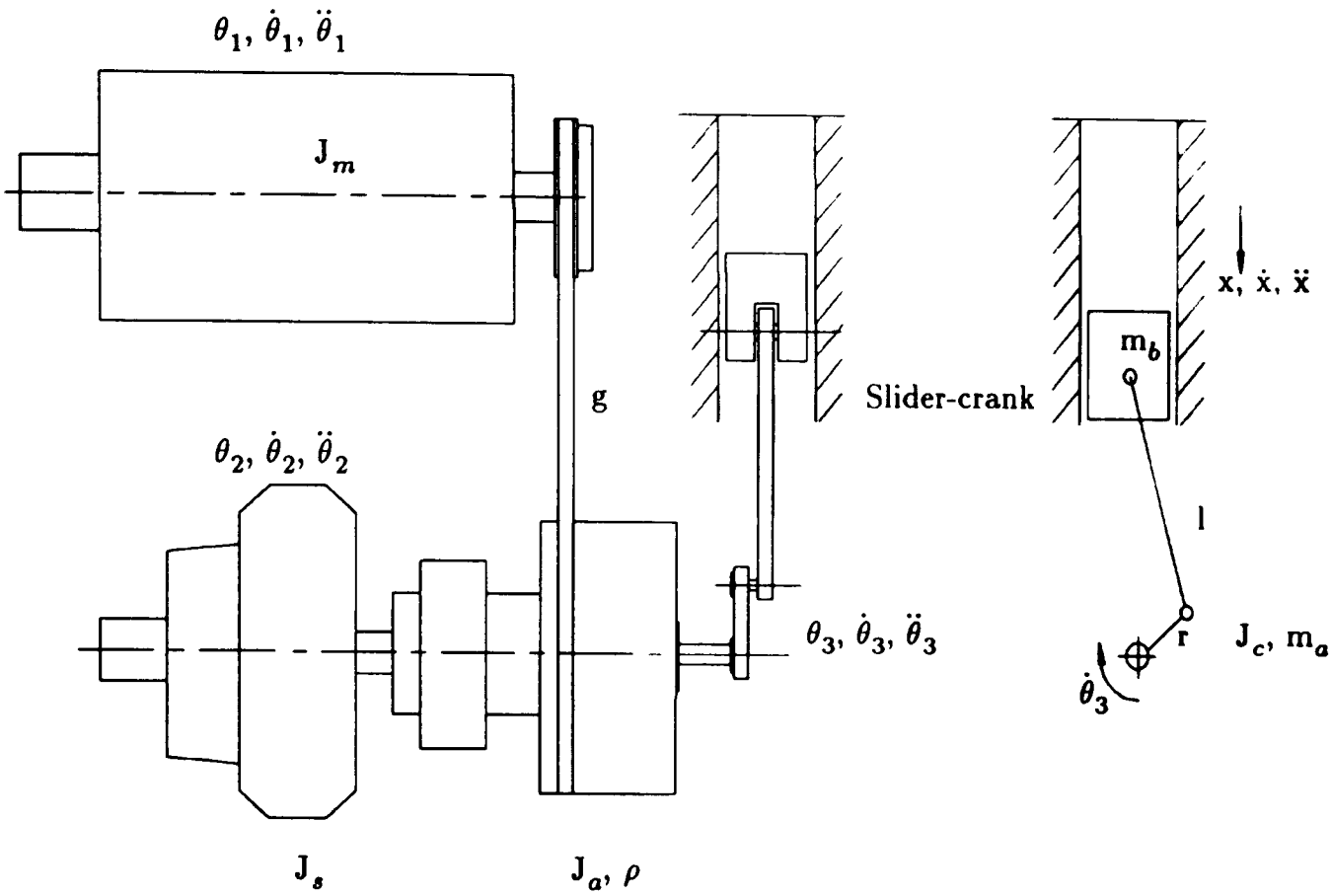

Figure 4.1. The components and their assigned notations.

The kinetic energy of the system consists of the rotational energy of the dc constant speed motor, the rotational energy of the differential gear annulus, the rotational energy of the dc servo-motor, the rotational energy of the crank and the translational energy of the total mass on the slider.

The total kinetic energy is expressed as:

$$T_t = \tfrac{1}{2}J_m\dot{\theta}_1^{\,2} + \tfrac{1}{2}J_a g^2\dot{\theta}_1^{\,2} + \tfrac{1}{2}J_s\dot{\theta}_2^{\,2} + \tfrac{1}{2}(J_c + m_a r^2)\dot{\theta}_3^{\,2} + \tfrac{1}{2}m_b\dot{x}^2 \tag{4.2}$$

Referring to the Lagrange's equations from chapter 3, equation (3.11), the total kinetic energy results in the two equations of motion in partial derivatives form as;

$$(J_m + J_a g^2)\,\ddot{\theta}_1 + (J_c + m_a r^2)\ddot{\theta}_3\left(\frac{\partial\theta_3}{\partial\theta_1}\right) + m_b\ddot{x}\left(\frac{\partial x}{\partial\theta_1}\right) = Q_1(t,\theta_1,\dot{\theta}_1) \tag{4.3}$$

$$J_s\ddot{\theta}_2 + (J_c + m_a r^2)\ddot{\theta}_3\left(\frac{\partial\theta_3}{\partial\theta_2}\right) + m_b\ddot{x}\left(\frac{\partial x}{\partial\theta_2}\right) = Q_2(t,\theta_2,\dot{\theta}_2) \tag{4.4}$$

where

θ_1– angular displacement of the dc constant speed motor,

θ_2– angular displacement of the dc servo-motor,

θ_3– angular displacement of the crankshaft,

x– linear displacement of the slider,

r, l– are the crank radius and the connecting rod length,

J_m, J_s, J_a, J_c– are the moments of inertia of the line of parts at the dc constant speed motor axis, the dc servo-motor axis, the differential annulus (casing) and the crankshaft correspondingly,

m_a, m_b–are the lumped masses representing the coupler and slider placed at the crank pin and slider gudgeon pin respectively,

$Q_1(t,\theta_1,\dot{\theta}_1)$ and $Q_2(t,\theta_2,\dot{\theta}_2)$– are the generalized torques acting on the respective generalized coordinates.

The kinematic relationships for the differential gear-unit are expressed in terms of the generalized coordinates in the form;

$$\dot{\theta}_3 = \rho\dot{\theta}_2 + (1-\rho)g\dot{\theta}_1 \tag{4.5}$$

where

ρ– the internal gear ratio of the differential gear-unit, is equal to 828/1120.

g– the pulley ratio between the dc constant speed motor output and the differential gear annulus, is equal to 1/1.875.

The displacement the slider is written in its explicit form by using kinematic displacement loop equations for a slider-crank from chapter 3 as:

$$x = r+l-r\cos\theta_3 - [\, l^2 - (y - r\sin\theta_3)^2 \,]^{1/2} \tag{4.6}$$

where y, the slider offset, is equal to zero in this arrangement.

Hence substitution of equations (4.5), (4.6) and time derivatives of equation (4.6) directly into equations (4.3) and (4.4) and taking the partial derivatives with respect to each generalized displacement yields the complete expressions as two nonlinear differential equations. The detailed form of the individual energy terms for the components are given in Appendix 3.

The final form of the equations of motion are given for the corresponding generalized coordinates as follows.

The equation of motion for the coordinate θ_1 is;

$$\ddot{\theta}_1\Big((J_m+J_a g^2)+(J_c+m_a r^2)(1-\rho)^2 g^2+ m_b\Big(r\sin\theta_3 + r\cos\theta_3(y - r\sin\theta_3)/[l^2 - (y - r\sin\theta_3)^2]^{1/2}\Big)^2$$

$$(1-\rho)^2 g^2\Big) + \ddot{\theta}_2\Big((J_c+m_a r^2)(1-\rho)\rho g+ m_b\Big(r\sin\theta_3+r\cos\theta_3(y - r\sin\theta_3)/[l^2 - (y - r\sin\theta_3)^2]^{1/2}\Big)^2$$

$$(1-\rho)\rho g\Big) = Q_1- m_b[\rho\dot{\theta}_2+(1-\rho)g\dot{\theta}_1]^2 \Big(\Big(r\sin\theta_3+r\cos\theta_3(y - r\sin\theta_3)/[l^2 - (y - r\sin\theta_3)^2]^{1/2}\Big)$$

$$\Big\{r\cos\theta_3+ \Big\{ \Big([-r\sin\theta_3(y - r\sin\theta_3) - r^2\cos^2\theta_3]\ [l^2 - (y - r\sin\theta_3)^2]^{1/2} - r^2\cos^2\theta_3(y - r\sin\theta_3)^2/$$

$$[l^2 - (y - r\sin\theta_3)^2]^{1/2}\Big)/[l^2 - (y - r\sin\theta_3)^2]\Big\}\Big\} (1-\rho)g\Big) \tag{4.7}$$

The equation of motion for the coordinate θ_2 is;

$$\ddot{\theta}_2\Big(J_s+ (J_c+m_a r^2)\rho^2+ m_b\Big(r\sin\theta_3+ r\cos\theta_3(y - r\sin\theta_3)/[l^2 - (y - r\sin\theta_3)^2]^{1/2}\Big)^2\rho^2\Big) +$$

$$\ddot{\theta}_1\Big((J_c+m_a r^2)(1-\rho)\rho g+ m_b\Big(r\sin\theta_3+ r\cos\theta_3(y - r\sin\theta_3)/[l^2 - (y - r\sin\theta_3)^2]^{1/2}\Big)^2(1-\rho)\rho g\Big)$$

$$= Q_2- m_b\,[\rho\dot{\theta}_2+(1-\rho)g\dot{\theta}_1]^2 \Big(\Big(r\sin\theta_3+r\cos\theta_3(y - r\sin\theta_3)/[l^2 - (y - r\sin\theta_3)^2]^{1/2}\Big)\Big\{r\cos\theta_3+$$

$$\Big\{\Big([-r\sin\theta_3(y - r\sin\theta_3) - r^2\cos^2\theta_3]\ [l^2 - (y - r\sin\theta_3)^2]^{1/2} - r^2\cos^2\theta_3(y - r\sin\theta_3)^2/[l^2 -$$

$$(y - r\sin\theta_3)^2]^{1/2}\Big)/\ [l^2 - (y - r\sin\theta_3)^2]\ \Big\}\Big\}\rho\Big) \tag{4.8}$$

In addition to the above equations, the schematic diagram of the armature-controlled dc motor is shown in Figure 4.2.

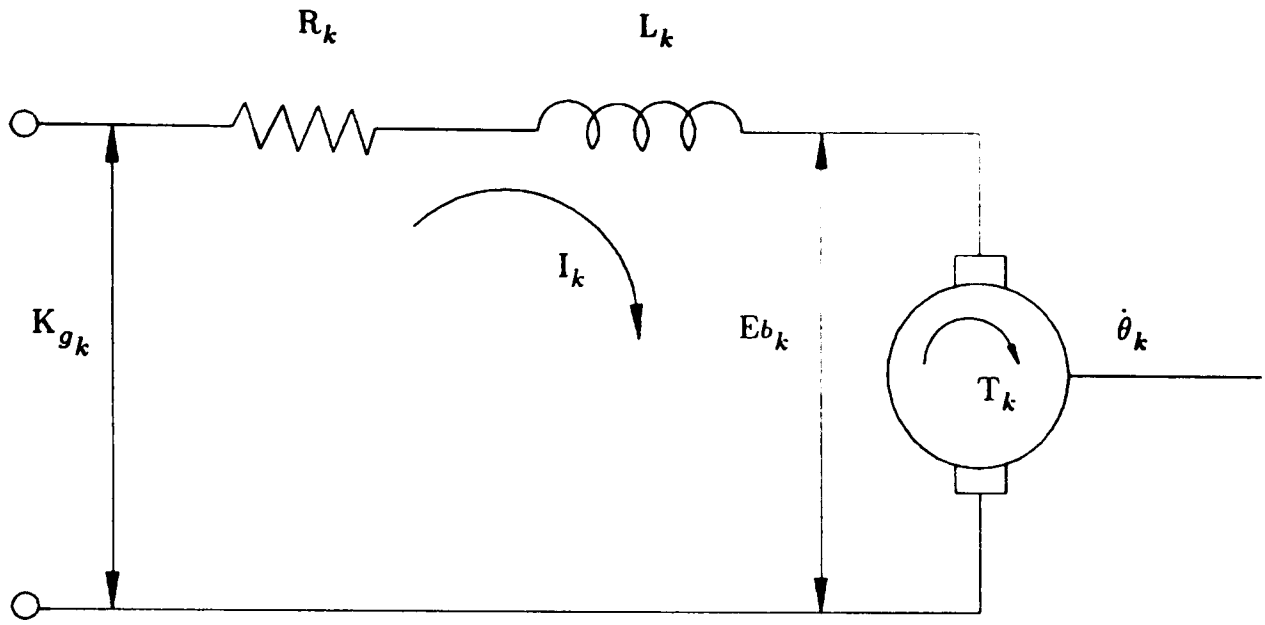

Figure 4.2. Motor Armature Circuit.

By using given notations from Figure 4.2, the differential equation for the armature circuit of the motor can be written as;

$$L_k \frac{dI_k}{dt} + R_k I_k + E_{b_k} = K_{g_k}(\theta_{k_c} - \theta_k) + K_{v_k}(\dot{\theta}_{k_c} - \dot{\theta}_k), \tag{4.9}$$

where the speed of the armature of a dc motor is controlled by its armature voltage represented on the right hand side of the equation (4.9). E_{b_k} represents the back emf which is directly proportional to the angular velocity $\dot{\theta}_k$. It can be written as:

$$E_{b_k} = K_{e_k}\dot{\theta}_k \tag{4.10}$$

and the motor torque is taken to be related to the armature current by the following form as a generalized torque term like:

$$Q_k = K_{t_k} I_k \tag{4.11}$$

where

R_k — motor resistance, Ohms

L_k — motor inductance, Henrys

I_k — armature current, Amperes

K_{t_k} — motor torque constant, N.m/A

K_{e_k} — emf constant, Volt/rad/s

K_{g_k} — proportional gain, Volt/rad

K_{v_k} – derivative gain, Volt/rad/s

θk_c – positional command to the kth coordinate

θ_k – current position of the kth coordinate

k– equal to 1 for the dc constant speed motor and 2 for the servo motor.

The right hand side of the equation (4.9) includes the feedback terms. For the constant speed motor, the right hand side of the equation (4.9) becomes K_{g_1} representing a constant voltage value for the motor armature. When this voltage is applied, the motor accelerates to reach its required constant velocity.

Finally the differential equations of motion given in equations (4.7), (4.8) and the armature circuit equation (4.9) are arranged in the following forms to give the differential equations separately as the first for the motor armature circuit and the second for the equations of motion for each coordinate. The mathematical model parameters are also based on information that was either from equipment suppliers or by simple measurement and usual calculation.

The derived equations for the coordinate θ_1 are:

$$L_1\dot{I}_1 + R_1I_1 + K_{e_1}\dot{\theta}_1 = Kg_1 \tag{4.12}$$

$$\ddot{\theta}_1\Big((J_m+J_ag^2) + (J_c+m_ar^2)(1-\rho)^2g^2 + m_b\big(r\sin\theta_3 + r\cos\theta_3(y-r\sin\theta_3)/[l^2-(y-r\sin\theta_3)^2]^{1/2}\big)^2$$

$$(1-\rho)^2g^2\Big) + \ddot{\theta}_2\Big((J_c+m_ar^2)(1-\rho)\rho g + m_b\big(r\sin\theta_3 + r\cos\theta_3(y-r\sin\theta_3)/[l^2-(y-r\sin\theta_3)^2]^{1/2}\big)^2$$

$$(1-\rho)\rho g\Big) = K_{t_1}I_1 - m_b[\rho\dot{\theta}_2 + (1-\rho)g\dot{\theta}_1]^2\Big(\big(r\sin\theta_3 + r\cos\theta_3(y-r\sin\theta_3)/[l^2-(y-r\sin\theta_3)^2]^{1/2}\big)$$

$$\Big\{r\cos\theta_3 + \Big\{\Big([-r\sin\theta_3(y-r\sin\theta_3) - r^2\cos^2\theta_3]\,[l^2-(y-r\sin\theta_3)^2]^{1/2} - r^2\cos^2\theta_3(y-r\sin\theta_3)^2/$$

$$[l^2-(y-r\sin\theta_3)^2]^{1/2}\Big)/[l^2-(y-r\sin\theta_3)^2]\Big\}\Big\}(1-\rho)g\Big) \tag{4.13}$$

where the machine data used for dc constant speed motor in the differential equation of armature circuit in (4.12) is;

$R_1 = 1.93\ \Omega$ $L_1 = 0.040$ H

$K_{e_1} = 1.146$ V/rad/s $K_{t_1} = 1.146$ Nm/A

and the numerical values for the crank radius, the connecting rod length, lumped masses and the moment of inertias are;

$r = 0.060$ m $l = 0.20$ m

$m_a = 0.3330$ kg $m_b = 1.3532$ kg

$J_m = 0.0062$ kg.m.m $J_s = 0.0012$ kg.m.m

$J_a = 0.029$ kg.m.m $J_c = 0.0050$ kg.m.m

The equations for the coordinate θ_2;

$$L_2\dot{I}_2 + R_2I_2 + K_{e_2}\dot{\theta}_2 = K_{g_2}(\theta_{2_c} - \theta_2) + K_{v_2}(\dot{\theta}_{2_c} - \dot{\theta}_2) \tag{4.14}$$

$$\ddot{\theta}_2\Big(J_s + (J_c + m_a r^2)\rho^2 + m_b\Big(r\sin\theta_3 + r\cos\theta_3(y - r\sin\theta_3)/[l^2 - (y - r\sin\theta_3)^2]^{1/2}\Big)^2\rho^2\Big) +$$

$$\ddot{\theta}_1\Big((J_c + m_a r^2)(1-\rho)\rho g + m_b\Big(r\sin\theta_3 + r\cos\theta_3(y - r\sin\theta_3)/[l^2 - (y - r\sin\theta_3)^2]^{1/2}\Big)^2(1-\rho)\rho g\Big)$$

$$= K_{t_2}I_2 - m_b\,[\rho\dot{\theta}_2 + (1-\rho)g\dot{\theta}_1]^2\Big(\Big(r\sin\theta_3 + r\cos\theta_3(y - r\sin\theta_3)/[l^2 - (y - r\sin\theta_3)^2]^{1/2}\Big)\Big\{r\cos\theta_3 +$$

$$\Big\{\Big([-r\sin\theta_3(y - r\sin\theta_3) - r^2\cos^2\theta_3]\,[l^2 - (y - r\sin\theta_3)^2]^{1/2} - r^2\cos^2\theta_3(y - r\sin\theta_3)^2/\,[l^2 -$$

$$(y - r\sin\theta_3)^2]^{1/2}\Big)/[l^2 - (y - r\sin\theta_3)^2]\Big\}\Big\}\rho\Big) \tag{4.15}$$

where the machine data used for the servo motor in equation (4.14);

$R_2 = 0.460\ \Omega$ $L_2 = 0.0001$ H

$K_{e_2} = 0.2435$ V/rad/s $K_{t_2} = 0.244$ Nm/A

and the numerical values for the crank radius, the connecting rod length, lumped masses and the moment of inertias are the same as above.

4.3.2. Matrix form representation of equations of motion

The armature circuit and the differential equations of motion can be represented in matrix form also. For this purpose, the armature equations are modelled by first order differential equations. Equations (4.12) and (4.14) are arranged in the following form

$$\begin{bmatrix} \dot{I}_1 \\ \dot{I}_2 \end{bmatrix} = \begin{bmatrix} \frac{-R_1}{L_1} & 0 \\ 0 & \frac{-R_2}{L_2} \end{bmatrix} \begin{bmatrix} I_1 \\ I_2 \end{bmatrix} + \begin{bmatrix} \frac{-K_{e1}}{L_1} & 0 \\ 0 & \frac{-K_{e2}}{L_2} \end{bmatrix} \begin{bmatrix} \dot{\theta}_1 \\ \dot{\theta}_2 \end{bmatrix} + \begin{bmatrix} \frac{K_{g1}}{L_1} \\ \frac{K_{gv}}{L_2} \end{bmatrix} \tag{4.16}$$

The above equation may be written in compact notation as:

$$\dot{\underline{I}} = A\,\underline{I} + B\,\dot{\underline{\theta}} + \underline{K} \tag{4.17}$$

where A is the matrix including resistance elements, I is the current vector, B is the matrix representing emf constants, $\dot{\theta}$ is the angular velocity vector and K is the gain voltage vector. Here the gain vector of the servo motor voltage is indicated as a total K_{g_v} to get the right hand side of equation (4.14) in a simplified form. It includes proportional-plus-derivative control action in the servo-control system.

The matrix forms of equations (4.13) and (4.15) are written in closed form with the representation of matrix elements of M in the left hand side. By arranging the angular velocity terms with masses, $\lambda\theta_1$ and $\lambda\theta_2$ are given in the right hand side.

Finally the differential equations of motion are expressed in a matrix form as

$$\begin{bmatrix} M(1,1) & M(1,2) \\ M(2,1) & M(2,2) \end{bmatrix} \begin{bmatrix} \ddot{\theta}_1 \\ \ddot{\theta}_2 \end{bmatrix} = \begin{bmatrix} Q_1 + \lambda\theta_1 \\ Q_2 + \lambda\theta_2 \end{bmatrix} \tag{4.18}$$

more concisely equation (4.18) looks like

$$M\,\ddot{\underline{\theta}} = \underline{Q} \tag{4.19}$$

where M is the mass and inertia matrix, $\ddot{\theta}$ is the angular acceleration vector and Q is the generalized torque vector.

In general an nth-order differential equation can be represented by a system of n first order differential equations in vector-matrix form. If n elements of the vector are a set of *state variables* then the vector-matrix differential equation is called as a *state equation* which gives the system a so called *state space representation*. Since the order of the system is specified by the minimum number of state variables needed in the state equation, the number of necessary state variables is already fixed.

If we consider the system equations, the armature circuit is first order and the equations of motion, (4.13) and (4.15) are order of two. For the equations of motion, the number of state variables needed is two. So by using state variables, these second order differential equations are written as a set of two first order differential equations. For each one of the generalized coordinates three first order state equations are, therefore, obtained, representing the whole arrangement.

In order to obtain time responses of the system, the equations of motion must be solved numerically by using a step-by-step process in which a sequence of points for t_{i+1}-t_i is generated. So in order to solve these initial value problems a computer program is written in pascal.

In this program to carry calculations, many system parameters are required like motor data, mechanism parameters and initial conditions. Firstly a data file including the angular displacements and velocity of the crankshaft which was found from the inverse solution in chapter 3, is required as motion command points for both motors. The constant speed motor and the servo-motor parameters are then given with proportional and derivative gains as the second requirement. The slider-crank mechanism parameters; link lengths, lumped masses, link inertias and initial conditions for both motors are set next. Having given all necessary parameters and initial conditions for θ_1, $\dot{\theta}_1$, $\ddot{\theta}_1$ and θ_2, $\dot{\theta}_2$, $\ddot{\theta}_2$, the state equations of the system are integrated through time using the *4th order Runge-Kutta formula*, which is one of the most widely used numerical methods of integration for systems of nonlinear differential equations. By using the kinematic relationship for the differential gear-unit with given the internal gear ratio of the unit and the belt reduction, equation (4.5) θ_3, $\dot{\theta}_3$, $\ddot{\theta}_3$ are further calculated.

The Runge-Kutta step size is specified by the incremental time Δt, which is equal to t_{i+1}-t_i for computation. It is chosen to be small enough to get a reasonably accurate integration by assuming that the accuracy of the numerical integration increases as Δt decreases. However,

if Δt is too small, the round-off error can be excessive. Whence, a suitable value of Δt is required to be established from the beginning of the integration. Since the algorithm is a fourth-order one, the truncation error remained relatively small, even for a relatively large step size, in trials.

4.4. Example Tests for The System Response

A simple mathematical model characterizing the behaviour of the system is obtained taking the elements separately first. From Figure 4.1, we already know that the system components are a constant speed motor, a servo-motor, a differential gear-unit and a slider-crank mechanism. If these components are disconnected from each other, the whole system can be considered as two separate motors, like in the first part of the computer model study. Standard functions can, therefore, be used for investigating the dynamic characteristics of a motor.

Usually standard input functions considered are the *step function, pulse function, impulse function, exponentially decaying function* and *sinusoid.* Here the response of the system is determined only for particular inputs of θ_2 such as a finite impulse function and square waveform function. Initially the system equations are tested with zero load inertias and masses and reduced to two uncoupled motors without a gear-reducer and a linkage mechanism.

The system is considered to be running in ideal conditions without any friction and losses.

4.4.1. DC-Motor Characteristics

The lumped masses and the moment of inertias of the components are assumed zero except the inertias of two motors. Figure 4.3 shows the system as two uncoupled motors with their resultant form for dc-motor characteristics after simplifying assumptions made. The given model parameters are:

$m_a = 0.0$ kg $\qquad$ $m_b = 0.0$ kg

$J_c = 0.0$ kg.m.m $\qquad$ $J_a = 0.0$ kg.m.m

By using the above zero parameters, the equations (4.13) and (4.15) are reduced to a form that represent only the dynamic equations of a dc constant speed motor and a servo-motor. The motor armature equations remained the same. The motor data sheets are used in the motor armature circuits during the calculations. These equations are given in the following forms.

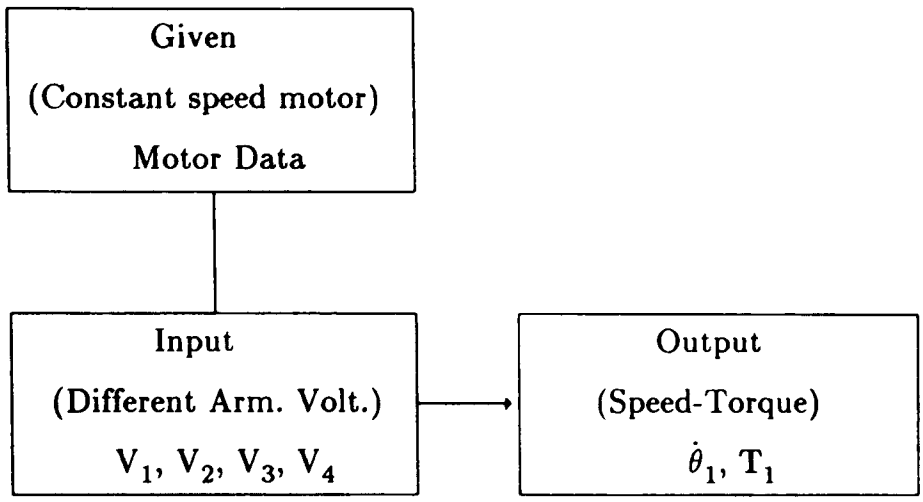

(a)

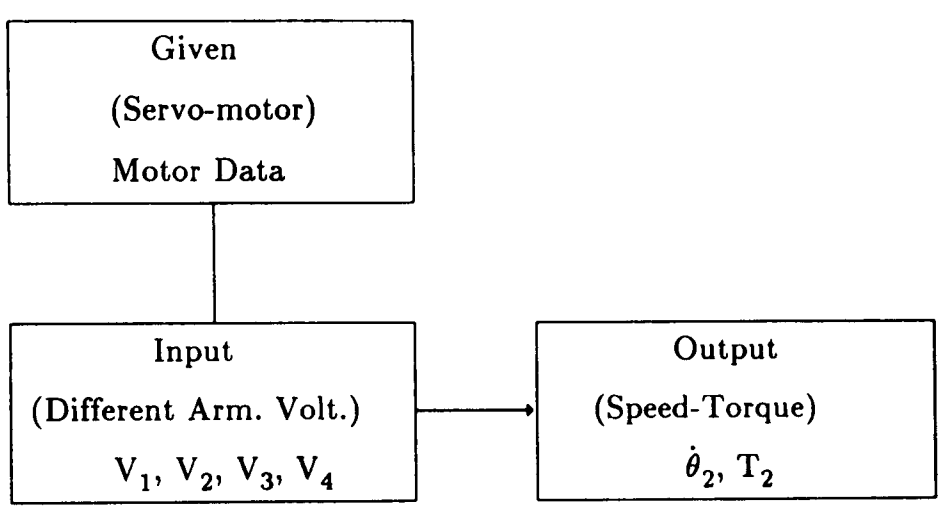

(b)

Figure 4.3. The mathematical model for two uncoupled motors without a linkage mechanism.

The differential equations for the dc constant speed motor:

$$L_1\dot{I}_1 + R_1I_1 + K_{e_1}\dot{\theta}_1 = K_{g_1} \tag{4.20}$$

$$J_m\ddot{\theta}_1 = K_{t_1}I_1 \tag{4.21}$$

The differential equations for the pancake type servo-motor:

$$L_2\dot{I}_2 + R_2I_2 + K_{e_2}\dot{\theta}_2 = K_{gv} \tag{4.22}$$

$$J_s\ddot{\theta}_2 = K_{t_2}I_2 \tag{4.23}$$

Equations (4.20) to (4.23) are then solved numerically by using the written program which was described above. Figure 4.4.(a) shows a set of typical speed-torque curves at different voltage inputs with $V_4 > V_3 > V_2 > V_1$ by changing K_{g1} for dc shunt motor. Figure 4.4.(b)

shows a set of speed-torque curves for various values of control voltages for the pancake type motor.

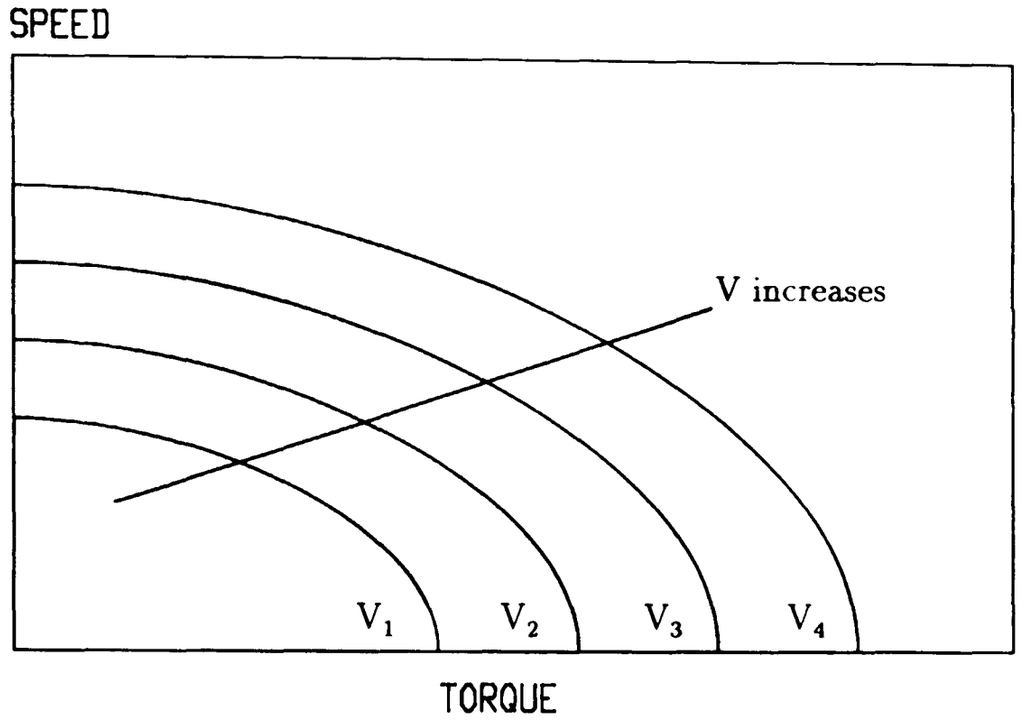

(a)

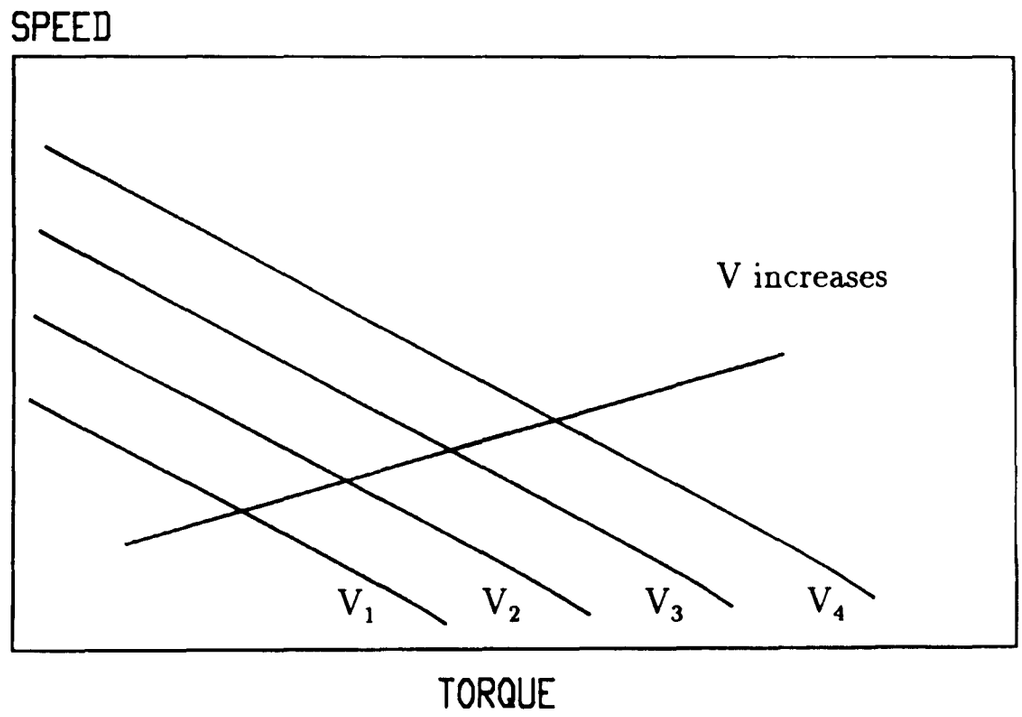

(b)

Figure 4.4. DC-Motor Characteristics.

As expected, the servo-motor provides a large torque at zero speed. This is necessary for required rapid acceleration. The torque decreases linearly when the speed increases. The values of K_{gv} is kept constant rather than with included feedback terms for the servo-motor.

4.4.2. The Servo-Motor Response for Standard Inputs

Here the model is studied as a single servo-motor for different commands. A finite impulse of known shape and a square waveform are applied to the system and the corresponding motor responses are obtained. The representative system model can be seen in Figure 4.5.

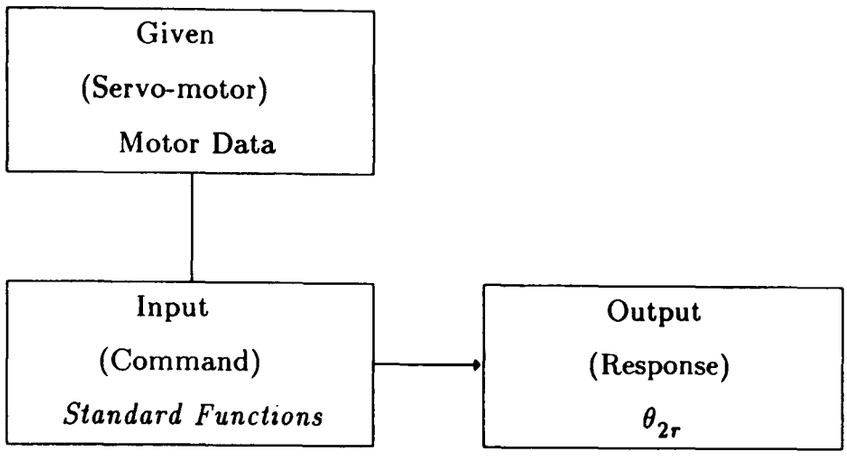

Figure 4.5. The programmable servo-motor model.

The servo-motor is assumed to be uncoupled from the dc constant speed motor. For the calculations zero voltage is given to the armature of the constant speed motor so that the system is only activated by the servo-motor. The system equations are, therefore, based on the servo-motor armature and the motor dynamic equations as the following.

$$L_2\dot{I}_2 + R_2I_2 + K_{e_2}\dot{\theta}_2 = K_{g_2}(\theta_{2_c} - \theta_2) + K_{v_2}(\dot{\theta}_{2_c} - \dot{\theta}_2) \tag{4.24}$$

$$J_s\ddot{\theta}_2 = K_{t_2}I_2 \tag{4.25}$$

where the servo-motor is subjected to a finite impulse input as a command motion in the right hand side of the equation (4.24) with proportional-plus-derivative control.

In a system, if gains are optimized, the proportional-plus-derivative control action can be considered as anticipatory and reduces the time to come near to the desired steady state value. It achieves an acceptable transient response behaviour and acceptable steady state behaviour for the system output.

In general, the response to standard functions is usually used as a means of evaluating the dynamic performance of a system. This type of input is a kind of disturbance where the change in θ_2 is considered to be instantaneous. For instance, the applied finite impulse-input to the above armature equation is mathematically defined as:

$\theta_{2_c} = 0.0$ $\quad$ 0<t<100 ms

$\theta_{2_c} = B$ $\quad$ 100<t<200 ms

$\theta_{2c} = 0.0$ $\quad$ 200<t<300 ms $\quad$ (4.26)

where B represents a constant, the angular displacement in radians.

The equations (4.24) and (4.25) are solved with the assumption of zero lumped masses and moment of inertias. The initial values for θ_2, $\dot{\theta}_2$ and $\ddot{\theta}_2$ are set to zero for Runge-Kutta method. The incremental time for Runge-Kutta step, Δt is chosen to be equal 1.66666 ms. To assure the accuracy of the integration, an inner loop has also been performed during the calculation of each output variable. In the inner loop, Δt is reduced to 0.16666 ms for the calculation of the servo-motor output.

Figure 4.6 shows the servo-motor responses for this representative system model. The amount of damping in the system can also be altered by increasing derivative gain K_{v2}. The impulse function occurs at t=100 ms and continues about 100 ms. In the upper plot, the proportional and derivative gains are set to K_{g_2}= 100.0 Volt/rad and K_{v_2}= 0.10 Volt/rad/s respectively. The system returns to its equilibrium state after having a definite transients. This is the characteristic behaviour of an underdamped system. In the middle plot, The proportional gain is kept same and the derivative gain is increased four times. The behaviour of the system is observed to be less oscillatory. In the lower plot, the proportional gain is still the same and the derivative gain is nearly doubled. Resultantly the oscillatory behaviour has not been seen, the system reaches its equlibrium state quickly. This is accepted nearly as critically damped system behaviour.

The second set of examples are the response curves for the *square waveform function* input which includes two step changes during the cycle. Mathematically a square waveform function is described as:

$\theta_{2_c} = B$ $\quad$ 0<t<150 ms

$\theta_{2_c} = -B$ $\quad$ 150<t<300 ms $\quad$ (4.27)

where B is a constant representing angular displacement in radians.

In this function, a step at the beginning signifies a sudden change. The same equations (4.24) and (4.25) are used. At this time only the square waveform input is given as motion command in the right hand side of the equation (4.24). The responses for the second order system are for a square waveform where the changes occur at t=0 and t=150 ms. They are given in Figure 4.7 with the action of derivative gains.

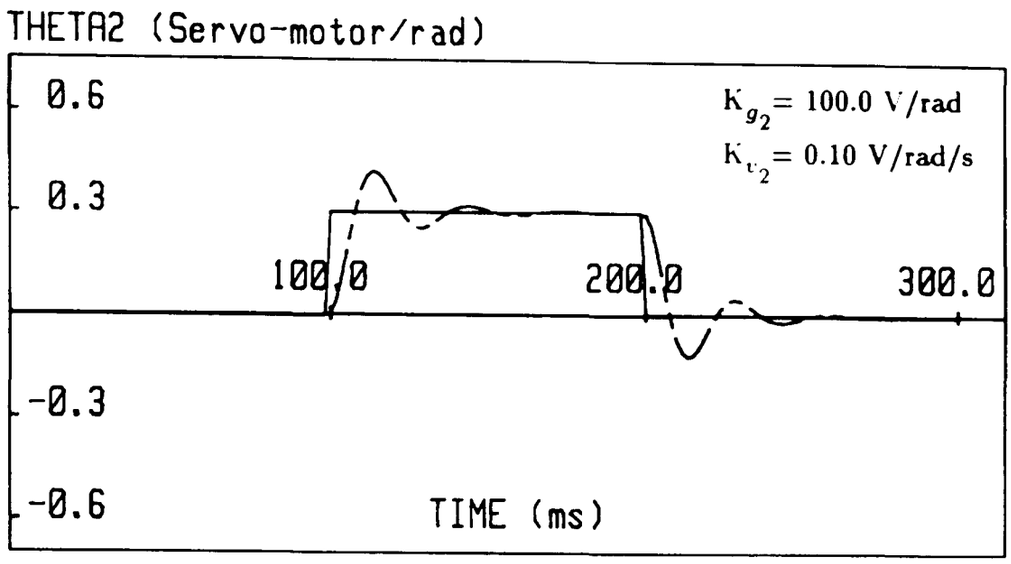

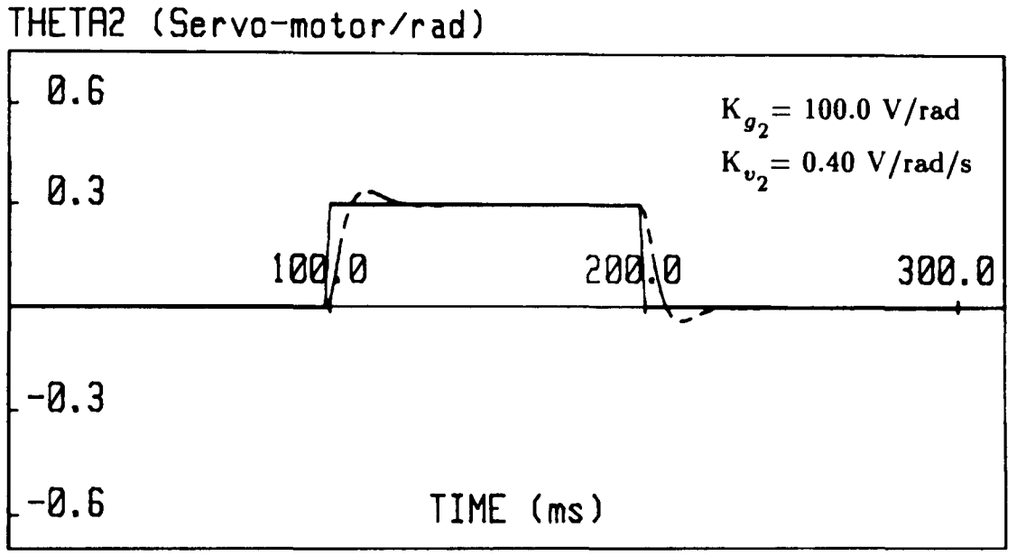

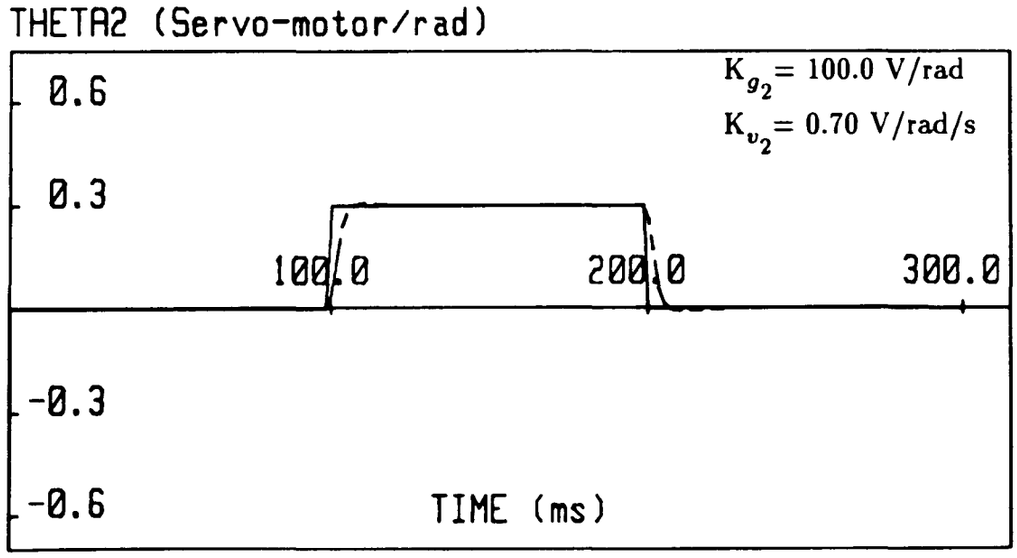

Command ———— Modelled response — – – —

Figure 4.6. The servo-motor responses for Finite Impulse Function.

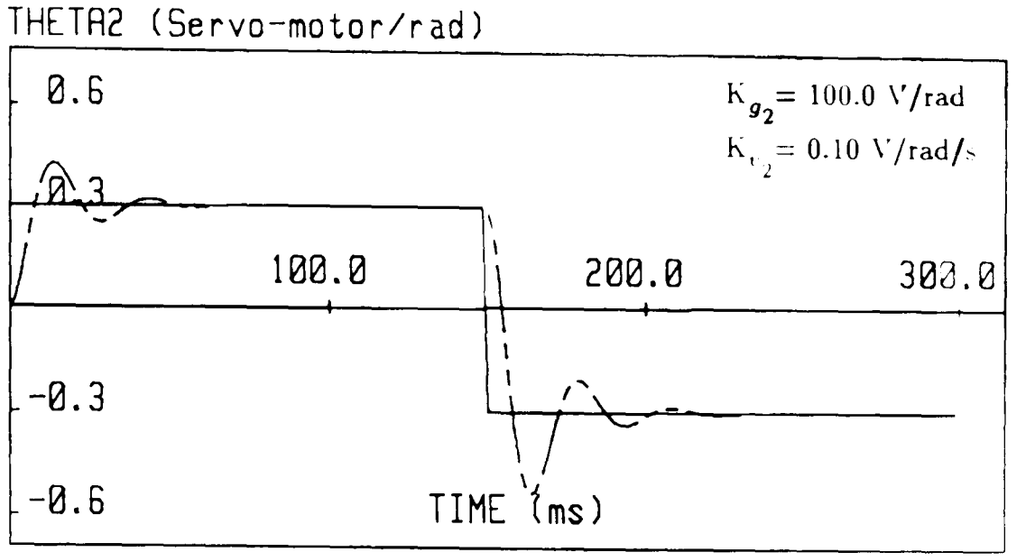

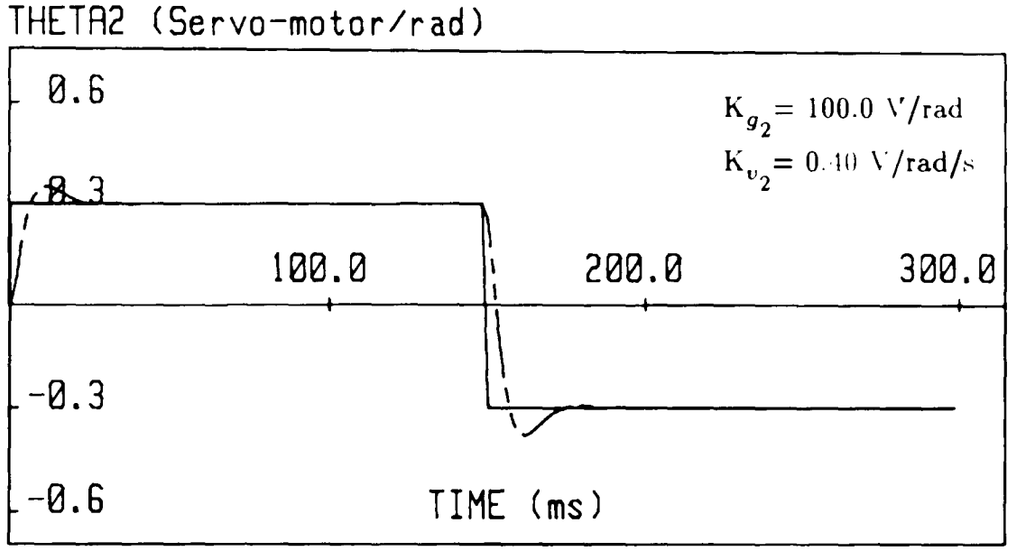

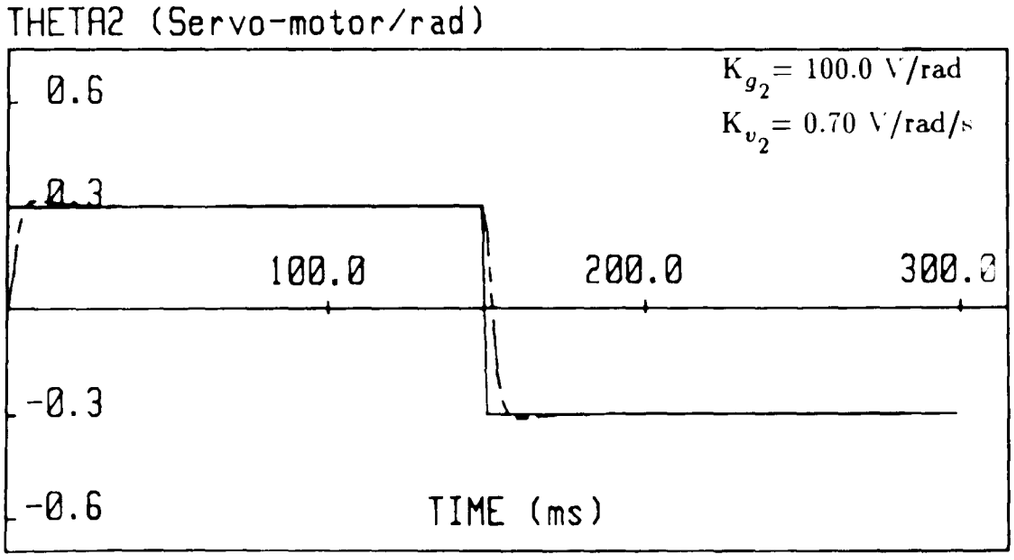

Command ———— Modelled response — — — —

Figure 4.7. The servo-motor responses for Square Waveform Function.

The same proportional and derivative gains used for the above example are applied for this example also. With increasing derivative action, the existing transients are entirely eliminated as expected.

4.5. The System Responses for the Hybrid Arrangement

After studying simplified examples, when all details and components are included, the hybrid arrangement is studied as a whole with two separate inputs θ_1 and θ_2. Figure 4.8 shows the two input model with coupled motors, the differential gear-unit and with a slider-crank.

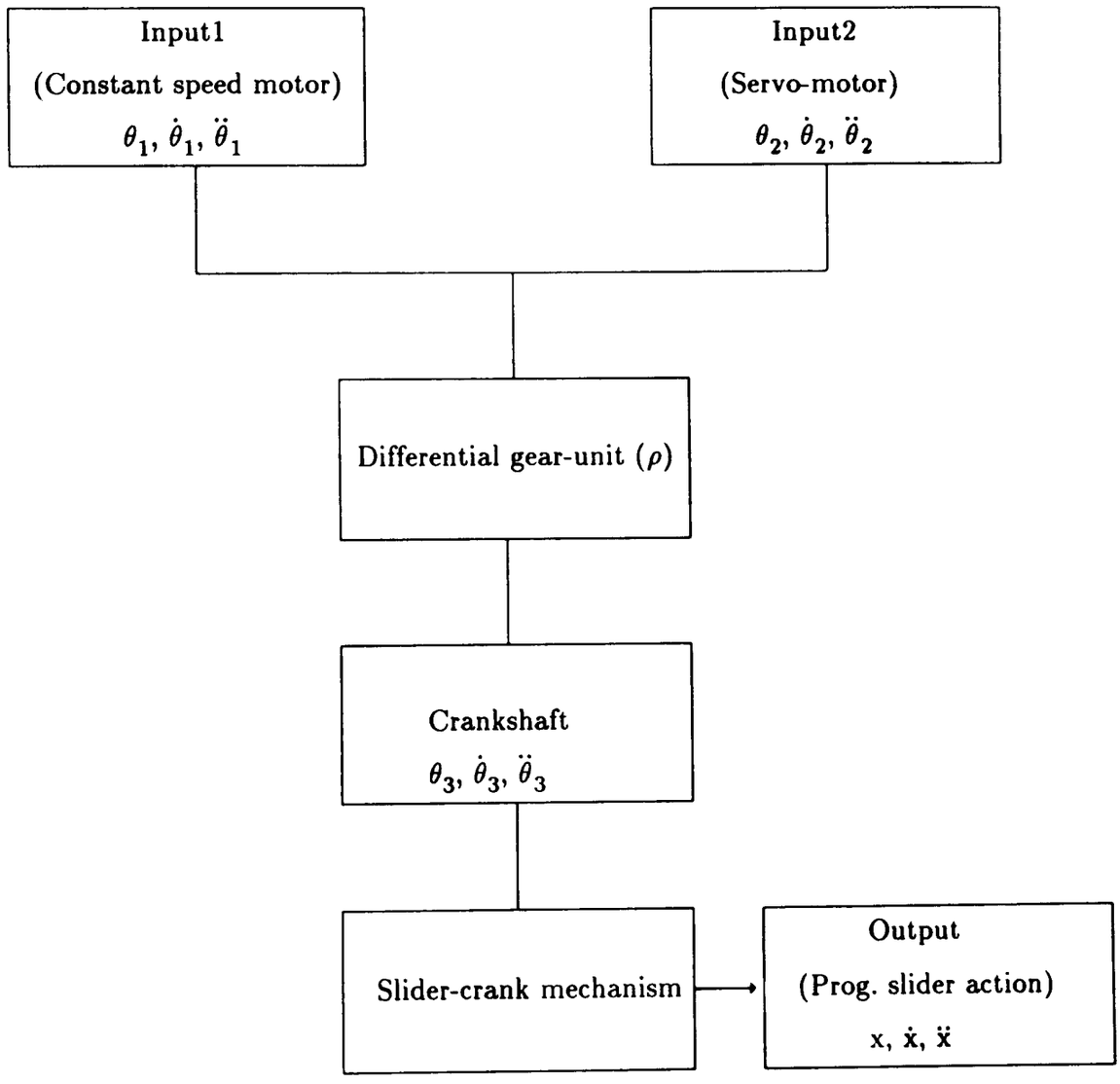

Figure 4.8. Two coupled motors, the hybrid arrangement.

Equations (4.12) to (4.15) are used to obtain the general form of the mathematical model. They describe a two degrees of freedom system subjected to a ramp input for the first coordinate, θ_1 from the constant speed motor and a continuously varying form of sinusoidal input for the second coordinate, θ_2 from the servo-motor. The numerical data for the links lengths and the motors are the same as given in the above section. The system is assumed to be running in ideal conditions free from losses and friction.

4.5.1. The System Response for the R-R Motion

First the response examples are obtained for the R-R motion. In this the specific motion the requirement is to provide quicker forward and slower return stroke also control the slider velocity during the return motion by superimposing the input from the servo motion on the fundamental constant speed motion.

Here we have two first order linear and two second order nonlinear equations. Using the Runge-Kutta integration program, these equations are solved separately for each motor by using zero initial values for θ_1, $\dot{\theta}_1$, $\ddot{\theta}_1$ and θ_2, $\dot{\theta}_2$, $\ddot{\theta}_2$. The incremental time, Δt is 1.66666 ms in the entire motion cycle. In order to improve the accuracy in the calculations, an inner loop is included for the current and angular displacement of the motor in the program. This loop repeats itself for the same data point by reducing Δt to 0.16666 ms. The calculations are continued for two cycles, about 600 ms and dc constant speed motor rotates approximately 1500 rpm. By using equations (4.12) and (4.13) with required voltage values and solving them together with equations (4.14) and (4.15), the following system responses are obtained.

Figure 4.9 shows the responses for the first axis, θ_1 and $\dot{\theta}_1$ with proper gain values in an open loop control. $\dot{\theta}_1$ reaches its required steady state value after nearly 200 ms starting from zero. The optimum proportional and derivative gains are found to be K_{g_1}=171.0 V/rad and K_{v_1}=0.0 V/rad/s.

Previously, the necessary servo-motor input command points θ_2 and $\dot{\theta}_2$ had been found from the inverse solutions in the previous chapter. They were stored, from the beginning, as a data file and when necessary they had been loaded as input command points for the R-R motion.

Figure 4.10 shows the responses for θ_2 and $\dot{\theta}_2$ starting from zero initial conditions and running for two cycles. Equation (4.14) has been used for the calculation of the current value of the servo-motor as a result of proportional-plus-derivative control action. The transients are not dominant in this part. The gain values for the servo-motor are K_{g_2}=80.0 V/rad and K_{v_2}=3.0 V/rad/s. It must also be noticed here that both response calculations are needed to be calculated simultaneously. This was because of the nonlinear coupling characteristics of the derived differential equations, such that each axis includes the time derivatives of the other one in it.

Finally after obtaining the response curves for two motors separately, the crankshaft output is found by using kinematic relationship from the differential gear-unit. This relationship is given in equation (4.5). Figure 4.11 gives the system response on the crankshaft, the angular displacement and velocity as θ_3 and $\dot{\theta}_3$ with command points.

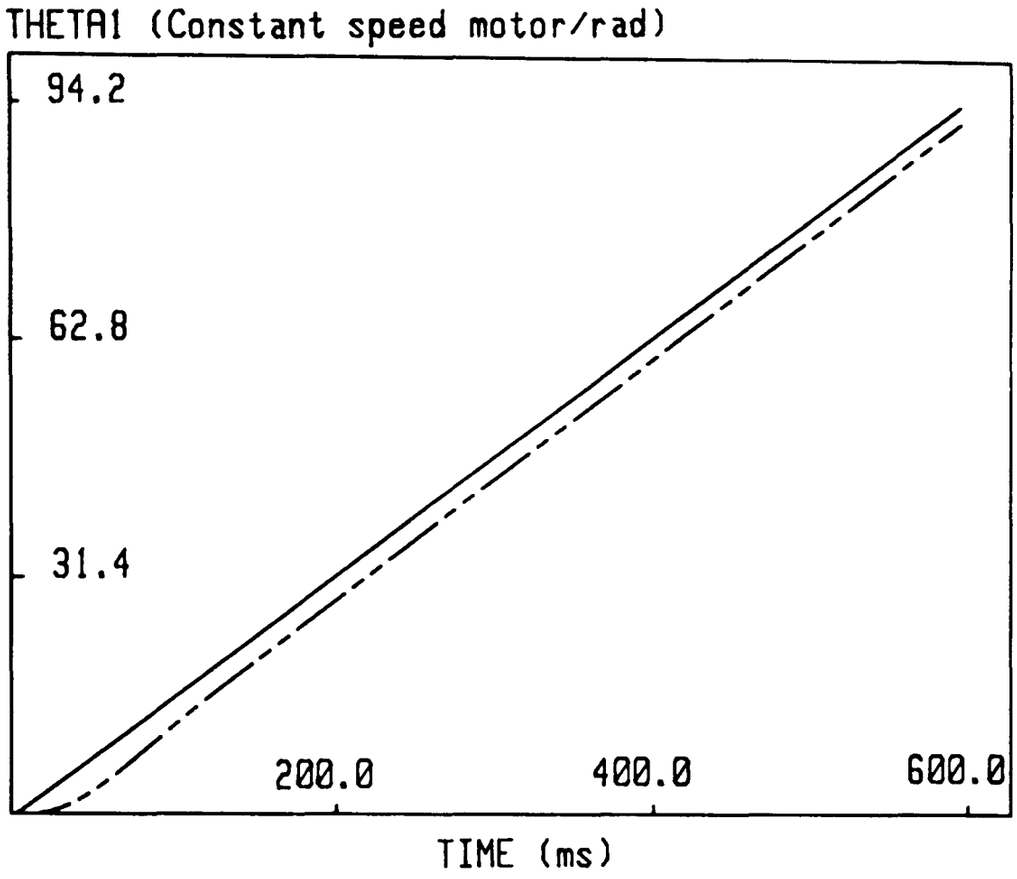

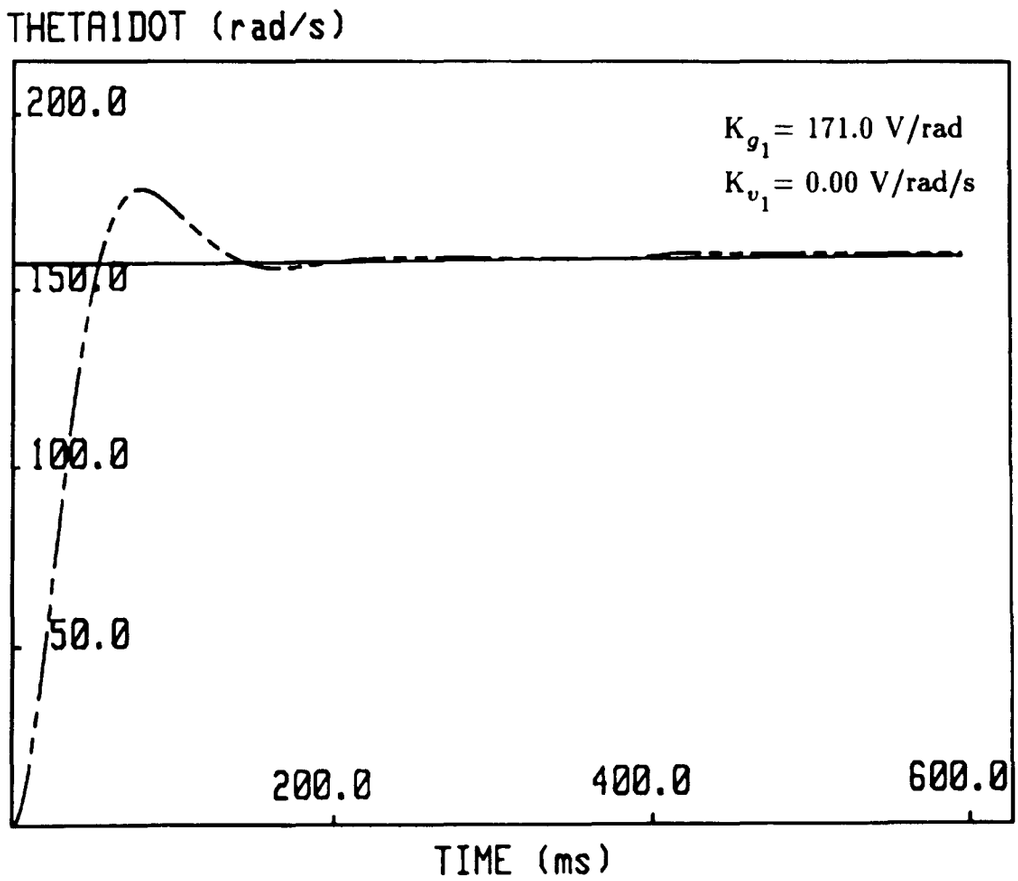

Figure 4.9. The constant speed motor response for the R-R motion.

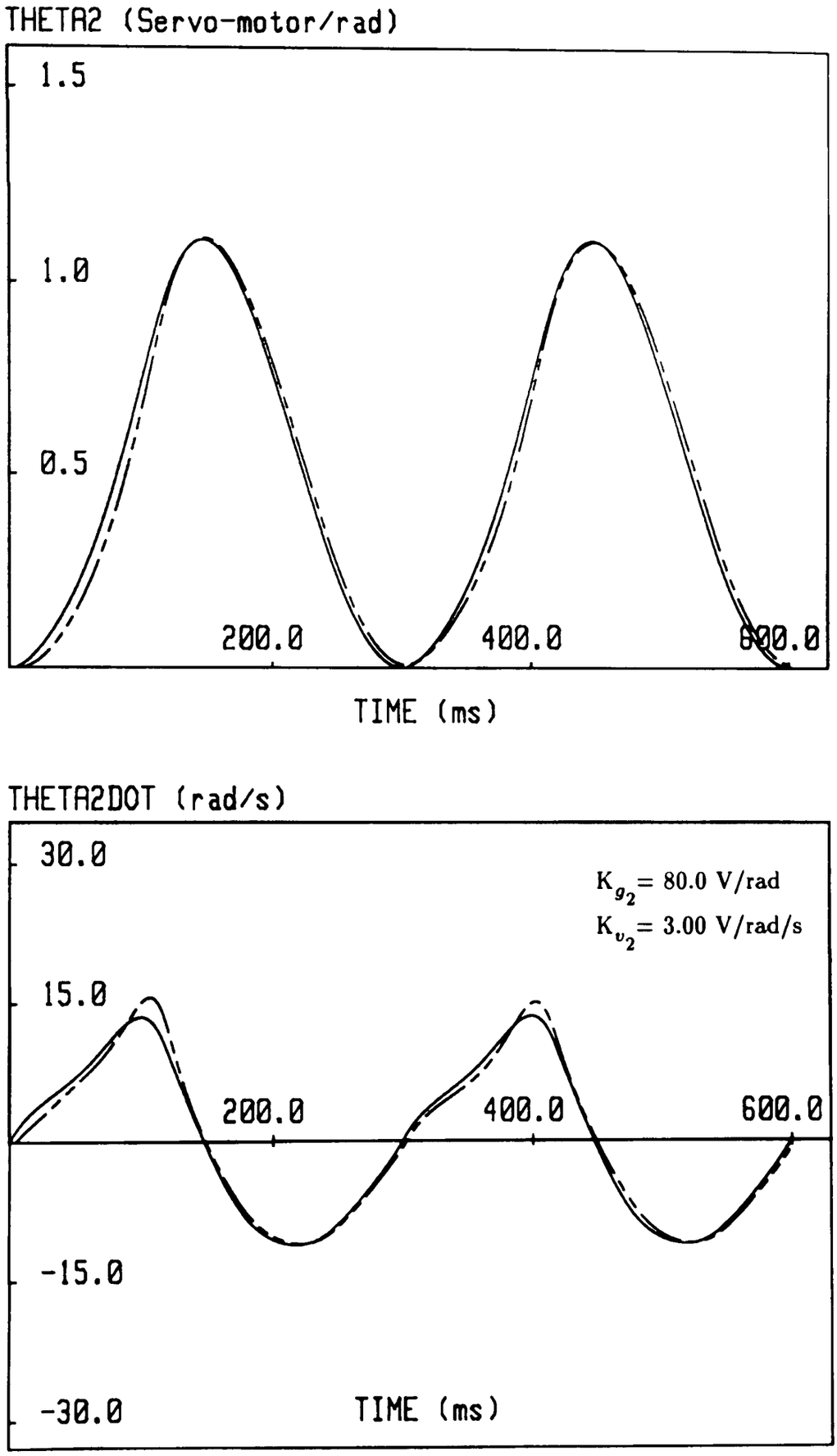

Figure 4.10. The servo-motor response for the R-R motion.

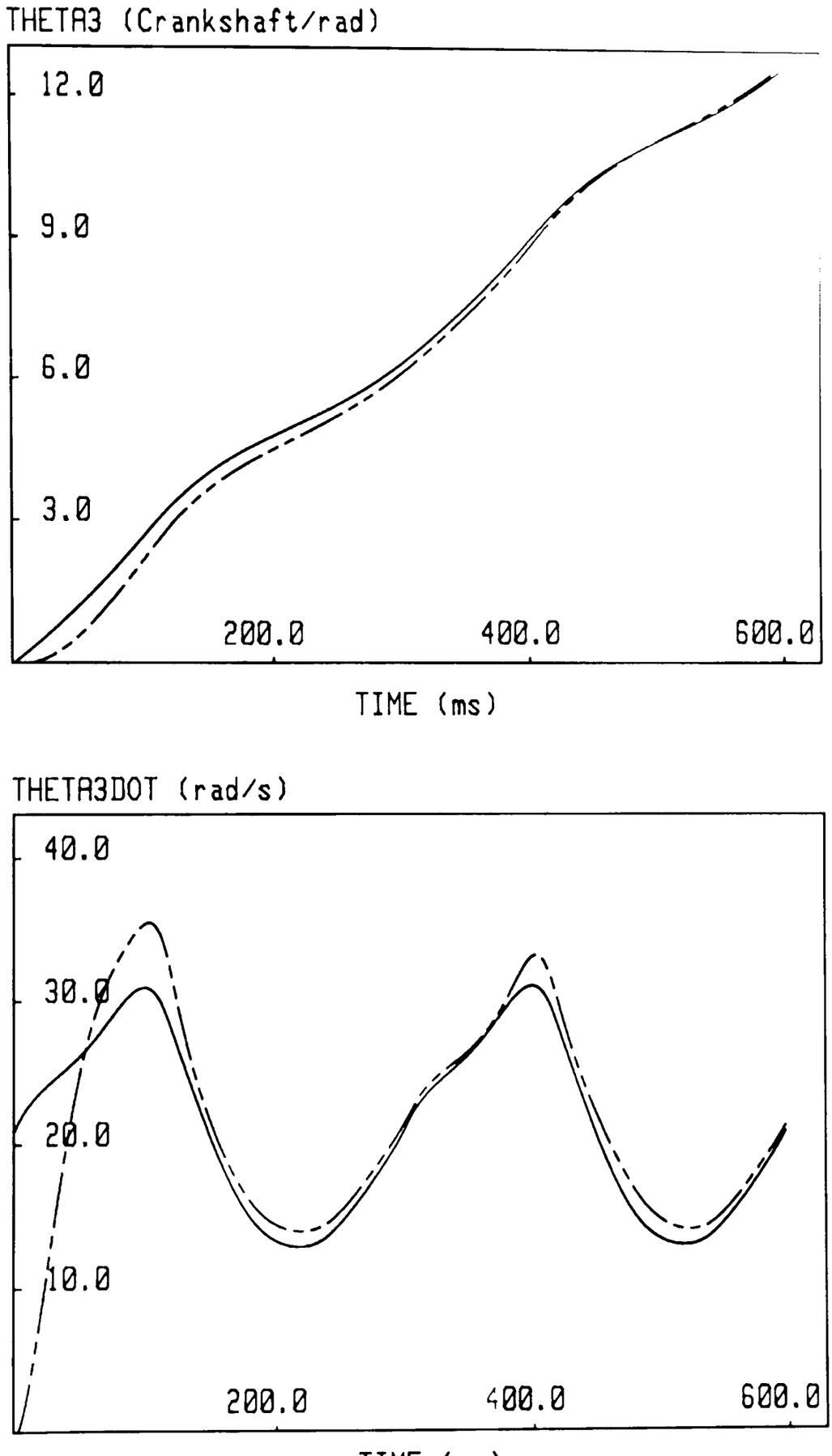

Figure 4.11. The crankshaft output for the R-R motion.

Because of the initial transients at the dc constant speed motor, from Figure 4.9, the effect of these transients is observed in the first running cycle of Figure 4.11. But it can be noticed here that transients diminish as a result of damping and smooth response curves are obtained in the second cycle.

4.5.2. The System Response for the R-D-R Motion

The second example is the R-D-R motion. In this motion, the dc constant speed motor rotates at approximately 750 rpm while synhcronizing with the servo-motor. The necessary servo-motor motion points have been found from the inverse solutions in the previous chapter. The motion data points were prepared to be used here as the servo-motor input command. The motion is continued over 600 ms, longer than first example. The time interval, Δt is taken to be equal to 3.33333 ms. Equations (4.12) to (4.15) are then solved by loading new input motion command points by changing Δt in Runge-Kutta integration program.

Figure 4.12 represents the responses for the dc constant speed motor over about 1200 ms for a given ramp input. As it can be seen from the angular velocity response, after starting from zero initial conditions with a given fixed voltage, $\dot{\theta}_1$ reaches its required steady state in about 300 ms. The proportional and derivative gains are set as K_{g_1}=85.0 V/rad and K_{v_1}=0.0 V/rad/s respectively.

Since the mixed acceleration terms for the constant speed motor and the servo-motor are included in the differential equations of motion because of nonlinearity, the constant speed motor angular velocity response shows some kind of cyclical variation as expected. This variation is a very small percentage of the rated output velocity indeed. It does not effect the overall motor output very much.

While solving the equations for the constant speed motor, by repeating same solution procedure with the equations for the servo-motor, the motor responses in Figure 4.13 are obtained with suitable values of proportional and derivative gains which are K_{g_2}=50.0 V/rad and K_{v_2}=1.70 V/rad/s respectively.

Finally these responses from Figure 4.12 and Figure 4.13 are summed by using the kinematic relationship for the differential gear-unit given in equation (4.5) to get the crankshaft output as total θ_3 and $\dot{\theta}_3$. They are given in Figure 4.14.

Here because of the initial transients in Figure 4.12, their effect is seen in the first running cycle in Figure 4.14. But they are completely eliminated in the second cycle.

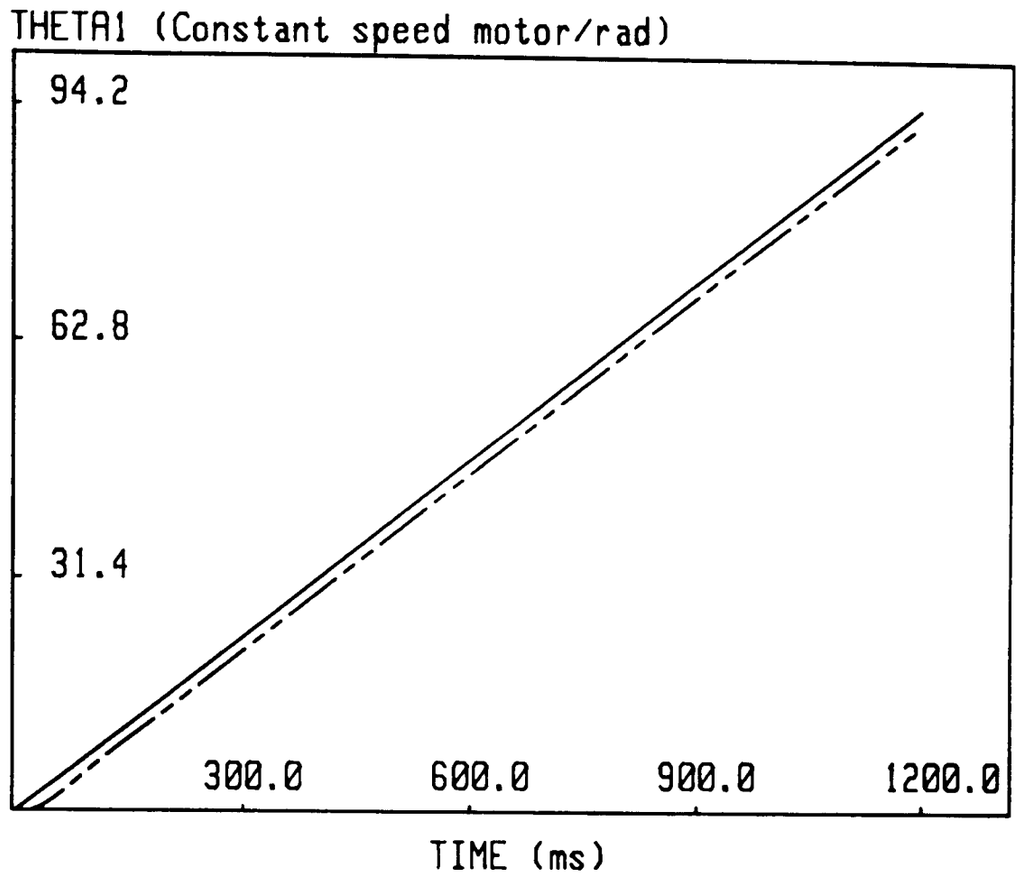

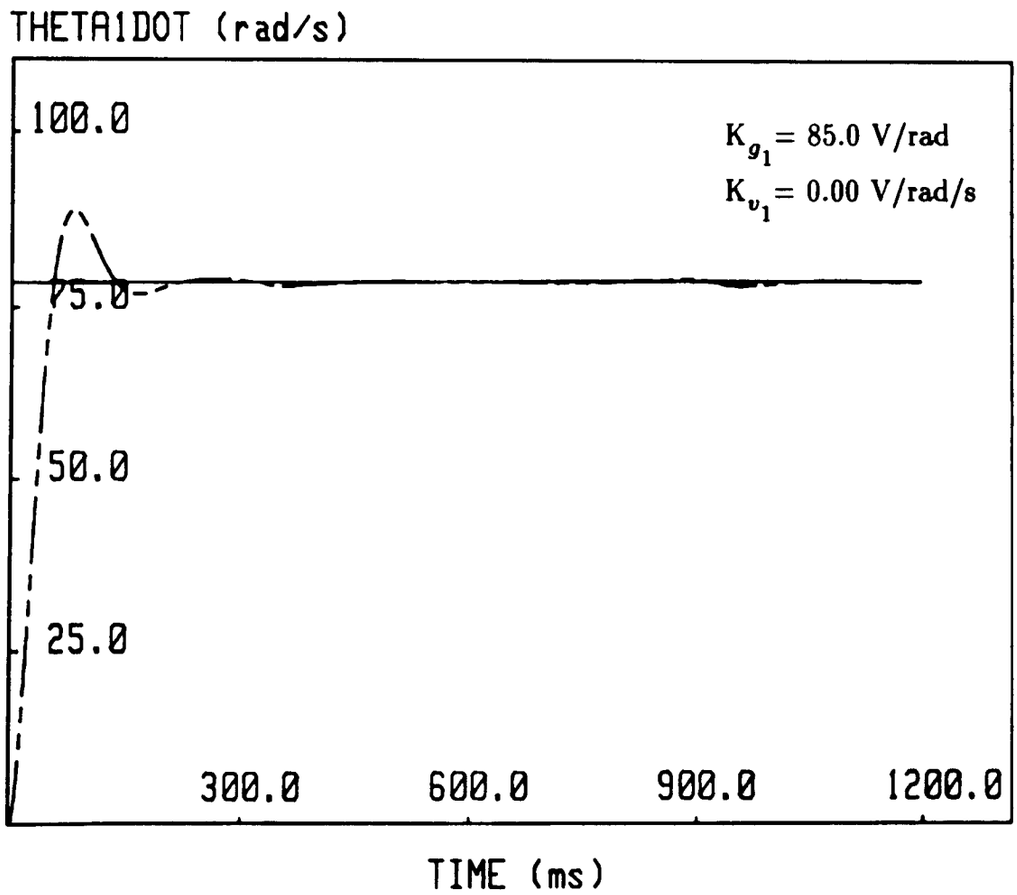

Figure 4.12. The constant speed motor response for the R-D-R motion.

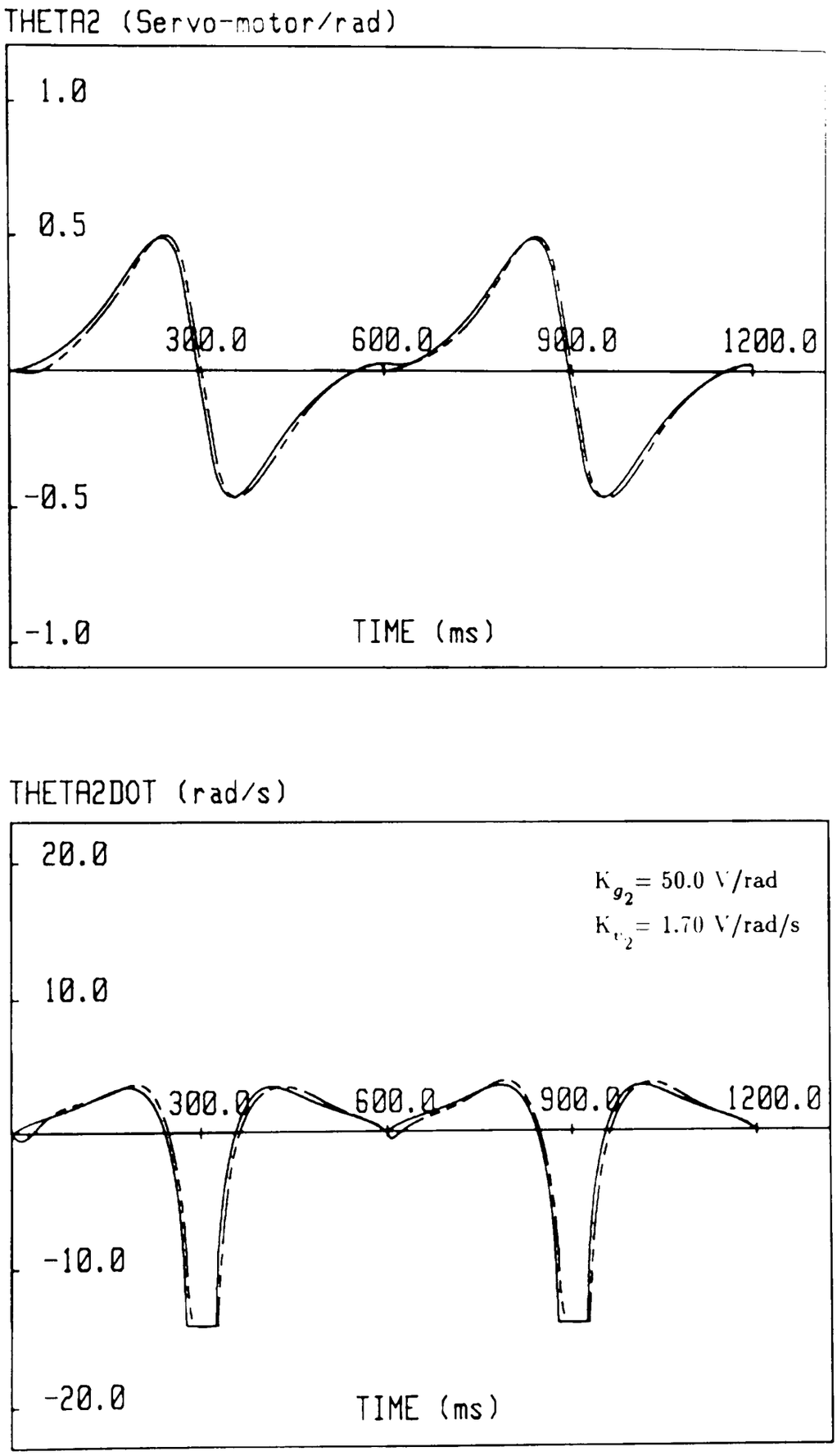

Figure 4.13. The servo-motor response for the R-D-R motion.

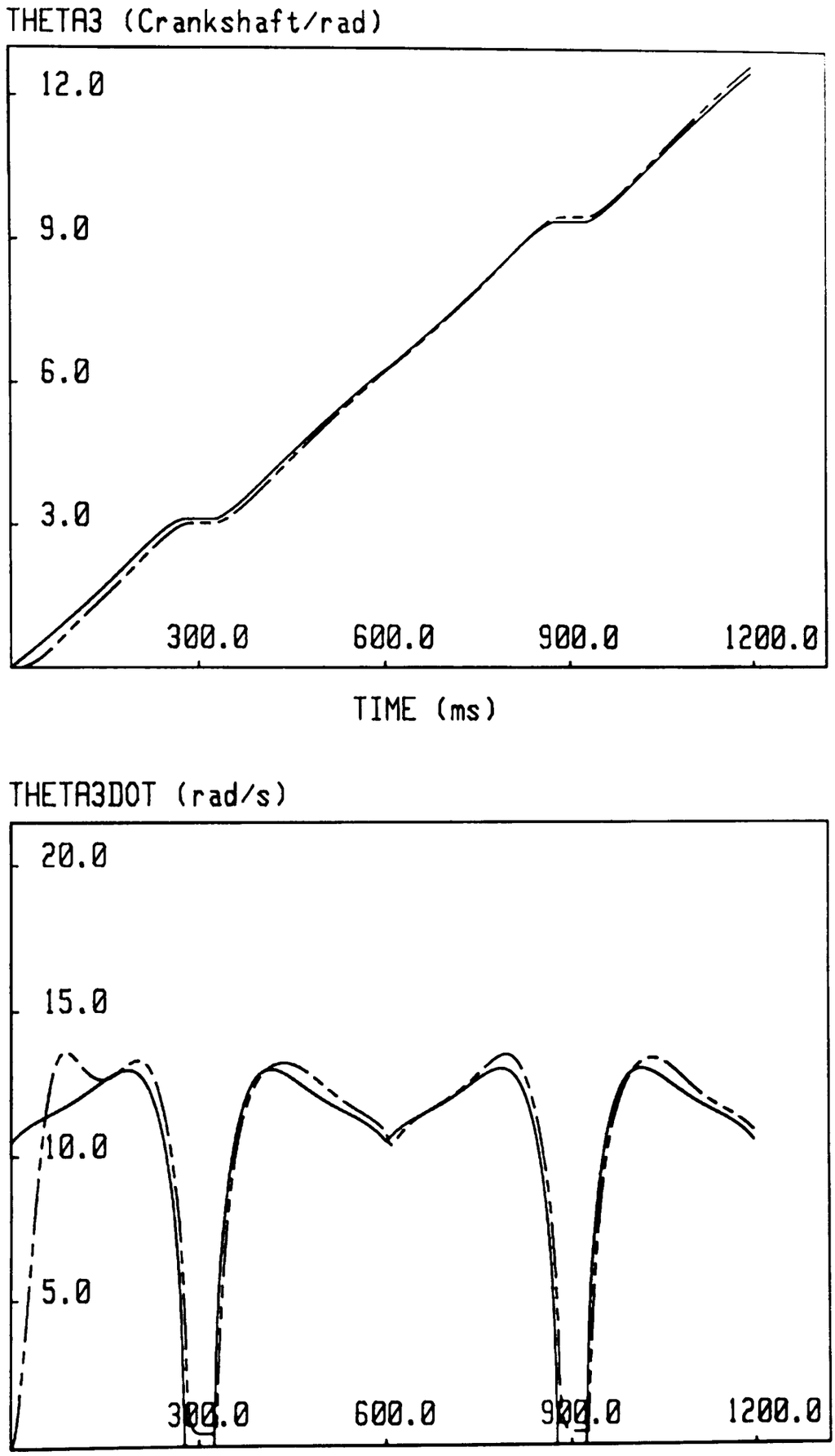

Figure 4.14. The crankshaft output for the R-D-R motion.

Obviously it is possible to obtain various response characteristics by continuous alteration of the gain values. First the proportional gain is adjusted without the action of damping. After finding a suitable K_{g_2} value, K_{v2} is changed to attain the best matching output response curve. When the value of K_{v2} is decreased, the responses in the vicinity of the dwell happened to be more oscillatory. However, when its value is increased slowly, the response is recovered to give a smooth 50 ms period of dwell as required.

4.5.3. The System Response for the R-R-D Motion

The final example for the system is studied for its response to the R-R-D motion. The input for θ_1 is a ramp function, giving approximately constant speed output, and the other one for a varying input θ_2 found from the inverse solution in chapter 3. It is given in Figure 3.11.

In this motion, the operating conditions are similar to the previous dwell motion which requires the dc constant speed motor to run at 750 rpm. The interval used Δ t is 3.33333 ms. The applicable dwell period is about 60 ms. Equations of the system from (4.12) to (4.15) have been solved here by using the same program again. The first set of outputs for θ_1 and $\dot{\theta}_1$ are nearly same as the ones obtained from the previous example in Figure 4.12. Here all system responses results are presented for two running cycles.

The constant speed motor response is given in Figure 4.15 where a fixed voltage is applied to the armature. The steady state response is obtained in about 300 ms. The optimum gains for the constant speed motor responses are found as K_{g_1}=85.0 V/rad and K_{v_1}=0.0 V/rad/s for the proportional and derivative action respectively. These gains are the same as used in the previous motion example.

The servo-motor response is shown in Figure 4.16 by using K_{g_2}=50.0 V/rad and K_{v_2}=1.70 V/rad/s as proportional and derivative gains respectively.

Finally by summing these two response curves, one for the constant speed motor and one for the servo-motor with a previously known relation for the differential gear-unit using equation (4.5) , Figure 4.17 is found as total crankshaft output. In Figure 4.17 the effect of initial transients from Figure 4.15 is seen in the first motion cycle. But they are eliminated completely in the second motion cycle like in the previous motion examples.

The alteration of gain values made possible to observe different motor response curves. Evidently all the responses for the R-R-D motion are obtained smooth as expected with good following characteristics as a result of properly set gains.

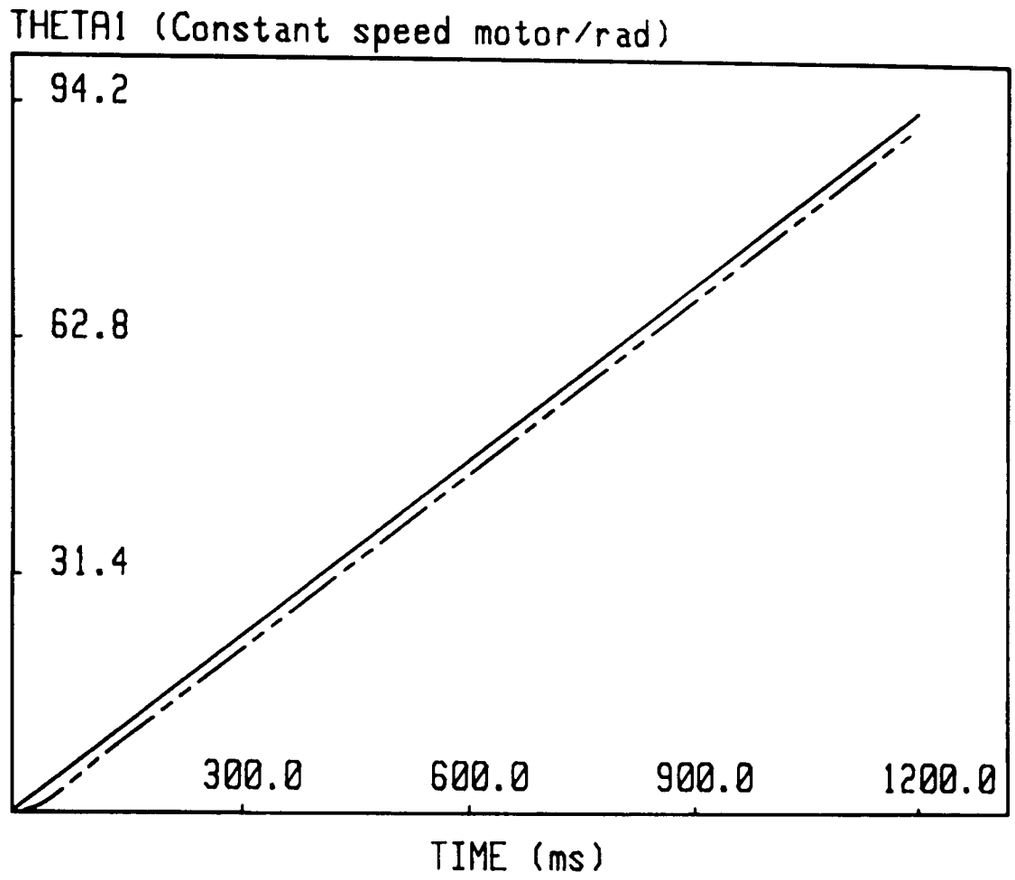

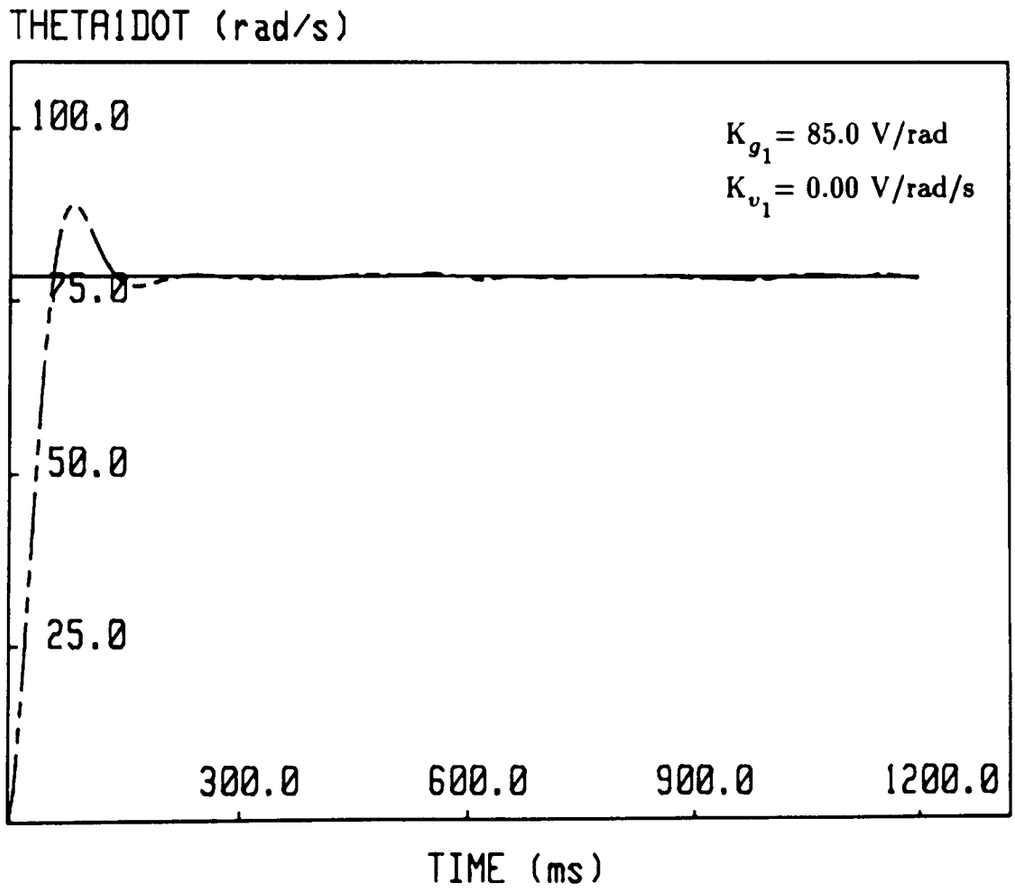

Figure 4.15. The constant speed motor model response for the R-R-D motion.

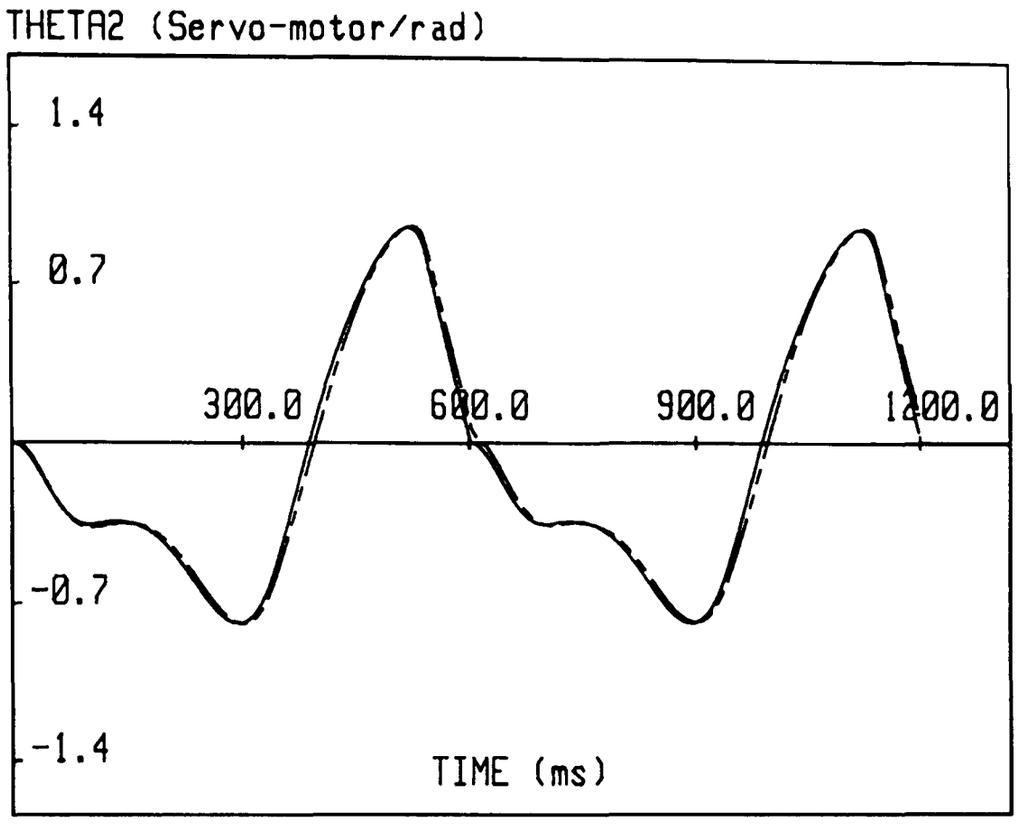

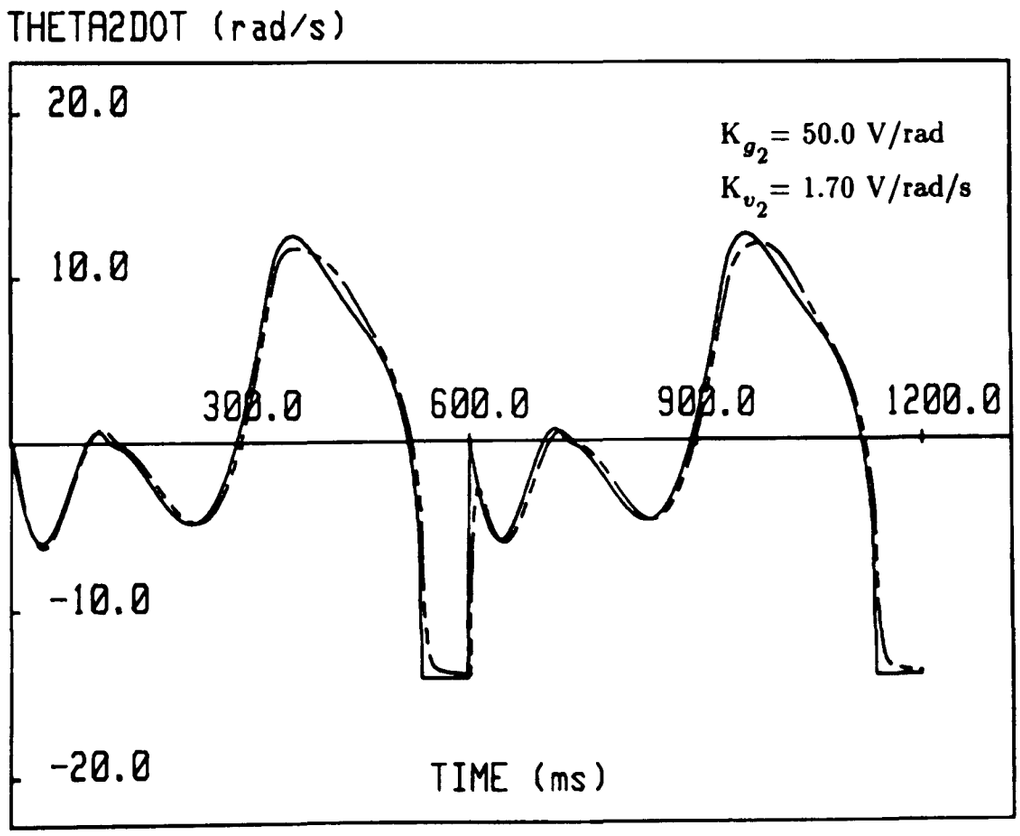

Command ———— Modelled response — — — —

Figure 4.16. The servo-motor response for the R-R-D motion.

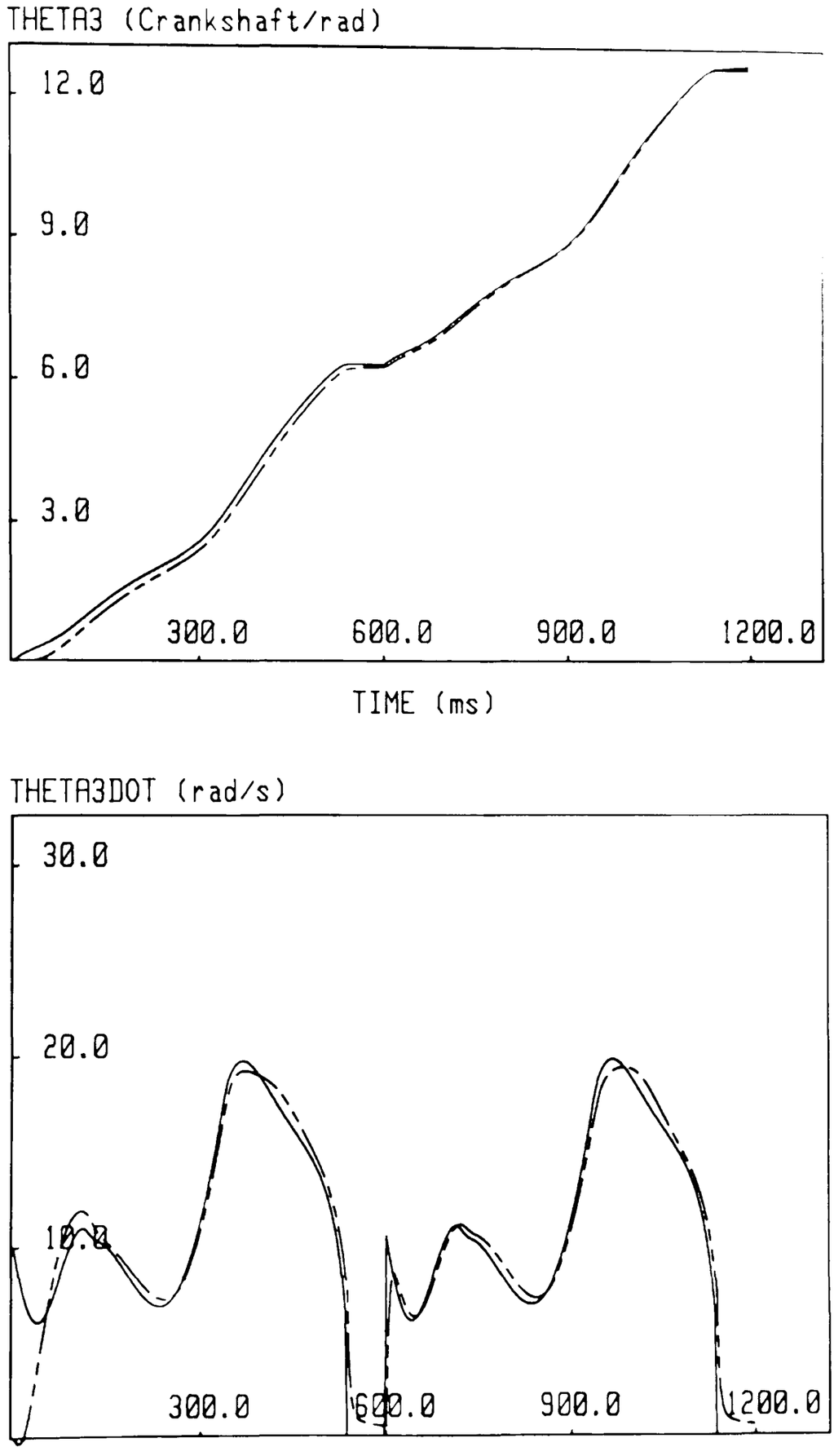

Figure 4.17. The crankshaft output for the R-R-D motion.

4.6. Conclusion

A mathematical model of the hybrid arrangement has been presented in this chapter. The differential equations of motion describing the dynamics of the system were utilized to understand and control this arrangement. The derived system equations of motion were studied for different running conditions, whether the system represents single degree of freedom or two degrees of freedom depending upon the assumptions made from the beginning.

Within the general layout of this chapter, the static and dynamic characteristics of dc motors were obtained, as dc motor characteristic curves. Standard functions were applied to verify the derived equations together with various assumptions for the total time response of the system. The hybrid arrangement was then studied for three different motion cases.

Having observed good matching between the system command and responses, at this point it could be said that the derived mathematical model has formed a basis for the investigation of the behaviour of hybrid machines. In the developed mathematical model, a compromise between the simplicity of the model and the accuracy of the results of the analysis has been achieved.

CHAPTER 5
COMPUTER CONTROL ISSUES

5.1. Introduction

In any computer control system, before used for any machine motion purpose the system functional tasks and the required levels of control have to be decided upon. The hardware requirements are then considered to accomplish these tasks, i.e: the control algorithm, computer program, sampling, conversion between analog and digital signal domain requirements.

The purpose of this chapter is to present an extensive discussion on the computer control issues for the hybrid arrangement. Initially a summary of the main control scheme and its functional levels is included. Shannon's sampling theorem is used as a guide in determining the minimal sampling rate. The specification and design of the control hardware is then presented. Using the control system, some response examples are studied and presented for the characteristically different motion profiles. Command motion tuning is introduced to the system. In this the command is modified to minimize the error between the required input and the actual output and to attain the desired response.

5.2. Control Scheme

By referring to chapter 1, Figure 1.1, the hybrid arrangement includes the basic components necessary for a motion control system, the motors, sensors and the mechanism. The motion is generated by a dc constant speed motor and a servo-motor which is driven by an amplifier. The sensors are the incremental encoders whose functions are simply to sense the shaft positions for both motors.

In order to achieve the programmable slider motion using the hybrid arrangement, three different levels of control are required in the control strategy.

i) Closed-loop position control of the servo-motor is necessary. The output position is to be measured, fed back and compared to the desired input. The difference between the desired position and actual position is the error. This is amplified and a voltage equivalent is used to minimize that error.

ii) The constant speed motor would be a reference or master that the servo-motor input should be coordinated with irrespective of the speed of operation. Incremental changes in its rotation would generate a new position command for the servo-motor. These values would need to be read from a look-up table during the operation of the system.

iii) A correlation between the crank angle position and the slider displacement must be provided, such that, zero position of the crank should be sensed to start the main position control loop in (i). This is necessary to obtain the slider displacement data from its datum position.

The above control requirements are implemented and developed one by one to satisfy their functional tasks. An harmonic analysis of the required motions is carried out to find the minimum sampling rate.

5.2.1. Sampling Rate

The harmonic content of the desired command motion is very important in digital control systems. It basically determines the sampling rate necessary for the control scheme, and the following characteristics for the servo-motor.

The performance of a servo-motor is essentially limited by the bandwidth of the control system. It is desirable that the command motion possesses only harmonics within the bandwidth for good following. If high harmonics exist in the command then the motion will not be followed as well and saturation of the motor is likely to be unavoidable as a result of excessive current on the windings. Since the digital controllers require time sampled inputs and produce time sampled outputs, it is necessary that the sampling interval satisfies the system requirements and the system keeps all desired information about the sampled signal.

Shannon's Sampling Theorem [5.1] provides a guide on the question of how frequently the points must be sampled. The theorem specifies that *the sampling must take place at a rate at least twice the highest signal frequency of interest.* In other words, a sampled data system must sample the current value and convert the command value at a rate at least equal to twice the signal frequency under consideration. This frequency is typically increased by a factor 5 to 10 to improve performance.

Motions that are periodic and non-uniform can be expressed in terms of Fourier series. In order to determine the dominant harmonics of the motion a Fourier analysis is taken. To carry out the analysis a computer program is prepared. It is written in pascal. The servo-motor command data points which are found in chapter 3 are loaded into this program for the three designed motion cases one by one. The amplitude of each harmonic is then calculated and normalized against to the first harmonic. This is performed upto the 20th harmonic. The original motion is then displayed by using the built-up profile and the following points are determined.

a) the necessary bandwidth that the closed loop must achieve.

In the application of the R-R motion, the constant speed motor rotates at 1500 rpm resulting in 200 rpm at the crank. This gives a motion period of 300 ms. If the motion harmonics are noticeable up to 10th, then the 10th harmonic has a period of 30 ms and the closed-loop bandwidth must therefore envelop 33.333 Hz frequency.

b) the necessary sampling time of the controller.

The selection of the sampling frequency depends on various system characteristics. In general, it is dictated by noise, data quantization etc. in the system. Starting from the system's highest frequency of interest, *Shannon's theorem* is satisfied at 10 times of the highest frequency.

5.2.2. Coordination of the Constant Speed Motor and the Servo-Motor

The hybrid arrangement seeks to obtain coordination between both inputs. It is essential to have an electronic link between the constant speed motor and the servo-motor. This can be achieved by an incremental encoder fixed on the constant speed motor shaft to provide coordinating pulses.

Since the bandwidth criterion dictates 3 ms sampling interval for the R-R motion, 100 data points must be loaded from the servo-motor. This is to achieve its closed loop position control in 300 ms motion cycle. By taking 100 data points and going back from the crank to the differential gear-unit and the belt reduction, the constant speed motor has to produce 14 ppr (pulses per revolution) for complete motion matching.

However, here the position information is obtained from the nearest available encoder pulse derived at 40 ppr from the constant speed motor. This shows 100 samples would not be adequate. In other words, the points must be sampled in less than 3 ms. What is needed is to

provide more data points for the servo command to compensate with the available pulses from the second input, the constant speed motor. The phase difference between two inputs must essentially be avoided. Otherwise two motions would be out of phase at this speed with obvious disastrous results for the programmable slider output. Whence the motion derived from the servo-motor would not be successfully superimposed on that produced by the constant speed one and the complete motion matching will obviously be lost after some cycles.

We may start using 40 ppr, then, considering the belt and the differential gear-unit reductions, 288 samples are resultantly required to be loaded from the servo-motor. This provides a sampling time of 1.041 ms for 300 ms overall cycle time. Therefore, the servo motion command data files are prepared for 288 samples from the inverse solutions given in chapter 3.

Sampling time is also found as 6 ms from the bandwidth criterion in the dwell included motion examples. Since the motion coordination between both motors is essentially required, 288 samples have been loaded for the implementation of the R-D-R and R-R-D motions. The sampling time is found to be 2.04 ms for each sample.

5.2.3. Other Issues

Another important issue in the control scheme is the correct phasing between the measured crank position and the slider displacement. This can be provided from the generation of a reference pulse which allocates a certain angle position. Such as zero crank angle corresponds to zero datum displacement of the slider. Whence the encoder marker pulse can act like an electronic trigger that activates the main servo-control loop. The slider displacement can then be measured by a linear potentiometer and digitized in the control hardware arrangement.

Although the sampling time of 3 ms is found from the bandwidth criterion for the R-R motion, by considering available sensors the sampling time of 1 ms is applied for perfect following using 288 samples. The system operated at lower speeds for the R-D-R and R-R-D motion examples, so the selection in their case is made about 2 ms.

The above mentioned points are found during the practical application. There are also some other problems and limitations on the system hardware that are tackled during the study. They are described below.

In order to attain good results, the cost of the control-system is considered to be an effective factor in the selection of an acceptable sampling time. How fast sampling can be achieved

depends on the speed of the digital devices and the clock frequency of the available computer. A faster sampling rate leaves less computational time. But sampling at too high a rate can detect noise and other system disturbances which are not wanted for better system performance. Another point is that making the sampling interval very short necessitates greater resolution in the feedback sensor. Generally a compromise between required accuracy and cost gives the optimal sampling frequency for the system.

The resolution of an encoder is the total number of signal cycles per revolution and corresponds to the number of line in the encoder grating. The resolution of 10000 on the servo-motor is equivalent to a measuring step of 0.036° at the motor shaft. This is adequate for the servo-system requirement. The same encoder resolution is also used on the crankshaft for data acquisition reasons.

The function of a Digital-to-Analog Converter (DAC) is to transform a digital number into a voltage output which can be used to drive the amplifier and the servo-motor. Its resolution depends on the number of bits in the digital signal which have to be converted. The commonly available types are 8 or 12 bits; i.e: 8 bits allowing a resolution of 256, 12 bits allowing a resolution of 4096. High resolution DAC's transmit smoother voltage output for the changes in inputs.

Similarly an Analog-to-Digital Converter (ADC) transforms an analog signal to a digital number through the slider output measurement. The number of bits used to code the incoming analog signal determine the resolution of the digital representation of that signal. The commonly available ADC's are of 4, 8 and 12 bits resolution.

In signal conversion, 12-bit DAC and ADC's are used in the designed control hardware arrangement.

5.2.4. Controller Hardware Requirements

To summarize the above, it is found that the controller is required to:

- sample not less than 1 kHz
- read incremental counts from the motor encoder
- provide a 12-bit resolution DAC for the feedback
- read slider displacement data with 12-bit resolution ADC's
- coordinate the constant speed motor with the servo-motor
- perform the required non-uniform displacement motions.

Coming section explains the controller hardware arrangement in detail.

5.3. Hardware Architecture and Interface for the Controller

The above control requirements are implemented with a digital control hardware arrangement developed by 'Mechanisms and Machines Group' of Liverpool Polytechnic. It had previously been successfully applied in the control and coordination of a pantograph type linkage for a carton erection machine [2.1].

The control system is built around the memory mapped Input/Output (I/O) channel of a VME/10 68010 microprocessor development system. The main controller software is written in two parts, one in pascal and the other in Motorola 68000 machine code. The schematic representation of the control hardware arrangement is shown in Figure 5.1. The parts are explained individually as follows.

The Input/Output (I/O) Channel

The I/O channel provides a communications path through to the 68010 microprocessor and I/O devices. The I/O channel provides the following features:

- 12 bit address bus
- 8 bit bidirectional databus
- asynchronous operation
- up to 2-megabyte transfer rate
- four interrupt lines
- reset line
- 4-MHz free running clock-line

I/O channel interface links the local on-board bus to the I/O channel cable for communication to any optional I/O cards installed. The I/O channel allows the master 68010 to perform read and write operations to I/O slave devices such as controller cards.

The Arbitrator Board

The arbitrator board is responsible for the protocol between the controller hardware and 68010 microprocessor. It is housed within the VME/10 system using a single euro-card.

In data transfer protocol, all data transfers on the I/O channel are between the master 68010 and the slave and are initiated by the master.

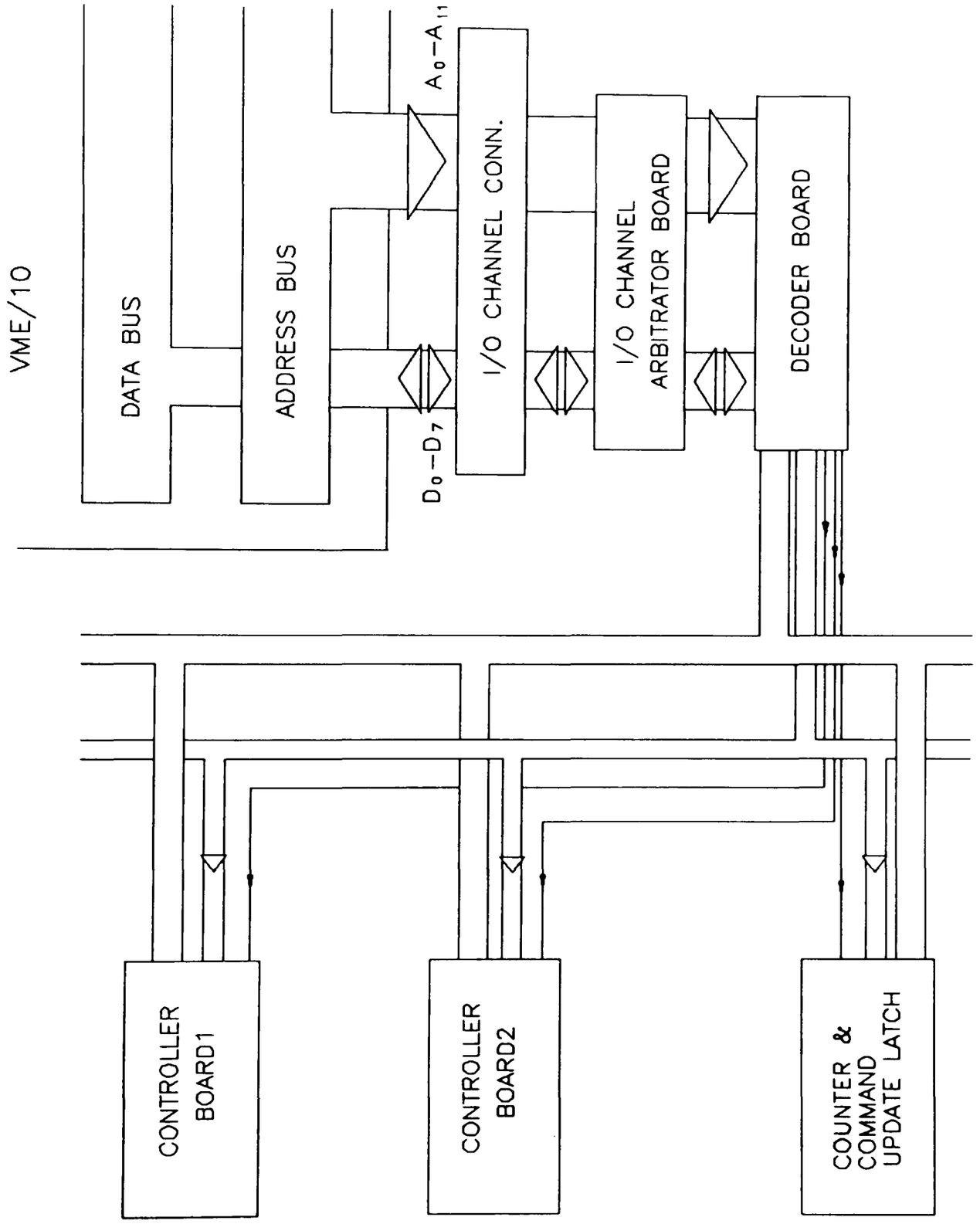

Figure 5.1. Control Hardware Arrangement.

All data transfers are asynchronous and dependent on two interlocked signal lines, STB (strobe) and XACK (data acknowledge) which are both provided by the 68010 architecture. STB is generated by the master and initiates a data transfer. XACK is generated by the addressed slave to show data transfer has been acknowledged.

I/O channel signal lines for data and address are identified as A_0-A_{11} (address channel) and D_0-D_7 (data channel).

The Decoder and Timer Board

The decoder board can read the 12-bit address bus available to the memory mapped I/O Channel. Depending upon the bus address in the VME, bits A_3 to A_5 allow a board to be selected and bits A_0 to A_2 assign the devices on this board.

The I/O channel only has 8-bit data bus. Therefore, the decoder board arbitrates between the least or most significant bytes of the interface devices on the controller boards.

The Controller Boards

Two controller boards are available. One provides an interface with the programmable input of the differential gear-unit. The other has been used for experimental data acquisition and is not included in the control loop. The second board performs digital data conversion for the slider displacement also.

The communication between the decoder board and the controller boards is assigned as following. Each board has four address lines, A_0-A_2 and the controller board select lines from the decoder. Using the board select line, the controller boards can be assigned and four available devices are individually selected from each one of them.

The present specification for each board is:

- two 16-bit counters, as up-down counters for incremental encoders,
- a 12-bit Analog-to-Digital Converter (ADC),
- a 12-bit Digital-to-Analog Converter (DAC).

There is a reference address that corresponds to a different device on each board. The counters are HCTL2000 or equivalent THCT12016, incremental encoder interface chips. They

can operate in 8 different function modes as up-down counters to determine the direction and displacement of an axis based on two input signals from incremental encoders; it can measure a pulse width using a known clock rate, or a frequency by counting input pulses over a known time interval. In order to enable operation of different modes, proper jumper connections must be chosen on the board. 12-bit ADC and DAC can also be set $\mp$ 5 Volts or 10 Volts using jumpers available on each board.

The Counter and Command Update Latch

In the hybrid arrangement, the servo-motor interacts with any other driving motor which means that the coordination of both motors is essentially required. There must be an electronic master which drives the set of points to control the other axis. Thus the slave axis can be position locked with the master axis giving its position as a function of the master's. However, if the system is restricted to controlling the servo-motor without any other interaction, a closed-loop position control would be adequate.

The above requirement has been achieved within the hardware using a single board referred as a 'Counter and Command Update Latch' (CCUL). This board includes a counter and a device that may latch the leading edge of a pulse supplied by an encoder on the constant speed motor. In the control loop cycle, the counter is set to sample at 2 kHz whatever the constant speed motor input is. The clocked counter has a value to decrement to zero in 0.5 ms. After the zero value has been recognized, the counter is reset by the microprocessor causing the latch to be addressed. It's state determines whether an encoder pulse has been received or not. If not, the control loop is performed around the same data point. If it has been processed, a new command point is then read from the 'look up' table and the error is determined.

The reference position for zero datum of the slider is enabled by using the crank encoder marker pulse. This pulse is processed in CCUL and occurs once per revolution in rotary encoders. The correlation between the zero crank position and the slider displacement data has been therefore provided. When the encoder marker pulse is recognized, the servo-control loop starts and measures exact displacement of the slider from its datum within the required control cycle time.

5.4. Command and Response Curves

The aim in this section is to get quicker servo-motor responses and also minimize the error between command and response without having any instability problem in the servo-system. This is achieved by adjusting the gain potentiometers that are one for the proportional and

the other one for the derivative action in the servo-motor amplifier board which is housed in the servo-amplifier.

Initially the servo-system is studied with an finite impulse function and a square waveform as well-known test signals. The hybrid system is reduced to have single degree of freedom, with input from the programmable drive only for these examples. The casing of the differential gear-unit is fixed so that it acts as a simple gear reducer. There is no requirement for the motion coordination.

In the present system, the microprocessor addresses the up-down counters. Therefore, the command data is stored in terms of encoder counts. Figure 5.2 shows a block diagram representation of the position control loop used for the servo-motor. In this position control loop, the microprocessor obtains a reading from the incremental encoder and generates an error value in the form of difference between the desired and the actual position. This error is expressed in units of resolution, such as encoder counts. It is then applied to the servo-amplifier via a DAC to drive the motor. The DAC interfaces between the digital output of the controller and the amplifier. Here additional feedback signal is generated by a tachometer which is integral with the servo-motor.

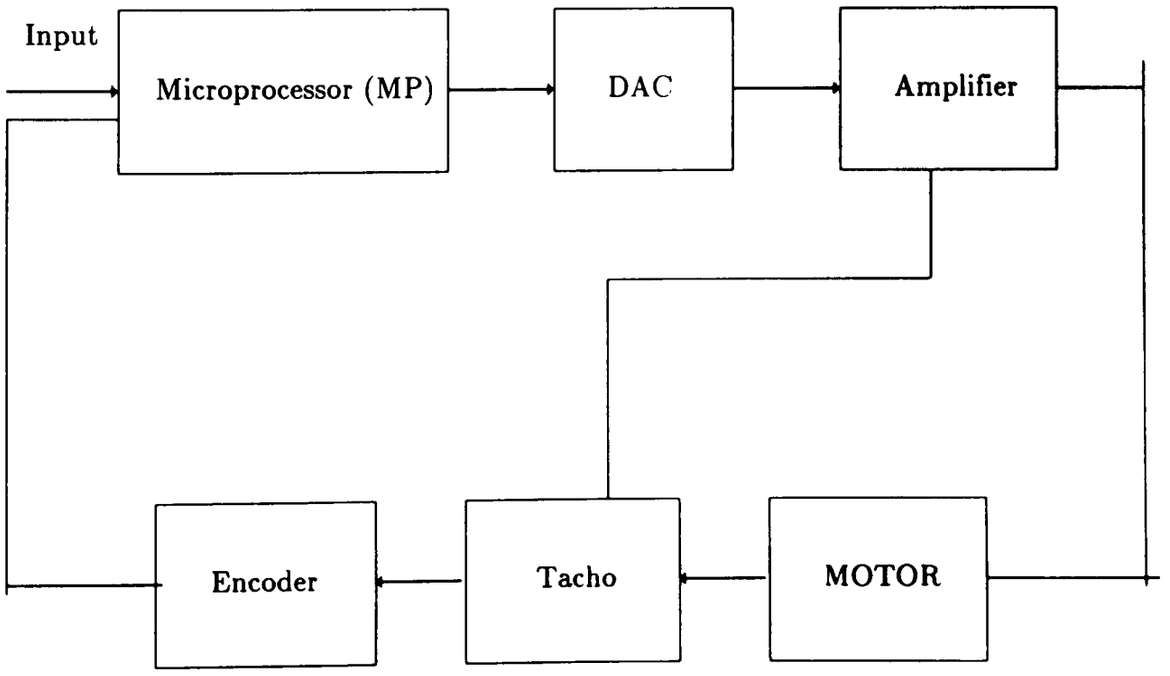

Figure 5.2. Position Control Loop.

Figure 5.3 shows the servo-motor command, response and error curves for a finite impulse and square waveform test input signals using 288 data points. The vertical axis is given in encoder counts and the horizontal axis in samples.

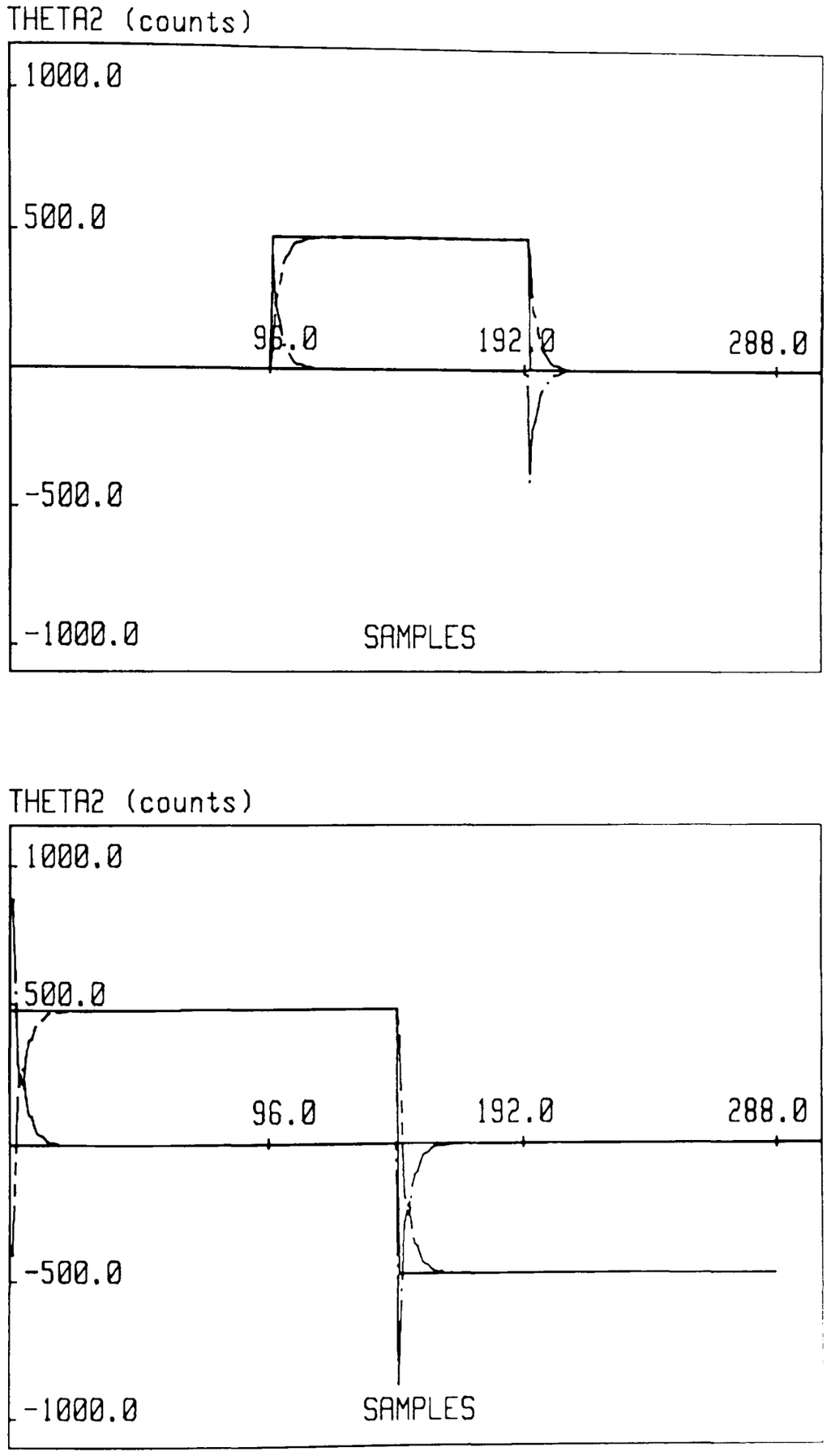

Figure 5.3. The Servo-Motor Responses for Standard Inputs.

The gain adjustment is carried on the step function as a start. The proportional and derivative gain potentiometers are then set to values so that the motor response is the equivalent of a critically damped system free from unnecessary oscillatory behaviour.

After achieving the above input examples, the other motions, the R-R, R-D-R and R-R-D are studied for a system having two degrees of freedom with a differential gear-unit in use.

Figure 5.4 illustrates the command, response and error curves for the implementation of the R-R motion. The upper plot represents the necessary programmable input as a result of the closed-loop control and the lower plot is the measurement on the crank shaft from the open-loop. The motion coordination of the two motors is provided using pulses from the constant speed motor which runs nominally at 1500 rpm.

Figure 5.5 represents the command, response and error curves for the R-D-R motion for the servo-motor and the crankshaft. The system operates at lower speeds than the previous case with the constant speed motor rotating at 750 rpm.

Figure 5.6 illustrates the servo-motor command, response and error curves and the crankshaft output for the R-R-D motion having same operating conditions as the previous R-D-R motion.

In the measured responses, it has been observed that the error is caused by a phase lag of the command from the system hardware. This is thought to be resulted from the control algorithm itself and as a result of the command digitization. The dynamics of the system and real operating conditions are also considered as other sources of error. To minimize the error, a phase advance for the command curve is needed. This is achieved by introducing command motion tuning into the system. The tuning algorithm is given in the following section.

5.5. Command Motion Tuning

The Mechanisms and Machines Group, Liverpool Polytechnic has developed some expertise in the field of command motion tuning [2.1], [5.6], [5.7] and [5.8].

The main purpose is to minimize the error between command and response and to get improved output characteristics. The use of tuned motion command significantly reduces the closed-loop error, the difference between desired and actual system output. Tuning utilizes system response to calculate the input required to get an output with the specified characteristics.

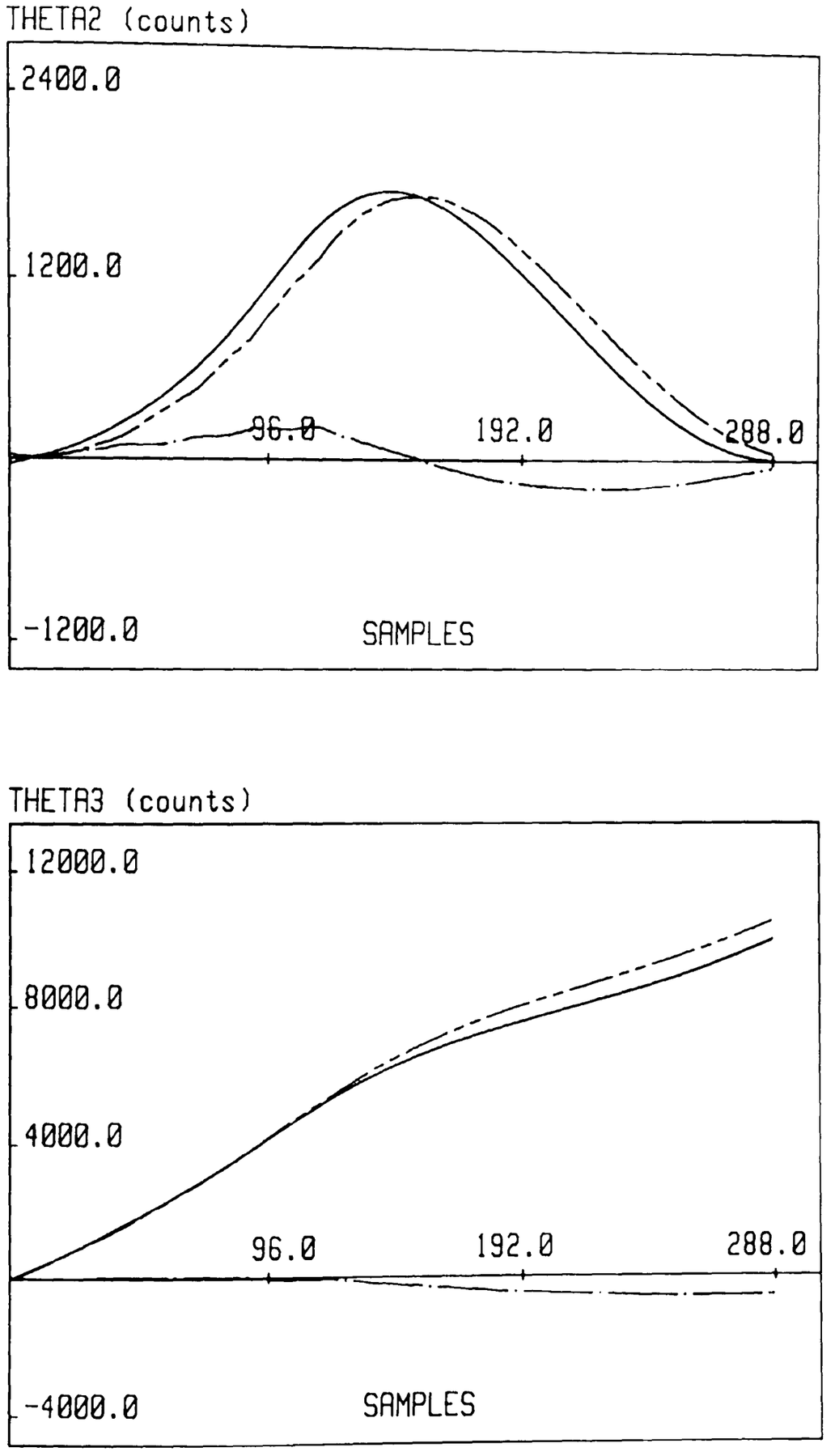

Figure 5.4. Measured System Responses for the R-R motion.

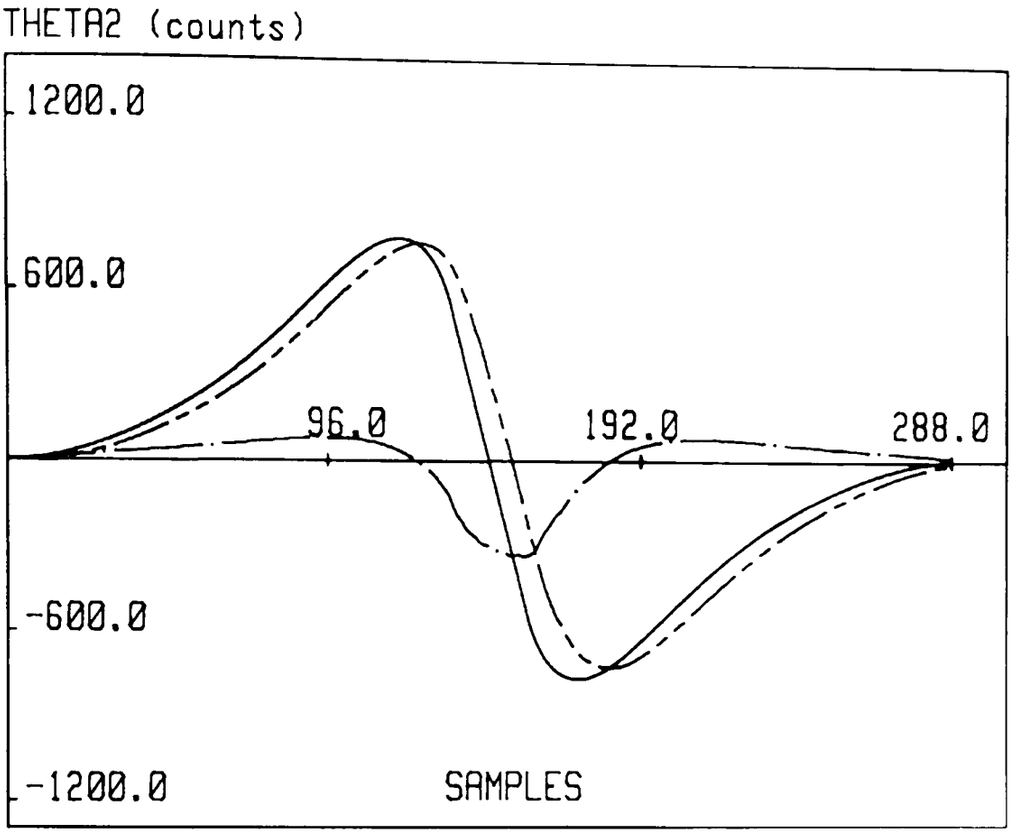

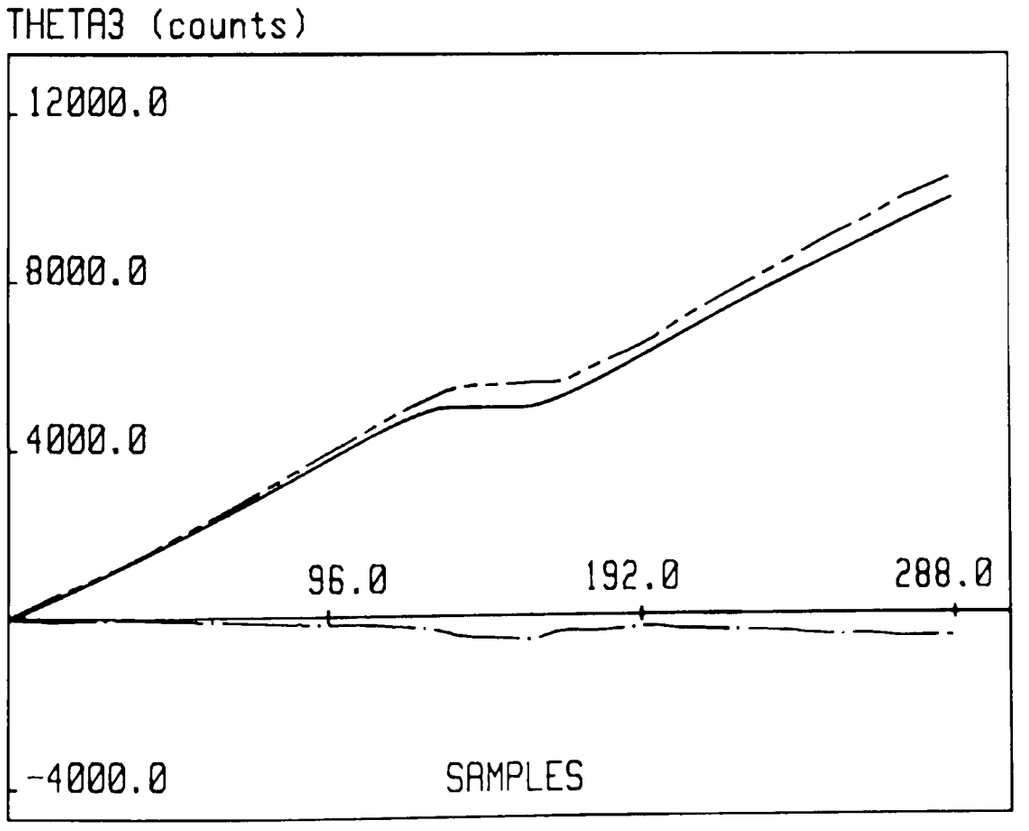

Command ———— Response — — — —

Error ——·——

Figure 5.5. Measured System Responses for the R-D-R motion.

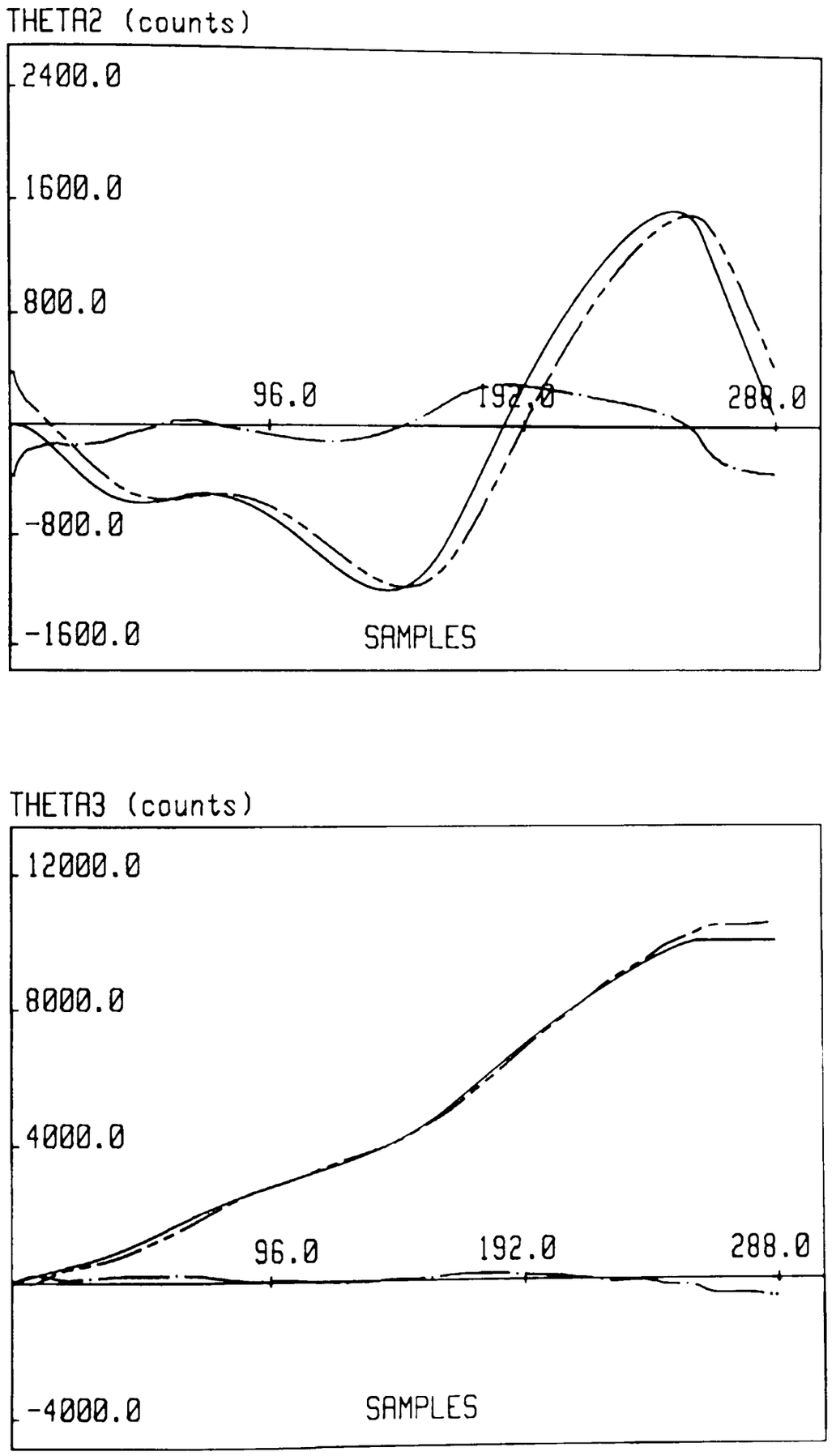

Figure 5.6. Measured System Responses for the R-R-D motion.

As an instance, the approach studied [5.7] implies that response improvement can be achieved by utilizing previous cycle response. This enables the system response to improve cycle by cycle. Since the final tuned motion command contains response information from the number of previous run cycles, this approach to tuning can be termed as *self learning*. This technique has been applied for the pantograph type linkage in [2.1], quite satisfactory results were obtained.

5.5.1. Tuning Algorithm

In the applied tuning algorithm, the difference between the nominal command and the dynamic response, the absolute error or portion of it is added sample by sample and cycle by cycle into the tuned command and a new dynamically tuned command computed based on it. This algorithm is described as the following.

$$C_{k+1,i}{}^{T} = C_{k,i}{}^{T} + G\,(C_{1,i}{}^{N} - R_{k,i}) \tag{5.1}$$

where

C^T – the tuned command

C^N – the nominal command

R – the response

G – gain

i – sample number

k – cycle number

In the assembly program, G is chosen as 1, 1/2, 1/4 etc. by shifting the binary data to the right.

A reasonable servo-motor response is required by using the above algorithm. This algorithm has to run continuously, monitoring the response and errors and adapting a tuned command repeatedly.

Figure 5.7 shows the improved servo-motor response after 2nd, 5th and later 8th cycles for the R-R motion. Other cycles are not included here. The comparison of the error curves is given in terms of encoder counts.

The peak error is found around 200 counts without tuning at the required speed. After introducing tuning algorithm, the peak error is reduced to 100 counts in 5 cycles, and 36 counts in the 10th cycle; nearly 1/5th of the previous error value. If the tuning algorithm is continued for 12-13 cycles, the peak error is found as 5 counts.

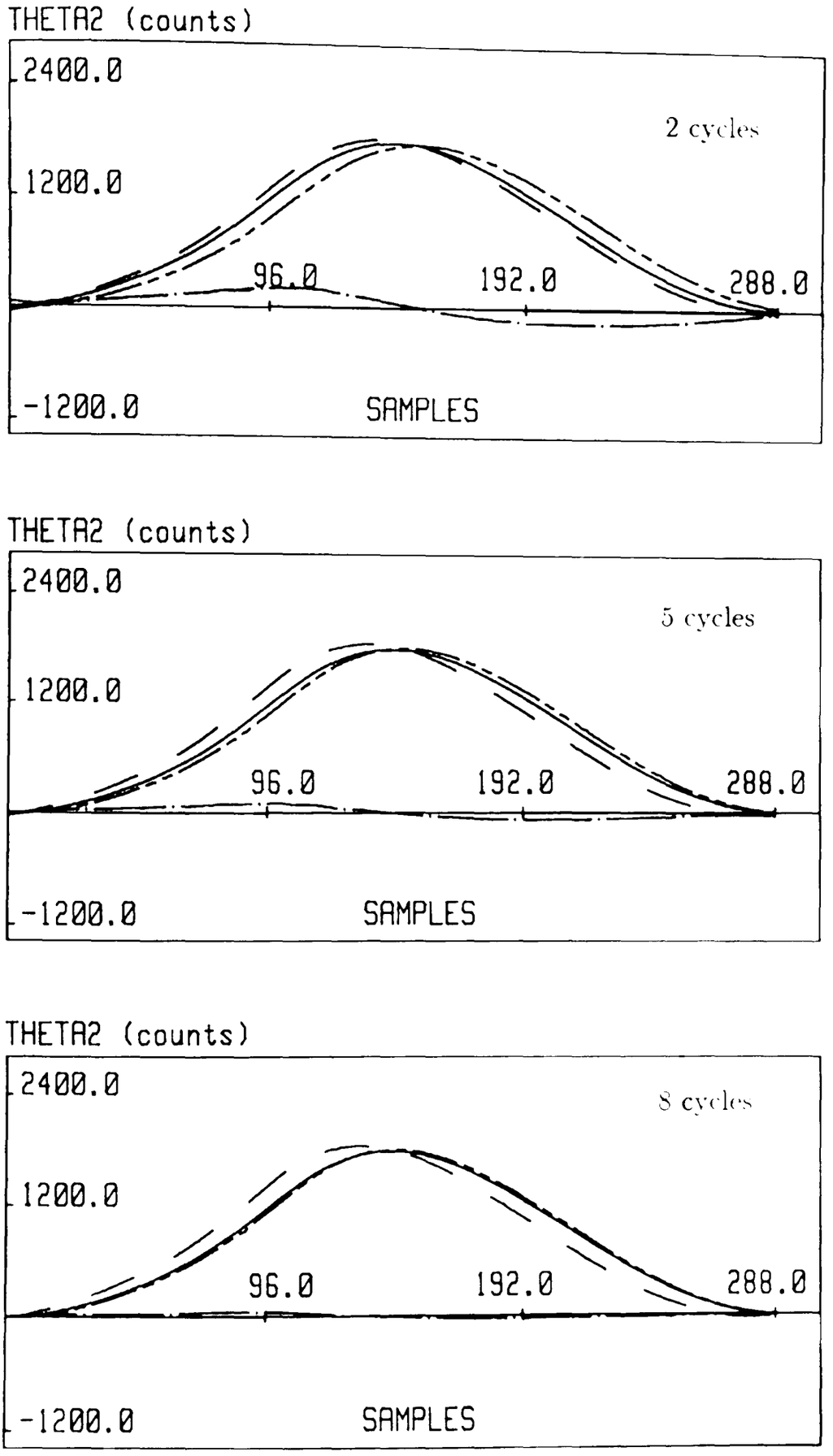

Figure 5.7. Progression of Tuning Algorithm.

If higher gains (G) are applied, the improvement in response is observed to be quicker and the number of cycles necessary is reduced.

Up to this point, it can be said that the tuning algorithm is successfully applied. However, some problems are observed during the algorithm application that should be mentioned here. If the system is kept running continuously with the tuning algorithm applied, some disturbances are observed on the resultant tuned command and the corresponding response. For instance, the system response matches with the command with some disturbance in the 20th cycle. After this cycle, the error but it starts to oscillate. This effects the system output with a resultant oscillatory response. When the same algorithm is tried with higher system gains, this happened quicker than 20th cycle.

In order to overcome the above problem which indicates some form of coming instability, the approach taken is to observe the system response up to an acceptable minimum error and then to stop the tuning algorithm. The optimum number of cycles is found to be 12 in terms of acceptability of the error for this example. Tuning is then paused. Thus the actual command stays as the tuned command without causing any further problems with minimized error as desired.

In this section, the progression of the tuning algorithm is presented only for the R-R motion not for the other two motions. The reason for this is that one motion example is thought to be enough to show the result of the algorithm applied. The R-D-R and R-R-D motions are also studied. In the application of the tuning algorithm the results are found similar to the R-R motion. For instance, if the system runs with included tuning algorithm oscillatory system responses are observed after some motion cycles. To avoid this problem, the same approach is taken as the above.

5.6. Conclusion

The necessary computer control system, control functions and the design of control hardware arrangement have been studied in this chapter.

The system responses were presented for the three designed motion examples. The command motion tuning was then investigated briefly. The motion command was tuned to have a response with minimum error to that of the desired output. The progression of tuning algorithm was presented for one motion case to show how the system response improved cycle by cycle. However, disturbances were observed in the tuned command and the corresponding system responses after some motion cycles. This problem was eliminated by pausing the tuning algorithm after optimum number of motion cycles depending upon the servo motion

required.

The control hardware arrangement had been developed by Mechanisms and Machines Group and it has performed satisfactorily for the required functional tasks up to this point. We may also add here that the controller boards are not designed for general purpose. However, modifications can be made for the specific purpose in these controller boards. Alternatively, the same functional tasks can be achieved by using controller cards available on the market. This latter approach will also help one who wants to utilize the hybrid arrangement for different purposes with less complication.

CHAPTER 6
POWER TRANSMISSION AND FLOW IN THE HYBRID ARRANGEMENT

6.1. Introduction

Power is transmitted in mechanical systems by means of friction, interlocking or contact. The transmission is usually performed at constant speed with shaft-mounted rotating members such as couplings, belts, chains and gears. With these elements, power is either transferred directly or by way of speed-torque multipliers. When transmission at variable speed is required, linkages, cams, and differential gears are applied.

Power transmission in the hybrid arrangement herein is achieved both at constant and variable speed. The first power path is found from the dc constant speed motor through belts, the casing of a differential gear-unit and then couplings to the crankshaft. Similarly, the second power path is found from the servo-motor through the gears and couplings to the crankshaft.

To see what is actually happening during the power transmission in the available set-up, this chapter presents a brief literature survey for differential transmission systems and then studies the basics of a differential gear, fundamental relations such as torque distribution and power flow. To complete the theoretical study achieved, it describes the experimental set-up with a torque transducer. It further presents measurements taken from this set-up with related torque and power outputs for the three motion cases.

6.2. Differential Transmissions

Macmillan 1961 [6.1] studied the fundamental relations connecting the torques, the velocities and the power flows for a general differential mechanism. He, in 1964 [6.2] described general shunt transmissions and four-shaft differentials which contain an assemblage of fixed ratio torque and speed differential units with possible arrangements, including two or four units. He then studied a regenerative system based on a speed differential in which the flywheel was

coupled to the transmission through the differential.

In 1965 Macmillan [6.3] described, analysed and compared divided-power transmission systems. Four assigned arrangements, which contained one or two differentials with a variable-speed unit, were investigated in terms of power flow and efficiency characteristics. They were called *bifurcated power transmission* systems.

In the following year 1965 Davies [6.4] presented a progress review about variable ratio drives with single and double differential mechanisms. The variator-single-differential arrangement connected one of the three members of a single differential to the input, another to the output and the third either to the input or to the output, via a variator. For a double differential arrangement, equilibrium was achieved between four components instead of three.

White 1967 [6.5] studied properties of differential transmissions composed of one differential gear and one variable-speed unit. An arrangement of a differential transmission was described in terms of principles of operation. The power input to a differential transmission was divided into two or more flow paths by gear trains, so that part of the power flowed directly to the differential gear and the remainder passed through the variable-speed unit. The differential gear then combined these separate power paths for a variable output. Possible arrangements of a variable-speed unit and a differential was also studied, for example, one shaft of the variable-speed unit was coupled either to the input shaft or the output shaft of the transmission. When the variable-speed unit was coupled to the input of the differential mechanism, the arrangement was termed as *input coupled* or *torque-divided* system. Similarly, the variable-speed unit was connected to the output shaft of a differential gear and it was termed an *output coupled* or *speed-divided* system.

In the same year White and Christie 1967 [6.6] revealed an improvement on the speed holding ability of a variable-ratio transmission by means of a differential coupling. Describing relations were derived for all possible types of differential coupling along with directions of power flow. The variable-ratio unit exhibited some variation of speed ratio with load during its applications. With a differential transmission, however, any undesirable change of speed ratio with load changes was eliminated. The positive action from the differential gear provided no change of speed ratio with load.

White 1970 [6.8] then examined multiple-stage, split-power transmissions. By using different possible arrangements such as the direct-drive and input-coupled transmission, the direct-drive and output-coupled transmission, two output-coupled and two input-coupled, two-stage speed changes were achieved. In single-stage split-power transmissions, a variable-ratio unit was connected in parallel with a fixed-ratio differential unit where they were grouped into

input-coupled and output-coupled systems as above. Multiple-stage split-power transmissions were used where a wide range of output speed was required. Two stage transmissions were obtained with one variable-ratio unit and two differential gears with several possible arrangements such that the transfer between speed stages occuring at a synchronous speed. The three possible cases of a two-stage transmission were both speed stages input-coupled or one-input coupled and one-output coupled speed stage. Two clutches were required for this application.

Further, Sanger 1971 [6.9] presented his work on the determination of power flow in multiple-path systems and expression in terms of speed ratios. The power transmitted was found from the each part of the system without torque analysis.

The following year 1972, White and Christie [6.10] described a variable ratio differential transmission with power flow relations. A three-stage variable-ratio transmission was described. High torque conversions were obtained over a wide speed range.

Basically all the above transmissions were meant to provide a wider range of output speeds and both a differential gear and a variable-speed unit were used. For the same purpose, Molian 1982 [1.4] later described a transmission in which a single differential gear-unit was used to combine the speed of a large constant speed motor with a small variable speed motor. Instead of using a variable-speed unit in the transmission, a motor with variable speed properties was applied to extend the range of the output speed from one of the inputs of the differential gear.

When a general overview is made about the study and application of differential transmissions it is found that the differential gear has always been used as a *uniform transmission mechanism.* However, in some circumstances, where the programmability is required, it is seen that the available differential transmissions could not cope with demands of this work. In the hybrid arrangement, the variable-speed motor has been replaced by a programmable servo-motor. The differential gear is then used as a single unit of fixed-ratio to add or subtract the motions from a constant speed motor and a servo-motor. So the hybrid arrangement is considered to be the basis of a search for its use as *non-uniform transmission mechanism,* which has not been explored before, by combining both uniform and programmable inputs.

6.3. General Analysis of a Differential Mechanism

Geared mechanisms are the most common form of the differential arrangements. In these mechanisms, the motion of one member or shaft is linearly related to the motion of other two

members.

A general differential can be represented by a gear casing and two integrated shafts with angular velocities $\dot{\theta}_1$, $\dot{\theta}_2$ and $\dot{\theta}_3$ under the torques T_1, T_2 and T_3 respectively. Figure 6.1.(a) shows this mechanism with its equivalent block diagram in Figure 6.1.(b). Here P_1, P_2 and P_3 are defined as positive power flows into the differential [6.3].

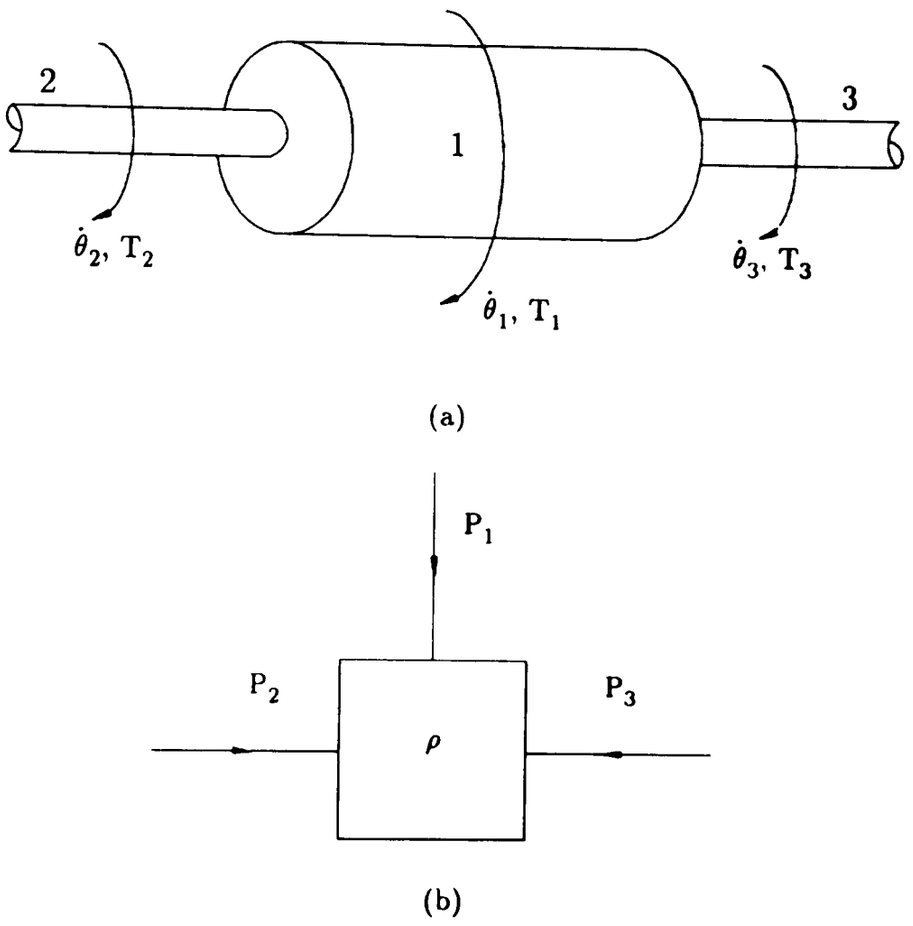

Figure 6.1. The general differential and its equivalent block diagram.

6.3.1. Torque Distribution

The operation of the differential is found by fixing one member and calculating the speed ratio of the two remaining members. The speed ratio between members 2 and 3 relative to member 1 is ρ in Figure 6.1. Additionally the belt reduction between the constant speed input and the annulus is g in the hybrid arrangement. This follows that

$$\dot{\theta}_3=\rho\dot{\theta}_2+ (1-\rho)g\dot{\theta}_1 \tag{6.1}$$

where $\dot{\theta}_1$ is the casing or dc-constant speed motor input, $\dot{\theta}_2$ is the servo-motor input and $\dot{\theta}_3$ is the crankshaft output. For steady operation, the requirement is that the differential gear

must be in equilibrium under the action of the three torques applied to it. Thus

$$T_1+T_2+T_3 = 0 \tag{6.2}$$

and if no losses are present, a power balance yields the algebraic sum of all power flows to the differential gear to be

$$T_1\dot{\theta}_1+T_2\dot{\theta}_2+T_3\dot{\theta}_3= 0 \tag{6.3}$$

As a result of multiplication of the torque relation, equation (6.2), with $\dot{\theta}_1$ and subtraction from the power relation, equation (6.3) an expression between T_2 and T_3 is found. Similarly, by using this relation in equation (6.2) an expression between T_1 and T_3 is obtained. They are given as the following.

$$-T_3 = \frac{T_2}{\rho} = \frac{T_1}{(1-\rho)g} \tag{6.4}$$

where represents a constant relationship for the ratio of torques carried by any two shafts of a differential gear. This equation gives the torque distribution on a differential gear. The preceding minus sign indicates the system output. This ratio is independent of the velocities between the members, but is dependent on the relative gear sizes [6.1].

Power flow can then be rewritten with power notations by using equation (6.3). The convention adopted defines power delivered by each shaft as positive if the product of its speed and torque is positive which indicates power flow into the differential through from a particular element. Neglecting losses the input power is equal to the output power that is

$$- P_3 = P_1 + P_2 \tag{6.5}$$

which is definitely true for the hybrid arrangement.

In addition to the above relations that are presently available, during the progress of this chapter the torque distribution on a differential gear has been considered in further detail. The reason for this is the necessity to clear some points on differentials when they are applied as a two degrees of freedom mechanisms rather than as isolated alternative inputs for the hybrid arrangement.

In the previous studies, it was noticed that the torque distribution was always calculated by considering only one input at a time. That is by fixing one member and calculating the ratio of the other two members. Undoubtedly this provided a considerable simplification in the

analysis of the mechanism and gave a constant ratio of the torques carried, like in equation (6.4). However, when two members are driving and the third is an output, the ratio of torques carried changes by depending on both relative gear sizes and velocities. The torque expression in equation (6.4) is true but not complete for a two degrees of freedom system.

To show this point more clearly for the hybrid arrangement application, the energy equation is rearranged. Equation (6.3) is then written without gear ratios, only the ratios of angular velocities from the power relation as:

$$-T_3 = T_2 \frac{\dot{\theta}_2}{\dot{\theta}_3} + T_1 \frac{\dot{\theta}_1}{\dot{\theta}_3} \tag{6.6}$$

If $\dot{\theta}_3$ is replaced from the equation (6.1) into equation (6.6), the torque expression becomes

$$-T_3 = T_2 \frac{\dot{\theta}_2}{[\rho\dot{\theta}_2+(1-\rho)g\dot{\theta}_1]} + T_1 \frac{\dot{\theta}_1}{[\rho\dot{\theta}_2+(1-\rho)g\dot{\theta}_1]} \tag{6.7}$$

where the ratio of $\dot{\theta}_2/\dot{\theta}_3$ is $1/\rho$ when the casing is fixed, $\dot{\theta}_1 = 0.0$, and the ratio of $\dot{\theta}_1/\dot{\theta}_3$ is $1/(1-\rho)g$ when the torque arm sleeve is fixed, $\dot{\theta}_2=0.0$.

The above relation is completely true for the one input and gives the general torque expression given in equation (6.4). It also satisfies the condition where two driving input exist at the same time.

6.3.2. Effect of Losses

The differential gear is accepted as a positive action device [6.5] because of no change of speed ratio with changing load. However, in practice, during its operation, any losses from tooth-action or bearings lead to a reduction in output torque and power flow. A single parameter η is assigned to represent these losses. The above expressions are then derived by including η.

MacMillan [6.1] has studied the concept of efficiency and its effect during the differential transmission by using equation (6.4). The internal friction losses are added with η to T_2 first and T_1 then is derived back. The new torque expression is found as:

$$-T_3 = \frac{\eta}{\rho} T_2 = \frac{\eta}{(\eta-\rho)g} T_1 \tag{6.8}$$

Similarly, the power flow equation is obtained by using equations (6.1) and (6.8), and multiplying them together the following power expression is found.

$$-P_3 = \eta\, P_2 + \frac{\eta(1-\rho)}{(\eta-\rho)} P_1 \tag{6.9}$$

The power equation is then replaced by the multiplication of torques and angular velocities and the torque expression is found as:

$$-T_3 = \frac{\eta\dot{\theta}_2}{\dot{\theta}_3} T_2 + \frac{\eta(1-\rho)\dot{\theta}_1}{(\eta-\rho)\dot{\theta}_3} T_1 \tag{6.10}$$

or, written in its explicit form:

$$-T_3 = \frac{\eta\dot{\theta}_2}{[\rho\dot{\theta}_2+(1-\rho)g\dot{\theta}_1]} T_2 + \frac{\eta\,(1-\rho)\dot{\theta}_1}{(\eta-\rho)\,[\rho\dot{\theta}_2+(1-\rho)g\dot{\theta}_1]} T_1 \tag{6.11}$$

Compared with equation (6.7), the above expression looks a bit more complex. Since the losses in a differential are small, sometimes they are ignored in the calculations. In a real system model, the efficiencies are usually added to complete the details for the systems real characteristics.

If the total frictional power lost in the mechanism is considered, all power inputs and outputs can be written as a summation of power terms as the following.

$$P_l = P_1 + P_2 + P_3 \tag{6.12}$$

P_3 is substituted from the equation (6.9) into the above summation to give

$$P_l = P_1 + P_2 - \left(\eta\, P_2 + \frac{\eta(1-\rho)}{(\eta-\rho)} P_1\right)$$

$$= (1-\eta)\, P_2 - \left(\frac{\rho(1-\eta)}{(\eta-\rho)} P_1\right) \tag{6.13}$$

When the mechanism operates as a differential with power flow at three members, the overall efficiency would be

$$1 - \frac{\text{power loss}}{\text{power input}}$$

By assuming P_1 and P_2 were positive power flow, the expression can be written in the following form

$$\eta_o = 1 - \frac{P_l}{P_1+P_2} \tag{6.14}$$

which includes both ρ and η for the overall efficiency.

6.3.3. Torque and Power Calculation in the Program

In order to complete the computer model study, the torque and power expressions are included in the mathematical model for the R-R, R-D-R and R-R-D motion cases. The torque and power relations which are given in equations (6.5) and (6.7) are the ones used.

Firstly the R-R motion is studied. The generated and output torques for this motion are given in Figure 6.2. These torques are found by using the same gains given in Chapter 4. The first plot shows the generated torque from the dc-constant speed motor, the second plot shows the generated torque from the servo-motor and the third plot represents the torque output T_3 on the crankshaft. Figure 6.3 then gives the supplied power P_1, P_2 and transmitted power P_3 by multiplying the torques T_1, T_2 with angular velocities $\dot{\theta}_1$, $\dot{\theta}_2$ respectively and summing them together.

For the second case, when the slider-crank is at its top dead centre, the servo-motor stops running system for nearly 50 ms by increasing its angular velocity equal to the other input velocity. In this specific motion, the differential gear-unit acts as a control element to keep the output shaft steady by equating speeds of the two driving inputs. However, when equation (6.7) is used for torque calculations, a numerical problem appears during the dwell period. The value of $\dot{\theta}_3$ becomes very small or zero, especially when $\dot{\theta}_3$ goes to zero, T_3 goes to infinity. The behaviour of the system can not be known by looking at equation (6.7) during the dwell. To find torque values corresponding to dwell, the equation of motion for a slider-crank, equivalent lumped masses is derived. Calculated θ_3, $\dot{\theta}_3$ and $\ddot{\theta}_3$ values are then used in this equation. So the corresponding torque values are replaced in the plot.

Figure 6.4 shows the generated torques as T_1, T_2 and output T_3 for the R-R motion. The corresponding supplied power and transmitted power outputs are given in Figure 6.5 as P_1, P_2 and P_3. The gain values are taken from chapter 4.

Finally the third motion, R-R-D introduces the dwell at the end of the return stroke for approximately 60 ms. The servo-motor stops running system to allow the coordination of an other object or a machine element. The value of $\dot{\theta}_3$ changes during 600 ms. But when the denominator of equation (6.7) or $\dot{\theta}_3$ goes to zero the same numerical problem as above appears. This is again eliminated by using the same approach taken for the previous motion. The generated torques and the crankshaft output are given in Figure 6.6 for the R-R-D motion. The supplied power and tranmitted power for this motion are shown in Figure 6.7.

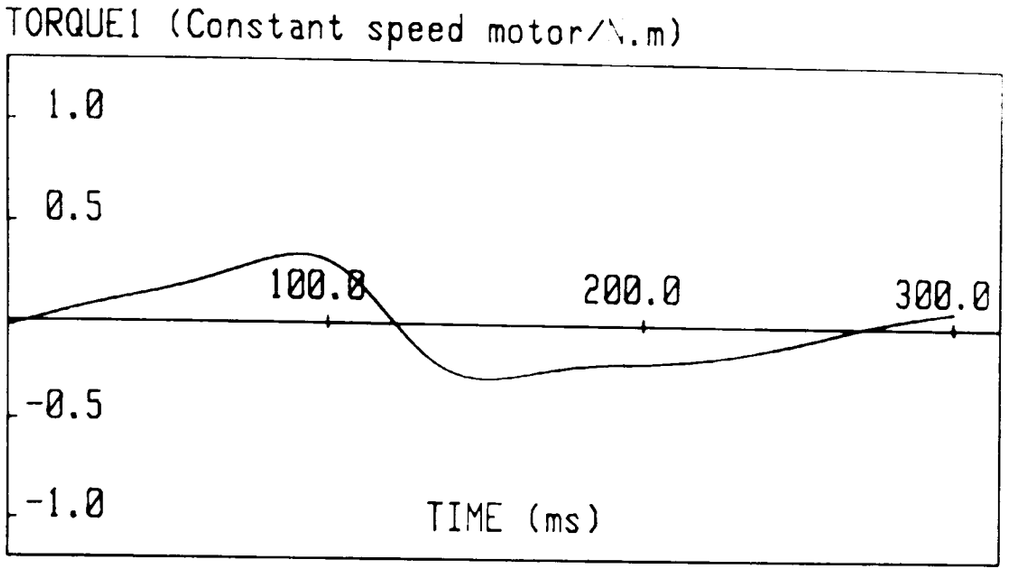

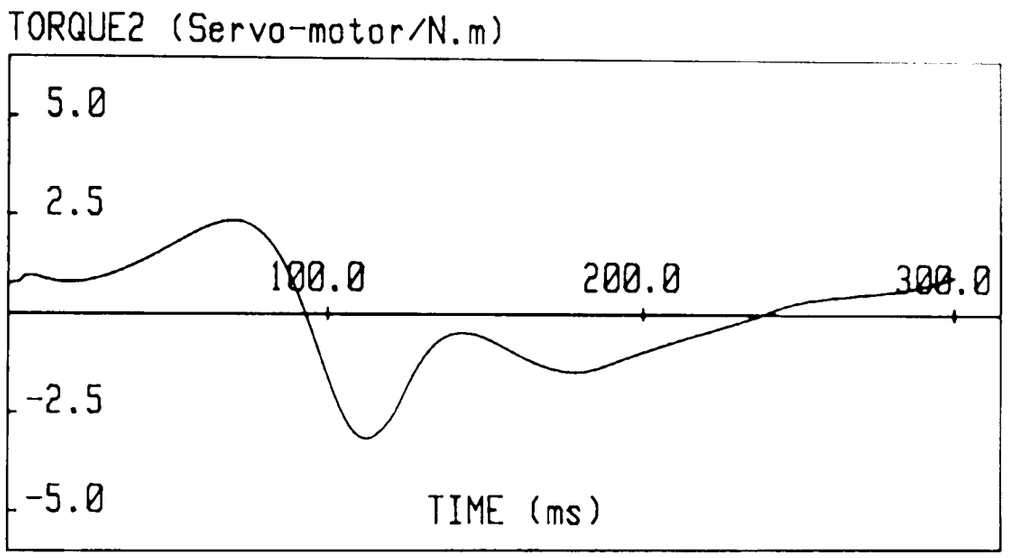

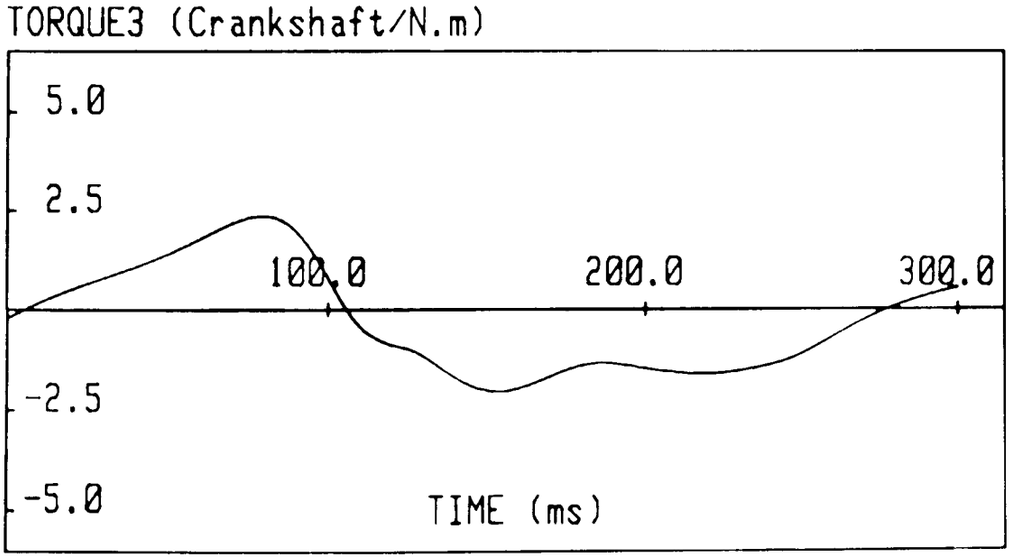

Figure 6.2. The generated torques T_1, T_2 and output T_3 for the R-R motion.

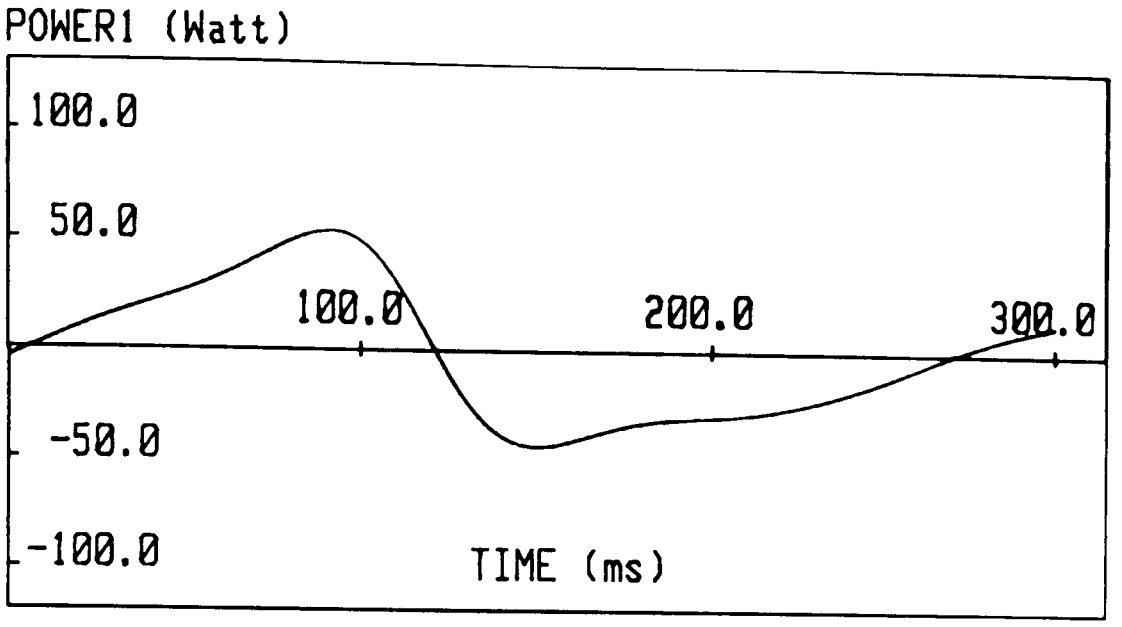

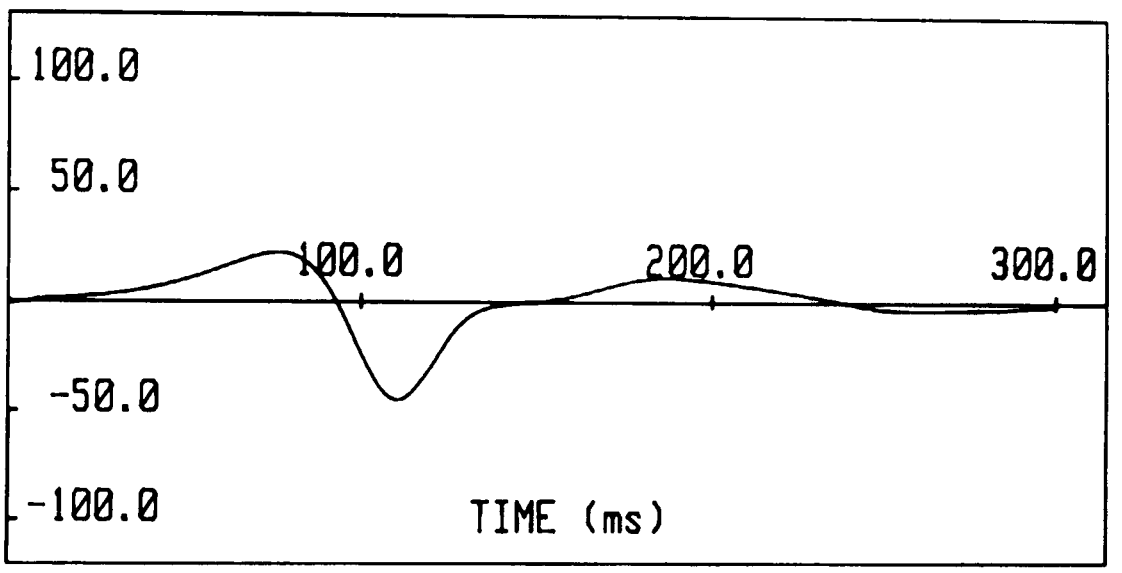

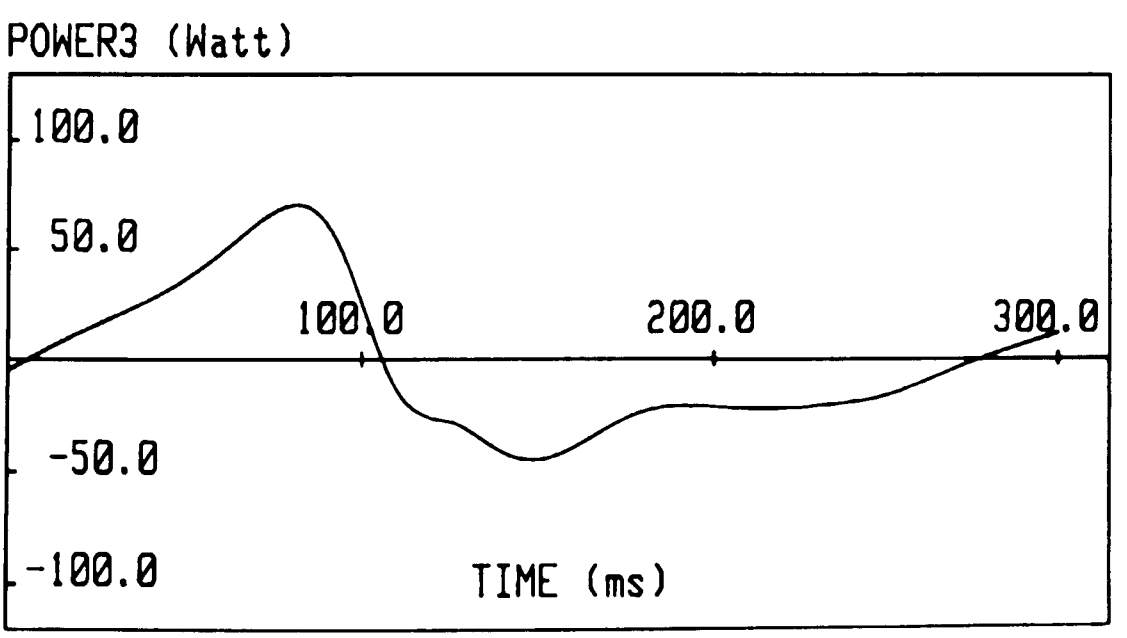

Figure 6.3. The supplied P_1, P_2 and transmitted power P_3 for the R-R motion.

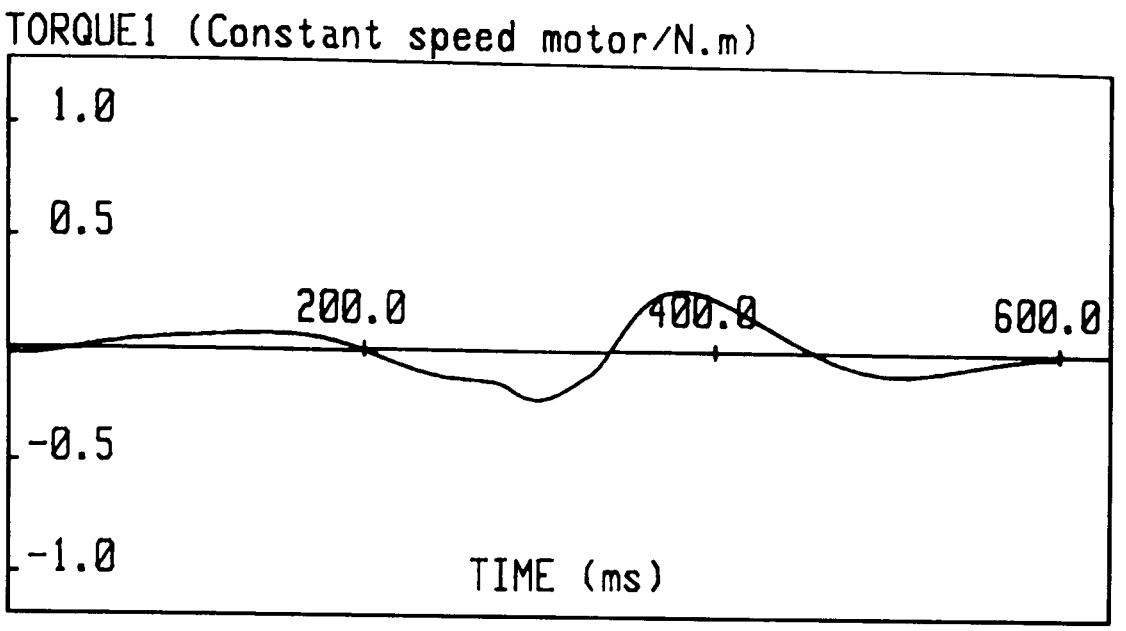

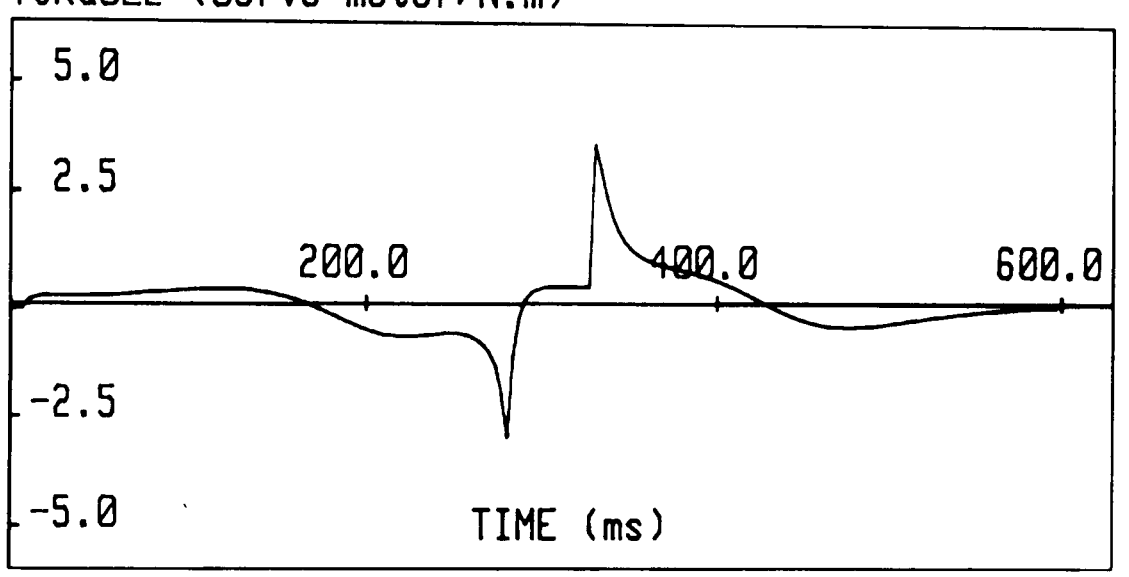

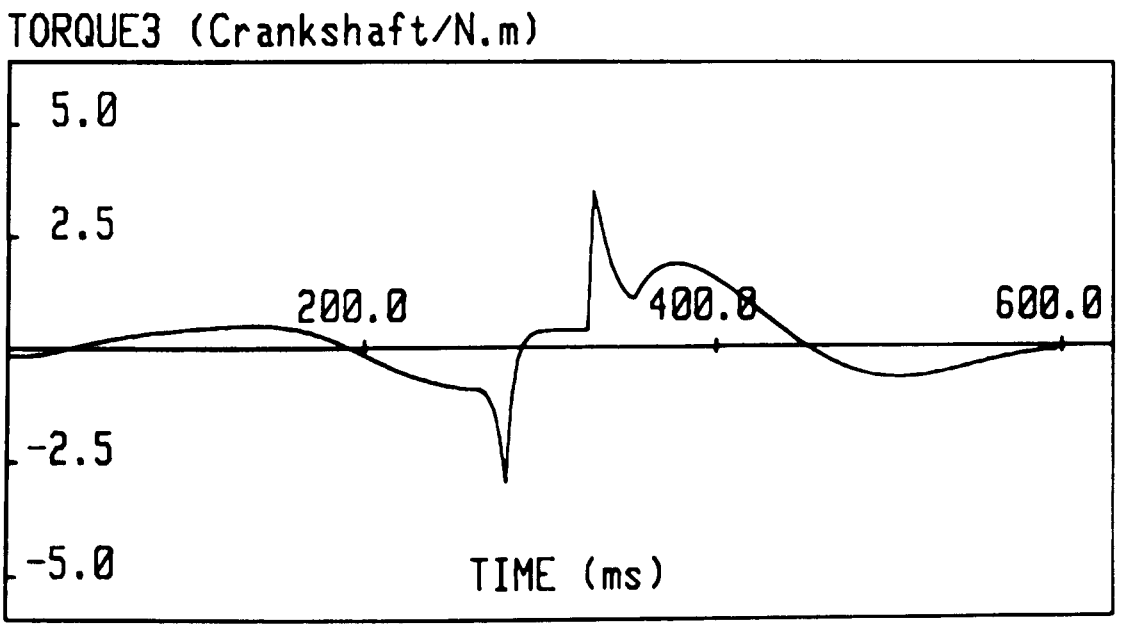

Figure 6.4. The generated torques T_1, T_2 and total T_3 for the R-D-R motion.

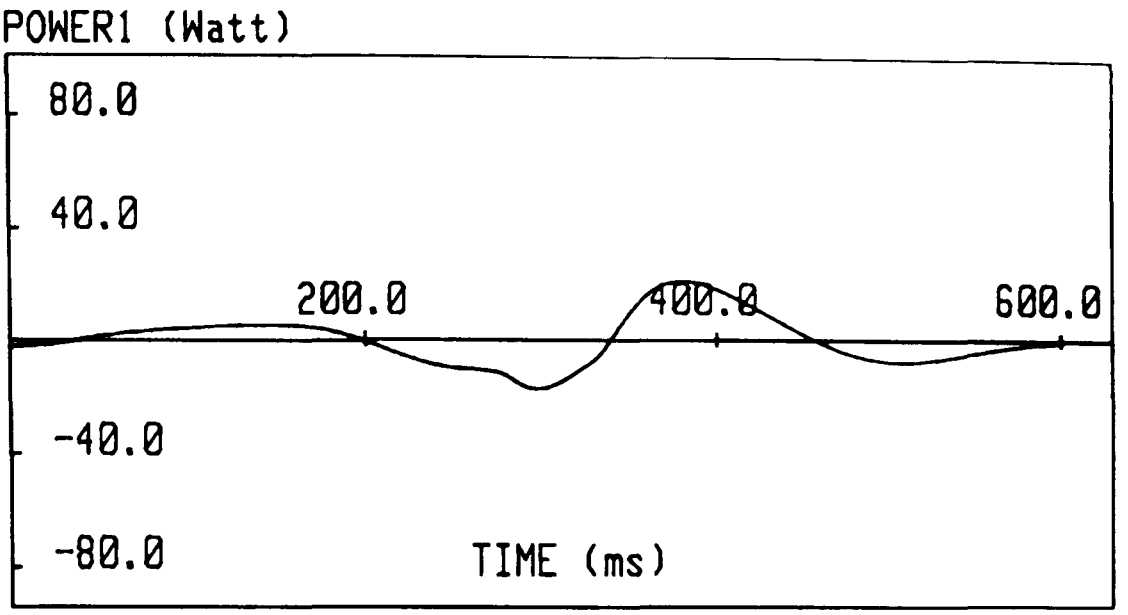

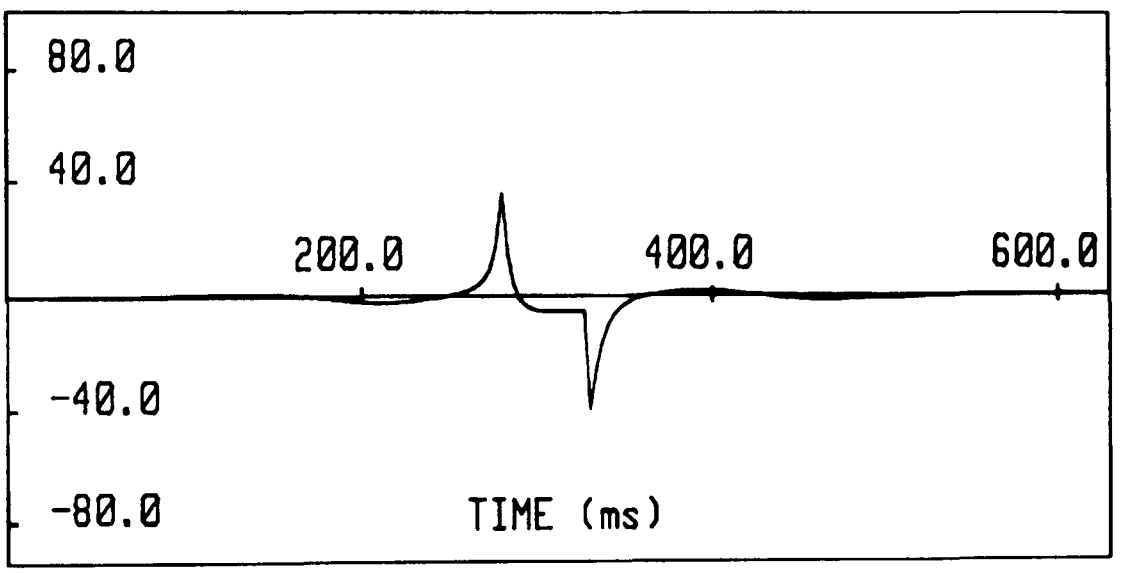

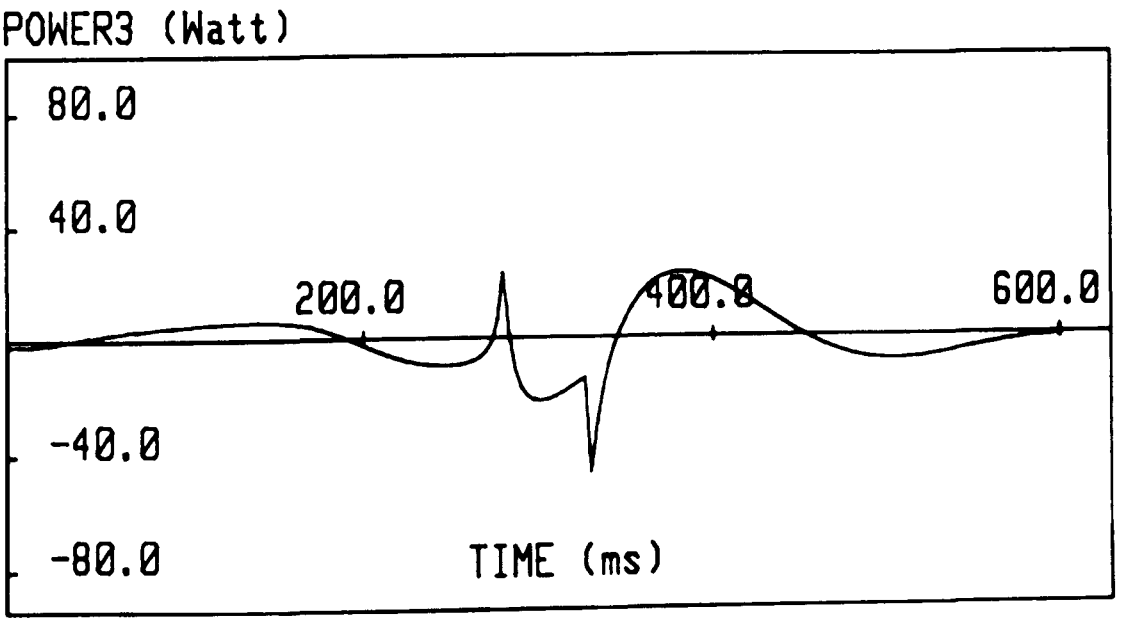

Figure 6.5. The supplied power P_1, P_2 and transmitted P_3 for the R-D-R motion.

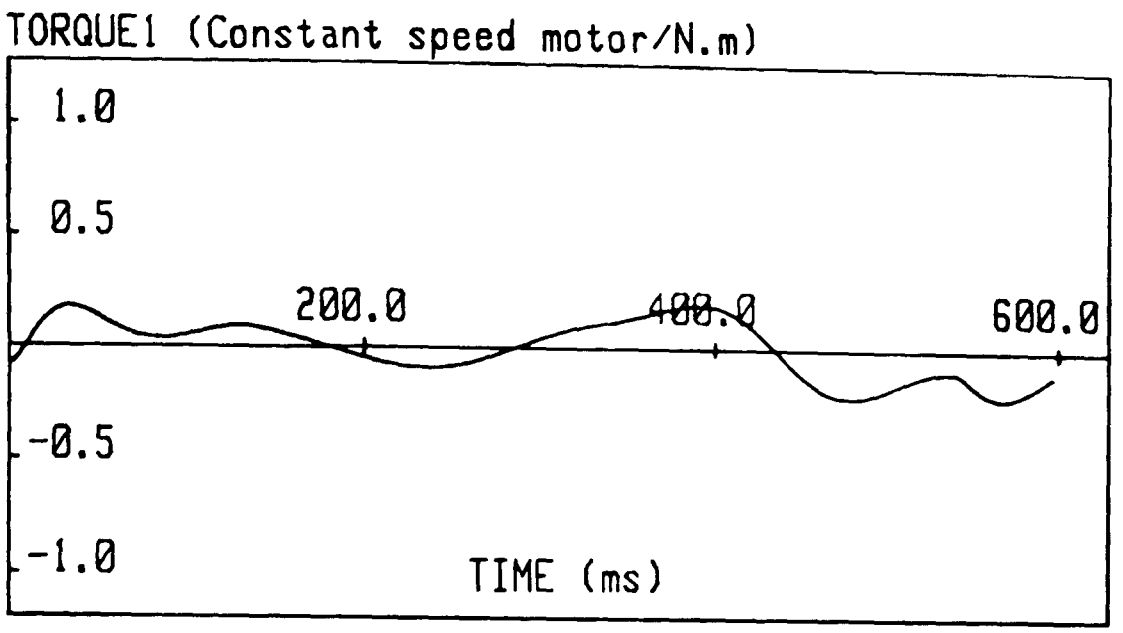

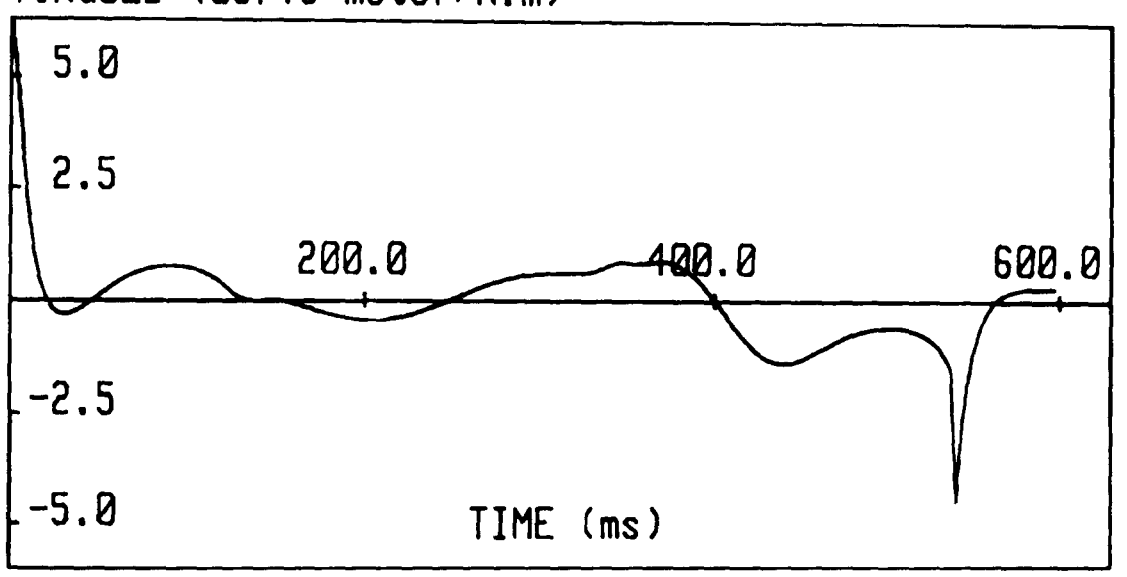

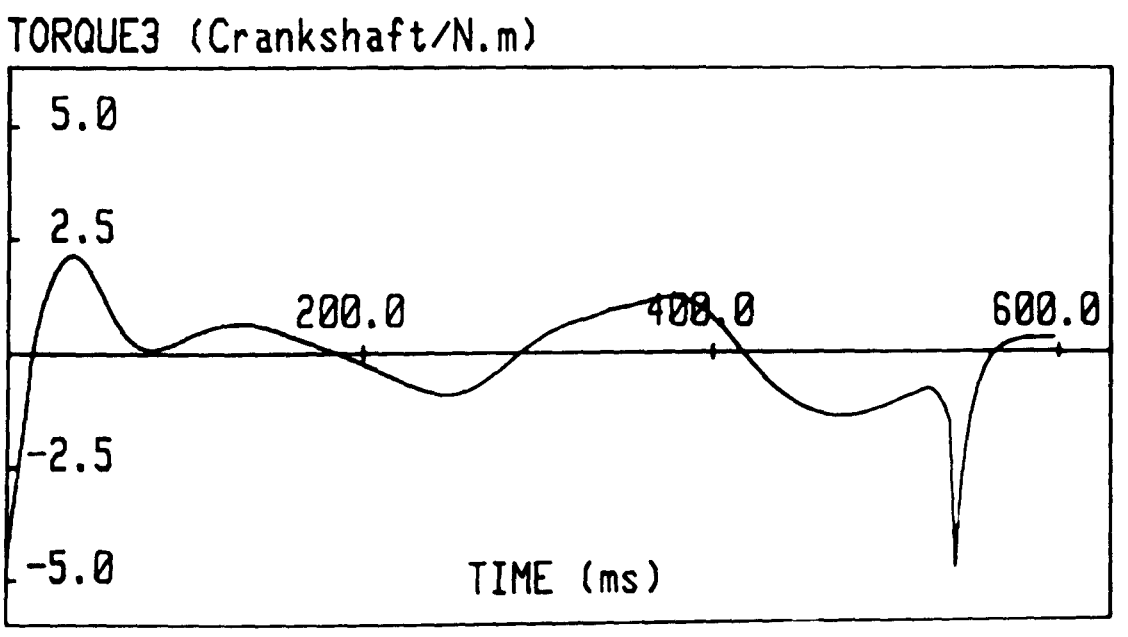

Figure 6.6. The generated torques T_1, T_2 and output T_3 for the R-R-D motion.

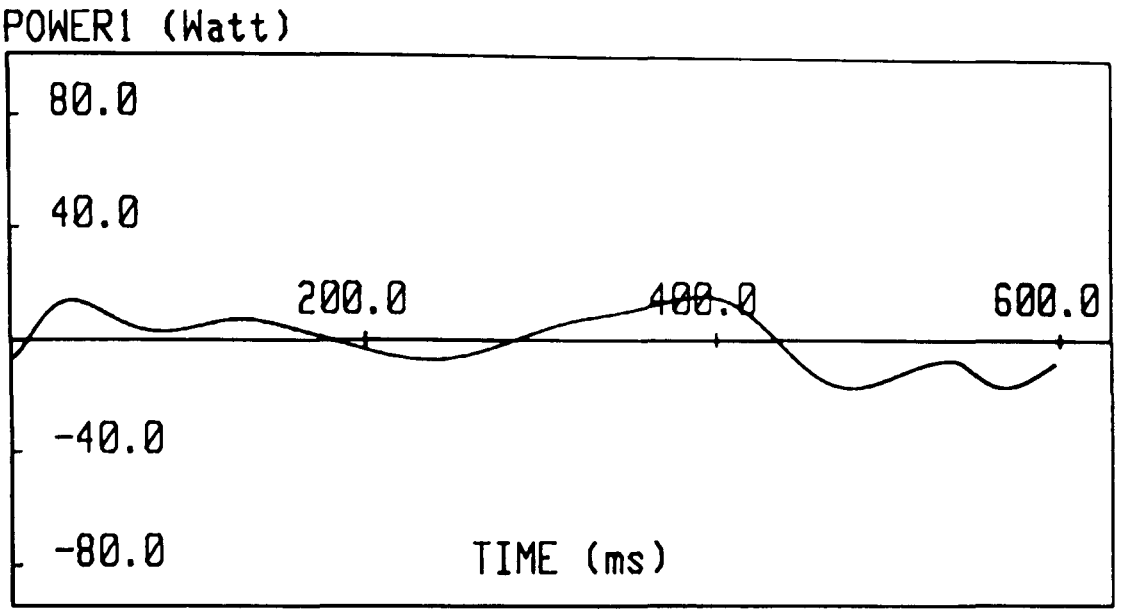

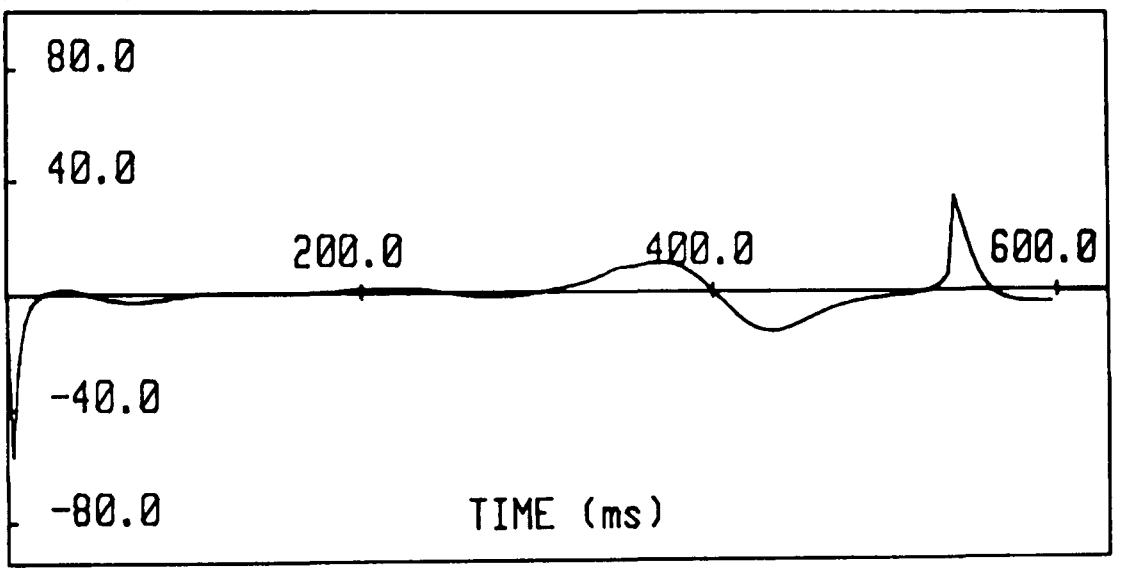

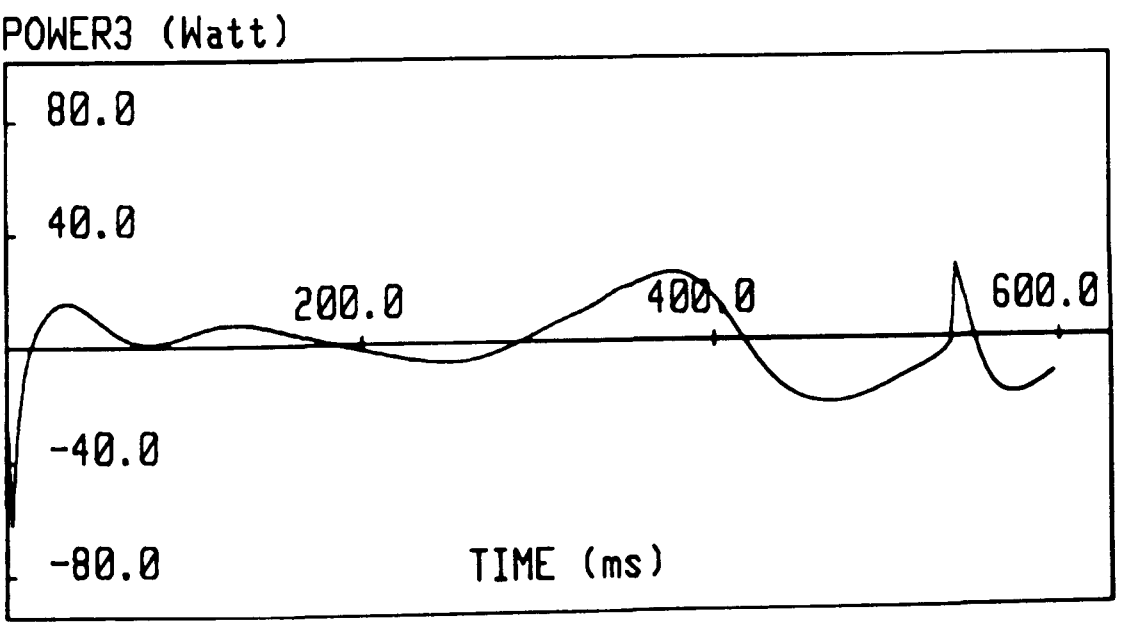

Figure 6.7. The supplied power P_1, P_2 and output power P_3 for the R-R-D motion.

6.4. The Experimental Set-Up

Figure 6.8 shows the experimental set-up. It has been used for the measurement of dynamic torques and angular velocities on the rotating crankshaft from which the experimental power flow is then found. In this set-up the generated torques can be isolated during the measurements. The input is provided either from the dc-constant speed motor or from the servo-motor with a differential gear-unit or from the combination of both.

6.4.1. Torque Measurement

An inductive torque transducer is integrally mounted between the differential gear-unit and the crankshaft by means of two flexible couplings. This transducer can measure torques in both directions irrespective of speed.

The measuring principle of the transducer is based on the distortion of the torque sensing zone under load. This is located in the central part of the transducer. The inductive measuring system forms a complete bridge which is supplied via a contactless rotary transformer with 10V, 8 Kc/s carrier frequency. The out of balance resulting in one of the bridge arm produces an amplitude modulated signal. This is fed to the carrier frequency amplifier (C.F.A) by means of a rotary transmitter. The output from the C.F.A is filtered, monitored and then stored on a digital scope. This torque output is later transferred to a digital computer (Hewlett Packard) through a RS232 communication interface for further calculations.

The calibration of the amplifier output is carried out statically. Static loads are arranged to apply a known pure couple to the transducer. Weights were applied in small increments up to 3 kg to a torque arm of 0.5 m length. By varying the gain of the carrier amplifier, a 3 Volt deflection is obtained for 14.715 N.m without overloading the device. The calibrated value of torque is later used when comparisons are made between the dynamic torque outputs and for the power flows.

6.4.2. Angular Velocity Measurement

A pulse pick-up transducer is mounted on the casing of the torque transducer to obtain the angular velocity information. The operation principle of this pick-up transducer is based on the incoming signal pulses whose frequencies are proportional to the angular velocities of the crankshaft. A frequency-to-voltage converter is required to process these incoming signals and convert them into a dc voltage output. A frequency-to-voltage conversion circuit has been built for the angular velocity measurement. Although this circuit has performed quite well

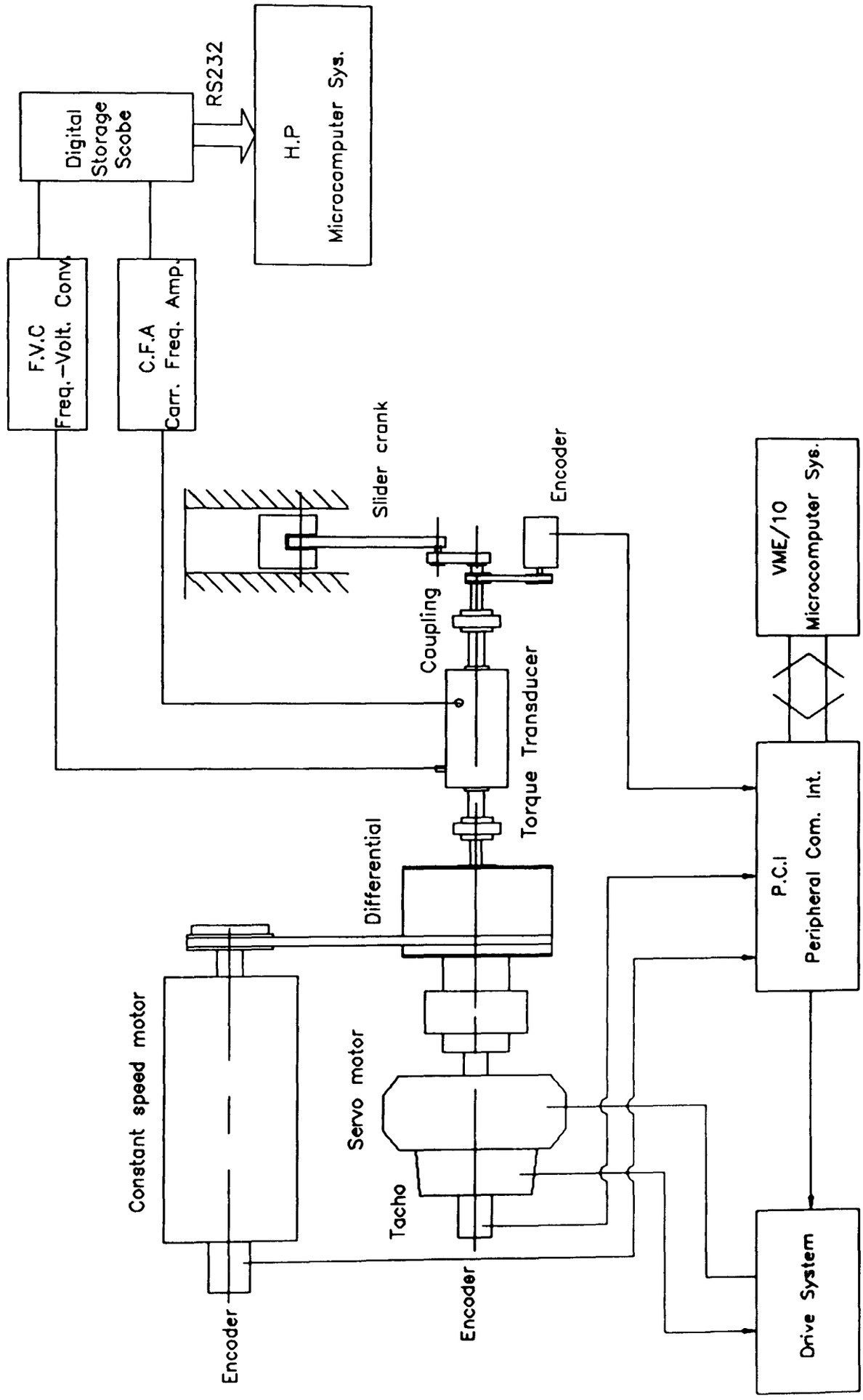

Figure 6.8. The Experimental Set-Up.

levels of voltage output at higher frequencies, the crankshaft output measurements were not very accurate. This was thought to be because of the very low operating frequency range.

Another alternative was searched for angular velocity measurement without changing anything in the set-up.

The output angular velocity $\dot{\theta}_3$ is later obtained from the incremental encoder, which is indirectly fixed on the crankshaft, by using a position counting technique [5.6]. The position that was measured in the previous control cycle is subtracted from the current position to give an incremental displacement that can be divided by the control cycle time. This manipulation produces the average velocity over the required time interval in the following form:

$$\dot{\theta}_{3_i} = \frac{(\theta_{3_i} - \theta_{3_{i-1}})}{R\, t_{c_t}} 2\pi \qquad \text{for } i=1,2,\ldots,n \tag{6.15}$$

where

$\dot{\theta}_{3_i}$ – angular velocity (rad/s)

θ_{3_i} – current angular position (rad)

$\theta_{3_{i-1}}$ –last angular position (rad)

R – encoder resolution (counts/revolution)

t_{ct}–control cycle time (sec).

The above calculations were performed within the control software. The resulting velocity has a resolution over the whole speed range of

$$\dot{\theta}_{res} = \frac{2\pi}{R\, t_{c_t}} \tag{6.16}$$

In this technique the velocity output is, however, very sensitive to the existing inaccuricies in the position signal obtained. Since a differentiation process is carried out, any noise in the coming signal is undoubtedly amplified. Although the technique can provide the necessary angular velocity information, in some circumstances, for example when the positional resolution is too low or the control cycle is too fast, this technnique can provide insufficient velocity resolution. It cannot satisfy the measuring accuracy requirements.

6.4.3. Experimental Torque, Angular Velocity and Power Curves

Finally a set of torque speed measurements are obtained from the hybrid arrangement. All the experimental data outputs are expressed in the number of samples in time scale

corresponding to actual motion cycle time. In order to find output shaft power in Watts, measured output torques are converted to N.m by using the calibration torque and then multiplied by output shaft angular velocity. Here 3 Volts correspond to 14.714 N.m from the previous section.

The shaft power P_3 developed by shaft torque T_3 N.m at angular velocity $\dot{\theta}_3$ rad/s is calculated from:

$$P_3 = T_3 \dot{\theta}_3 \tag{6.17}$$

Figure 6.9 shows torque, angular velocity and transmitted power obtained for the R-R motion while the dc-constant speed motor is rotating at 1500 rpm. The torque output is expressed in volts and in number of samples in the first plot. The resultant angular velocity, $\dot{\theta}_3$ is given in rad/s and against number of samples is shown in the second plot and while the third plot shows the corresponding power in Watts.

Figure 6.10 represents torque, angular velocity and transmitted power for the R-D-R motion where the dc-constant speed motor runs at 750 rpm. All plots are represented in same units as the previous example.

Figure 6.11 shows the measured outputs for the R-R-D motion. The plots are given in the same units as above. The results are measured when the constant speed motor runs at 750 rpm.

In order to get better output from the measurements, the experiments were performed over many cycles and one of the best for each is plotted here. Some noise is evident in the plots. This was simply due to the real operating conditions so that readings recorded from the experiments had errors of various kinds. When the experimental outputs are studied separately, the lower noise level was observed for slower motion examples like in Figure 6.10 and Figure 6.11.

Additionally, the digitization of the command points was found to be very effective in the calculations. In the control program, the system responses are stored as integer numbers and numerical methods, like numerical differentiation are then introduced to perform further calculations for the angular velocity. Since the transmitted power is found by multiplying the crankshaft torque and angular velocity, any noise and inaccuracy in reading during the torque and angular velocity measurement is directly reflected in the power outputs. Thus it is obvious that better torque and angular velocity measurement would result in more accurate calculation of transmitted power outputs.

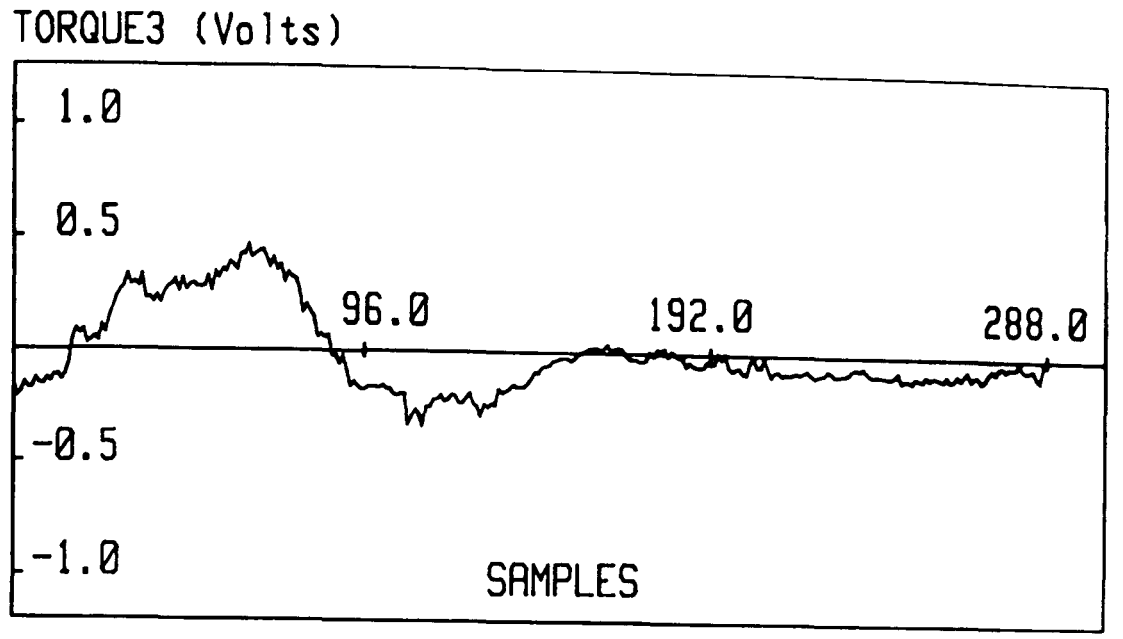

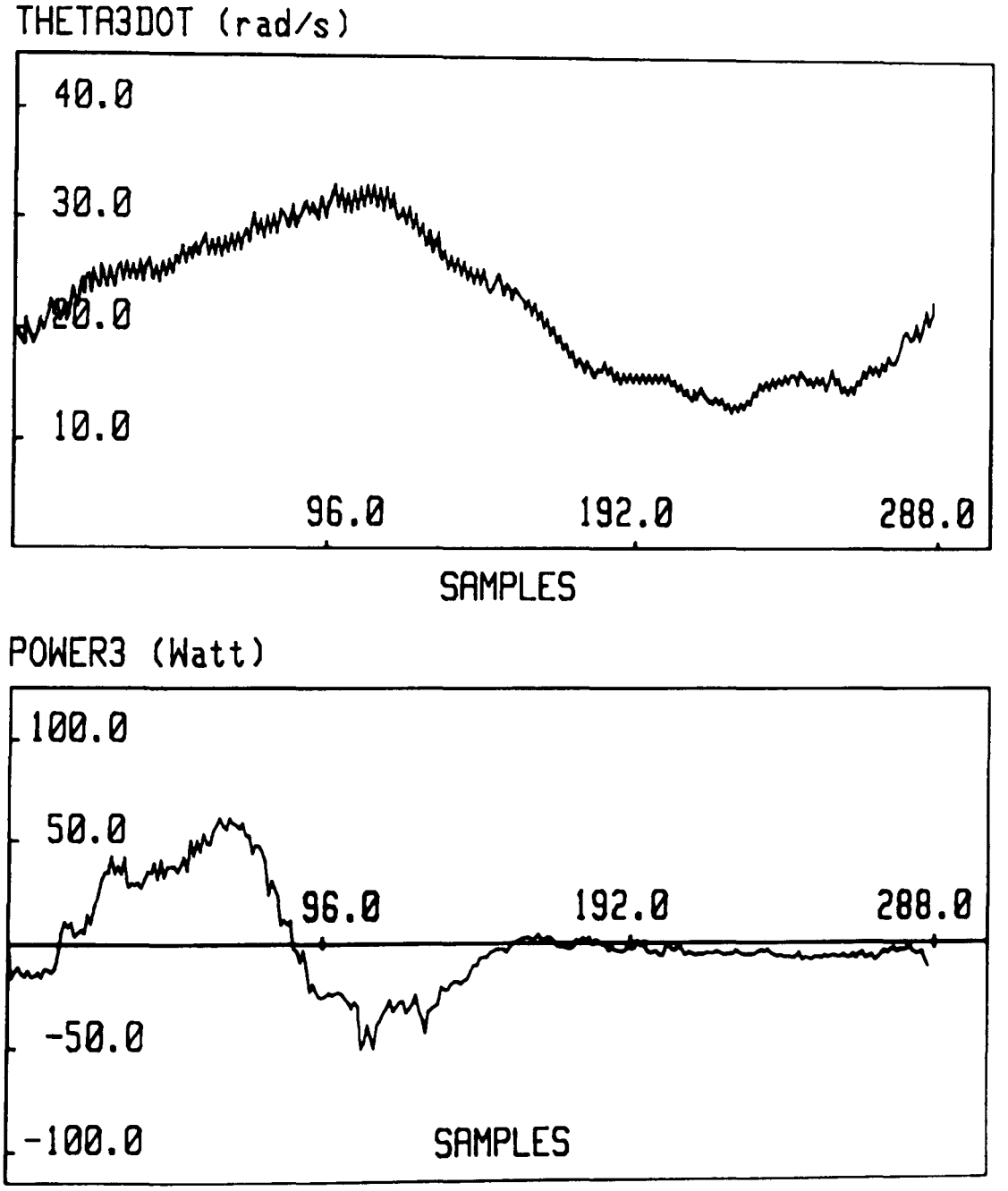

Figure 6.9. The output torque, angular velocity and power for the R-R motion.

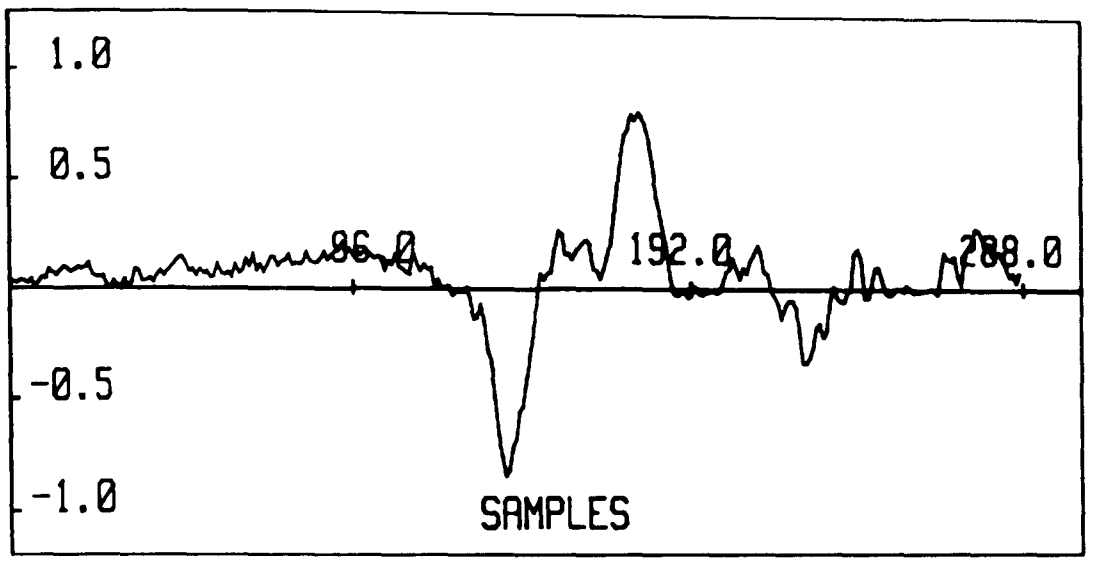

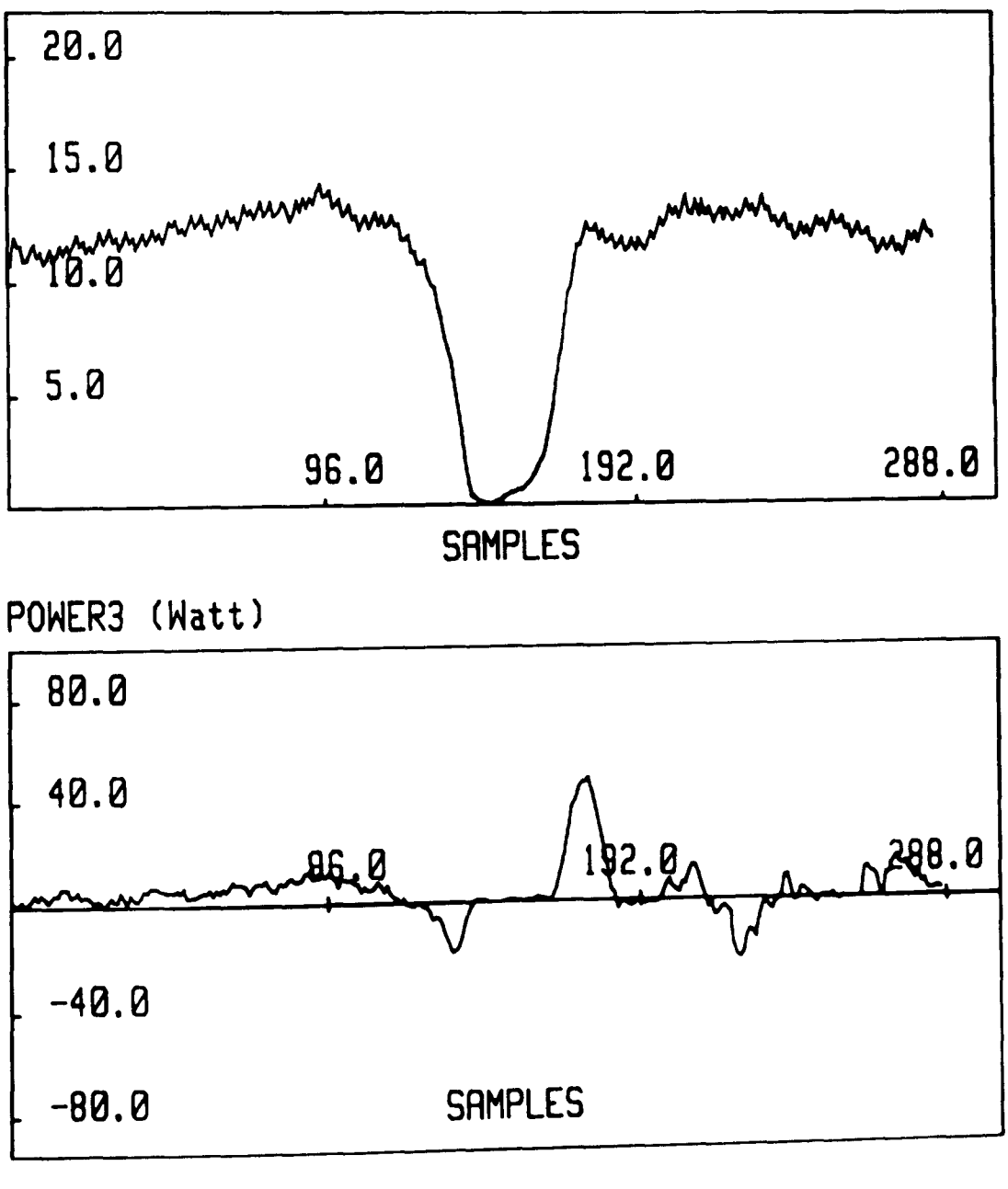

Figure 6.10. The output torque, angular velocity and power for the R-D-R motion.

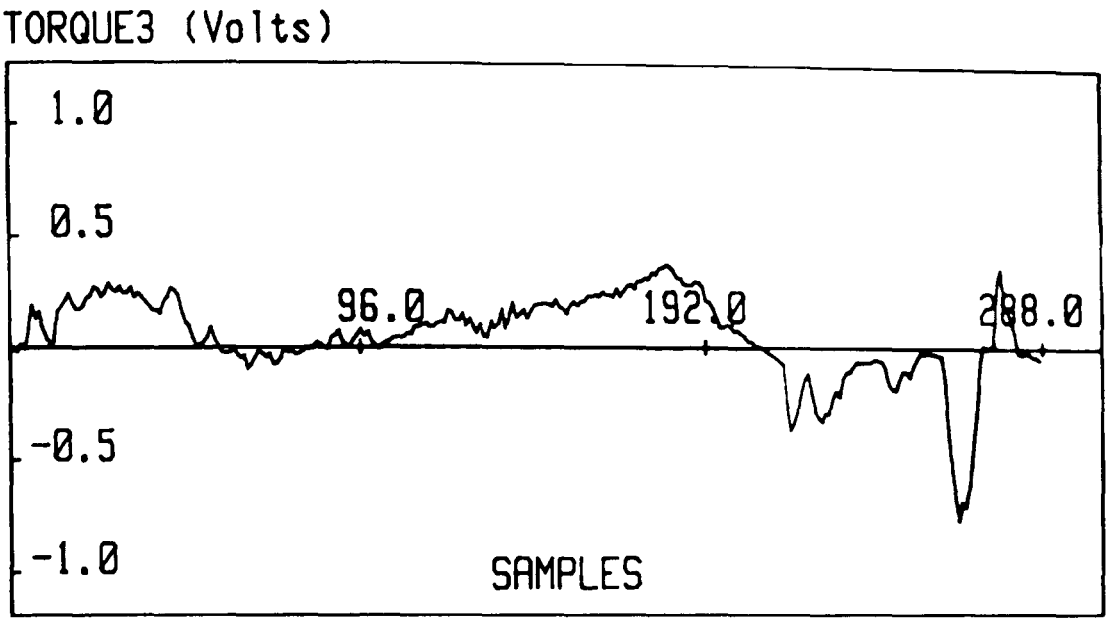

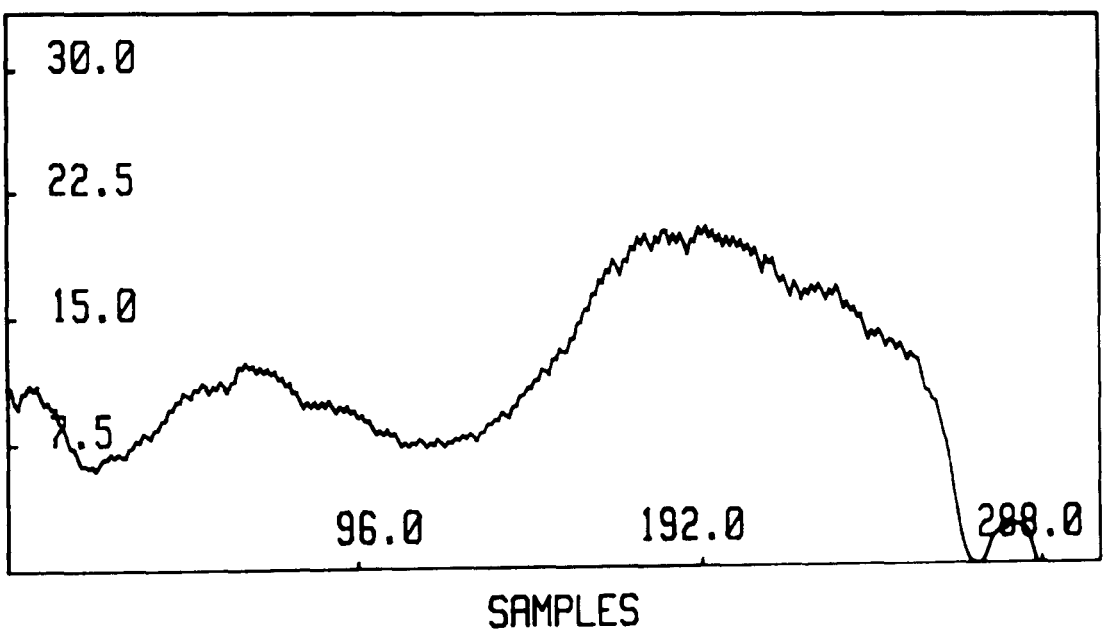

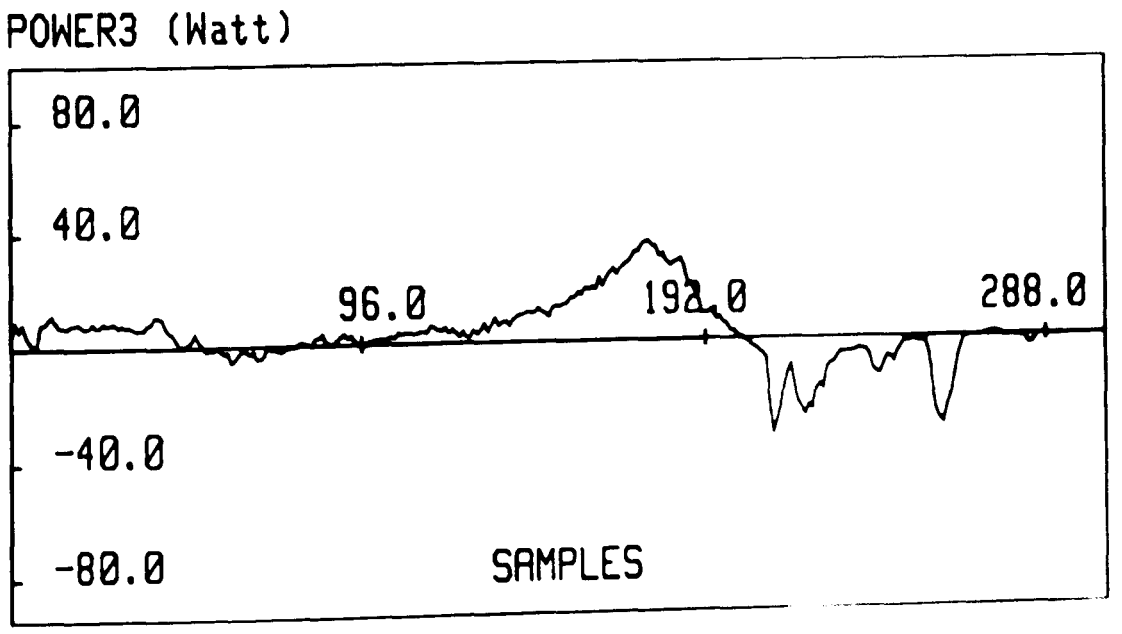

Figure 6.11. The output torque, angular velocity and power for the R-R-D motion.

6.5. Conclusion

A review has been included differential transmissions in this chapter. Fundamental relations for the torques, the angular velocities and the power flows have been derived for a differential gear and effect of losses were considered. Additional torque relations are presented, while two inputs are driving. These relations have been included into the computer model and the numerical problems have been tackled for the dwell included motions.

An experimental set-up has been built for the dynamic torque and angular velocity measurement. Power flow has been found for the each components of the hybrid arrangement. The experimental torque, angular velocity and transmitted power outputs were then presented. The comparisons and discussions about theoretical and experimental torque distribution and power flow are left to be included in the following chapter.

CHAPTER 7
COMPARISON OF THE MODEL AND THE EXPERIMENTAL RESULTS

7.1. Introduction

During the overall progress of work, a mathematical model is built up to describe the dynamic behaviour of the real system. Equivalent experiments are carried out on the real system and the model.

In this chapter the comparison of the model and the experimental results are presented into two parts. In the first part the model and the experimental servo-motor and the crankshaft responses are given and the designed slider displacements are included with their calculated and measured outputs. In the second part the torque distribution and power flow calculated from the model and measurements taken from the experimental set-up are presented. In generating non-uniform mechanism motion two alternative techniques; *the programmable drive only* and *the hybrid arrangement* are further studied to decide which alternative would offer a better choice. All comparisons made are based on torque and power requirements from the programmable drive. This part is carried out in theory only. At the end, regenerative programmable systems are considered.

7.2. Comparison of Model and Experimental Responses

The results for the model and experimental work are developed into two parts. One part concerns a single degree of freedom system, without a linkage mechanism, for standard inputs only. The second part concerns the two degrees of freedom system, the set-up as a whole, representing the hybrid arrangement.

7.2.1. Standard Inputs

Initially, to observe the dynamic response of the servo-motor different positional commands were applied. The chosen examples were a finite impulse and a square waveform function. It

is anticipated that, for these inputs, the servo-motor behaviour will be a kind of response which will include both transient and steady state parts. The transient part of the response dies away with increasing time in stable systems. The system then shows its steady state behaviour.

Figure 7.1.(a) and (b) show typical command and responses for these test signals. The results are found from the model, after simplifying assumptions are made, and from the experimental set-up after disconnecting the mechanism, the differential gear-unit and the constant speed motor.

The first plots on the left hand side of Figure 7.1.(a) and (b) demonstrate the response for the pulse function of finite period, when an instantaneous change occurs in θ_2, under proportional plus derivative control action. The full line curves represent the command functions and the dotted line curves are for the corresponding responses. The model responses are given in radians and milliseconds and the proportional and derivative gains are set at K_{g2}=100.0 V/rad and K_{v2}=0.80 V/rad/s. The recorded servo-motor responses are represented as encoder counts and samples. In the command function, the step change occurs at 100 ms on a time basis which is equivalent to the 96th sample and continues for about 100 ms up to 192nd sample.

The second plots on the right hand side of Figure 7.1.(a) and (b) represent the computed and measured responses for a square waveform input and indicate the close matching. The first step change occurs at time equal to zero and the second step change happens at 150 ms half of the cycle which corresponds to 144th samples. The servo-motor model responses are calculated using K_{g2}=100.0 V/rad and K_{v2}=0.90 V/rad/s for the proportional and derivative gains respectively.

Evidently these responses demonstrated that the behaviour described above was observed during the application of both functions. In the model, continuous alteration of the gains made it possible to obtain different response characteristics, for example, the effect of transients is easily observed in the model responses under the action of small derivative gains. The model response is made practically identical to the experimental one only by altering K_{v2} in the calculation here. In the experimental responses, the transient behaviour is not observed and the steady state part is directly seen as constant encoder counts indication of a constant amplitude. This was because of the gains used in the closed loop to get a critically damped response to avoid oscillatory conditions.

Briefly the reason for choosing the first input function was to observe the servo-motor behaviour for zero displacement at the beginning. The servo-motor response is recorded before

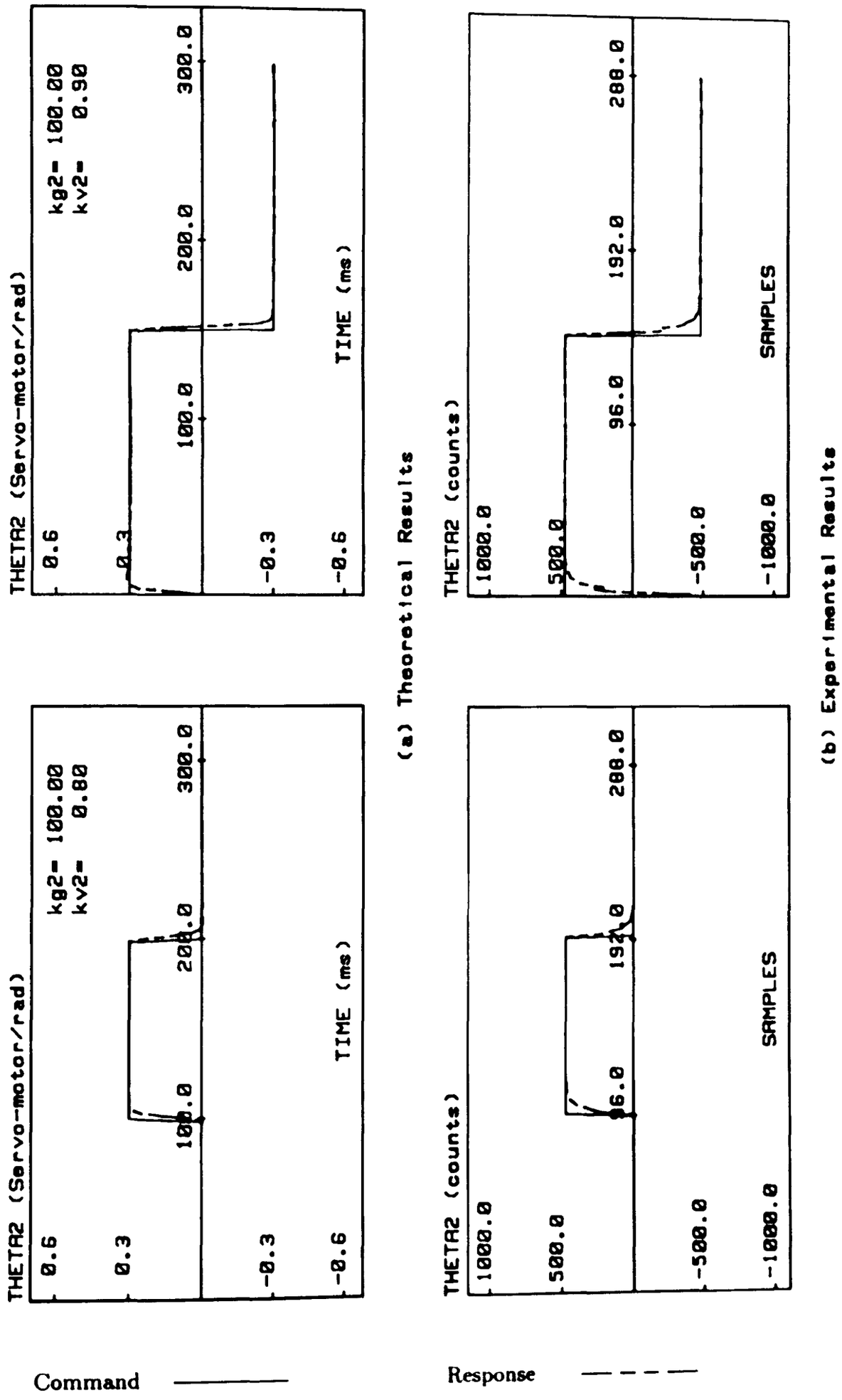

Figure 7.1. The model and the experimental servo-motor responses for standard inputs.

applying the input function, during the application of the function and after the function has been applied. For the second input, it is required to see what happens when there is a step change at t=0.0 ms and subsequently another step change at t=150 ms, but in the opposite sense, with twice the original magnitude is made.

The servo-motor has exhibited a good response albeit without load and linkage mechanism. However, the anticipation is that the same motor would not respond that well when it is complete with the linkage mechanism and the other transmission elements.

7.2.2. Different Motion Examples

The three designed slider motions are presented with their modelled and experimental responses here. In the computer model, the slider displacement is calculated from a kinematic relationship used previously in chapter 3 as:

$$x = r+l-r\cos\theta_3 - [l^2-(y-r\sin\theta_3)^2]^{1/2} \tag{7.1}$$

where r and l are the crank radius and connecting rod length, y is the zero-offset and θ_3 is the crankshaft displacement found using the kinematic relationship for the differential gear-unit, given in chapter 4, in equation (4.5) and the model responses from the constant speed motor and the servo-motor. In the experimental set-up the slider displacement is measured by means of a linear potentiometer during the control cycle. In the control program used in chapter 5, the result taken corresponds to the last cycle of the motion. The number of motion cycles is defined by the system user.

The model and the experimental system responses can be seen in Figure 7.2.(a) and (b) for the R-R motion.

The first plots on the left hand side of Figure 7.2.(a) and (b) show the command and responses for the closed loop servo-system. The 1st controller board, which was explained in chapter 5, has been used for this purpose. The variables are scaled consistently, whether they are model or experimentally based. In the model, they are found as radians and time, correspondingly as encoder counts and samples in the experimental results.

The second plot, shown in the middle of Figure 7.2.(a), gives the response of the crankshaft. θ_3 is calculated by using the kinematic relationship for a differential unit. For the second plot in the middle of Figure 7.2.(b), the 2nd controller board of the digital hardware arrangement has been used. The crankshaft output is taken as encoder counts in an open loop measurement taken over the control cycle.

The third plot on the right hand side shows the slider displacement found from the model measured on the exprerimental set-up by a linear potentiometer. It is expressed in meter in Figure 7.2.(a) and correspondingly in ADC counts in (b). The experimental measurement is performed in the 2nd controller board which was described in chapter 5. When the servo-motor started providing the required motion, the slider data is read from the linear potentiometer at the same time. This potentiometer is fed by a voltage supply. It's output is sent to the ADC's in the 2nd controller board. It is then stored with the other responses and plotted simultaneously.

Figure 7.3.(a) and (b) represent the model based and experimental test rig system command and responses for the R-D-R motion at the slider output. The variables are given in the same scale and units as before. The plots are given in the same order as above.

The first plot on the left hand side of Figure 7.3 shows the servo-motor command and responses, the second plot on the middle represents the command and responses on the crankshaft and the third plot on the right hand side finally shows the calculated and the measured slider displacements.

For the third example, the R-R-D motion, the model based and experimental system responses are given in Figure 7.4.(a) and (b) with the slider outputs. They are consistently scaled as the above.

In general, compared with the modelled responses, similar following characteristics for the servo-motor, the crankshaft and the slider are obtained in the experimental responses. The following error is found in lesser degree in the modelled responses. This was simply because of the assumption made in calculations, like an ideal system without friction and losses and sampling and computing overheads.

For the servo-motor, the correlation between the model and actual responses for the three motion cases is good. In the modelled responses, it is possible to get exactly matching curves by altering available gains in the controller action. But in the experimental servo-motor responses, under the available controller action, a following error is observed as a response lag between the desired and the actual output for all motion cases. This lag was less in slower motions used with the R-D-R and R-R-D cases. To eliminate this following error, it is realized that the servo-motor command would need to be tuned. This is already achieved in chapter 5 using the tuning algorithm given in equation (5.1). The command motion is modified for the next cycle by using the position information obtained during the previous cycle in the control program.

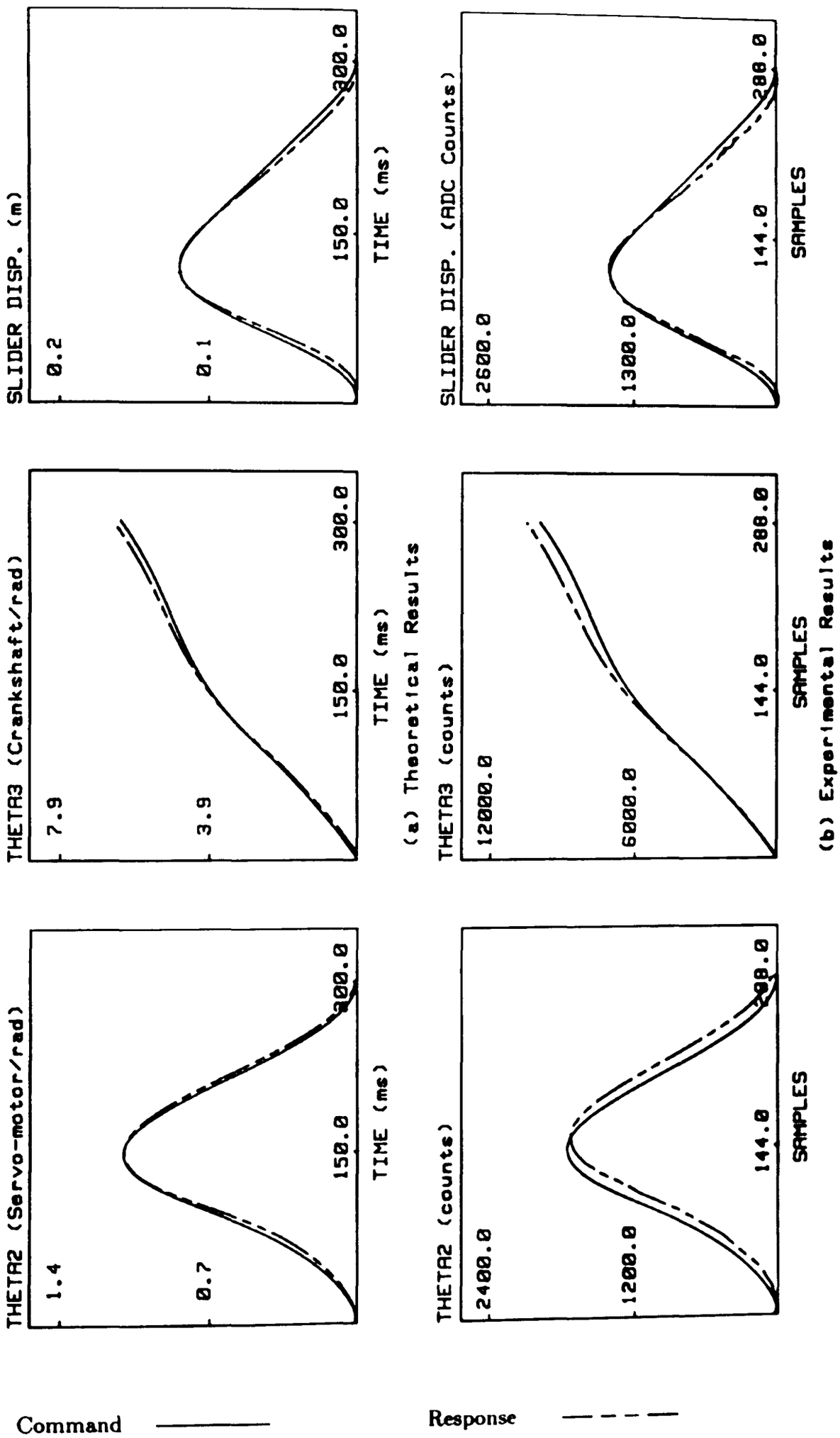

Figure 7.2. The model and the experimental responses for the R-R motion.

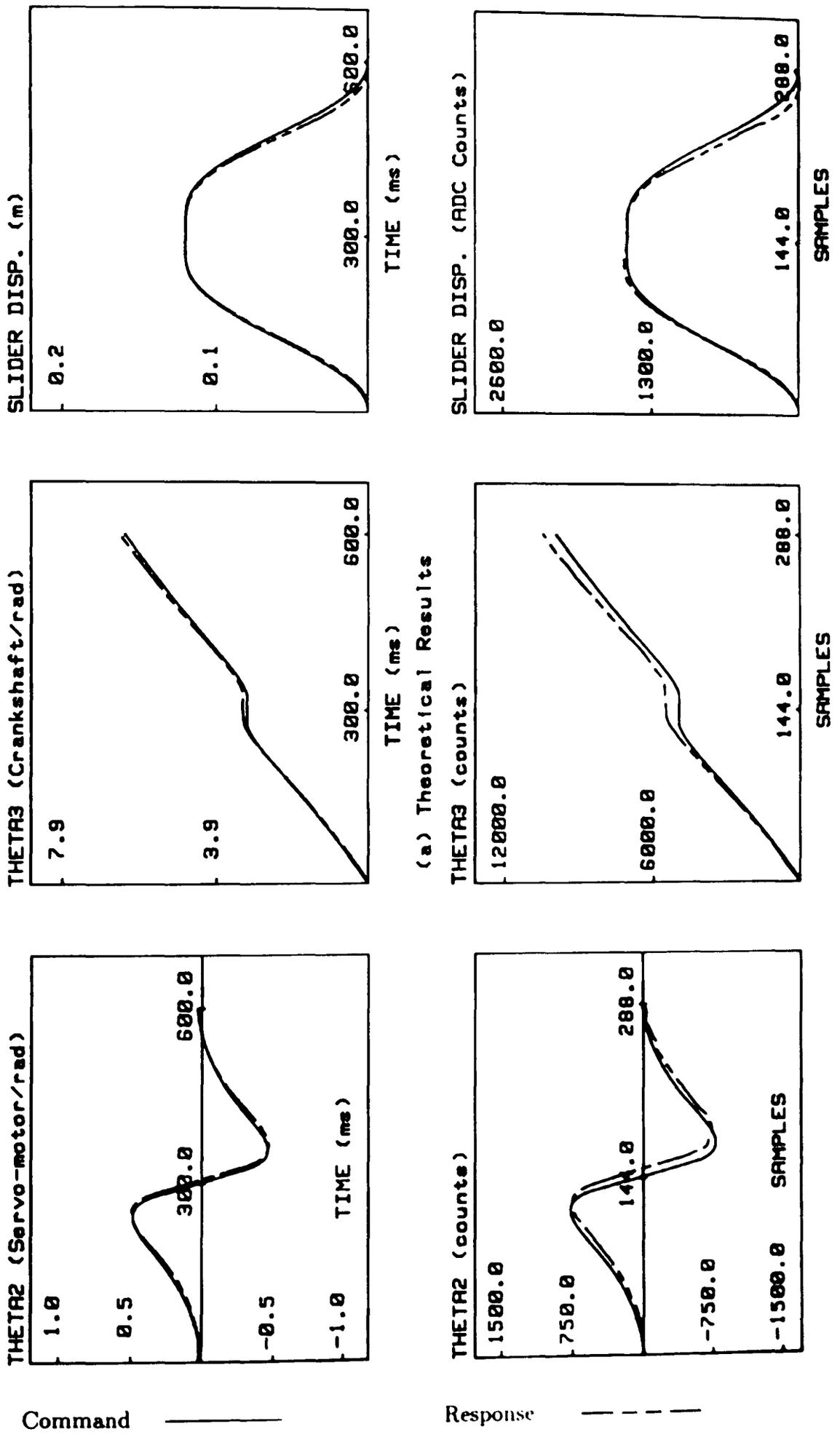

Figure 7.3. The model and the experimental responses for the R-D-R motion.

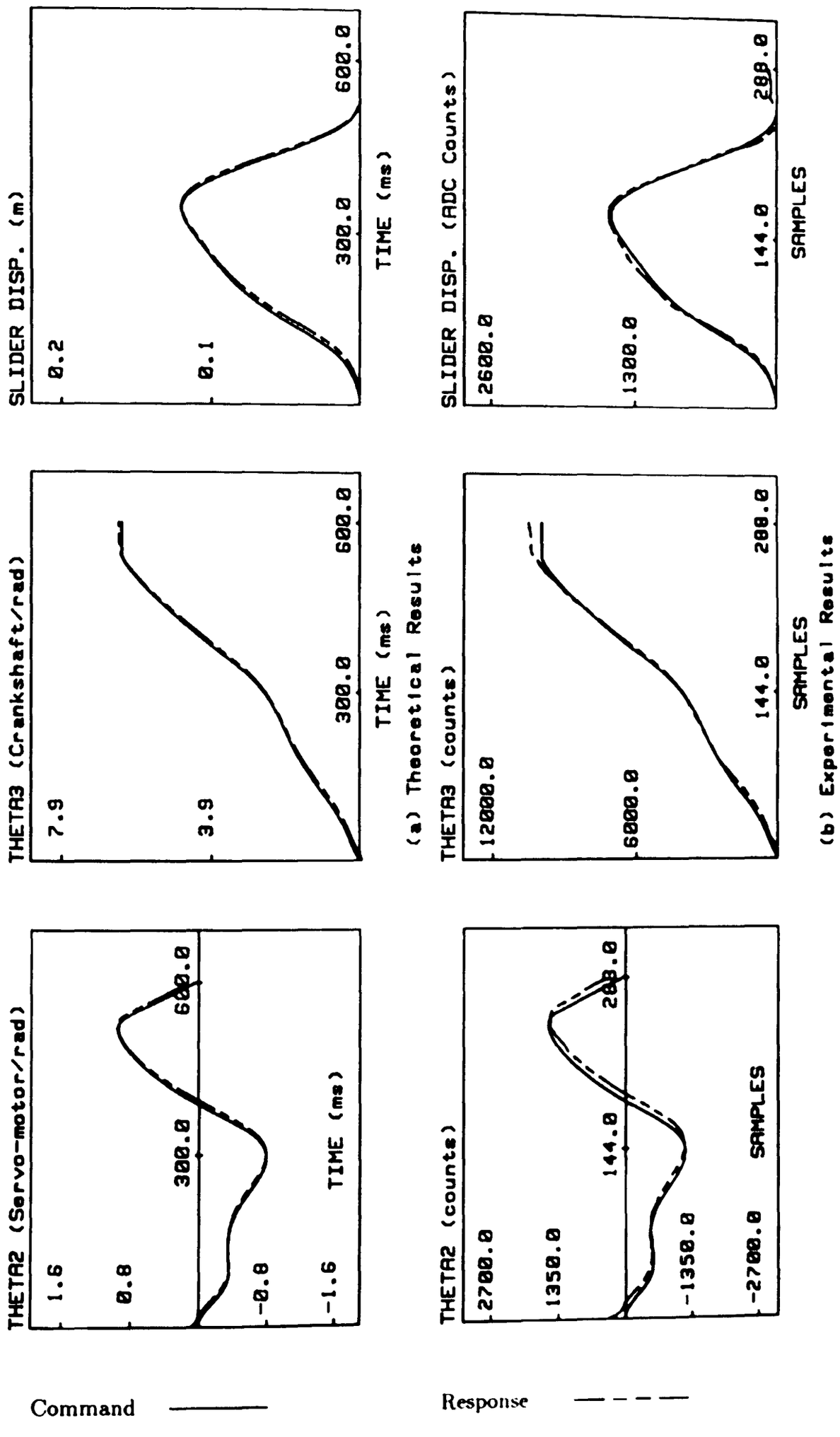

Figure 7.4. The model and the experimental responses for the R-R-D motion.

From the crankshaft leading responses are obtained for the three motion cases. In other words here the experimental response proceeds before than the required command. In the modelled crankshaft outputs this is negligible. Depending on the gain values set during the calculation of the constant speed motor and the servo-motor responses, the crankshaft response is determined. Evidently a leading response results in lagging slider displacements for the R-R and R-D-R motions. In the third motion the matching between the crankshaft command and response was quite good. Only measurement error is observed during the dwell period which caused an offset other than zero slider displacement.

Finally we may add some numerical values by looking at the actual slider displacements. The main concern is to see how well the slider met the requirements for the programmable action in the characteristically different motion cases. Here the values used in the calculation of the relative error contain experimental errors of measurement.

For the R-R motion the relative error is observed between 5 and 8 % in the rise period. When the slider is near to top dead centre, the error is reduced to 1.5 %. At top dead centre, it is found between 0.10 and 0.2 %. During the return period of the motion, because of the leading response observed in the crankshaft output, the relative error became bigger, in the range of 5 to 10 %.

During the implementation of the R-D-R motion, the relative error is observed between 2 to 4 % in the rise period. This is reduced to 0.2 % during the dwell. Compared with the first part of the slider motion, however, the relative error got five times bigger in the return period. This is caused by leading response observed in the crankshaft output similar to the prevoius example.

For the last motion case, R-R-D, during rise and return periods, the relative error is found in the range of 1.5 to 4 %. Here instead of getting zero slider displacement a positive displacement offset is observed. The reason for this was the leading crankshaft response seen during dwell like the previous examples.

7.3. Comparison of Torque, Angular Velocity and Power Curves

In the second part of the result comparisons, further calculations and measurements are carried out for the crankshaft torque, angular velocity, and the power output. This is achieved by including a set of calculation routines in the computer model for the torque distribution and power flow relations, given in chapter 6 for a differential gear-unit and correspondingly introducing a torque transducer into the experimental set-up.

Figure 7.5.(a) and (b) show a quantitative comparison of torque, angular velocity and transmitted power for the R-R motion.

The first plots on the left hand side of Figure 7.5.(a) and (b) represent the output torques calculated from the relations between the input torques in the model and those taken from a carrier amplifier, representing the crankshaft torque. The variables in each plot is scaled and presented with the same units for both studies. The torque axis is given in N.m and time in milliseconds. A calibration value has been used for the experimental torque, i.e: 3 volts represent 14.714 N.m. The measured torque is given in N.m and time in samples by using the calibration torque value.

In the second plots in the middle of Figure 7.5.(a) and (b), the angular velocities of the crankshaft can be seen. They are calculated by using the kinematic relation between the inputs of a differential gear-unit and also applying pulse-counting. Both outputs are given in rad/s and on a time basis in milliseconds and samples in the same figure.

The third plots on the right hand side of Figure 7.5 show the calculated and transmitted power in Watts and against time in milliseconds and samples. These values are found by multiplying given torque and angular velocity results from the previous plots. It is seen that the agreement between the model and the experiments is reasonable in terms of amplitude and characteristics. It indicates the validity of torque, power calculation for two driving input conditions previously given in chapter 6.

Figure 7.6 represents the calculated and measured torque, angular velocity, and transmitted power for the R-D-R motion. All variables in these plots are given with similar scales and identical units as above R-R motion.

Figure 7.7 represents the model and measured experimental torque, angular velocity and transmitted power for the R-R-D motion with same units and scale previously given for other two motions.

When these curves for the R-R, R-D-R and R-R-D motions are studied one by one, further comments may be added for the existing differences between the theoretical and the experimental results.

In the R-R motion in the Figure 7.5, the experimental output torque measurement shows some differences from the modelled results in the second half of the torque curve. The interesting point here is that, this output torque characteristic is found to be similar to the servo-motor torque calculated rather than the crankshaft torque.

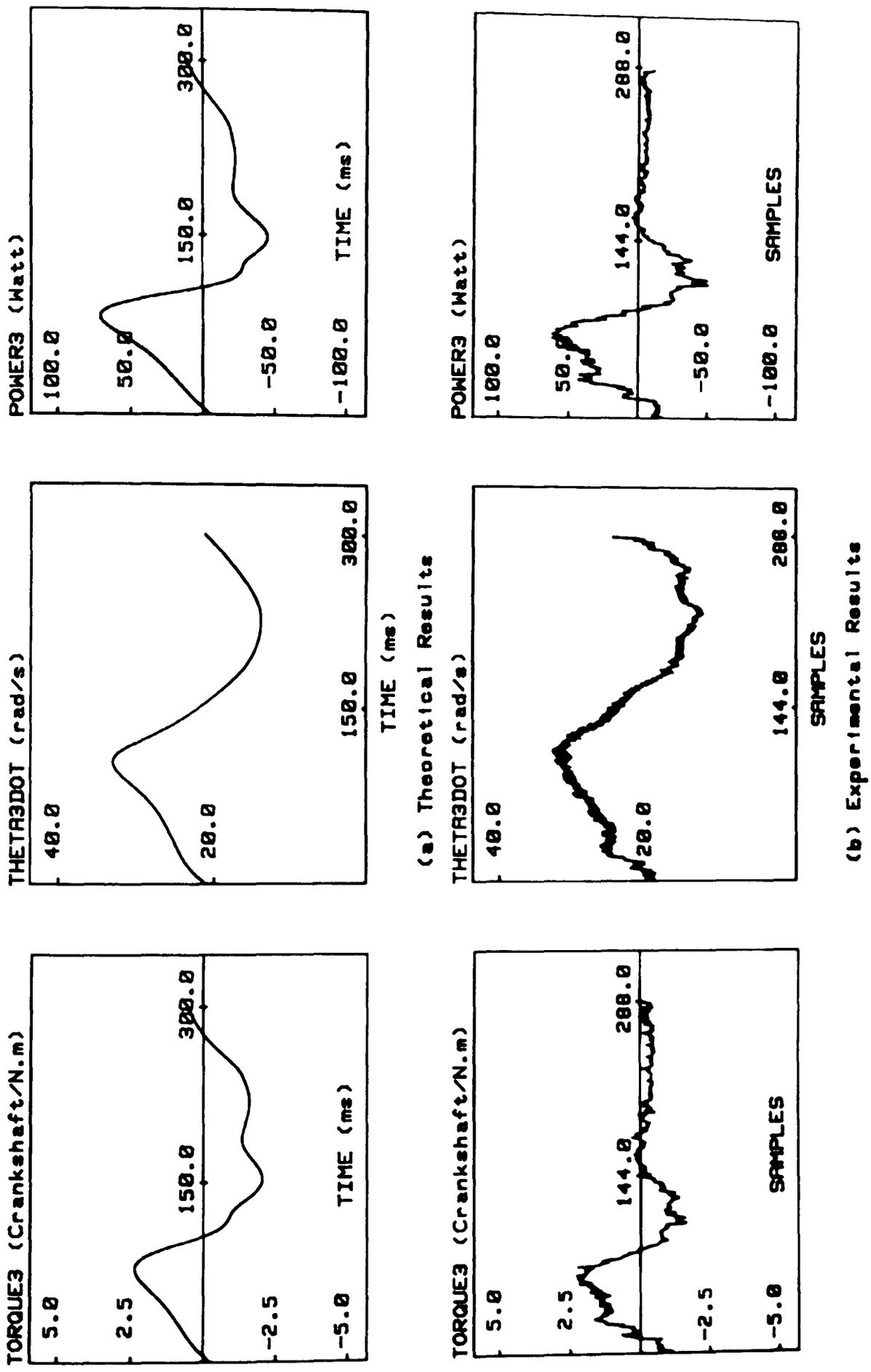

Figure 7.5. The model and experimental torque, angular velocity and power for the R-R motion.

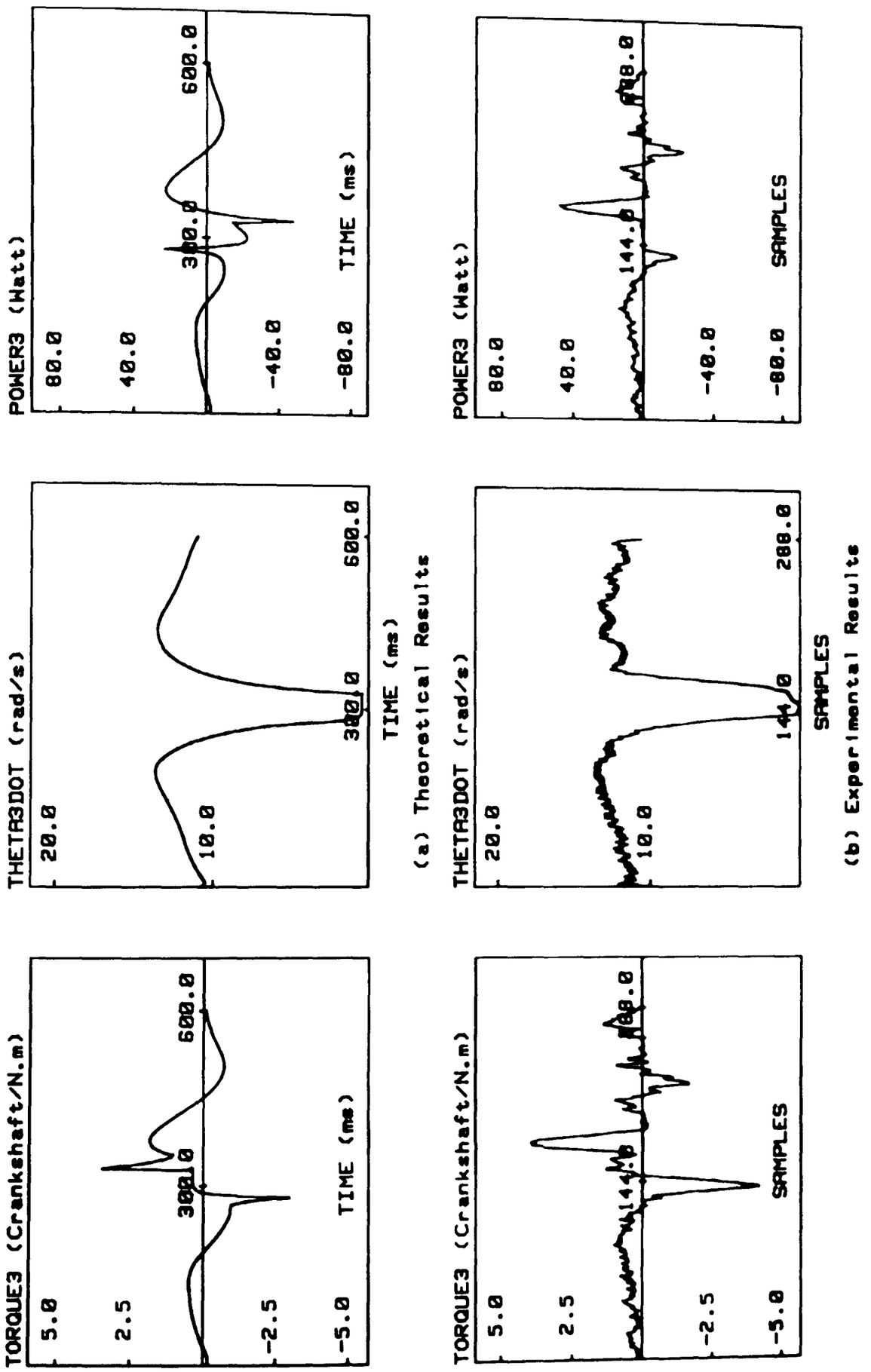

Figure 7.6. The model and experimental torque, angular velocity and power for the R-D-R motion.

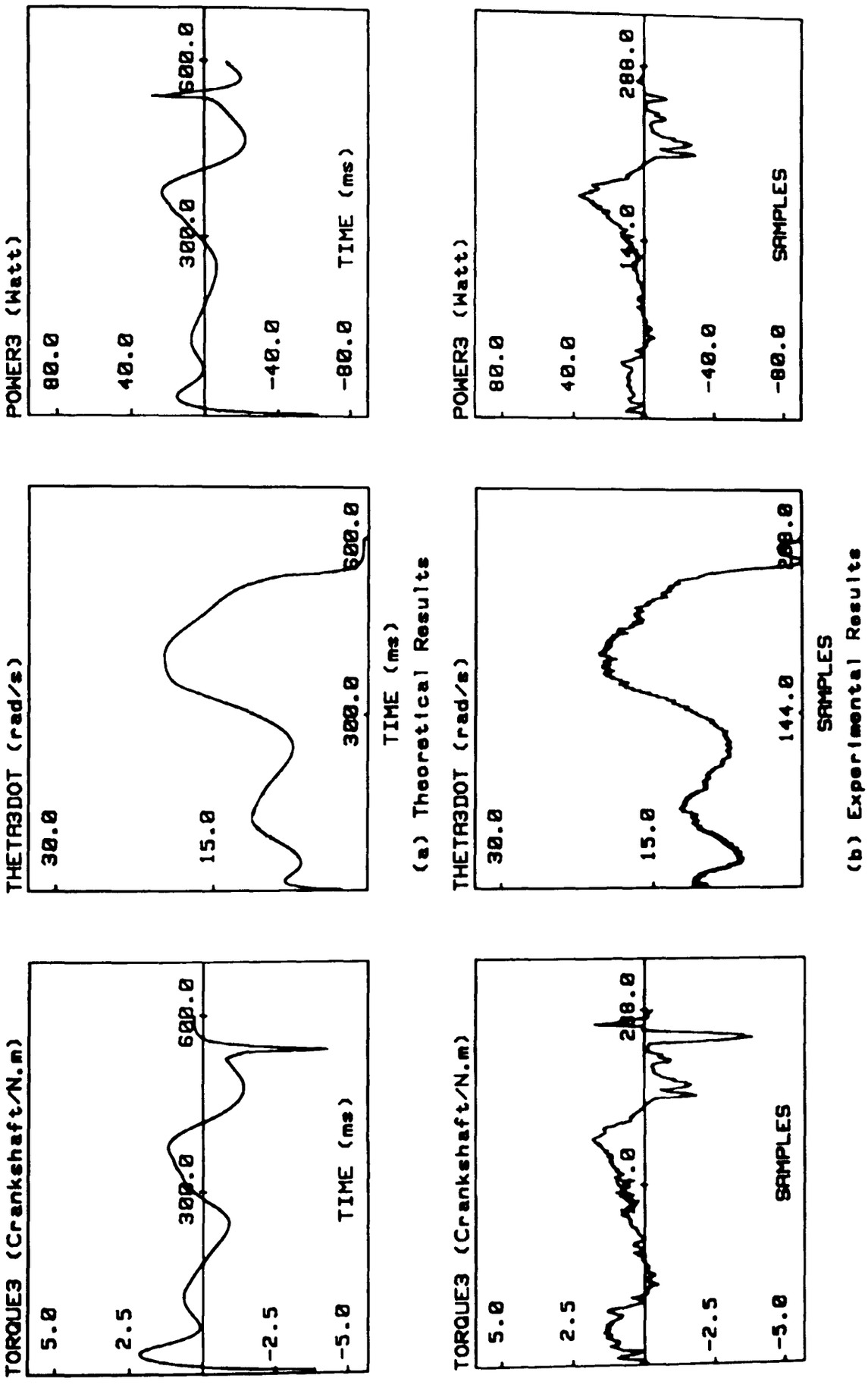

Figure 7.7. The model and experimental torque, angular velocity and power for the R-R-D motion.

This is simply thought to have resulted because of the developed model which introduced nonlinear coupling characteristics into the equations of motion. In real the system, this is becoming less obvious than the model. Since all accelerations and decelerations are performed by the servo-motor, whole torque characteristics are dominated by the servo-motor. The experimental result is much closer than the measured torque but still with higher noise levels in the second plot on the middle. The amplitudes of the high frequency components are noticable too.

As given in the Figure 7.6, quite good dwell period is found from the model for the R-D-R motion. However, while measuring the torque, some oscillatory behaviour is observed after the dwell period. Although similar motion characteristics have been obtained before the dwell, after then, it become oscillatory. A similar behaviour is observed in the crankshaft angular velocity. This is thought to be caused not only the result of imperfect dwell but also with inclusion of other transmission elements. In the angular displacement curves of chapter 4, this behaviour can not be traced. However, it is noticable enough in the actual system. It should be pointed here that before connecting the flexible couplings, the oscillatory behaviour seen was not the same. Inclusion of transmission elements with longer transmission line certainly amplified this undesirable behaviour.

Quite good correlation between results are found for the R-R-D motion in Figure 7.7. Especially the crankshaft angular velocity which is much closer to the model results and was reduced noise levels. The reason was, therefore, the operation at lower speeds so the amplitudes of the higher frequency components are greatly reduced. After performing dwell, similar oscillatory behaviour is seen in the beginning of the next motion cycle and then these oscillations die and the system output is become smooth. The results are given only for one cycle here. Actually without flexible couplings on the transmission line, these oscillations were not that obvious.

7.4. Comparison of The Programmable Drive Only and The Hybrid Arrangement

Here the mathematical model is used for the comparison of the two alternative techniques; the programmable drive only and the hybrid arrangement. In order to define a reference basis for comparisons, the same slider motions are achieved using both alternatives. They have then been investigated in terms of their input torques, angular velocities and power requirements from the programmable servo-motor.

All comparisons in the following section are based on the three designed motions, R-R, R-D-R, and R-R-D.

7.4.1. Considerations on The Servo-Motor Power Requirements

Initially the R-R motion is studied. By using the representative model equations, the calculations are carried out for the servo-motor angular velocity, torque and power. Figure 7.8 shows the torque-angular velocity diagram calculated for this motion. The full line represents the programmable drive only and the dotted line shows the hybrid arrangement.

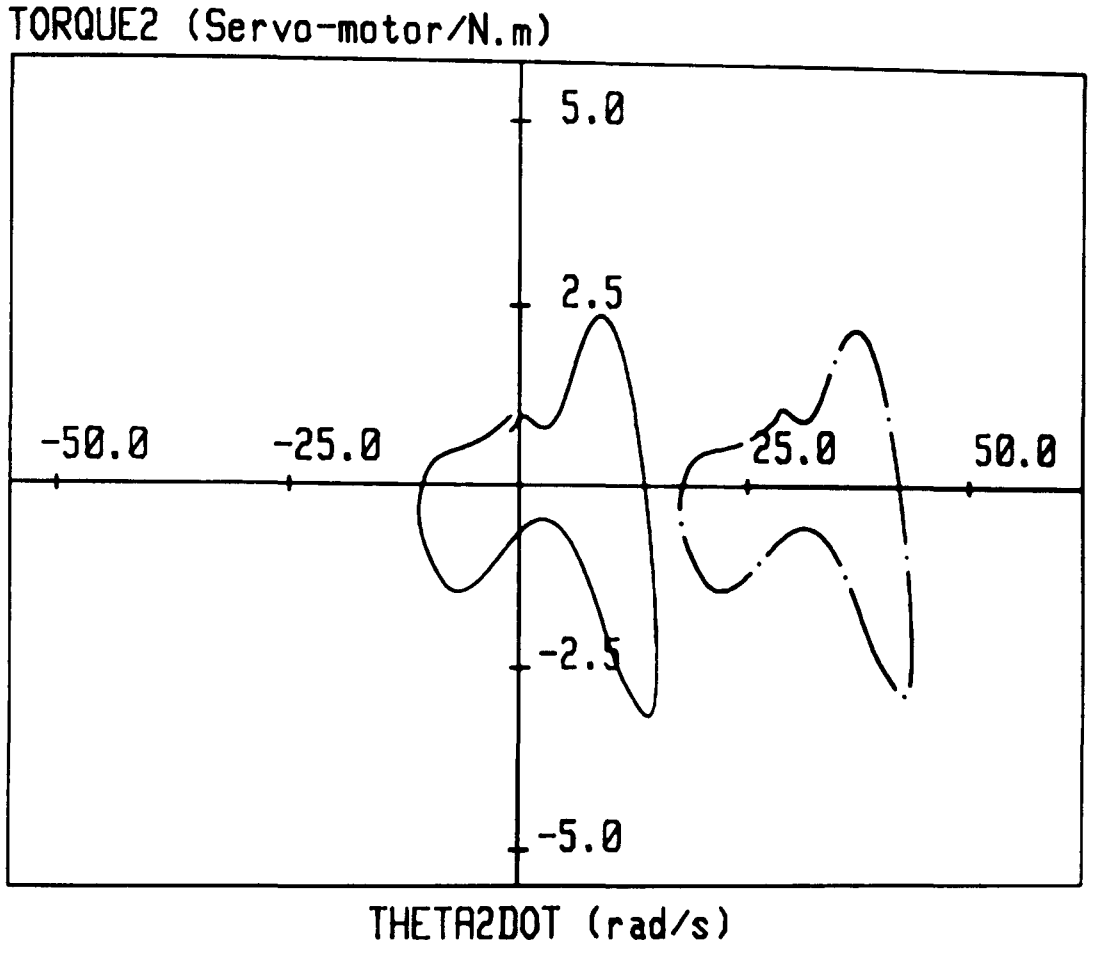

Programmable drive only arrangement — · —

Hybrid arrangement ————

Figure 7.8. Torque-angular velocity diagram for the R-R motion.

The servo-motor used is capable of operating in four quadrants of the torque-angular velocity diagram. It is possible to accelerate the mechanism connected to the motor and also decelerate by electro dynamic braking and then reverse the rotation. In two quadrant operation, the mechanism is either accelerated in the clockwise direction (operation in the 1st quadrant) or anti-clockwise (operation in the 3rd quadrant). When the mechanism is required to be slowed down, the braking action is achieved operating in the 2nd and 4th quadrant.

As it can be seen from Figure 7.8 that the programmable drive only arrangement requires two quadrant operation, always in clockwise direction. All quadrants of operation are required for the hybrid arrangement and the torque-angular velocity diagram is shifted to the left with

lesser angular velocities.

Figure 7.9 represents the time variation of $\dot{\theta}_2$, T_2 and P_2 for the R-R motion. The servo-motor requirements are shown with a full line for the programmable drive only and the dotted line is for the hybrid arrangement.

When the curves are studied one by one with reference to a few salient points, we can see the obvious power reduction for this motion case. To achieve the designed slider output, the programmable drive only arrangement requires the following maximum and minimum peak servo-motor torques, angular velocities and power;

$T_{2_{max}}$ = 2.2294 N.m $T_{2_{min}}$ = -3.07300 N.m
$\dot{\theta}_{2_{max}}$ = 43.9840 rad/s $\dot{\theta}_{2_{min}}$ = 17.1910 rad/s
$P_{2_{max}}$ = 82.8306 Watt $P_{2_{min}}$ = -131.7738 Watt

For the hybrid arrangement, the servo-motor requirements are:

$T_{2_{max}}$ = 2.3551 N.m $T_{2_{min}}$ = -3.1958 N.m
$\dot{\theta}_{2_{max}}$ = 15.8008 rad/s $\dot{\theta}_{2_{min}}$ = -11.1643 rad/s
$P_{2_{max}}$ = 22.0188 Watt $P_{2_{min}}$ = -47.9724 Watt

At the above salient points, the main difference is found in the angular velocity requirement of the servo-motor, not much from the servo-motor input torques. By looking at $P_{2_{max}}$, we can say that power reduction is more than 1/3 of the programmable only, also nearly 1/3 for mimimum power requirements.

The difference is seen in the last plots of Figure 7.9. This reveals that the same input torques but smaller power ratings would be required to accomplish the same task just by introducing lower angular velocities from the programmable input, the servo-motor.

R-D-R and R-R-D motion examples have been considered further to see whether there will be any use for the dwell introduced slider motions in terms of the servo-motor torque and power requirements.

Figure 7.10 represents the torque-angular velocity diagram for the programmable drive only and the hybrid arrangement where Figure 7.10.(a) is for the R-D-R and Figure 7.10.(b) for the R-R-D motion respectively. Two and four quadrant operation are found with similar servo-motor input torque requirements for both motion cases.

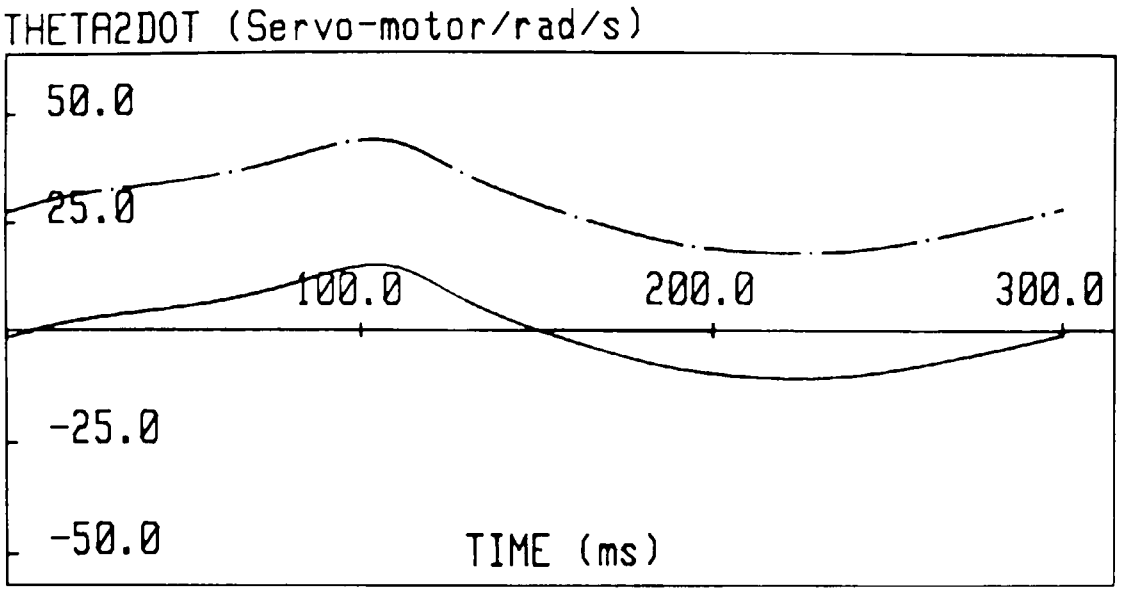

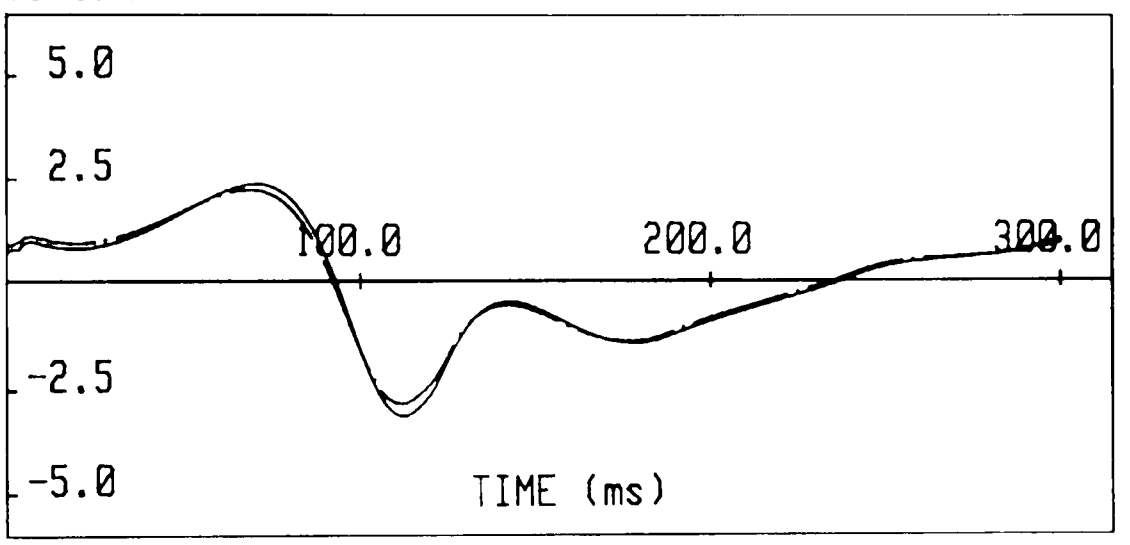

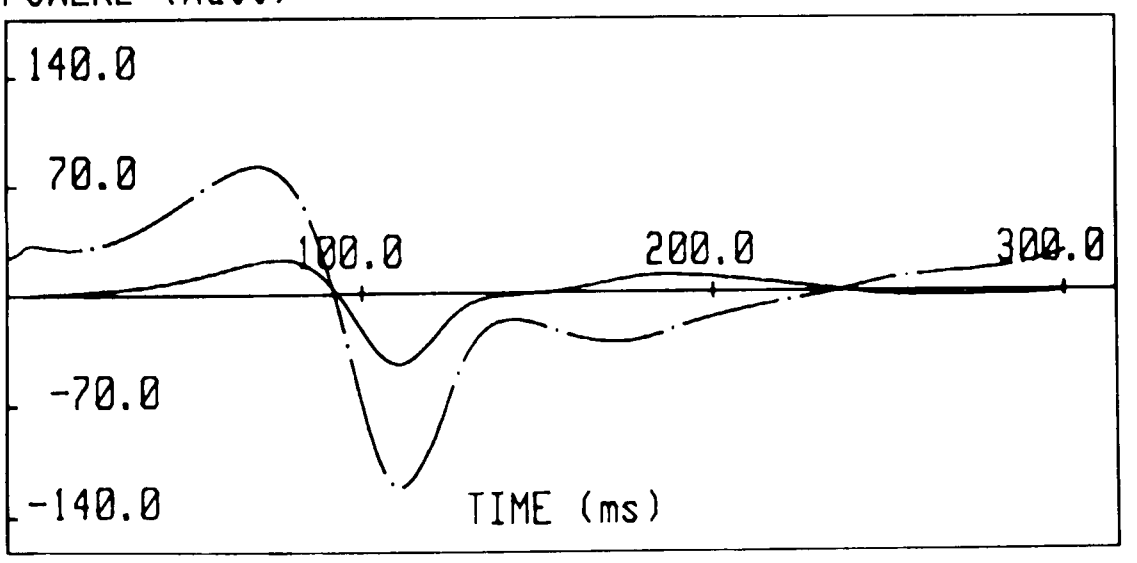

Programmable drive only arrangement — · —

Hybrid arrangement ————

Figure 7.9. The servo-motor requirements for the R-R motion.

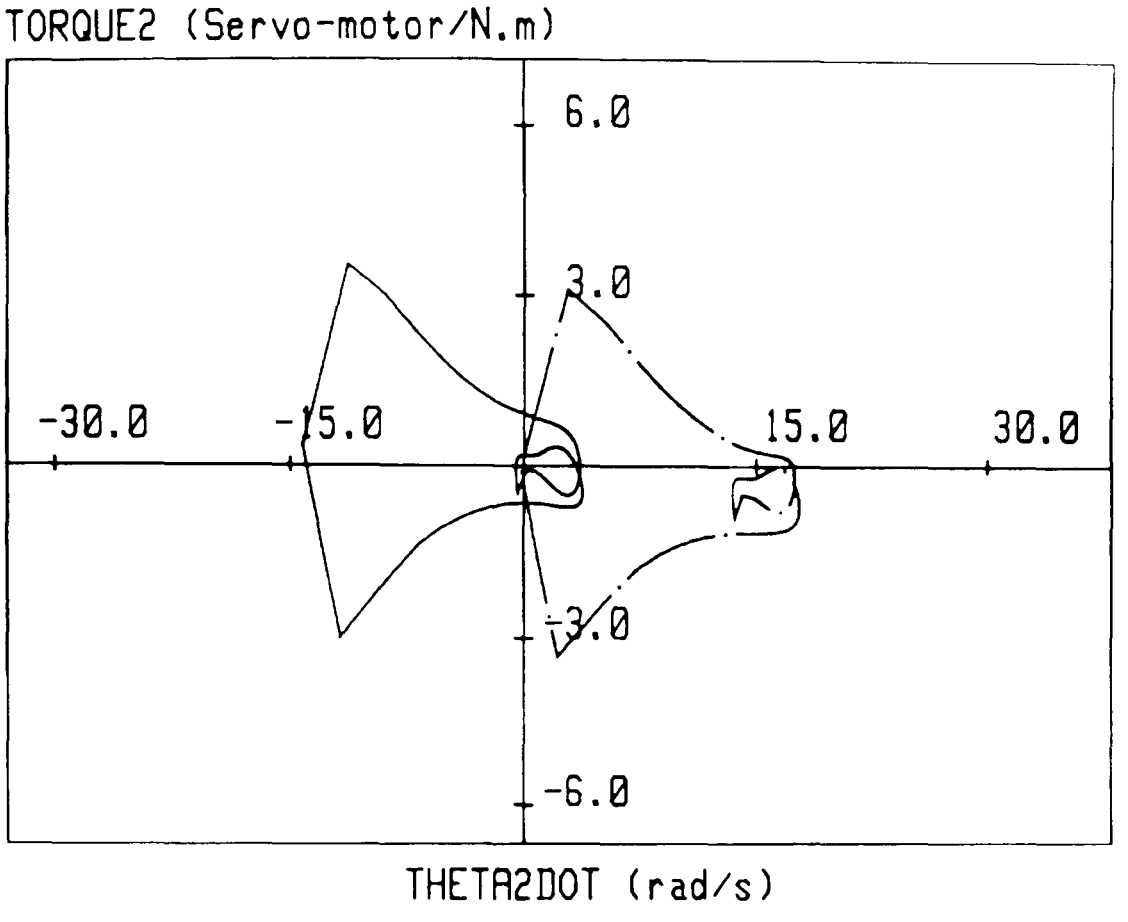

(a)

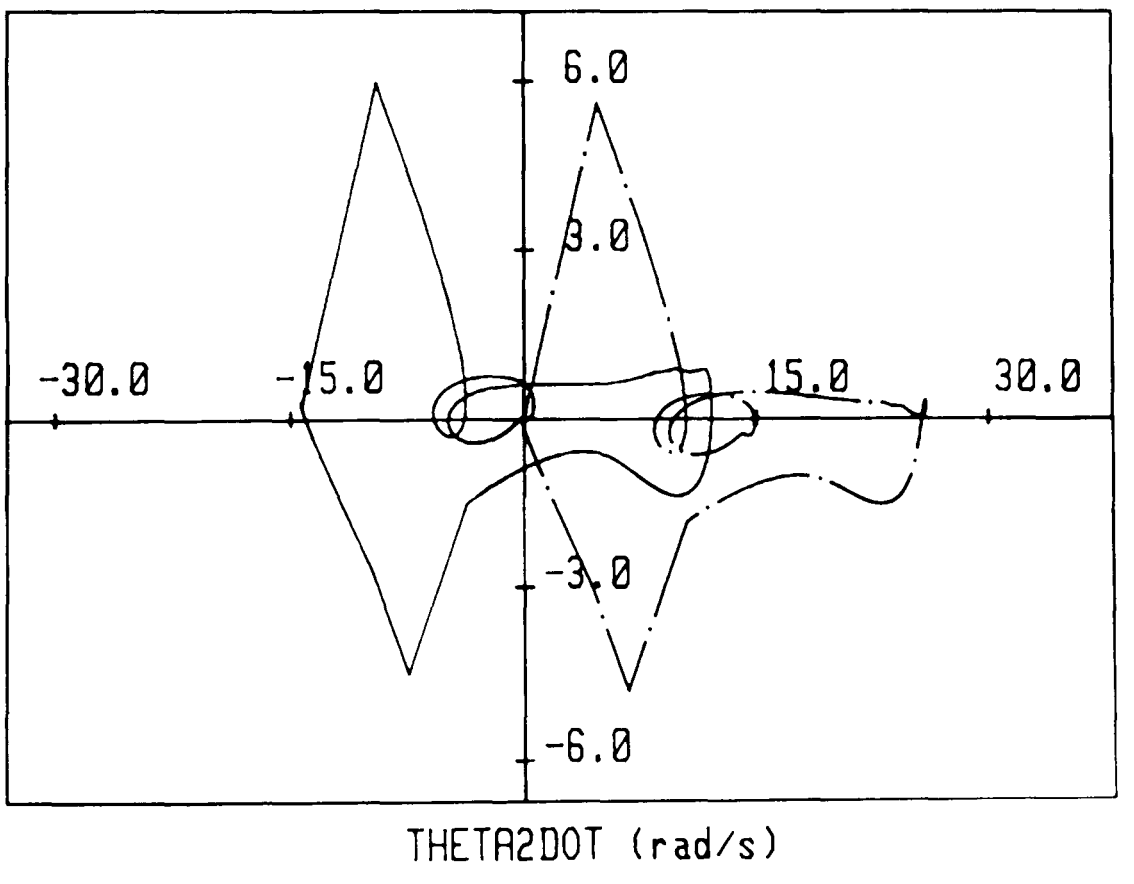

(b)

Programmable drive only arrangement — · —

Hybrid arrangement ———

Figure 7.10. Torque-angular velocity diagram for the R-D-R and R-R-D motions.

Figure 7.11 then demonstrates the servo-motor requirements for the programmable drive only and the hybrid arrangement for the R-D-R motion. The outputs are $\dot{\theta}_2$, T_2, and P_2 and plotted in the same order as above. The programmable drive only results maximum and minimum peak torques, angular velocities and power as the following:

$T_{2_{max}}$ = 3.0975 N.m
$\dot{\theta}_{2_{max}}$ = 17.8327 rad/s
$P_{2_{max}}$ = 13.6407 Watt

$T_{2_{min}}$ = -3.3464 N.m
$\dot{\theta}_{2_{min}}$ = -0.1389 rad/s
$P_{2_{min}}$ = -19.3226 Watt

For the hybrid arrangement, the servo-motor requirements are:

$T_{2_{max}}$ = 3.540045 N.m
$\dot{\theta}_{2_{max}}$ = 3.7529 rad/s
$P_{2_{max}}$ = 35.4713 Watt

$T_{2_{min}}$ = -2.998809 N.m
$\dot{\theta}_{2_{min}}$ = -14.2010 rad/s
$P_{2_{min}}$ = -40.0806 Watt

It is seen that there is not much difference in the servo-motor input torques. The servo-motor angular velocities indicate one and two directions of operation. In this example, however, the expected reduction in power requirement has not been found. The hybrid arrangement required higher servo-motor power. It is found as 2.6 times the maximum power requirement which is not desirable at all.

Finally the servo-motor requirements are calculated for the R-R-D motion. The plots are given in Figure 7.12. The programmable drive only requires maximum and minimum value torques, angular velocities and power as the following:

$T_{2_{max}}$ = 5.6525 N.m
$\dot{\theta}_{2_{max}}$ = 25.8388 rad/s
$P_{2_{max}}$ = 25.4824 Watt

$T_{2_{min}}$ = -4.7910 N.m
$\dot{\theta}_{2_{min}}$ = -0.2357 rad/s
$P_{2_{min}}$ = -35.1112 Watt

For the hybrid arrangement, the servo-motor requirements are:

$T_{2_{max}}$ = 5.9589 N.m
$\dot{\theta}_{2_{max}}$ = 12.0600 rad/s
$P_{2_{max}}$ = 33.4879 Watt

$T_{2_{min}}$ = -4.4968 N.m
$\dot{\theta}_{2_{min}}$ = -14.3158 rad/s
$P_{2_{min}}$ = -56.4564 Watt

Higher power requirements are found for the hybrid arrangement in generating the R-R-D motion. The maximum power is higher 1.3 times than the equivalent programmable requirement.

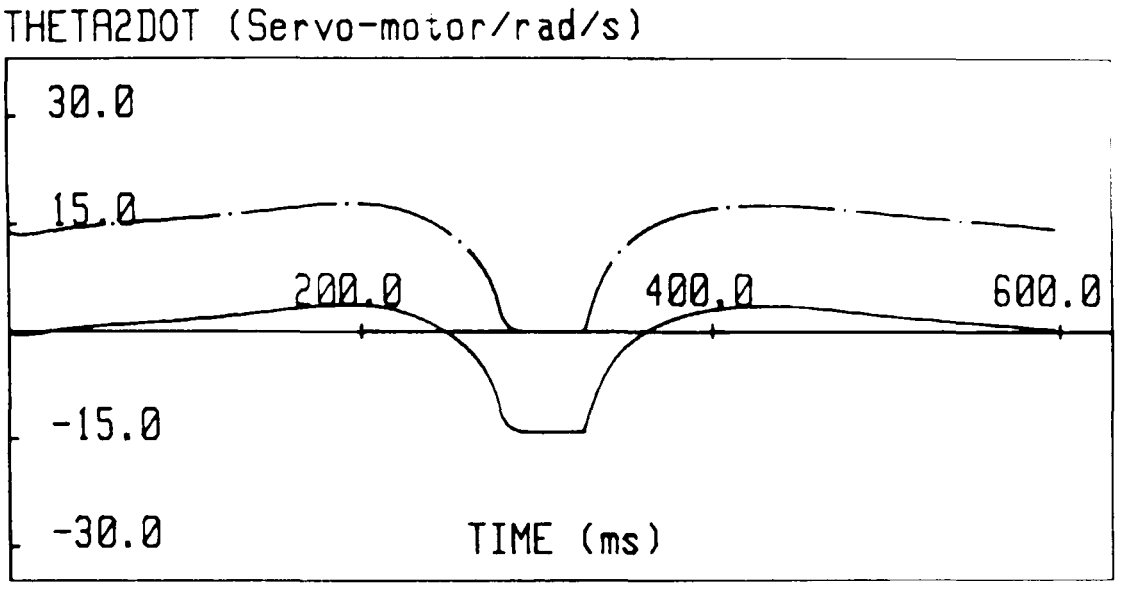

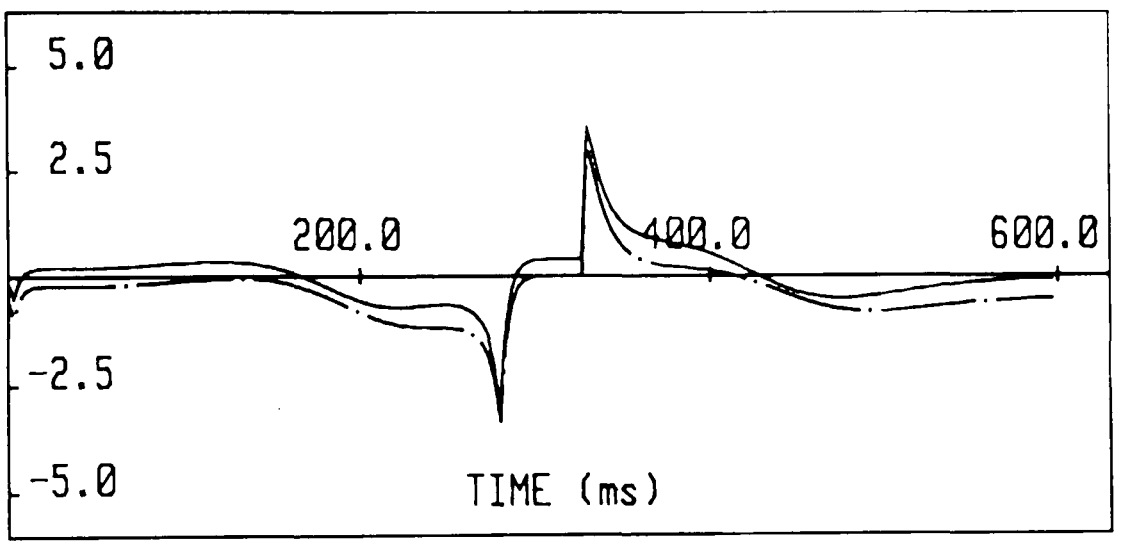

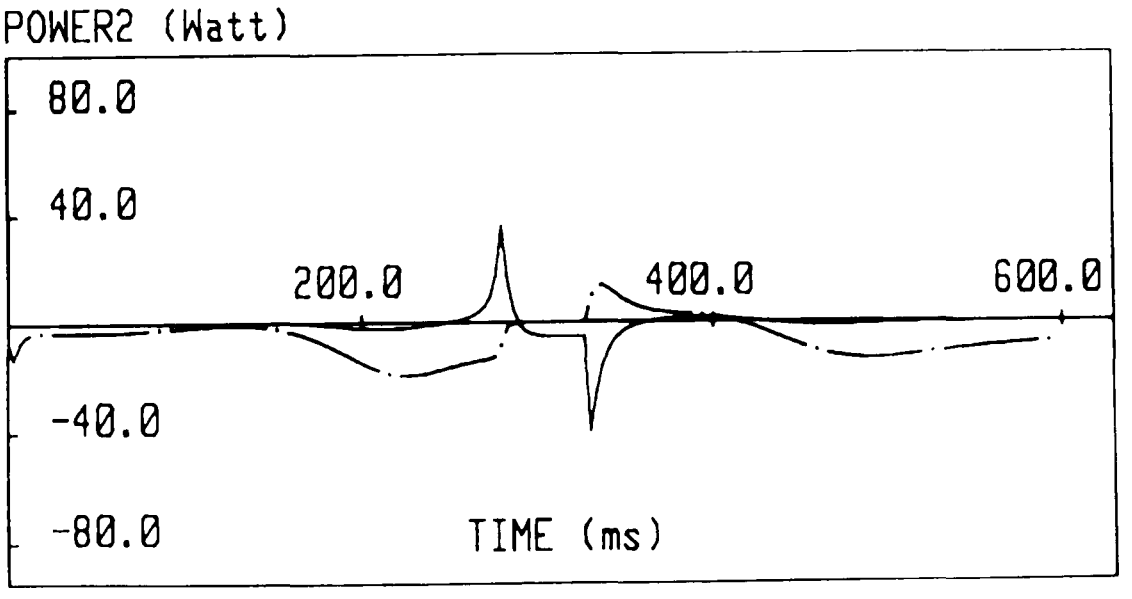

Programmable drive only arrangement — · —

Hybrid arrangement ———

Figure 7.11. The servo-motor requirements for the programmable drive only and the hybrid arrangement for the R-D-R motion.

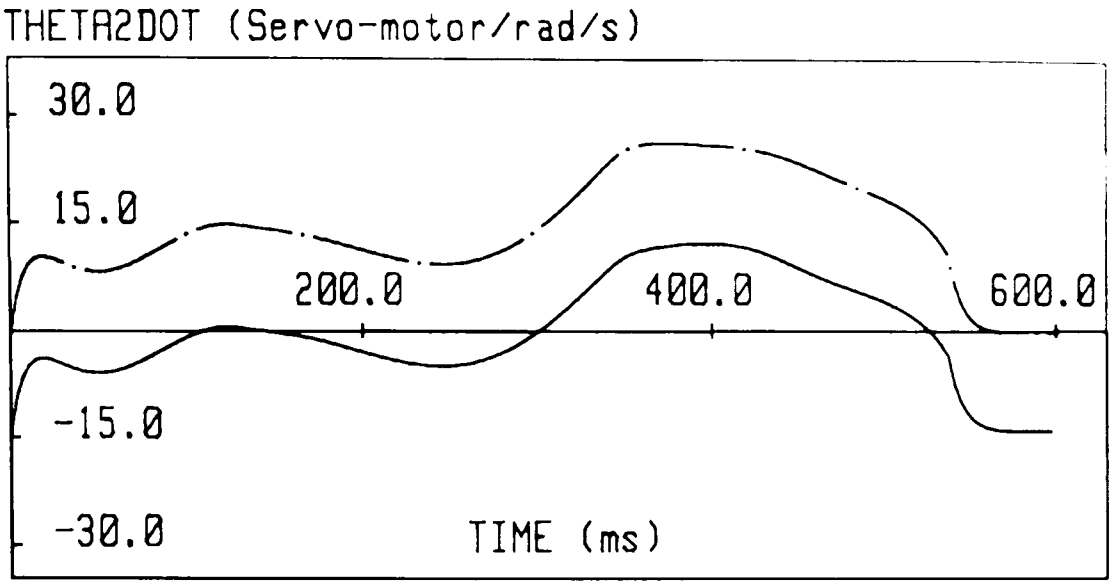

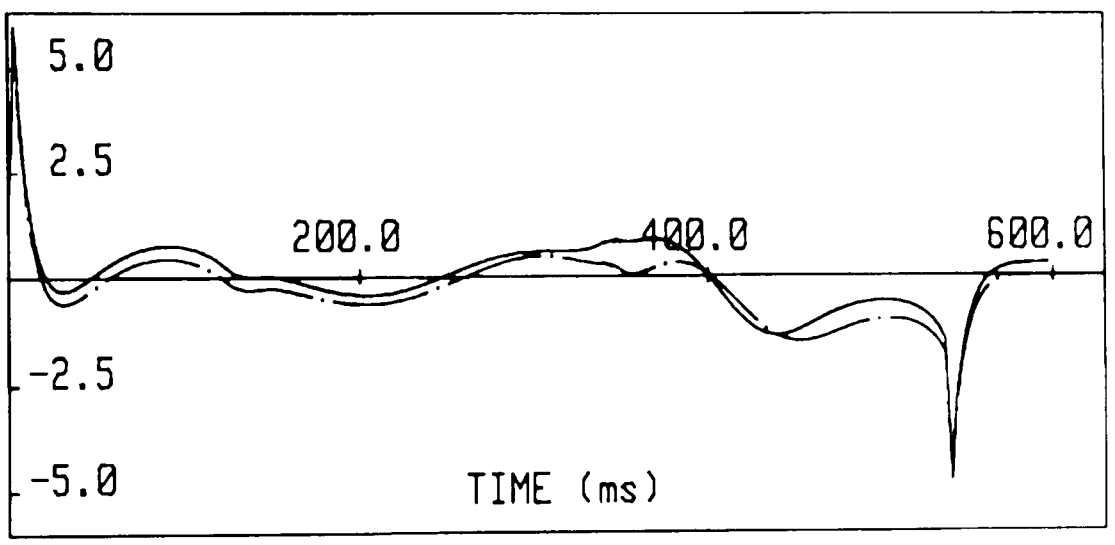

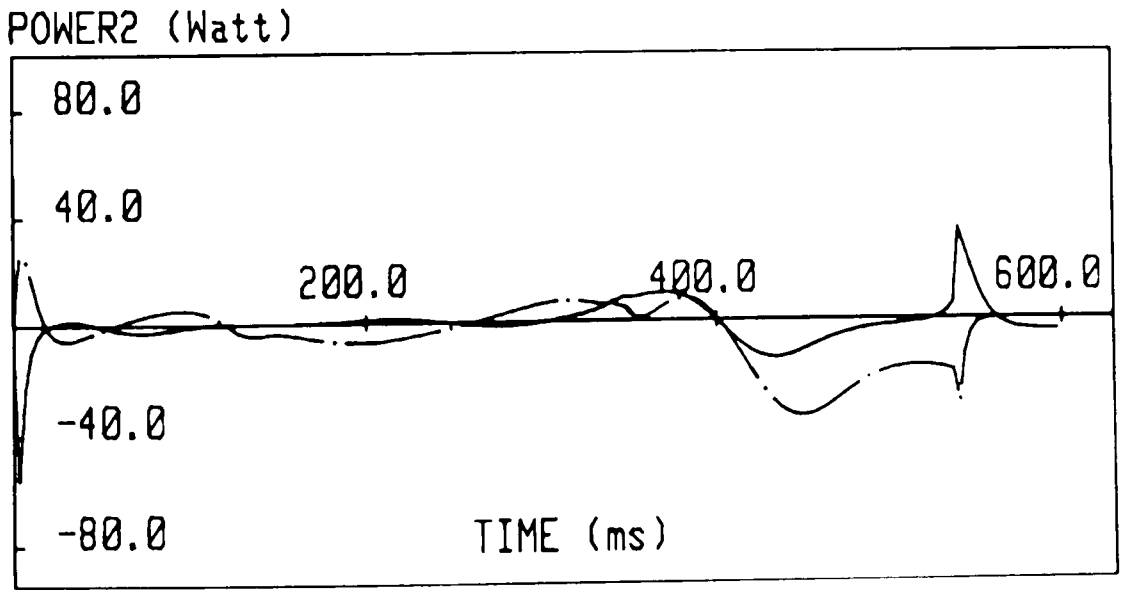

Programmable drive only arrangement — · —

Hybrid arrangement ———

Figure 7.12. The servo-motor requirements for the programmable drive only and the hybrid arrangement for the R-R-D motion.

So by looking at these figures we can make a conclusive statement about the characteristics for the implemented motion. Thus if small modulations, like R-R motion characteristics are introduced there will be no doubt about reduction from the servo-motor power requirements. However, when a dwell is introduced, the hybrid arrangement does not offer the expected reduction on the servo-motor power requirements. On the contrary, it nearly doubles the requirements and power ratings.

The observations for the comparisons of the programmable drive only and the hybrid arrangement are given in the following table.

MOTION	ARRANGEMENT	POWER REQ.	TORQUE REQ.	VELOCITY REQ.
R-R	Programmable	P_{2max}, P_{2min}	T_{2max}, T_{2min}	$\dot{\theta}_{2max}(+),\dot{\theta}_{2min}(+)$
	Hybrid	0.26 P_{2max} 0.36 P_{2min}	T_{2max} T_{2min}	$\dot{\theta}_{2max}(+)$ $\dot{\theta}_{2min}(-)$
R-D-R	Programmable	P_{2max}, P_{2min}	T_{2max}, T_{2min}	$\dot{\theta}_{2max}(+),\dot{\theta}_{2min}(+)$
	Hybrid	2.60 P_{2max} 2.07 P_{2min}	T_{2max} T_{2min}	$\dot{\theta}_{2max}(+)$ $\dot{\theta}_{2min}(-)$
R-R-D	Programmable	P_{2max}, P_{2min}	T_{2max}, T_{2min}	$\dot{\theta}_{2max}(+),\dot{\theta}_{2min}(+)$
	Hybrid	1.30 P_{2max} 1.60 P_{2min}	T_{2max} T_{2min}	$\dot{\theta}_{2max}(+)$ $\dot{\theta}_{2min}(-)$

7.5. The Regenerative Programmable Systems

This section discusses the energy considerations for the two alternative techniques involving a slider-crank mechanism. In order to achieve a programmable slider action, presently available which is a constant speed motor with a flywheel and proposed the hybrid arrangement are investigated. The system is assumed to be ideal without losses due to friction in these examples.

The constant speed motor/flywheel driving a slider-crank

In conventional mechanical systems, the excess energy can be stored as kinetic energy of rotation or it is totally lost from the system by conversion to heat or noise etc. Standard linkage mechanisms with large flywheels experience typical regenerative system in practical applications.

The flywheel is capable of storing and delivering kinetic energy depending on the requirements for the supply and demand. The flywheel buffers out the energy flow between the motor and the mechanism, and its moment of inertia also controls the output fluctuations acting as a mechanical filter. So energy is transferred back to the motor during one part of the slider motion and is available for use during other part of the slider motion according to the slider speed achieved. In the absence of external loads, the mechanism would run indefinitely.

Here the motion of the slider is fixed by the rotational speed of the flywheel and the output is totally *regenerative* but *non programmable.*

The servo-motor driving a slider-crank

In direct generating non-uniform motion, the programmable drive only arrangement achieves the motion by providing the required accelerating and decelerating torques. Although the desired variability in slider motion is achieved, the energy interchange between mechanical and electric components does not allow very efficient use of energy. Since there is no simple way of storing re-usable energy, their regenerative capacity is very limited.

The hybrid arrangement driving a slider-crank

By using a differential gear-unit and a flywheel the motion of the slider can possibly be made both *regenerative* and *programmable.* By use of a low energy control input, the transfer of energy between the flywheel input and the crankshaft could be regulated. Energy could be transferred from the crank to the flywheel even when the rotational speed is less than that of the flywheel.

In principle, the hybrid arrangement offers both programmable and regenerative output.

7.5. Conclusion

A theoretical study must always be supported by an experimental verification. For this purpose, a complete check of the model was thorougly obtained by using the experimental set-up and quantitative comparisons were presented in this chapter. While testing the computer model against the experimental work, great care was taken to ensure that the results were reliable and verification was good enough.

The model based and experimental set-up slider outputs have given complete satisfaction. The slider has met the requirements of the three designed motions. As already mentioned,

however, during the output torque measurement, the measurements obtained on the crankshaft and the computer model have shown some discrepancies. They were thought to be the result of noise, unbalanced masses and the carrier amplifier used. The developed model was also thought to be another source in terms of introduced high nonlinearity in the equations of motion of the system. In addition to this, the model results were calculated for an idealized system free from real effects.

This chapter has also given an oppurtunity to reveal the comparative advantages and disadvantages of the programmable drive only versus the hybrid arrangement for the servo-motor power requirements and their potential regenerative capacity for future applications. It has seen that depending upon the modulations required either the hybrid arrangement was advantageous or disadvantageous. This result made clear that modulation amount was a very important and determining point for future applications of the hybrid machines.

CHAPTER 8
BOND GRAPHS FOR THE HYBRID ARRANGEMENT

8.1. Introduction

Bond graphs were first used in 1959 by Prof. H.M. Paynter at M.I.T (Cambridge, Mass. U.S.A) as a new concept utilizing power and energy as input-output variables to simplify the intensive use of block diagrams for servocontrols and simulation problems. (For a bibliography the reader is referred to [8.1]). Since then the bond graph structure has been further developed in the last decade particularly by Prof. Dean Karnopp and Prof. Ronald Rosenberg [8.2].

Bond graphs consist of signs, lines and simple symbols for the representation of engineering systems. Both energy and signal exchanges can be shown in this linear graph and a clear picture of the relationship between the variables of a dynamic system can be obtained.

In the past, most applications of bond graphs have been almost entirely applied to mechanical systems. However, like all systems that involve mixed engineering components of all types, mechanical, electrical, hydraulic, pneumatic and thermal, can be conviniently represented by bond graphs.

In its applications, bond graphs are used in a variety of ways. For example, either bond graph of a system is constructed with a given Lagrangian [8.5] or the reverse is achieved, a given bond graph is used in writing the equations of motion [8.9]. The second approach also provides a suitable way to establish the generalized coordinates, the generalized forces and to compute state functions for a variety of systems. The structure of the graph contains all, or almost all, of the information if the system is linear or mildly nonlinear. However, in systems that are highly nonlinear, the graph structure can contain relatively little information and serve rather little purpose.

Compared with other techniques of representation, such as differential equations, transfer

functions, block diagrams and signal flow graphs a bond graph has the advantage of

–providing a graphical representation of the interactions between all components in a system,
–mixing the energy systems that can be bonded together without regard to the form of energy,
–presenting a powerful tool in developing a systematic approach to obtain state equations for dynamic systems.

It has been accepted that bond graphs can bridge the gap between control engineering and the parts of the engineering science whose power has greater importance in energy conversion [8.8]. However, the emphasis is put on the studies that, *bond graph is only a graphical language rather than a solution technique.*

In this chapter, the bond graph concept is considered from the word bond graph, the power graph and the final bond graph form with the causality. The equations of motion are used to construct bond graphs. The exact equations of motion are modified during the logical procedure of bond graph modelling, like separate dc-motors and a differential gear-unit with a coupled slider crank mechanism. The reason for these changes was the result of high nonlinearity observed in the model equations developed in chapter 4. This is explained in the following section in detail.

8.2. Linear System Equations for Bond Graph Modelling

To carry out bond graph modelling for the hybrid arrangement, the equations of motion, equation (4.13) and (4.15) given in chapter 4 are reconsidered here. The characteristic of these equations is that each axis includes coupling terms from the other axis. For example, the equation of motion of the constant speed motor, equation (4.13) includes the displacement, velocity and acceleration terms of the servo-motor. Similarly, the equation of motion of the servo-motor, equation (4.15) includes the displacement, velocity and acceleration terms for the constant speed motor. All of these mixed terms introduce high nonlinearity to the system equations. Thus this makes bond graph representation for the hybrid arrangement more difficult and complicated.

The intention of using bond graphs here is to simplify the power structure of the system and to show energy exchanges clearly. To achieve this, a decision is made and the equations of motions are simplified. The coupling effects in the equations of motion are not taken into consideration. Therefore compared with the equations of motion of the system, relatively different set of equations of motion are used throughout this chapter. The representative system is thought with two separate motors and their inputs are summed by a differential

gear-unit to drive a slider-crank mechanism.

Consequently when the differential gear-unit is applied as a two degrees of freedom mechanism some difficulty is found in the bond graph representation. This is eliminated by doing some manipulations in the graph representation. These changes are explained the following sections.

Evidently because of simplified system equations some of the system details are lost, but an attempt is made to get some use from the bond graph representation for the hybrid arrangement.

8.3. Fundamentals of Bond Graphs

Before presenting the bond graph concept and derivation of models, the reader is recommended to look at the summary of the basic elements of bond graphs [8.4], [8.8] and their definitions with given examples in Appendix 4, Table A.4.1.

Here the bond graph technique is summarized with the help of the word bond graph, standard elements and the concept of causality.

8.3.1. The Word Bond Graph

The *word bond graph* form identifies an initial representation of the system with words and lines. The words represent the system components and the lines indicate power exchange between them. Each line carries a pair of signals whose product is power. This is a well-suited form to display the power structure of the systems.

Figure 8.1.(a) shows the principle of a word bond graph with an example of a dc constant speed motor coupled by a load (mechanism). This form can also be used to represent a closed control loop with feedback signals. This is exemplified by a servo-motor driven mechanism where position feedback is added.

In Figure 8.1.(b), feedback is represented by lines with arrows indicating one way signal flows. These are called as *degenerate bonds* [8.1] such that the information is communicated without power. Position and velocity signals are transmitted without any back effect.

By combining the above word bond graph representations the hybrid arrangement is shown in Figure 8.1.(c).

Figure 8.1. The Word Bond Graph.

In word bond graphs, the transfer functions for command, amplifier and controller are handled in a standard block diagram manner. However, in a true bond graph, the components are not represented by a full description instead they are replaced by the standard bond graph elements.

8.3.2. Standard Elements of Bond Graphs

The bond graphs employ a standard set of elements for modelling power flows in a dynamic system. The lines connecting the elements are named as *bonds*. Associated with each bond, there are two variables; *a cause* and *an effect* reacting with each other to provide new causes. They are the *effort*, e(t) and the *flow*, f(t) giving a product, the *power* P(t). So each bond is equivalent to two signals in conventional block diagram notation.

$$P(t) = e(t) \cdot f(t) \tag{8.1}$$

and this bond is represented as follows:

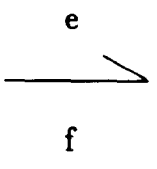

where the half-arrow describes the assumed direction of positive power flow. In mechanical devices, the effort and flow become the torque and angular velocity, whereas in electrical circuits the voltage and current respectively.

The standard elements of bond graphs are classified according to the number of bonds that they represent, as one-port, two-port and multiport. There are nine basic multiport elements that are grouped into four categories according to their energy characteristics. These elements and their definitions are summarized in the following part and also in Appendix 4 Table A.4.1.

One-ports are the elements exchanging energy with the system through one bond only including resistance-elements, called *R-elements;* capacitance-elements, called *C-elements;* and inertia-elements, called *I-elements.*

The resistance elements that dissipate energy are represented by R, ie: resistors, dampers, friction etc. The *R-elements* have a functional relation between effort and flow. They take power from the system and transform it into a considerable loss as heat. The storage elements store all kinds of energy forms are indicated by C and I, ie: capacitors, inductors, springs etc.

The *C-element* represents a relation between time derivative of effort and flow, whereas the *I-element* gives a relation between the time derivative of the flow and effort.

The *effort and flow sources* S_e, S_f are also included within the one-port elements, i.e: voltage and current sources. In an effort source, effort is independent of flow while in a flow source the flow is independent of effort.

Two-port elements have two bonds for energy exchange within the system. They are the transducers forming power flow from one physical domain into another domain without storing or dissipating energy but preserving it.

The *transformer* (TF) represents efforts and flows that are proportional due to the power conservation. The best examples are the gear reducers and the electrical transformers. The ratio of the efforts is called the *transformer ratio* (or modulus). The *gyrator* (GY) is defined where the input effort is proportional to the output flow and the output effort proportional to the input flow. An electric motor is a well-known example for the gyrator. The constants of proportionality are equal due to power conservation and are called as the *gyrator ratio* (or modulus). Both transformer and gyrator may be adjustable. Their conversion ratios can be modulated by a signal applied through an activated bond and they are represented by the symbols (MTF) and (MGY).

The *junctions* are the three-ports indicated by 0- and 1- are equivalent to parallel and series connections in electrical circuit diagrams. In some studies, they are represented by p- and s-junctions.

Zero represents a junction through which a common effort passes and into which the sum of the flows is zero. On the other hand, a one represents a junction through which the flows are equal and the efforts add up to zero. The junctions are power conserving at each instant and the power transports of all bonds add up to zero at all times.

8.3.3. The Causal Bond Graphs

In a bond graph representation, each bond can be marked by a vertical bar. This establishes a sense of input-output to each of the elements in the system and defines the *causality*. The assignment of causality gives a new capability for displaying the variables.

The effort causality exists in the direction towards to the bar and flow causality away from it. The open end of a bond indicates the causal direction of the flow signal. This is shown as the following.

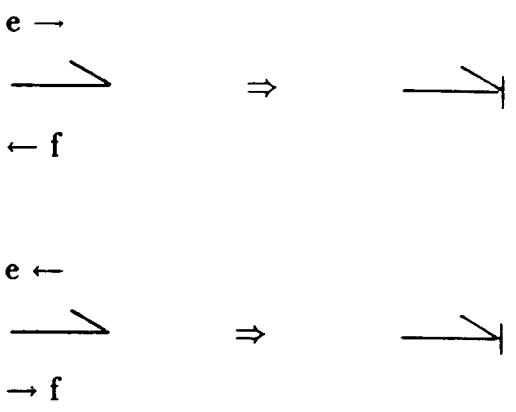

There are some rules for the selection of causality on the bond graphs. The ports of the elements are classified into four different groups for causality assignment.

–The ideal sources (S_e,S_f) have a *fixed causality*. Sources that impose an effort or a flow to the system are represented with an arrow pointing away from the source.

–The storage elements (C, I) have a *preferred causality*, like integral causality or derivative causality, depending upon the computational requirement. For I- and C-elements the energy flow is chosen into the element.

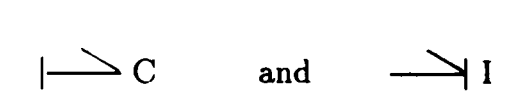

–Junctions, transformers and gyrators have *causal constraints*. The causality of one of the ports fixes the causalities of the others. A transformer transmits causality straight through itself with no change in direction. On the other hand, a gyrator inverts the direction of causality so that an effort causality into the gyrator will result in a flow causality out.

Referring to the junctions, an input effort determines all other efforts in a 0-junction. The 1-junctions contain a common flow, one input flow determines all output flows, whilst one effort is determined as a sum or difference of all input flows.

Some of the examples for gyrators and transformers are:

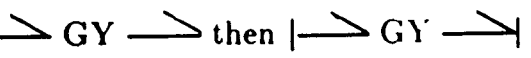

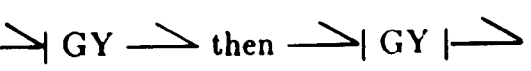

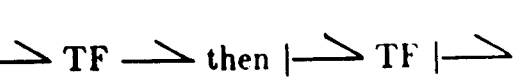

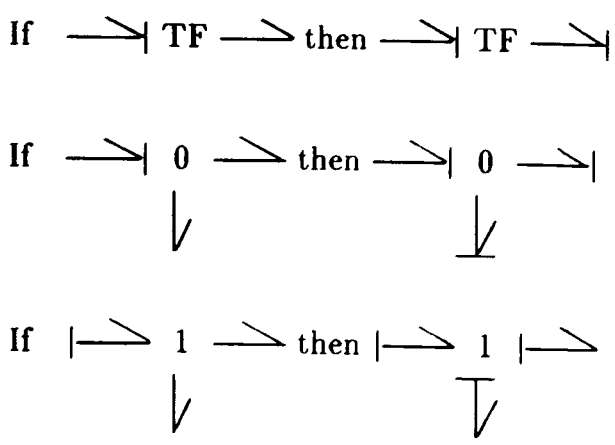

–The dissipative elements have a *free causality* which means that causal forms can be taken without any preference or constraint, such as a linear resistor. This can also be called as indifferent causality.

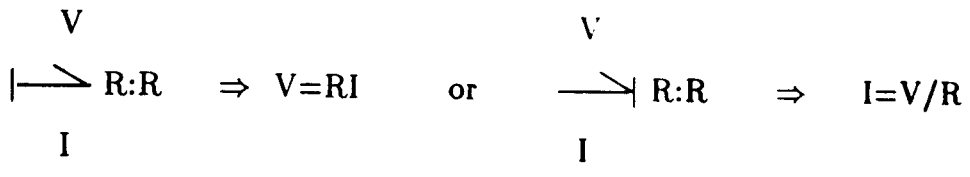

8.4. The Power Graph

The *power graph* provide a useful and clear way of displaying the relationships. It is the detailed form of the word bond graph with added effort and flow variables and power direction arrows.

To clarify the system's power structure, the hybrid arrangement is shown with two separate examples and related power graphs are presented. The first example is a constant speed motor with the annulus of a differential gear-unit driving a load (slider-crank mechanism). The second one is a servo-motor with a gear reducer driving a load.

The equation of the armature of the dc-constant speed motor is

$$L_1 \frac{dI_1}{dt} + R_1 I_1 + K_{e_1} \frac{d\theta_1}{dt} = K_{g_1} \tag{8.2}$$

where L_1 is motor inductance, R_1 is motor resistance, I_1 is armature current, K_{e_1} is emf constant, K_{g_1} is armature voltage and θ_1 is the angular displacement of the dc constant speed motor.

The dynamic equation of the constant speed motor

$$J_1 \frac{d^2\theta_1}{dt^2} + C_{d_1} \frac{d\theta_1}{dt} = K_{t_1} I_1 \tag{8.3}$$

where J_1 is the equivalent inertia, referred to the armature of the constant speed motor, the annulus of the differential gear-unit and the mechanism. C_{d_1} is the frictional resistance and K_{t_1} is motor torque constant. For simplicity K_{e_1} is taken equal to K_{t_1} and both are represented by K_1 as the gyrator ratio in the power graphs.

The relations to express electrical and mechanical power are given as;

$$P_{e_1} = E_{b_1} I_1 \tag{8.4}$$

$$P_{m_1} = T_{g_1} \dot{\theta}_1 \tag{8.5}$$

where T_{g_1} is the generated constant speed motor torque and E_{b_1} is the back emf and is directly proportional to $\dot{\theta}_1$. If all the electrical and mechanical losses in the electro-mechanical link are neglected other than C_{d_1}, then the power into the link can be taken to be equal to the power out.

The kinematic relationships for the inputs of the differential gear-unit used is also given with the belt reduction as;

$$\dot{\theta}_3 = \rho\dot{\theta}_2 + (1-\rho)g\dot{\theta}_1 \tag{8.6}$$

By using the above equations, the related power graph can be drawn. It is given in Figure 8.2.(a). This power graph represents a system which includes a dc motor with reduction in two stages, one by belts and the other by gears. At the end it drives a slider-crank mechanism.

The primary variables are the voltage and torque which are the efforts and the current and angular velocity are the flows in the system. he power is directed from the voltage source, as shown by half-arrow heads that represent the positive power flow, and goes to the armature resistance and inductance of the motor and to the mechanical link. $\dot{\theta}1$ and I_1 are the common variables. Only one input which is $\dot{\theta}_1$ exists on the differential gear-unit and it is applied from the casing. So equation (8.6) gives only a relation between $\dot{\theta}_1$ and $\dot{\theta}_3$.

Figure 8.2.(a) can be detailed with all the effort and flow variables to the bond. Figure 8.2.(b) shows the resultant power graph with added variables. The analysis of Figure 8.2.(b) allows us to write the equations in a very simple systematic way. For electrical elements they show that

$$K_{g_1} = E_{r_1} + E_{b_1} + E_{l_1} \tag{8.7}$$

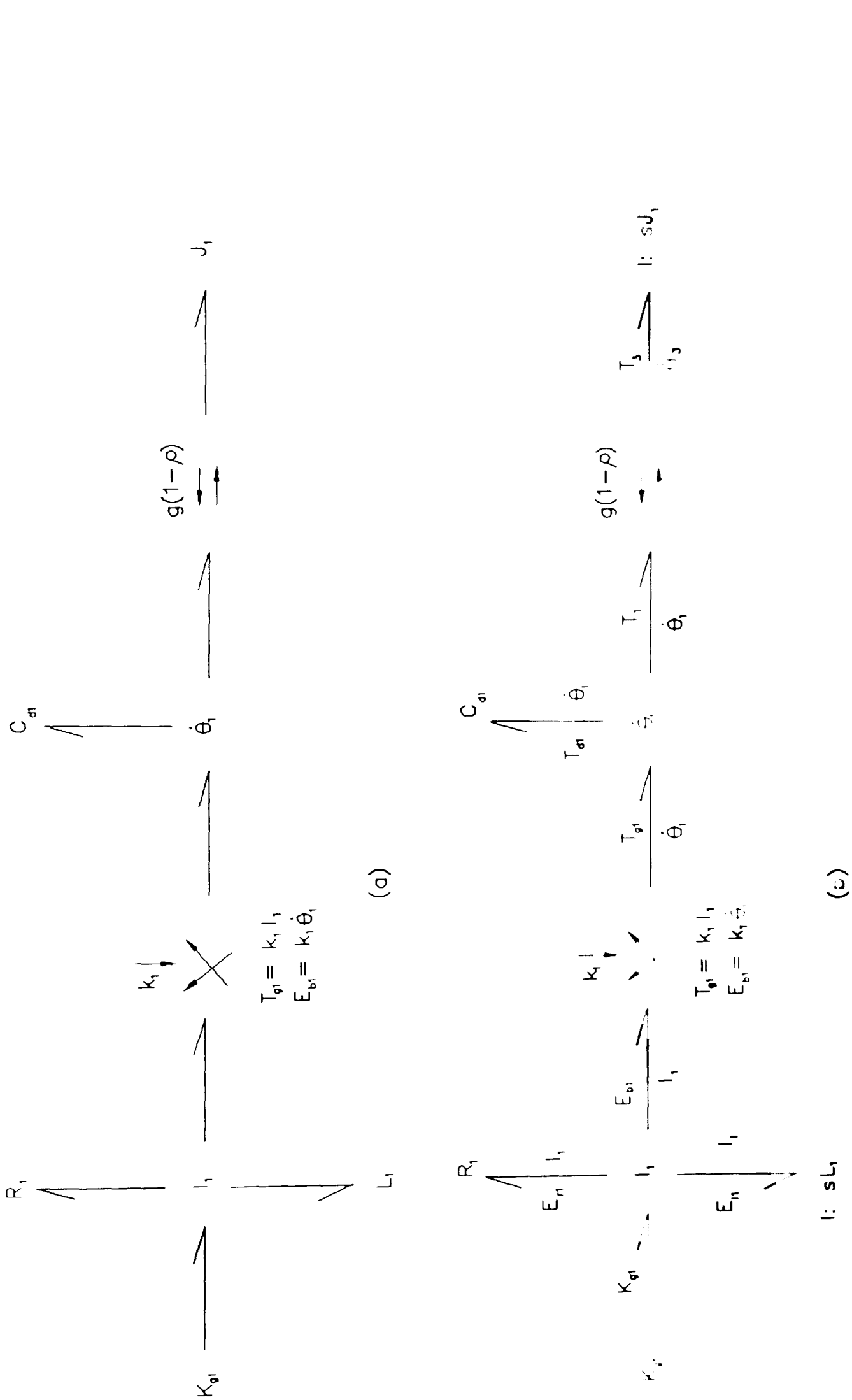

Figure 8.2. The power graph of the constant speed motor.

while in mechanical elements

$$T_1 = T_{g_1} - T_{d_1} \tag{8.8}$$

where T_1 is the required load torque and T_{d_1} is the torque lost by the friction.

We can also write from the power graph that;

$$E_{r_1} = R_1 I_1 \tag{8.9}$$

$$E_{l_1} = L_1 \frac{dI_1}{dt} \tag{8.10}$$

$$T_{d_1} = C_{d_1} \dot{\theta}_1 \tag{8.11}$$

and the storage element has a constitutive relation;

$$T_1 = J_1 \frac{d^2\theta_1}{dt^2} \tag{8.12}$$

In order to show the second derivative with respect to time the Laplace operators can be used as

$$T_1 = J_1 s \dot{\theta}_1 \tag{8.13}$$

In graph representation with the use of a colon (:) the related parameter like mass, inertia can be attached to the other elements in the bond graph model representing whether they are dissipative or storage.

In Figure 8.2.(a) and (b), gyrators and transformers are shown by crossed and parallel arrows respectively. In the same figure, the transformer ratio represents a constant parameter that includes both the gear sizes and the belt reduction and the transformer gives the following relations between the angular velocities and torques.

$$\dot{\theta}_3 = g(1-\rho)\dot{\theta}_1 \qquad \text{and} \qquad T_3 = \frac{1}{g(1-\rho)} T_1 \tag{8.14}$$

These relations have already been derived and given in chapter 6. In there T_3 is represented with a preceding minus sign to indicate the output.

Similarly, the armature equation is written for the servo-motor as:

$$L_2 \frac{dI_2}{dt} + R_2 I_2 + K_{e_2} \dot{\theta}_2 = K_{g_2}(\theta_{2_c} - \theta_2) + K_{v_2}(\dot{\theta}_{2_c} - \dot{\theta}_2) \tag{8.15}$$

the servo-motor dynamic equation is

$$J_2\frac{d^2\theta_2}{dt^2} + C_{d_2}\frac{d\theta_2}{dt} = K_{t_2}I_2 \tag{8.16}$$

where J_2 is the equivalent inertia which includes the servo-motor armature, gear reducer and the mechanism.

The constitutive relations are also written in the same order like as in the previous example with similar parameters. The only difference is the added feedback as an activated bond which represents proportional plus derivative control. In order to clarify the right hand side of the equation (8.15), the total resultant voltage is represented with K_{g_v} in the power graph. The common variables are I_2, $\dot{\theta}_2$ and the differential gear-unit gives a kinematic relation between $\dot{\theta}_2$ and $\dot{\theta}_3$ and acts as a simple gear reducer.

The power graph of a servo-motor driving a mechanism is given in Figure 8.3.(a) and (b). By looking at these power graphs, the analysis of Figure 8.3.(b) allows us to write the system equations in a simple systematic way. These equations are similar to the previous example except here the electrical elements give that

$$K_{g_v} = E_{r_2} + E_{b_2} + E_{l_2} \tag{8.17}$$

and the transformer gives the following relations for the angular velocities and torques.

$$\dot{\theta}_3 = \rho\dot{\theta}_2 \qquad \text{and} \qquad T_3 = \frac{1}{\rho}T_2 \tag{8.18}$$

The transformer ratio represents a constant parameter and it is dependent on the relative gear sizes.

To show the power graph of the whole arrangement the power graphs given in Figure 8.2.(b) and Figure 8.3.(b) are then combined. This graph is given in Figure 8.4. The common variables are I_1, $\dot{\theta}_1$ and I_2, $\dot{\theta}_2$. The differential gear-unit acts as a two degree of freedom mechanism and gives a kinematic relationship between $\dot{\theta}_1$, $\dot{\theta}_2$ and $\dot{\theta}_3$. In this power graph an important difference can be noticed in the representation of the transformer ratios. In the previous power graphs, Figure 8.2.(a) and Figure 8.3.(b) the transformer ratios are given as constant parameters. Here, however, they are given as ratios of two angular velocities. To obtain a correspondence between the bond graph representation and the operation of the differential gear-unit with two driving inputs, the transformer ratio for the constant speed motor is given as $\dot{\theta}_3/\dot{\theta}_1$ and the transformer ratio for the servo motor is given as $\dot{\theta}_3/\dot{\theta}_2$.

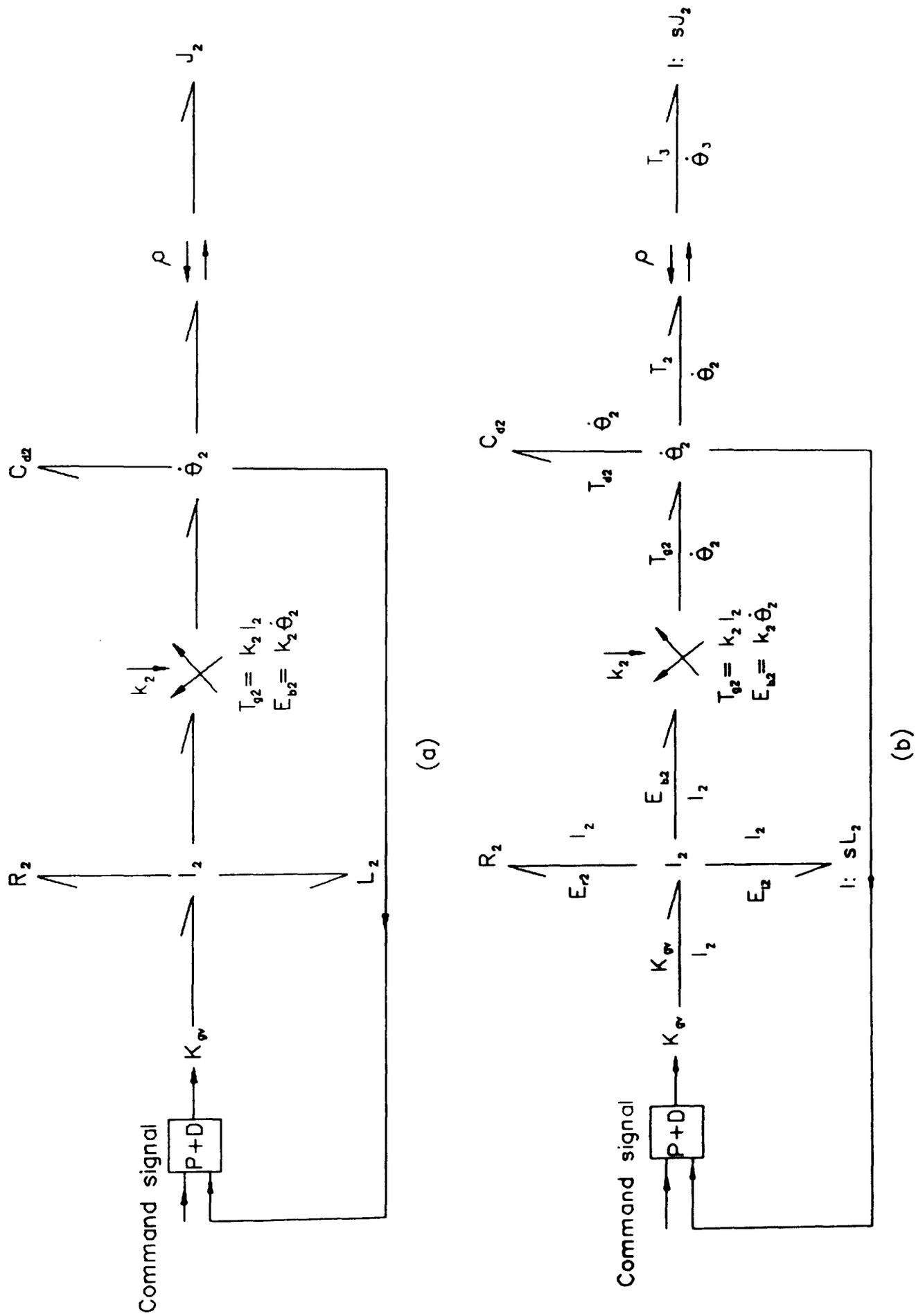

Figure 8.3. The power graph of the servo-motor.

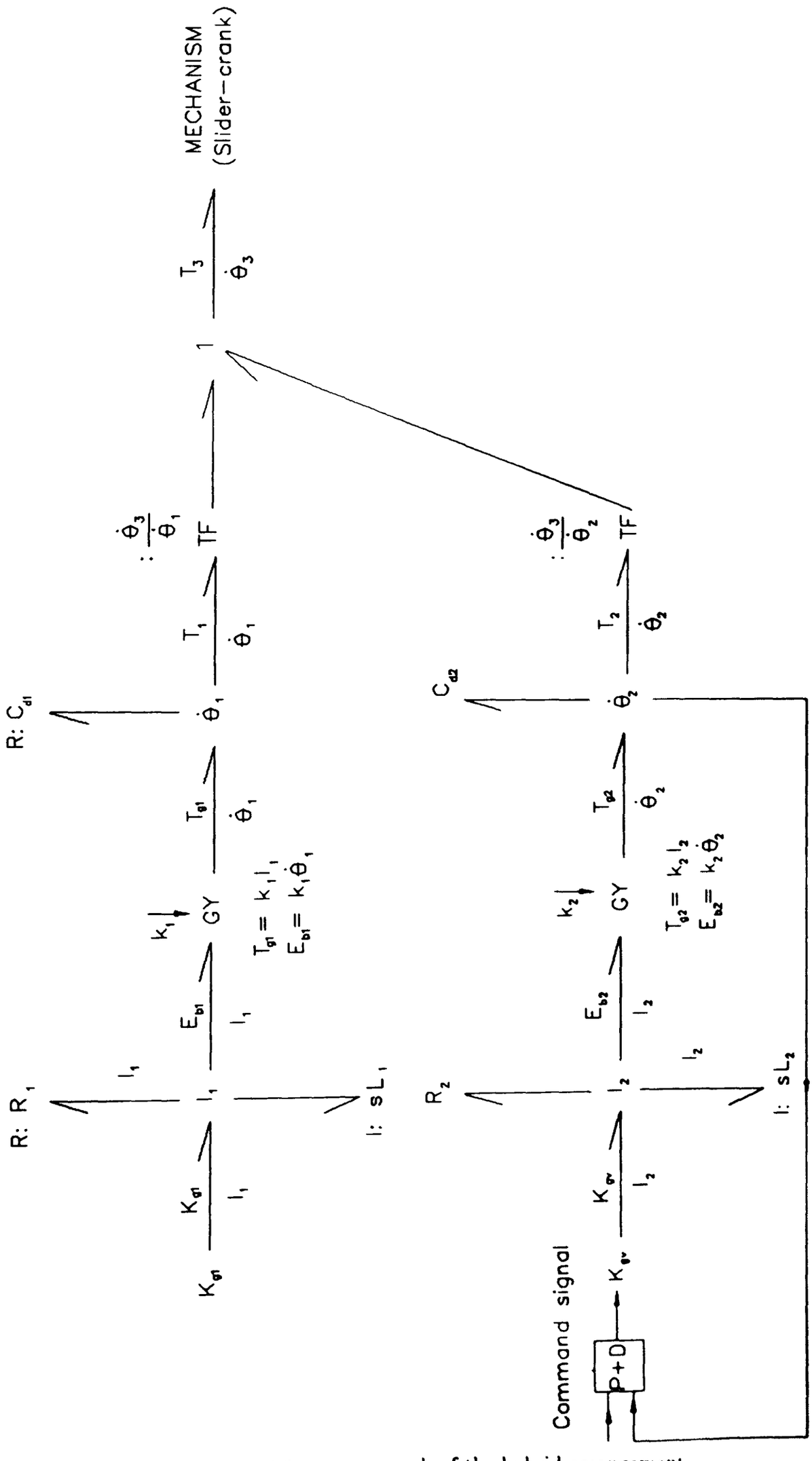

Figure 8.4. The power graph of the hybrid arrangement.

If one input exists at a time whether from the constant speed motor or from the servo-motor, $\dot{\theta}_3$ can be replaced from equation (8.6) and it gives a constant parameter again. This is studied and discussed in chapter 6 in detail.

Therefore, the analysis of 1-junction in Figure 8.4 gives the following torque expression.

$$T_3 = \frac{\dot{\theta}_2}{\dot{\theta}_3} T_2 + \frac{\dot{\theta}_1}{\dot{\theta}_3} T_1 \qquad (8.19)$$

This expression satisfies the operation of the differential gear-unit.

Finally the mechanical part of the system has simply been shown by the word 'mechanism' and two ports coming are the generalized coordinates θ_1 and θ_2. However, if required, a bond graph representation for the slider-crank mechanism can also be created. The procedure and more detail are given in references [8.7], [8.11].

Up to this point, the power graph has only been used as a graphical way of showing the all relationships on the system. It can not yet be called as a bond graph. For full representation, the causality assignment should be added. If required the detailed outline of the power graphs and their applications can be found in [8.14] with explicit examples.

8.5. Causal Bond Graph for The Hybrid Arrangement

Causality may now be assigned according to the above rules and by applying the following algorithm given in [8.17].

–assign all fixed causalities.
–apply all necessary constraints (like TF, GY etc.) of elements connected to the fixed causalities.
–assign all preferred causalities.
–apply all necessary constraints again. If there are causal conflicts, then they must be eliminated by changing the causality of some parts.

After performing these steps one by one, the causalities for the hybrid arrangement are properly assigned.

The final completed form of bond graph is given in Figure 8.5. Once established, causality gives an automatic formulation of the system equations. If I_1 junction in Figure 8.5 is taken as an example, the causality shows that the output voltage is to E_{r_1} and the inputs are from K_{g_1}, E_{b_1} and E_{l_1} so that

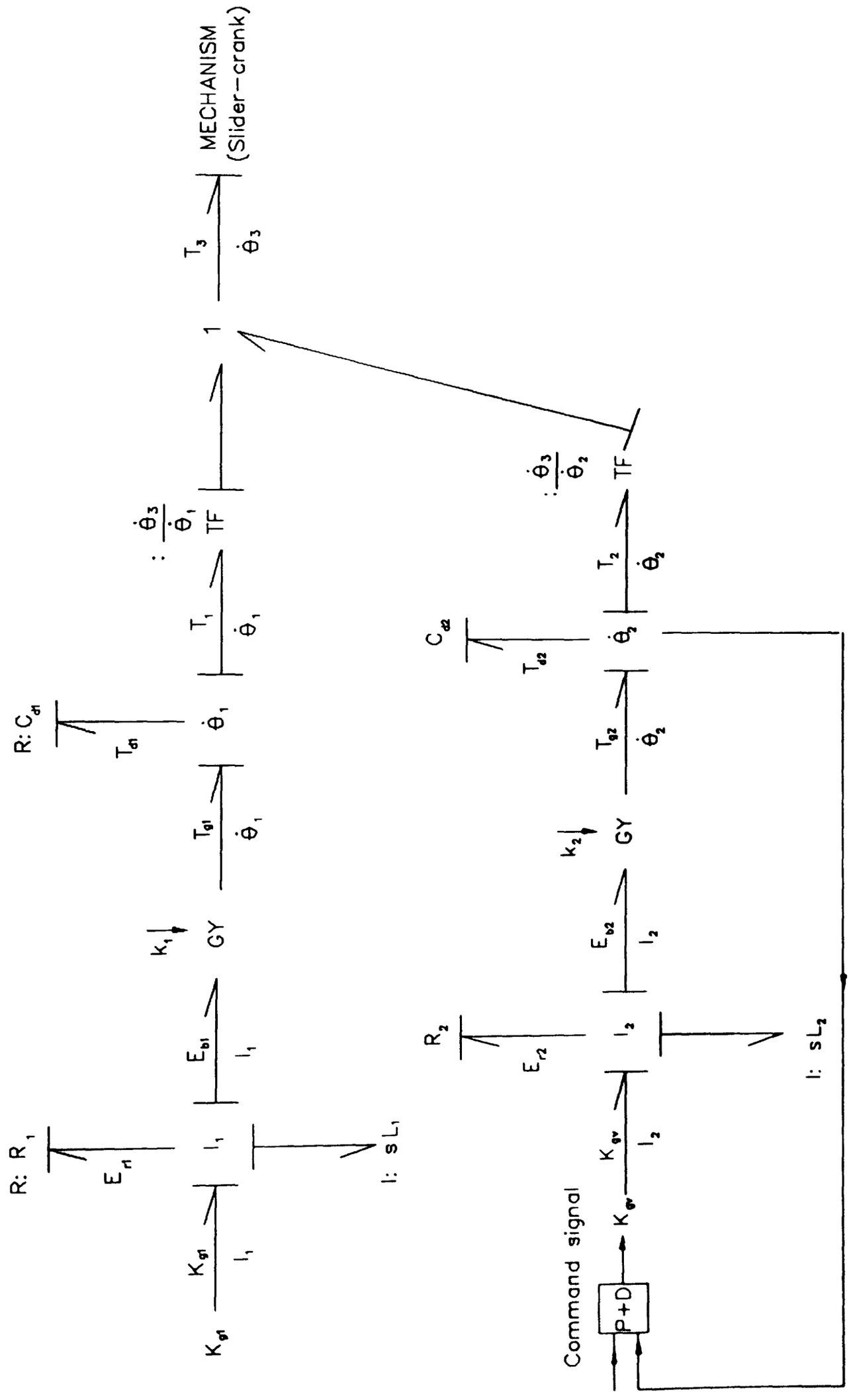

Figure 8.5. Causal bond graph for the hybrid arrangement.

$$E_{r_1} = K_{g_1} - E_{b_1} - E_{l_1} \tag{8.20}$$

At the $\dot{\theta}_1$ junction, we similarly obtain

$$T_{d_1} = T_{g_1} - T_1 \tag{8.21}$$

In the case of the gyrator, the equations are both identical.

$$T_{g_1} = k_1 I_1 \tag{8.22}$$

$$E_{b_1} = k_1 \dot{\theta}_1 \tag{8.23}$$

The constitutive relations for the storage and dissipative elements are;

$$I_1 = \frac{1}{R_1} E_{r_1} \tag{8.24}$$

$$\dot{\theta}_1 = \frac{1}{C_{d_1}} T_{d_1} \tag{8.25}$$

Basically equations from (8.21) to (8.25) can also be written for the servo-motor in the same order only by assigning causalities properly. The difference here is that if I_2 junction in Figure 8.5 is considered, the causality shows the output voltage is to E_{r_2} and the inputs are from K_{g_v}, E_{b_2} and E_{l_2} so that

$$E_{r_2} = K_{g_v} - E_{b_2} - E_{l_2} \tag{8.26}$$

where K_{g_v} includes proportional and derivative control action. Similarly, the causality for the differential gear-unit can be written using 1-junction.

8.6. Conclusion

This chapter was intended to present the basic definitions of bond graph language in general form and cover the method of practical assembly for the hybrid arrangement.

The whole idea was mainly based on splitting the main arrangement into separate components that exchange energy or power through identifiable connections or ports. This helped to see the power flow from separate electric motors and a differential gear-unit to a slider-crank mechanism. The bond graph representation relatively simplified the whole picture of the system while describing the behaviour of it.

The concept of bond graph has been taken with many assumptions in this study. Nonlinearity of the system has not been taken into account at all. More complex model can be built by including nonlinearity from the available reference studies. The purpose here was to simplify the power structure description of hybrid machines, that is why bond graphs were given briefly. But although some time was spent on bond graph modelling the method has not given full satisfaction for the representation of this system.

CHAPTER 9
CONCLUSIONS

9.1. The Present Work

This work has presented a comprehensive study of *hybrid machines*. The advantages and disadvantages of using two inputs were compared with a one using a single programmable input.

The systematic development of the work started with a brief description of the proposed hybrid arrangement and its components. Then the aim was to design characteristically different slider motions and implement them on this experimental arrangement. Subsequently three motion cases were decided and the kinematic and dynamic analyses were carried out for these motions. The inverse solutions were then presented in the form of inputs required from the constant speed motor and the servo-motor.

To provide a better understanding of the system and the importance of its parameters and their effects, a mathematical model was developed. Lagrange's method of formulation was used to derive the equations of motion. These equations were solved by using the 4th order Runge-Kutta method of integration. The importance of this model was realized in the progress of the work. For example, it was used to represent a single input programmable system, by simply eliminating the constant speed motor from the model. When all components were included, the model was used for the hybrid arrangement with a differential gear-unit, having two degrees of freedom and programmable output.

In order to observe the real system response, a set of experiments was carried out by using the designed control hardware arrangement. Error compensation techniques were then studied to get better responses from the servo-motor. When this was attempted by tuning, some unstable results were obtained from the algorithm. Although the problem was resolved during the implementation to the system, more work was required to eliminate the observed dissatisfaction.

A review was further included about differential transmission systems. The general analysis of a differential unit was presented with the fundamental torque and power relations. Numerical problems for two driving inputs have been tackled also. All of the results from the computer model and the experimental arrangement were compared in terms of their magnitude and characteristics.

Finally the bond graph technique has been reviewed and the hybrid arrangement has been represented graphically by using bond graphs. By doing this, the power relations were described in a more simplified manner. It was seen that the method was quite powerful to display energy storages, power flow, in a way of showing energy structure of the proposed arrangement clearly. Here the method has only been applied on a simple basis. Therefore most of the system details, such as motor coupling effects were not seen. The method requires more study on the system nonlinearity to show complete power structure of the hybrid arrangement.

9.2. Observations on the present work

Having studied both the model and experimental results, the observations were presented. They were based on the programmable drive only and the hybrid arrangement. Both were compared in terms of applicable optimum modulation and the power requirements from the programmable input. A reversed configuration was also studied by changing the inputs on the available system. The purpose for doing this was to decide a better configuration for the hybrid arrangement.

(i) Amount of Modulation

Three different slider motion cases; R-R, R-D-R, and R-R-D were studied primarily to conform or predict the optimum modulations and show the advantage of one characteristic to the another for the application.

The observations concluded, although it could be possible to perform a wide range of modulations such as; quicker forward stroke, slower return stroke, dwell period at top or bottom dead centre that there was a certain need to put some limitations on the magnitudes of modulation required for the optimum performance of the system to be obtained. Otherwise, the advantages behind the hybrid machines would be lost.

For the first motion case, R-R, the constant speed motor is operated at its full speed and the designed slider motion is achieved without any difficulty. In the second motion, however, when a dwell period is introduced to the slider motion, the requirement from the servo-motor

become severe. There was no doubt about system performance for a dwell, but the operating torques were much higher than a motion without a dwell period and with small modulation requirements. Although nothing was changed in the system, higher accelerations were found from the numerical calculations. This was the indication of higher torque requirements from the servo-motor. So the dwell requirement forced us to run the constant speed motor at slower speeds from the beginning. This was considered as the first important difference. Otherwise, the servo-motor used would not be able to move the mechanism and to stop when required.

The concluding point was that the optimum modulation applied would only be fine control requirements on the slider output. This could be achieved by providing quicker or slower motion or introducing a constant velocity period for some varying time to control output impact velocity of the slider. To be more general, the output could belong to any mechanism other than a slider-crank where the programmable action was required. But this point would still be the same for the modulations intended to be achieved.

Here the R-R type motion is recommended for use because of the suitability of its characteristics for any implementation.

(ii) Servo-Motor Power Requirements

It was anticipated that the size of the servo-motor would possibly come down after using the hybrid arrangement. A lot of time was devoted to search for the system power requirements for this purpose. The computer model has been studied for the programmable drive only and the hybrid arrangement in terms of application of the input torques and required power ratings.

After performing a set of calculations, the figures found were quite interesting and in a way it has supported the idea for smaller size servo-motor. When the search was over, for the R-R motion, when compared to the programmable drive only arrangement, there was obvious reduction (more than 1/3) in the servo-motor power requirements for the hybrid arrangement. The same programmable motion was accomplished with lesser angular velocity requirements from the servo-motor, but with similar input torques. That the same motion was achieved using a servo-motor with same rated torque capacity, but with lesser speeds and obviously smaller power ratings.

However, when severe modulations were introduced, like a dwell period, the servo-motor power reduction has not been found. Actually, instead of reducing the power requirement, the demand was multiplied or nearly doubled. This implied that an important decision must be

made to confirm what amount of modulation was acceptable or severe. Thus before implementing any motion, initially one had to examine the servo-motor requirements again to decide which type of motion would be the best for the programmable input without offsetting any one of the advantages.

During the study, the servo-motor power size is reduced only for the R-R motion characteristics.

(iii) Alternative Configurations

Lastly, the idea of a alternative transmission configuration was investigated by altering the inputs of the hybrid arrangement. The question was that of finding the best configuration by using the constant speed motor and the servo-motor inputs whether lower or higher gear ratios would be desirable.

In the proposed arrangement, the annulus, carries planets was driven by the constant speed motor. The servo-motor input was given from the torque arm sleeve, the sun gear and the differential gear-unit was then used for summing up these uniform and programmable inputs. For the servo-motor input, the differential mechanism used has provided $1/\rho$ (nearly 1.3528) reduction, only by gears. On the other side, the constant speed motor input has been reduced $1/(1-\rho)g$ (nearly 7.1898) with inclusion of belts and gears. The reduction ratio of the constant speed motor input was found to be nearly 5.3 times bigger than the servo-motor one. In the assumed reversed configuration, the servo-motor was introduced from the annulus, with higher reduction ratios, initially by belts and then gears. The constant speed motor input was then given the torque arm sleeve, the sun gear and the reduction is achieved only by gears. Here the reduction ratio of the servo-motor input was nearly 5.3 times bigger than the constant speed motor input.

In order to be certain about the idea, the equations of motion for the reversed configuration were derived by using Lagrange's method of formulation. They were then solved using 4th order Runge-Kutta method. Thus how these configurations differed was found by comparing the derived system equations and their solutions. To define a comparison basis, the same slider motions were achieved with both configurations; the programmable drive only and the hybrid arrangement without changing any parameters in the system. It was evidently found that the requirements from the servo-motor was increased nearly 6 times for the reversed configuration. The servo-motor used would not be able to perform the designed slider motions at all. However, when the reversed configuration was used, one point was clear about the results for the programmable drive only and the hybrid arrangement. In the reversed configuration, compared to the programmable drive, the hybrid arrangement still offered

reduction in the power requirements for the R-R motion but not for the R-D-R and R-R-D motion cases.

The best input configuration for the servo-motor was found be the case where it was applied from the input which introduces least gear reduction. Fortunately without being aware of this sharp outcome from the beginning of this work, the better input configuration for both motors happened to have been chosen. The reason was the suitability for the experimental set-up indeed.

Additionally it may be pointed here that, the annulus was considered to be showing flywheel effect. In the available computer model, the change in the annulus inertia has shown small effect on the servo-motor accelerations and torque requirements. Since the annulus inertia was included with the constant speed motor armature inertia, it was more effective for the calculations on the constant speed motor torque. In order to make this point clear, the computer model has been studied with different annulus inertias such as J_a, $2J_a$, $3J_a$ and the outputs were observed.

All of the observations were summarized in the following table for three slider motions at the end.

MOTION	ARRANGEMENT	MODULATION	SERVO REQ.	REGENERATIVE	REV. CONF.
R-R	Programmable	Good	High	Inefficient	Not good
	Hybrid	Good	Reduced	Good	
R-D-R	Programmable	Good	Normal	Inefficient	Not good
	Hybrid	Severe	Doubled	Good	
R-R-D	Programmable	Good	Normal	Inefficient	Not good
	Hybrid	Severe	Increased	Good	

Conclusion

The work has presented an introduction to programmable modulation of non-uniform motion using hybrid machines. Non-uniform motion outputs were obtained by tailoring the fundamental input motion to suit a wide range of requirements. flexibility in motion was

certainly introduced and the change-over time was reduced with full programmability. It was also pointed that different linkage geometries could be used to generate wider range of motions which are advantageous for the machine designer and user. An emphasis was made about the potential for the regenerative action capacity with required further verification and understanding.

In the hybrid machine application, some limitations were also realized. For example, one limitation was found as the optimum modulation to be implemented, only within fine modulation limits. A second was found especially during the experimental implementation on the controller arrangement. This was the essential motion coordination between both inputs. Thus the input from the servo-motor must always be coordinated with the input from the constant speed motor in which has introduced a synchronization issue for the control hardware arrangement. Otherwise, the required variability and accuracy would be lost cycle by cycle for the slider.

Lastly, we may possibly say the results of this work highlighted that the hybrid machines had encouraging promises and features. When the right decision is made for the applicable modulations, they could always be used as a programmable modulator for various motion applications without offsetting their advantages.

9.3. Recommendations for continuation of work

At this moment, one suggestion is to introduce a flywheel into the available experimental set-up and repeat the experiments for the carried torques and transmitted power with a real flywheel effect. These could be accomplished by using different sizes of flywheel to obtain a real regenerative action from the system. Similar work must also be carried on by including a flywheel into the mathematical model equations.

Another point is the differential gear-unit chosen. In the work presented, all observations are dependent upon the differential gear-unit used. In the studied arrangement, for example, standard driving methods, Vee belts and a reaction plate are used to drive the casing and the torque arm sleeve respectively. However, different driving methods can be applied depending upon the experimental set-up designed. Alternatively, the casing can be driven by a coupling, by gears, by worm and wheel or by chain. Similarly, the other input can be applied using available accessories such as a flange, a gearwheel, worm and wheel or timing belt pulley. One last point can be added for the gear-unit ratios. The differential gear-unit used only covers a specific gear ratio. But different gear-ratios can be investigated as a first step and one in the optimum can then be decided. Additionally, different differential gear-unit designs can be searched. Instead of using a differential with casing, a differential unit with two input shafts

can be studied. This can also answer the question of multiple hybrid arrangements more clearly.

In addition to the above, to obtain a better estimate for the system performance, it would be required to deal with a more complex model which includes real effects such as friction forces, losses and external forces on the slider also. To have a complete understanding on the hybrid machines this can be a further research.

REFERENCES

[1.1] Jones J. Rees,"Some Selection Issues in Non-Uniform Motion Generators for High Speed Applications",

[1.2] Hamilton H. Mabie, Ocvirk Fred W., "Mechanisms and Dynamics of Machinery", John Wiley and Sons Inc., 1975.

[1.3] Molian S, "Mechanism Design",1982.

[2.1] Vernon G. W., "Motion Design, Control and Implementation", Ph. D. Thesis, Department of Mechanical, Marine and Production Eng., Liverpool Polytechnic, 1988.

[2.2] Stamp K. J., "The Mechanisation of Carton Erection", Ph. D. Thesis, Department of Mechanical, Marine and Production Eng., Liverpool Polytechnic, 1989.

[2.3] Engineering Science Data Unit (E.S.D.U), Item no: 86026.

[2.4] Kirecci Ali, "Motion Design for High-Speed Machines", M.Phil./Ph.d. Transfer Report, Department of Mechanical, Marine and Production Eng., Liverpool Polytechnic, 1991.

[3.1] Haug Edward J., "Computer Aided and Optimization of Mechanical System Dynamics", Centre for Computer Aided Design, Published in Cooperation with NATO Scientific Affairs Division, 1984.

[3.2] Haug Edward J., "Computer Aided Kinematics and Dynamics of Mechanical Sytems", Allyn and Bacon Series in Engineering, 1989.

[3.3] Shigley Joseph Edward, Vicker John Joseph, J. R., "Theory of Machines and Mechanisms", Mc. Graw Hill, 1980.

[3.4] Deravi P.,"Computer Analysis of Multi-Cylinder diesel engine mechanism dynamics", Ph. D. Thesis, Department of Mechanical, Marine and Production Eng., Liverpool Polytechnic, 1980.

[3.5] Ginsberg Jerry H., "Advanced Engineering Dynamics", Harper and Rous Publishers New York, 1988.

[3.6] Baysec Sedat, "Simulation of the dynamics of hydraulically actuated planar manipulators", Ph. D. Thesis, Department of Mechanical, Marine and Production Eng., Liverpool Polytechnic, 1983.

[4.1] Nicholson H., "Modelling of Dynamical Systems", Vol.1, Peter Peregrinus Ltd., 1980.

[4.2] Nagrath I. J, Gopal M., "Systems Modelling and Analysis", TATA McGraw-Hill Publishing Company Ltd., 1982.

[4.3] Ogata Katsuhiko, "Modern Control Engineering", Prentice-Hall Inc., 1990.

[4.4] Bishop D. M., "What is Simulation?", Measurement and Control, Vol.7, pp.445-447, 1974.

[4.5] Fasol K. H., Jorgl P., "Principles of Model Building and Identification", Automatica, Vol.16, pp.505-518, 1980.

[4.6] Doebelin Ernest O., "System Modelling and Response", John Wiley and Sons, 1976.

[4.7] Dorf Richard C.,"Modern Control Systems", Addison-Wesley, 1986.

[4.8] Bunden Richard L., Raires J. Douglas, Reynolds Albert C., "Numerical Analysis", Prindle, Weber and Scmidth, Boston-Massachusetts, 1981.

[4.9] Shanhhikumar J. G., Sargent R. G., "A Unifying View of Hybrid Simulation /Analytic Models and modelling", Operations Research, Vol.31, No.6, Nov.-Dec. 1983.

[5.1] Houpis Constantine H., Lamont Gary B., "Digital Control Systems", McGraw-Hill, 1985.

[5.2] Richards R. J., "An Introduction to Dynamics and Control", Longman Group Limited, 1979.

[5.3] Wheeler Colin, "Microprocessors and Industrial Control", Hutchinson Computer Studies Series, 1988.

[5.4] Tal Jacop, "Motion Control by Microprocessors", Galil Motion Control Inc., 1986.

[5.5] Williams Steve, "Programming the 68000", SYBEX Inc., 1985.

[5.6] Soldner K., Jones J. R., Fischer P. J., "Dynamically Optimum Performance of Manipulators", Interim Report: S.E.R.C. Grant GR/B/51840, Mechanisms and Machines Group, Liverpool Polytechnic.

[5.7] Vernon G. W., Jones J. R., Rooney G. T., "Dynamic Command Motion Tuning for Robots: -A Self Learning Algorithm", VIth CISM-IFToMM Symposium, Ro.man.sy-86, Cracow, Poland, September 9-12, 1986.

[5.8] Vernon G. W., Jones J. R., Rooney G. T., "Automatically increasing the speed of industrial robots and multi-axis machines", Proceedings of the Institute of Mechanical Engineers-UK Research in Advanced Manufacture, pp.69-78, 1986.

[5.9] "DC Motors, Speed Controls, Servo Systems", Engineering Handbook by Electro-Craft Corp., 1980.

[6.1] Macmillan R. H., "Power Flow and Loss in Differential Mechanisms", Journal of Mech. Engng. Science, Vol.3, No.1, pp.37-41, 1961.

[6.2] Macmillan R. H., "The control of stepless variable speed transmissions in automobiles and their possible application to regenerative systems", 10th F.I.S.I.T.A Congress in Tokyo,

pp.277-303, 1964.

[6.3] Macmillan R. H., Davies P. B., "Analytical study of systems for bifurcated power transmission", Journal of Mech. Engng. Science, Vol.7, No.1, 1965.

[6.4] Davies W. John, "Steplessly Adjustable or Variable Ratio Drives", The Chartered Mechanical Engineer, Vol.12, No:9, pp.504-511, October-1965.

[6.5] White G., "Properties of Differential Transmissions", The Engineer, Vol.224, pp.105-111, July 1967.

[6.6] White G., Christie D. M., "Improving the speed holding ability of a variable-ratio transmission by means of a differential coupling", Int. J. Mach. Tool Des. Res., Vol.7, pp.155-168, Pergamon Press 1967.

[6.7] Fitzgeorge Dougles, "Synthesis of Single Differential Gear Units", Journal of Mechanisms, Vol.5, pp.311-336, 1970.

[6.8] White G., "Multiple-Stage, Split-Power Transmissions", Journal of Mechanisms, Vol.5, pp.505-520, 1970.

[6.9] Sanger D. J., "The Determination of Power Flow in Multiple-Path Transmission Systems", Mechanism and Machine theory, Vol.7, pp.103-109, 1971.

[6.10] White G., Christie D. M., "A variable Ratio Differential Transmission with wide speed range and high torque multiplication", Conference on Mechanisms, pp.68-77, 1972.

[6.11] Willis R. J. Jr., "On the kinematics of the closed epicyclic differential gears", Trans. ASME Journal of Mech. Design, Vol.104, pp.712-719, 1982.

[8.1] Bos A. M., Breedveld P. C., "1985 Update of the Bond Graph Bibliography", Journal of The Franklin Institute, Vol.319, No.1/2, pp. 269-276, January/February 1985.

[8.2] Karnopp D. C., Rosenberg R. C., "Power Bond Graphs: A New Control Language", Control Engineering, pp.79-82, May 1968.

[8.3] Karnopp Dean, "Power Conserving Transformations: physical interpretations and applications using bond graphs", Journal of The Franklin Institute, Vol.288, No.3, pp.175-201, 1969.

[8.4] Rosenberg R. C., Karnopp D. C., "A Definition of the Bond Graph Language", Trans. ASME Dynamic Syst., Measure. Control, Vol.94, No.3, pp. 179-182, 1972.

[8.5] Brown F. T., "Lagrangian Bond Graphs", Trans. ASME Dynamic Syst., Measure. Control, Vol.94, No.3, pp. 213-221, 1972.

[8.6] Martens H. R., Bell A. C., "A Logical Procedure for the Construction of Bond Graphs in Systems Modelling", Trans. ASME Dynamic Syst., Measure. Control, Vol.94, No.3, pp. 183-188, 1972.

[8.7] Rosenberg R. C., "Multiport Models in Mechanics", Trans. ASME Dynamic Syst., Measure. Control, Vol.94, No.3, pp. 206-212, 1972.

[8.8] Thoma Sc. Jean U., "Introduction of Bond Graphs and their applications", 1975.

[8.9] Karnopp Dean, "Lagrange's Equations for Complex Bond Graph Systems", Trans.

ASME Dynamic Syst., Measure. Control, Vol.99, No.4, pp. 300-306, 1977.

[8.10] Dixhoorn J. J. Van, "Simulation of Bond Graphs on Minicomputers", Trans. ASME Dynamic Syst., Measure. Control, pp. 9-14, 1977.

[8.11] Allen R. R., Dubowsky S., "Mechanisms as components of dynamic systems: a bond graph approach", Trans. ASME J. Engng Ind., Vol.99, No.1, pp. 104-111, 1977.

[8.12] Karnopp D., Margolis D., "Analysis and simulation of planar mechanism systems using bond graphs, Trans. ASME J. of Mechanical Design, Vol.101, pp.187-191.

[8.13] Margolis Donald L., "Bond-graphs for some classic dynamic systems", Simulation, pp. 81-87, 1980.

[8.14] Blundell Alan, "Bond Graphs for modelling engineering systems, 1982.

[8.15] Sirivadhna K., Richards E. F., Anderson M. D., "The application of bond graphs to electrical machinery and power engineering", IEEE Trans. on Power App. and Syst., Vol.PAS-102, No.5, 1983.

[8.16] Karnopp Dean, "Alternative bond graph causal patterns and equation formulations for dynamic systems", Trans. ASME Journal of Dynamic Syst., Measure. Control, Vol.105, pp. 58-63, 1983.

[8.17] Breedveld Peter C., "A systematic method to derive bond graph models", Proceedings of the 2nd Europena Simulation Cong., pp.38-44, 1986.

[8.18] Rosenberg R. C., "Exploiting bond graph causality in physical system models", Trans. ASME Journal of Dynamic Syst., Measure. Control, Vol.109, pp. 378-383, 1987.

[8.19] Beaman J. J., Rosenberg R. C., "Constitutive and modulation structure in bond graph modelling", Trans. ASME Journal of Dynamic Syst., Measure. Control, Vol.110, pp. 395-402, 1988.

[8.20] Breedveld P. C., "Fundamentals of bond graphs", University of Twente, Dept. of Electrical Engng., 1988.

[8.21] Zeid A., "Some bond graph structural properties: Eigen Spectra and Stability", Trans. ASME Journal of Dynamic Syst., Measure. Control, Vol.111, pp. 382-388, 1989.

APPENDICES

APPENDIX 1

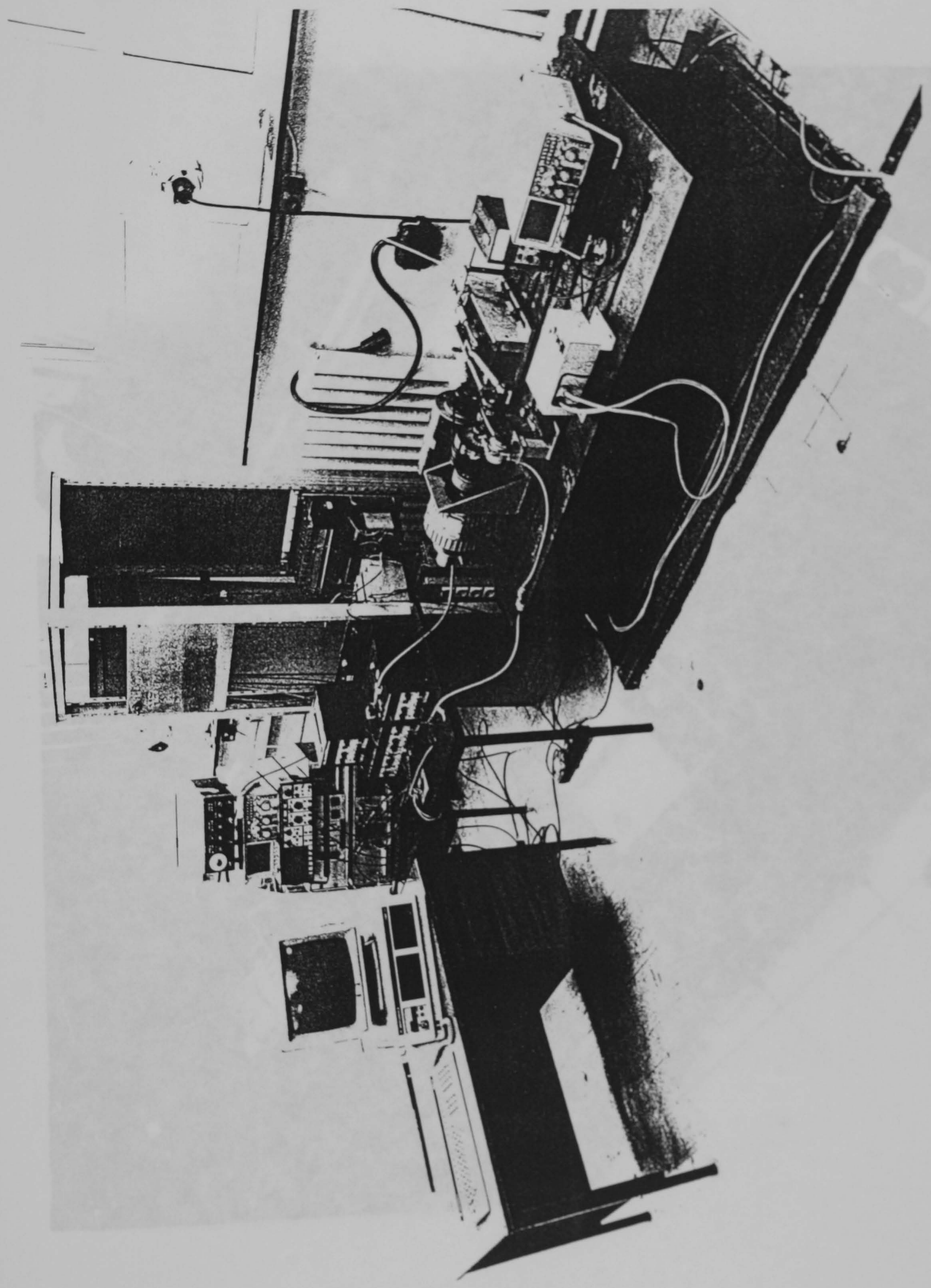

Figure A.1.1. General view of the hybrid arrangement.

Figure A.1.2. Top view of the hybrid arrangement.

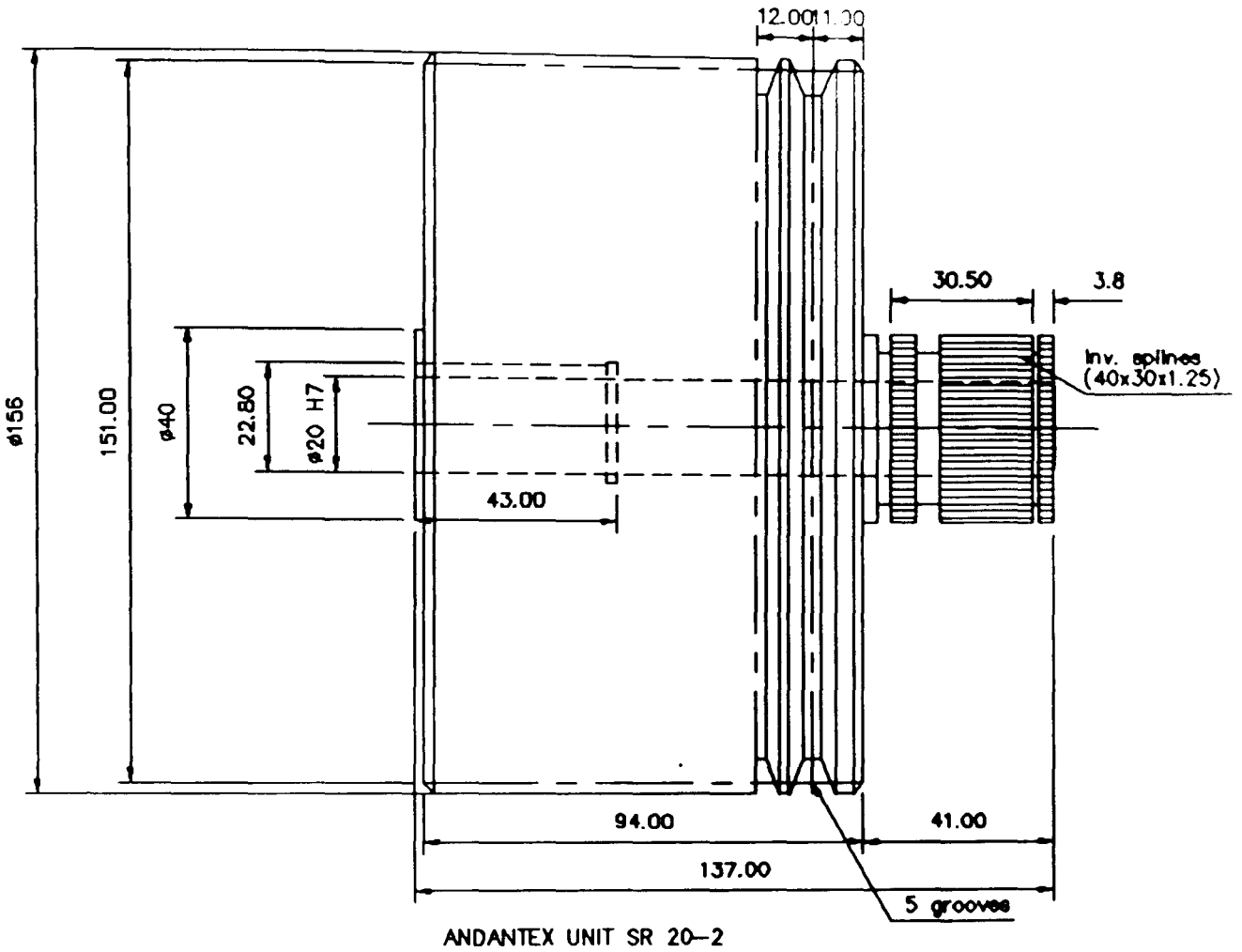

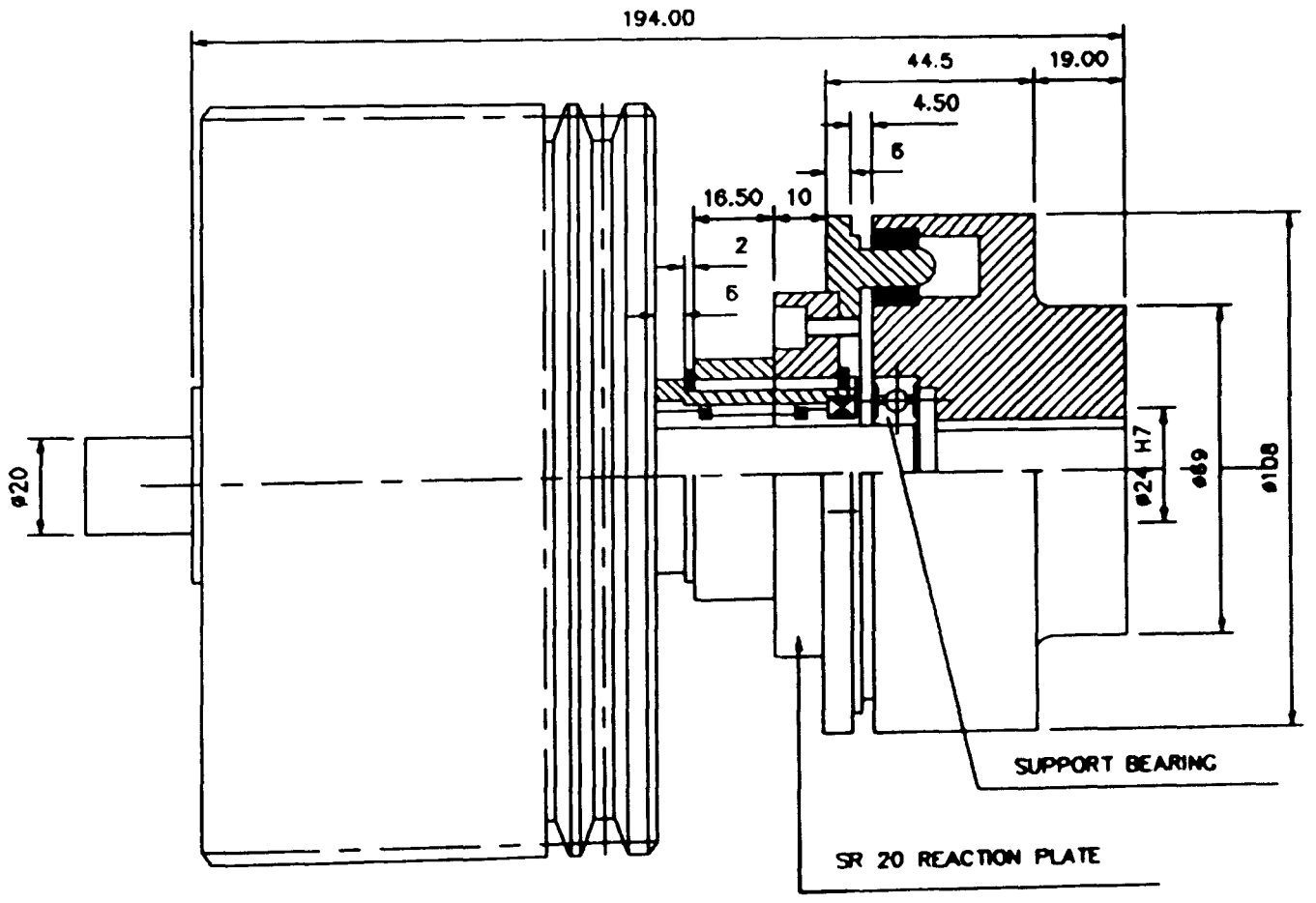

Figure A.1.3. The differential gear-unit and accessories.

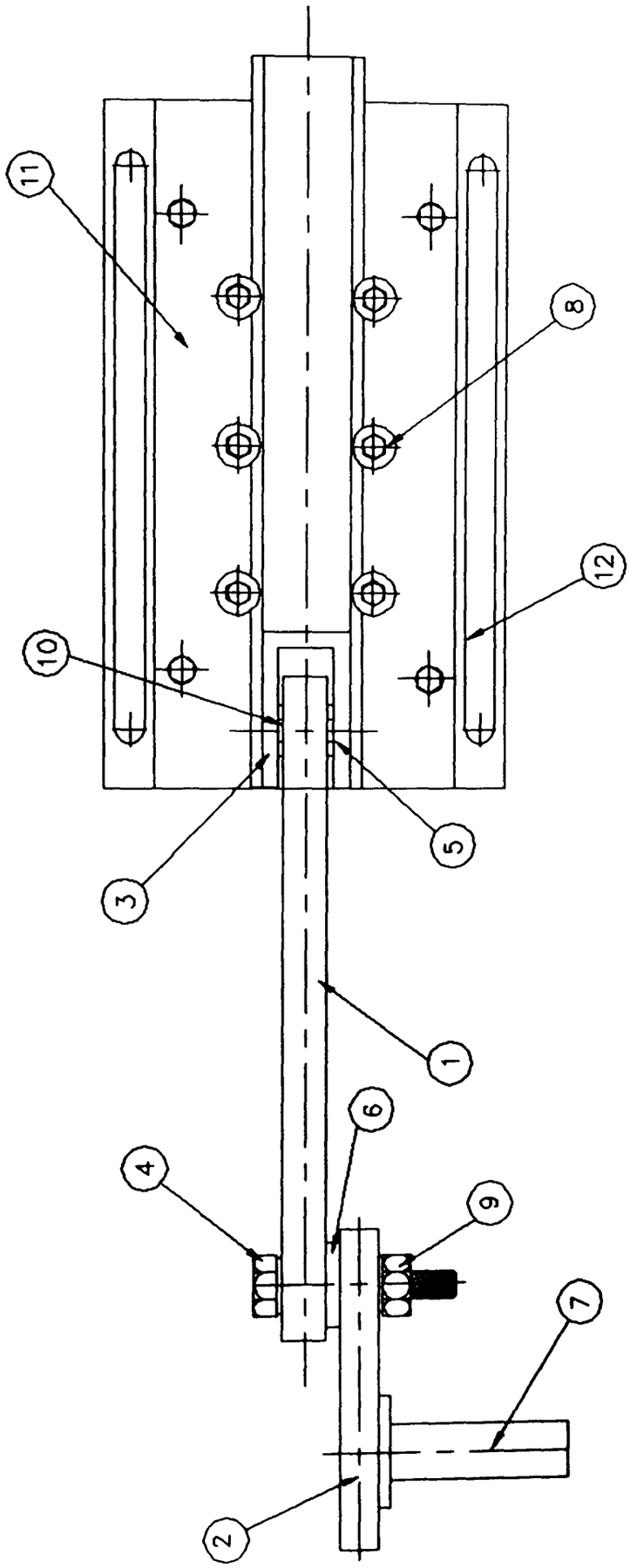

Part no.	Description	Quantity	Material
1	Connecting rod	1	Mild steel
2	Crank	1	Mild steel
3	Slider	1	Mild steel
4	Connecting rod pin	1	Mild steel
5	Slider pin	1	Mild steel
6	Spacer	1	Mild steel
7	Crank shaft	1	Mild steel
8	Rollers	6	Mild steel (Case hard.)
9	Nut	1	Mild steel
10	Thrust washer	2	Brass
11	Slideway plate	1	Mild steel (Normalized)
12	Slideway base	1	Mild steel

Figure A.1.4. Assembly drawing of slider-crank.

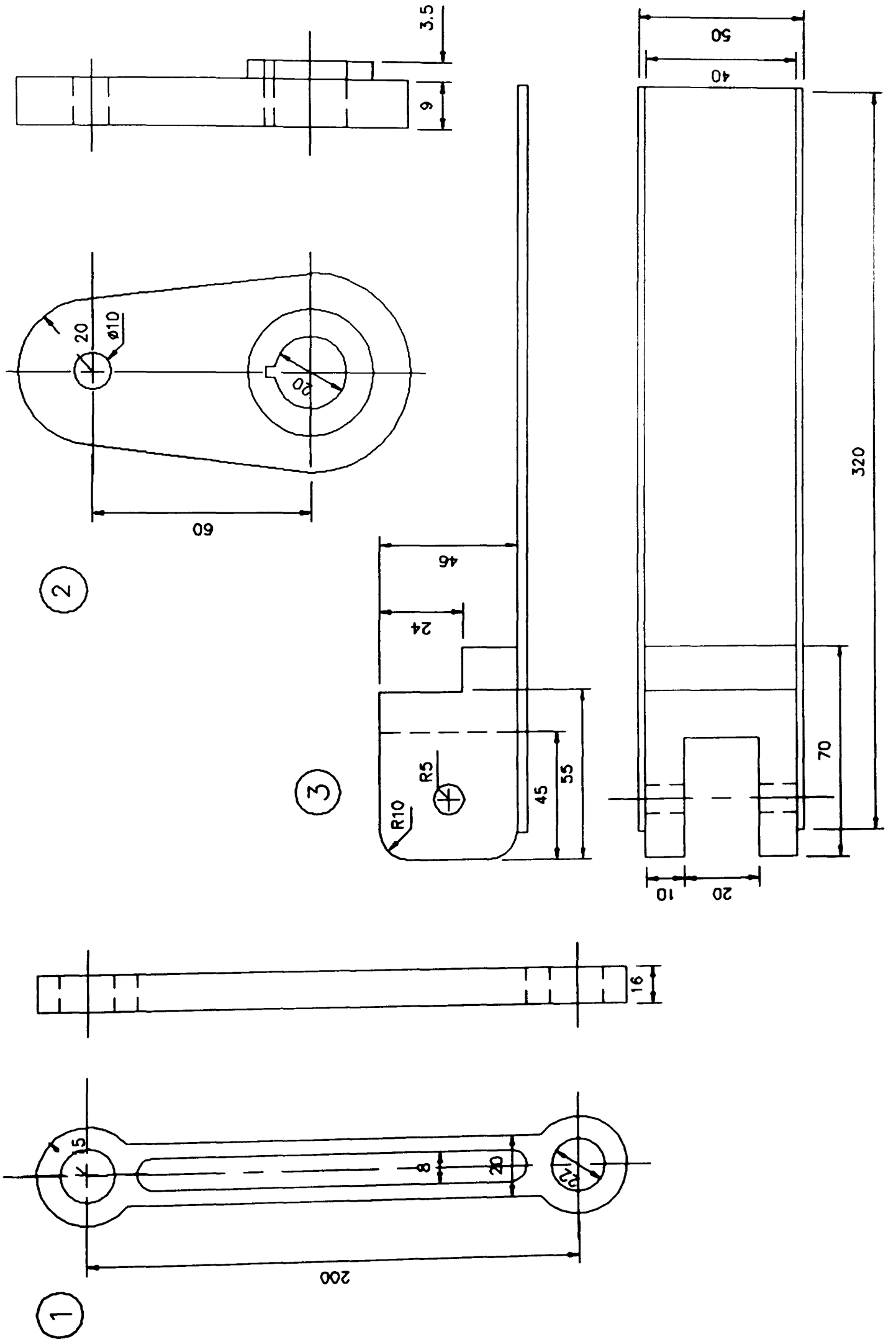

Figure A.1.4. Continued.

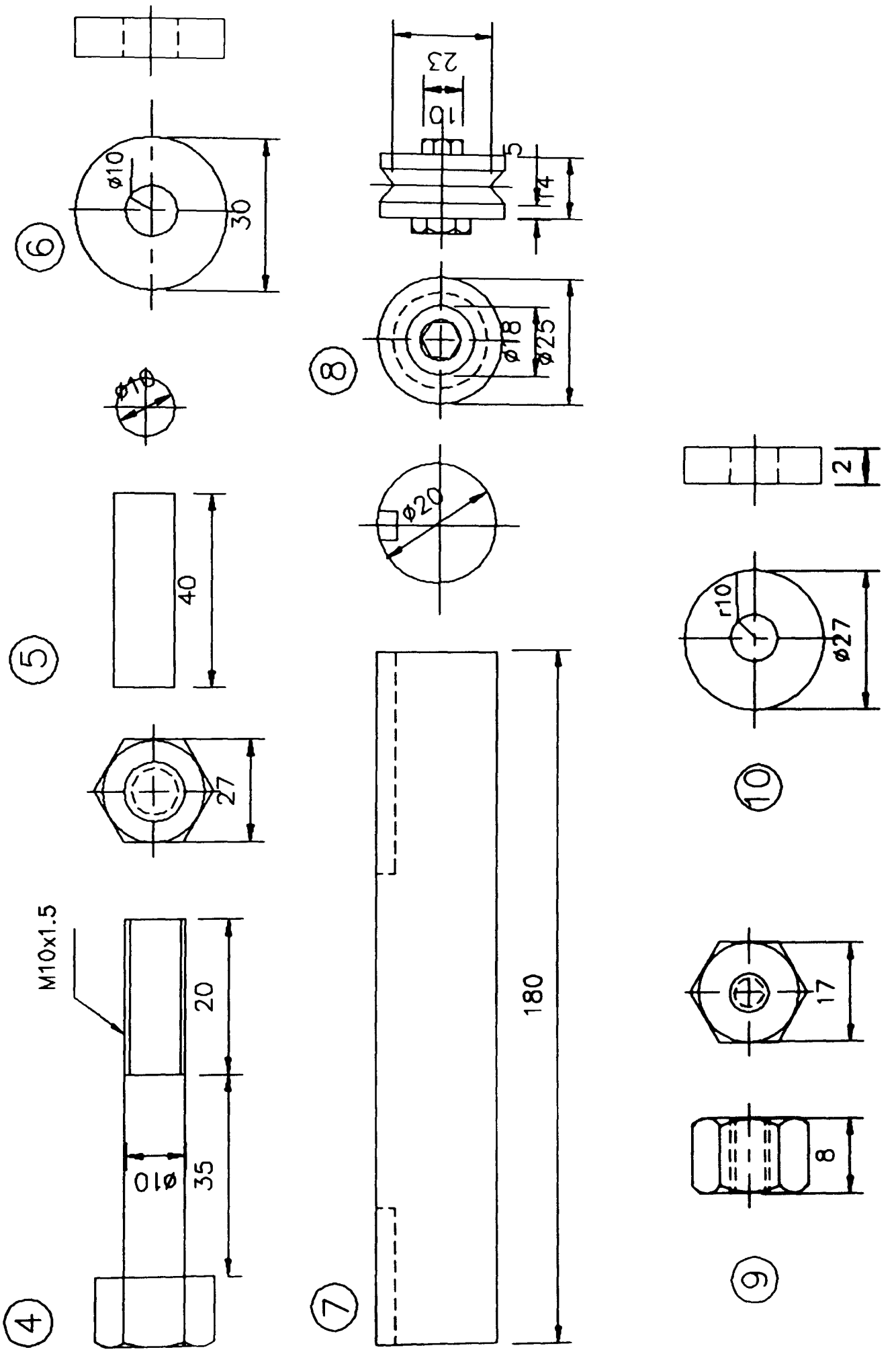

Figure A.1.4. Continued.

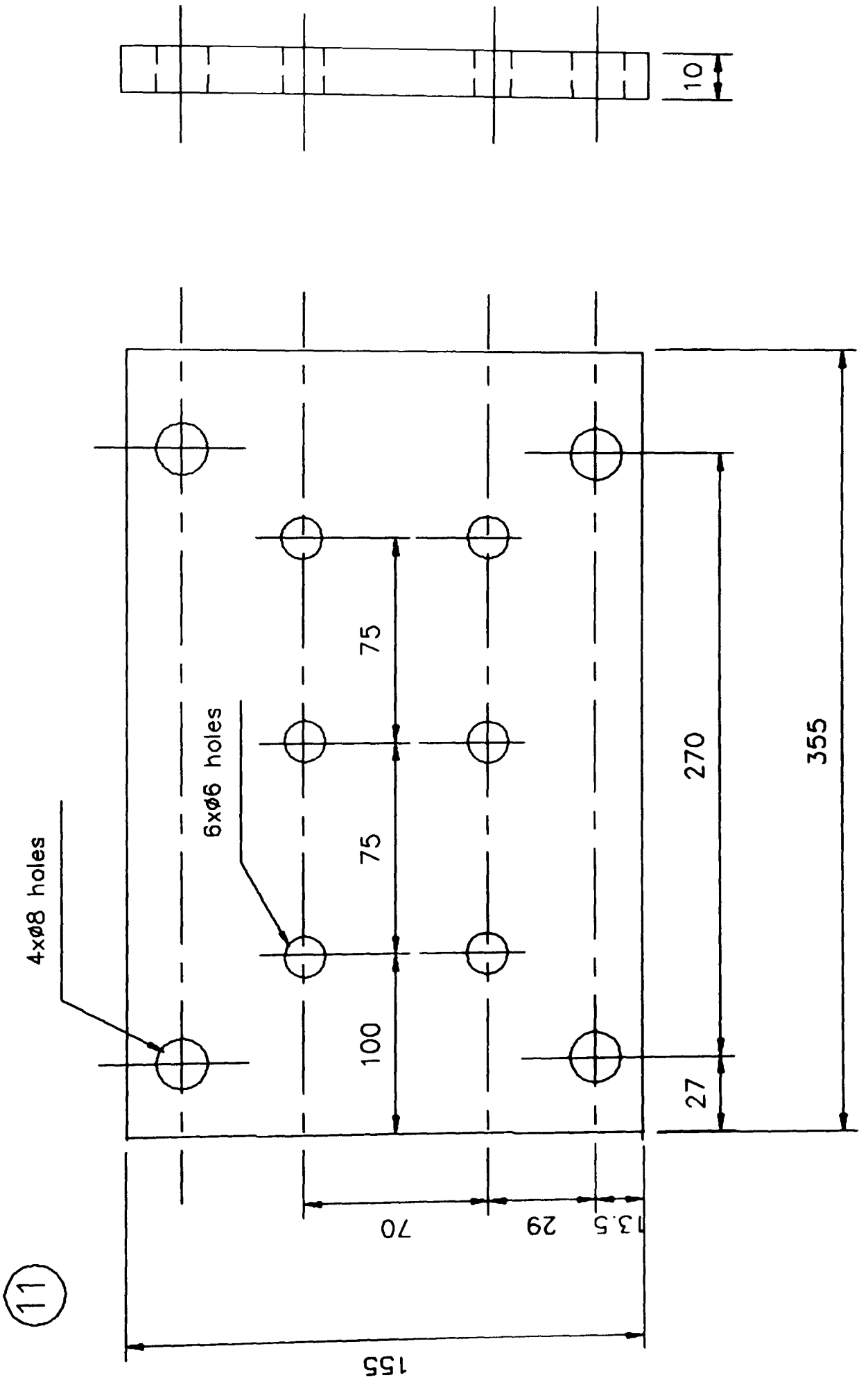

Figure A.1.4. Continued.

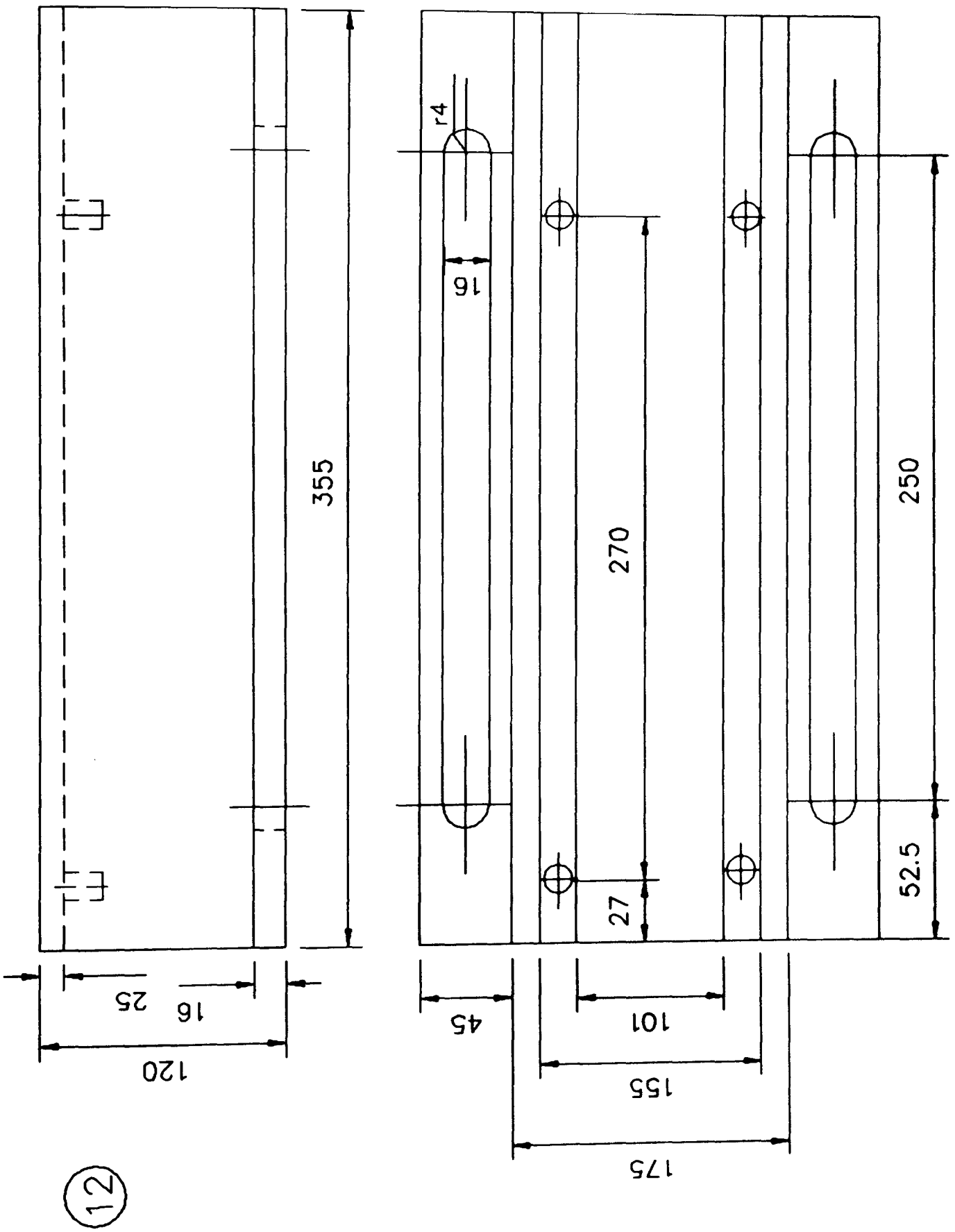

Figure A.1.4. Continued.

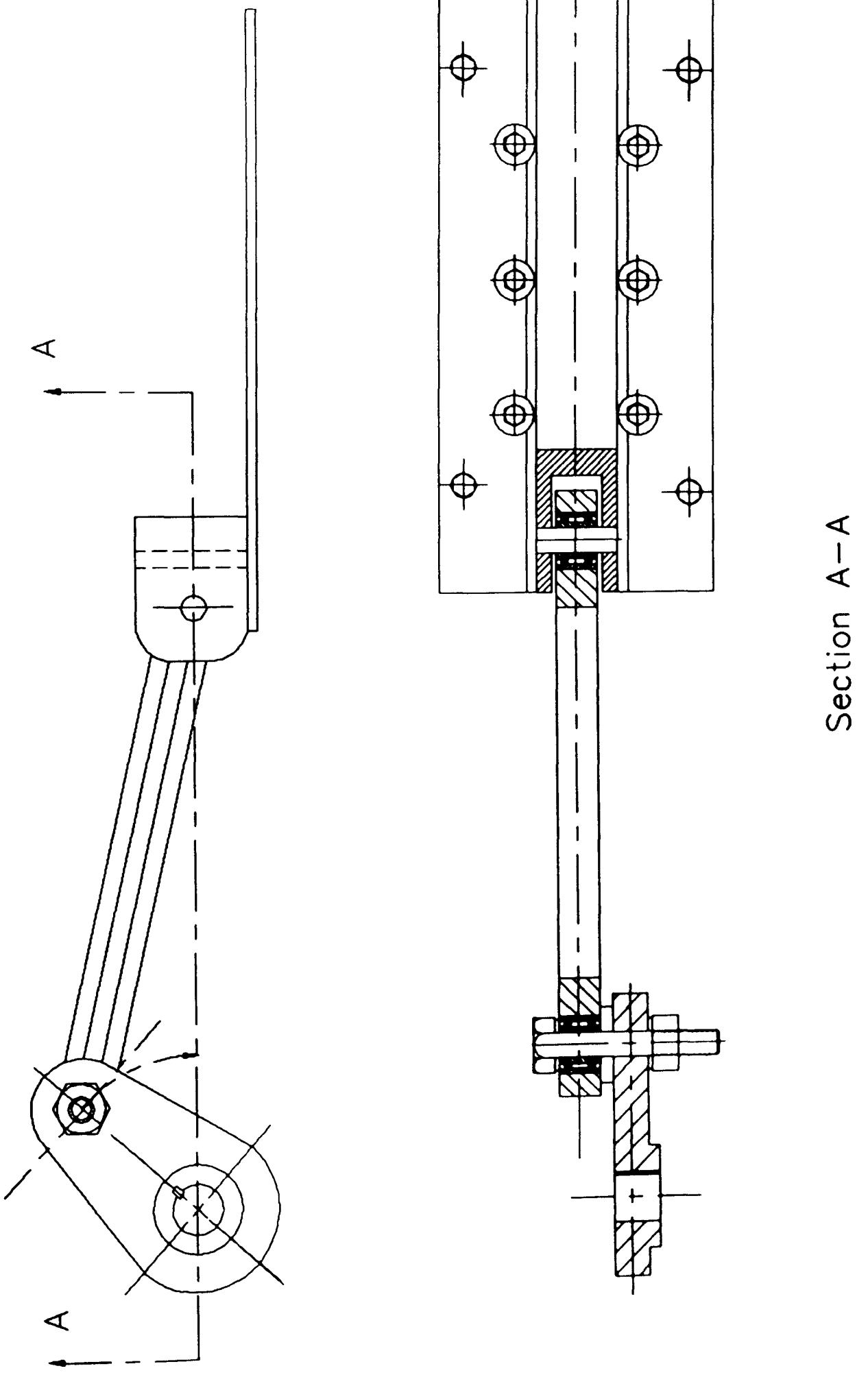

Figure A.1.5. Sectional view of slider-crank.

APPENDIX 2

LAGRANGE FORMULATION OF SLIDER CRANK

The slider-crank mechanism is given in Figure 3.5. T_t is the total kinetic energy of the mechanism as the summation of the energies of the individual links.

$$T_t = T_2 + T_3 + T_4 \tag{A.2.1}$$

$$T_t = \sum_{i=2}^{4} \frac{1}{2} m_i \dot{x}_i^2 + \frac{1}{2} J_2 \dot{\theta}^2 + \frac{1}{2} J_3 \dot{\phi}^2 \tag{A.2.2}$$

Energy expression for individual links are as follows.

Link 2:

$x_2 = r_1\cos\theta$; $\quad y_2 = r_1\sin\theta$

$\dot{x_2} = -r_1\dot{\theta}\sin\theta$; $\quad \dot{y_2} = r_1\dot{\theta}\cos\theta$

where x_2 is the distance from the centre of mass of link 2 in the x direction and y_2 is the height from the centre of mass of link 2.

$$T_2 = \frac{1}{2} J_2\dot{\theta}^2 + \frac{1}{2} m_2 r_1^2 \dot{\theta}^2 \tag{A.2.3}$$

Link 3:

$x_3 = r\cos\theta + l_1\cos\phi$; $\quad y_3 = l_1\sin\phi$

$\dot{x}_3 = -r\dot{\theta}\sin\theta - l_1\dot{\phi}\sin\phi$; $\quad \dot{y}_3 = l_1\dot{\phi}\cos\phi$

$$T_3 = \frac{1}{2} J_3 \dot{\phi}^2 + \frac{1}{2} m_3 [\, l_1^2\dot{\phi}^2 + r^2\dot{\theta}^2\sin^2\theta + 2rl_1\dot{\theta}\dot{\phi}\sin\theta\sin\phi \,] \tag{A.2.4}$$

Link 4:

$x_4 = r\cos\theta + l\cos\phi$; $\quad y_4 = 0$

$\dot{x}_4 = -r\dot{\theta}\sin\theta - l\dot{\phi}\sin\phi$;

$$T_4 = \frac{1}{2} m_4 [\, r^2\dot{\theta}^2\sin^2\theta + 2rl\dot{\theta}\dot{\phi}\sin\theta\sin\phi + l^2\dot{\phi}^2\sin^2\phi \,] \tag{A.2.5}$$

Total kinetic energy of the mechanism T_t is:

$$T_t = \frac{1}{2} J_2 \dot{\theta}^2 + \frac{1}{2} m_2 r_1^2 \dot{\theta}^2 + \frac{1}{2} J_3 [r^2\dot{\theta}^2\cos^2\theta/(l^2-(y-r\sin\theta)^2)] +$$

$$\frac{1}{2} m_3 [l_1^2 r^2\dot{\theta}^2\cos^2\theta/(l^2-(y-r\sin\theta)^2) + r^2\dot{\theta}^2\sin^2\theta + 2r^2 l_1\dot{\theta}^2\sin\theta(y-r\sin\theta)\cos\theta/(l^2-(y-r\sin\theta)^2)^{1/2} +$$

$$\frac{1}{2} m_4 [r^2\dot{\theta}^2\sin^2\theta + 2r^2\dot{\theta}^2\sin\theta\cos\theta\,(y-r\sin\theta)/(l^2-(y-r\sin\theta)^2)^{1/2} + r^2\dot{\theta}^2\cos^2\theta(y-r\sin\theta)^2/(l^2 -$$

$$(y-r\sin\theta)^2)]$$

(A.2.6)

Lagrange's equations are:

$$\frac{d}{dt}\left(\frac{\partial L}{\partial \dot{q}_i}\right) - \frac{\partial L}{\partial q_i} = Q_i \qquad \text{for } i=1,2,\ldots,n \tag{A.2.7}$$

where L is the Lagrangian given as the difference between the total kinetic energy and the total potential enery;

$$L=T-V$$

So the differentiation of individual energy terms with respect to the generalized coordinate and time derivatives with respect to the generalized velocities, the equation of motion is obtained for the slider-crank mechanism. Its complete form is given in chapter 3.

APPENDIX 3

LAGRANGE FORMULATION OF THE HYBRID ARRANGEMENT

The total kinetic energy of the system is expressed as individual energies of each component in the hybrid arrangement as:

$$T_t = T_c + Ta + T_s + T_{cr} + T_{sl} \tag{A.3.1}$$

where T_c is the rotational kinetic energy of the dc constant speed motor, T_a is the rotational energy of the differential gear annulus, T_s is the rotational energy of the dc servo-motor, T_{cr} is the rotational energy of the crank and T_{sl} is the translational energy of the total mass on the slider.

Individual energy terms for components are given as the following.

$$T_c = \tfrac{1}{2} J_m \dot{\theta}_1^{\,2} \tag{A.3.2}$$

$$T_a = \tfrac{1}{2} J_a g^2 \dot{\theta}_1^{\,2} \tag{A.3.3}$$

$$T_s = \tfrac{1}{2} J_s \dot{\theta}_2^{\,2} \tag{A.3.4}$$

$$T_{cr} = \tfrac{1}{2}(J_c + m_a r^2)\dot{\theta}_3^{\,2} \tag{A.3.5}$$

$$T_{sl} = \tfrac{1}{2} m_b \dot{x}^2 \tag{A.3.6}$$

Total kinetic energy of the system is then written as:

$$T_t = \tfrac{1}{2} J_m \dot{\theta}_1^{\,2} + \tfrac{1}{2} J_a g^2 \dot{\theta}_1^{\,2} + \tfrac{1}{2} J_s \dot{\theta}_2^{\,2} + \tfrac{1}{2}(J_c + m_a r^2)\dot{\theta}_3^{\,2} + \tfrac{1}{2} m_b \dot{x}^2 \tag{A.3.7}$$

The values of slider displacement and velocity x, $\dot{x}$ and $\dot{\theta}_3$ are written in open form here as:

$$x = r + l - r\cos\theta_3 - [l^2 - (y - r\sin\theta_3)^2]^{1/2} \tag{A.3.8}$$

$$\dot{x} = r\sin\theta_3\dot{\theta}_3 + \frac{r\cos\theta_3\dot{\theta}_3(y - r\sin\theta_3)}{[l^2 - (y - r\sin\theta_3)^2]^{1/2}} \tag{A.3.9}$$

the kinematic relationship for the inputs of a differential gear-unit is expressed as:

$$\dot{\theta}_3=\rho\dot{\theta}_2+(1-\rho)g\dot{\theta}_1 \tag{A.3.10}$$

If equations (A.3.8), (A.3.9) and (A.3.10) are substituted into equation (A.3.8), the total kinetic energy is written as the following.

$$T_t=\frac{1}{2}J_m\dot{\theta}_1^{\,2}+\frac{1}{2}J_ag^2\dot{\theta}_1^{\,2}+\frac{1}{2}J_s\dot{\theta}_2^{\,2}+\frac{1}{2}(J_c+m_ar^2)\left(\rho\dot{\theta}_2-(1-\rho)g\dot{\theta}_1\right)^2$$

$$+\frac{1}{2}m_b\left(r\sin\theta_3+\frac{r\cos\theta_3\,(y-r\sin\theta_3)}{[l^2-(y-r\sin\theta_3)^2]^{1/2}}\right)\left(\rho\dot{\theta}_2+(1-\rho)g\dot{\theta}_1\right)^2 \tag{A.3.11}$$

Partial differentiation of each term in the total kinetic energy with respect the generalized displacements and velocities as $\frac{\partial T_t}{\partial\theta_1}$, $\frac{\partial T_t}{\partial\dot{\theta}_1}$, $\frac{\partial T_t}{\partial\theta_2}$, $\frac{\partial T_t}{\partial\dot{\theta}_2}$ and further time derivatives for $\frac{d}{dt}\left(\frac{\partial T_t}{\partial\dot{\theta}_1}\right)$ and $\frac{d}{dt}\left(\frac{\partial T_t}{\partial\dot{\theta}_2}\right)$ by using equation (A.2.7) yield final form of the equations of motion as given in chapter 4.

APPENDIX 4

STANDARD ELEMENTS OF BOND GRAPHS

TABLE I:

name	constitutive relation	example
Sources		
S_e —— e-source	e(t) given	force source, voltage source
S_f —— f-source	f(t) given	velocity source, current source
S —— source	ψ(e,f) = 0	motor characteristics
Dissipators		
—— R resistance	ψ(e,f) = 0	mechanical damper, electrical resistance,
	e= Rf (linear)	
Storage		
—— C capacitance	ψ(e,q) = 0	spring, hydraulic reservoir
	e= e(0)+1/C $\int$ fdt (linear)	
—— I inertiance	ψ(f,p) = 0	hydraulic inertiance, mass, inductance
	f= f(0)+1/I $\int$ edt (linear)	

Transducers

— TF — transformer	$e_1 = ne_2$	rack and pinion,
	$f_2 = nf_1$	cylinder and piston
— GY — gyrator	$e_1 = rf_2$	electrodynamic tr.
	$e_2 = rf_1$	
|		
— MTF— modulated	$e_1 = ne_2$	kinematic mechanism
transformer	$f_2 = nf_1$	
|		
— MGY— modulated	$e_1 = rf_2$	electric motor
gyrator	$e_2 = rf_1$	

Junctions

— 0 — 0-junction	$e_1 = e_2 = e_3 = \ldots e_n$	equal forces
|	$f_1+f_2+f_3+\ldots f_n = 0$	parallel connection
— 1 — 1-junction	$f_1 = f_2 = f_3 = \ldots f_n$	equal velocities
|	$e_1+e_2+e_3+\ldots e_n = 0$	series connection